

David Arellano · Abdullah Tolga Özer
Steven Floyd Bartlett · Jan Vaslestad
Editors

5th International Conference on Geofoam Blocks in Construction Applications

Proceedings of EPS 2018

5th International Conference on Geofoam Blocks in Construction Applications

@Seismicisolation

David Arellano · Abdullah Tolga Özer
Steven Floyd Bartlett · Jan Vaslestad
Editors

5th International Conference on Geofoam Blocks in Construction Applications

Proceedings of EPS 2018



Springer

@Seismicisolation

Editors

David Arellano

Department of Civil Engineering

The University of Memphis

Memphis, TN

USA

Abdullah Tolga Özer

Department of Civil Engineering

Okan University

Istanbul

Turkey

Steven Floyd Bartlett

Department of Civil and Environmental

Engineering

The University of Utah

Salt Lake City, UT

USA

Jan Vaslestad

Norwegian Public Roads Administration

Oslo

Norway

ISBN 978-3-319-78980-4

ISBN 978-3-319-78981-1 (eBook)

<https://doi.org/10.1007/978-3-319-78981-1>

Library of Congress Control Number: 2018939132

© Springer International Publishing AG, part of Springer Nature 2019

This work is subject to copyright. All rights are reserved by the Publisher, whether the whole or part of the material is concerned, specifically the rights of translation, reprinting, reuse of illustrations, recitation, broadcasting, reproduction on microfilms or in any other physical way, and transmission or information storage and retrieval, electronic adaptation, computer software, or by similar or dissimilar methodology now known or hereafter developed.

The use of general descriptive names, registered names, trademarks, service marks, etc. in this publication does not imply, even in the absence of a specific statement, that such names are exempt from the relevant protective laws and regulations and therefore free for general use.

The publisher, the authors and the editors are safe to assume that the advice and information in this book are believed to be true and accurate at the date of publication. Neither the publisher nor the authors or the editors give a warranty, express or implied, with respect to the material contained herein or for any errors or omissions that may have been made. The publisher remains neutral with regard to jurisdictional claims in published maps and institutional affiliations.

Printed on acid-free paper

This Springer imprint is published by the registered company Springer International Publishing AG part of Springer Nature

The registered company address is: Gewerbestrasse 11, 6330 Cham, Switzerland

Contents

Part I Key Note, Geofoam Blocks in Civil Engineering Applications

Geofoam Blocks in Civil Engineering Applications	3
Roald Aabøe, Steven Floyd Bartlett, Milan Duškov, Tor Erik Frydenlund, Jnanendra Nath Mandal, Dawit Negussey, Abdullah Tolga Özer, Hideki Tsukamoto and Jan Vaslestad	

Part II Construction Applications

Dutch A4all Tramway EPS Embankment with Vertical Sides	41
Milan Duškov and Johan de Jongh	
Geofoam Eps Used in Bridge Abutment, E18 Farris Bridge	49
Jan Vaslestad, Jørn Einar Liveroed, Tseday Damtew, Staale Singstad and Dag Loevstad	
EPS Geofoam Used in E16 Sandvika–Wøyen	57
Ermias Hailu Mijena	
First Geofoam Roadway Embankment Application in Turkey	71
Abdullah Tolga Özer and Emre Akınay	
Dutch A76 Highway Widening Using EPS Embankment with a Vertical Side	81
Milan Duškov, Martin den Uil and Michaël Fütterer	
Dutch N201 Road Embankment with EPS Geofoam	89
Milan Duškov and Wim Erkelens	
Post-use Examination of EPS Block Characteristics:	
Finnish Case Histories	99
Gowthaman Sinnathamby, Leena Korkiala-Tanttu and Henry Gustavsson	

Analysis of Crack and Differential Settlement on Pavement in EPS After Highway Opening	111
Yongchai Chang and Nagyoung Kim	
Load Reduction on Buried Rigid Culverts, Instrumented Case Histories and Numerical Modeling	115
Jan Vaslestad and Murad Sani Sayd	
Improving the Behavior of Buried HDPE Pipe by Using EPS Geofoam	129
Emre Akınay and Havvanur Kılıç	
Part III Material Properties and Modeling	
Creep Behavior of Recycled-Content Expanded Polystyrene Geofoam Under Compressive Loading	151
Chuanqi Wang, David Arellano and Roger Meier	
The Influence of Strain Rate on the Stress-Strain Behavior of EPS Geofoam	161
Djiba Kaké, Engda Kassahun Temesgen and Dawit Negussey	
Evaluation of Interface Shear Strength Between Interlocked Geofoam Blocks and Precast Concrete	171
Abdullah Tolga Özer	
California Bearing Ratio (CBR) Behaviors of EPS Geofoam: Experimental and Numerical Studies	185
Yebelta Zerie Beju and Jnanendra Nath Mandal	
Non Destructive Testing for EPS Geofoam Quality Assurance	197
Engda Kassahun Temesgen, Luke Andrews and Dawit Negussey	
Evaluation of Interface Shear Strength Between Interlocked Geofoam Blocks and Cast-in-Place Concrete	207
Abdullah Tolga Özer and Özgür Ekincioğlu	
Stress-Strain Behavior of EPS Geofoam with Multiple Grades by Using FlexiForce Sensors	219
Chen Liu and Dawit Negussey	
Behavior of Expanded Poly Styrene (EPS) with Experimental and Numerical Methods	231
S. N. Moghaddas Tafreshi and S. M. Amin Ghotbi Siabil	
Effects of Installation of Different Density Geofoam and Continuous Vertical Gaps	239
Chen Liu and Dawit Negussey	

Effect of Using EPS Geofoam on Deformation Behavior of Square Footings on Clay Subjected to Static and Dynamic Loads: Experimental Study	251
M. El. Gendy, I. El. Araby, W. El. Kamash, E. Sallam and A. El. Labban	
Mechanical Properties of EPS Geofoam Under Various Loading Conditions	267
Vinil Kumar Gade and Satyanarayana Murty Dasaka	
Part IV New Concepts and Special Topics	
Bridge Foundations Supported by EPS Geofoam Embankments on Soft Soil	281
Jan Vaslestad, Steven Floyd Bartlett, R. Aabøe, H. Burkart, T. Ahmed and David Arellano	
Guidance on Use of Geofoam Lightweight Fill and Complementary Technologies Using <i>GeoTechTools</i>	295
Ryan R. Berg, Vernon R. Schaefer and Silas C. Nichols	
N222 Roundabout upon EPS Embankment with Integrated Corrugated Steel Tunnel Structure Without Pile Foundation	309
Milan Duškov and Jeroen Tameling	
Design and Evaluation of Seismic Stability of Free-Standing EPS Embankment for Transportation Systems	319
Steven Floyd Bartlett and Zahra Amini	
Expanded Polystyrene (EPS) Geofoam Columns in Expansive Soil: Preliminary Swelling Characteristics Evaluation	331
S. Selvakumar and B. Soundara	
The Effect of EPS Geofoam Thickness on the Seismic Performance of Quay Walls	339
Ayşe Edinçliler and Yasin Sait Toksoy	
Opening Traffic for a Temporarily Remediated EPS Road After the 2016 Kumamoto Earthquake: A World First	351
Keiichi Taneichi, Takeharu Konami, Hideki Tsukamoto, Tatsuro Kubota and Kazuya Yasuhara	
Development of Joint Metal Binder for Improving Earthquake Resistance of EPS Embankment	361
Keiichi Taneichi, Takeharu Konami, Hideki Tsukamoto, Tatsuro Kubota and Kazuya Yasuhara	
Shaking Table Test of Scaled 1/5 EPS Embankment Model	367
Keiichi Taneichi, Tsuyoshi Nishi, Takeharu Konami, Tatsuro Kubota, Junichi Koseki, Hiroyuki Kyokawa and Kazuya Yasuhara	

Part I

**Key Note, Geofoam Blocks in Civil
Engineering Applications**

Geofoam Blocks in Civil Engineering Applications



**Roald Aabøe, Steven Floyd Bartlett, Milan Duškov,
Tor Erik Frydenlund, Jnanendra Nath Mandal, Dawit Negussey,
Abdullah Tolga Özer, Hideki Tsukamoto and Jan Vaslestad**

Abstract In Norway the use of Geofoam blocks in road construction applications started in 1972. Excessive settlements of a road embankment adjoining a bridge abutment founded on piles to firm ground was then successfully halted by replacing a 1 m layer of road aggregate with blocks of Expanded Polystyrene (EPS). Boards of EPS had previously been successfully tested in road structures over several years in a major research project related to Frost Action in Soils. The use of Geofoam blocks for lightweight fill purposes, reduced earth pressure and several other applications for a variety of Civil Engineering purposes, has since been adopted and further developed in many countries worldwide. In this article the state of the art regarding various applications of Geofoam blocks are shown based on available information supplied by the authors.

Keywords Geofoam blocks · Lightweight · Stability · Bearing capacity
Settlements

R. Aabøe · J. Vaslestad
Norwegian Public Roads Administration (NPRA), Oslo, Norway

S. F. Bartlett
University of Utah, Salt Lake City, UT, USA

M. Duškov
InfraDelft, Delft, The Netherlands

T. E. Frydenlund (✉)
Geo Con, Oslo, Norway
e-mail: tofryden@vikenfiber.no

J. N. Mandal
Indian Institute of Technology, Bombay, India

D. Negussey
University of Syracuse, Syracuse, USA

A. T. Özer
Okan University, Istanbul, Turkey

H. Tsukamoto
Construction Project Consultants Inc., Tokyo, Japan

1 Introduction

Geofoam blocks are made of Expanded Polystyrene (EPS) initially produced for packaging and insulation purposes. The material is extremely light and can be produced in many shapes and densities, typical density $\rho = 20 \text{ kg/m}^3$. Geofoam blocks for civil engineering applications have typically dimensions $0.5 \times 1.0 \times 2.5\text{--}3.0 \text{ m}$ weighing some 25–30 kg. Material strength properties varies relatively linearly with density and a 20 kg/m^3 material may typically have a compressive strength of $\sigma = 100 \text{ kPa}$ at 10% strain. Geofoam blocks are produced in wide ranges of densities and strength characteristics. The term Geofoam is also used in connection with Extruded Polystyrene (XPS), but this production process limits the products to board formats.

When Geofoam blocks were first used as a lightweight fill material for road construction purposes in Norway in 1972 [1] it had already been demonstrated by a research project on Frost Action in Soils that boards of EPS could sustain the repetitive loads in a road pavement and that material properties did not deteriorate with time. When excessive settlements ($\sim 20 \text{ cm/year}$) occurred in a road embankment adjacent to a bridge founded on piles to firm ground, it was decided to replace 1 m of ordinary embankment materials with EPS blocks placed in two layers each with a thickness of 0.5 m. The embankment rested on 3 m of peat overlaying 10 m of soft clay deposits and due to repetitive adjustments of the road level, the embankment load on the subsoil increased resulting in accelerated settlements and risk of embankment failure. By replacing 1 m of embankment aggregate with Geofoam blocks, being nearly 100 times lighter than the replaced embankment material, the settlements were successfully halted.

The use of Geofoam blocks in civil engineering applications has since been adopted as a general practice in many countries and for a multitude of purposes. International conferences have been instrumental in the dissemination of information related to the properties and use of Geofoam blocks. The first conference was held in Oslo, Norway in 1985 attended by 150 participants from 11 countries [2]. With a strong Japanese engagement in using and further developing the method the second conference was held in Tokyo, Japan in 1996 where 300 participants from 15 countries attended [3]. Similarly, with an increased focus on the use of the method in the U.S. the third conference was held in Salt Lake City, Utah in 2001 [4]. The fourth conference was held in Lillestrøm, Norway in 2011 [5]. The present conference is in this respect a further landmark in disseminating information on the use of Geofoam blocks in civil engineering applications.

In addition to international conferences seminars and local arrangements on a national level have also further promoted the use of Geofoam blocks in addition to bilateral agreements between government agencies and private organizations in various countries and by direct contacts on a personal level.

Today projects using Geofoam blocks are known to have been completed in many European countries: Czech Republic, Denmark, Finland, France, Germany, Greece, Ireland, Netherlands, Norway, Poland, Russia, Serbia, Sweden and the UK,

but other European countries may also have adopted the method. In Asia the major user is Japan (Figs. 1 and 2), but China, Malaysia, Thailand, The Philippines, South Korea and Taiwan are also known to have used Geofoam blocks. India has recently shown an interest and several other Asian countries are likely potential users. The first road embankment with Geofoam blocks was recently completed in Turkey [6, 7]. In America the method is adopted in the US and Canada as well as in Argentina, and Columbia. Civil engineering projects involving Geofoam blocks have been reported from Victoria, New South Wales and Queensland in Australia. No African projects are known so far but situations where the use of Geofoam blocks may have an advantageous potential, are likely to exist there too.

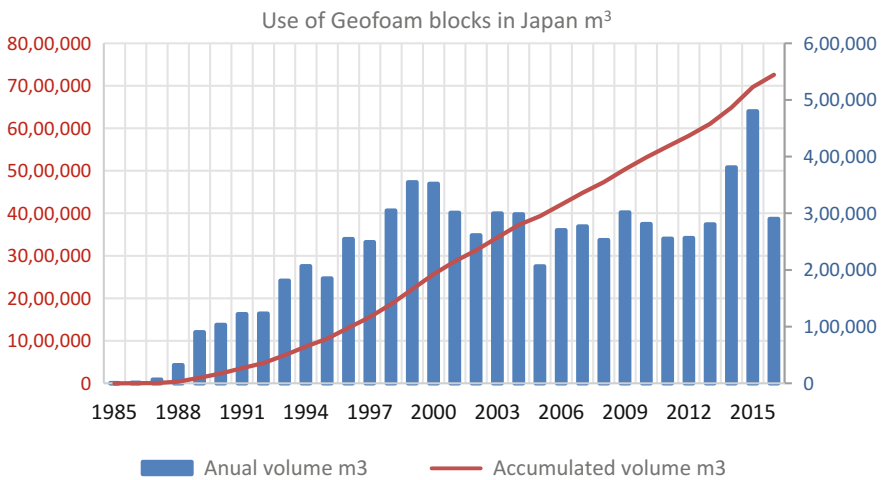
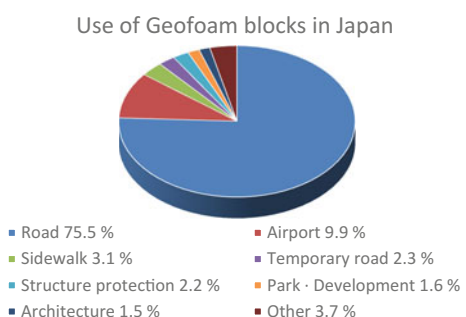


Fig. 1 Use of geofoam blocks for civil engineering purposes in Japan (EDO)

Fig. 2 Use of geofoam blocks in Japan by purpose (EDO)



2 Applications

2.1 Lightweight Fill

The major use of Geofoam blocks has so far been as a lightweight fill material, mainly for road construction purposes [8–17] but also for railroads [18, 19], airfields and other construction projects. The blocks may be applied to reduce the construction load on soft subsoils for both stability and settlement reasons. A typical road cross section with inclined and/or vertical side slopes may be as shown in Fig. 3. Normally the pavement structure above the Geofoam blocks will consist of a sparsely reinforced concrete slab of 10–15 cm thickness with a minimum bearing course (some 35 cm) above topped with an asphalt wearing course. In cases where the load on the Geofoam blocks is not critical, a normal pavement structure may be applied but a membrane is then usually added above the Geofoam blocks.

As indicated the Geofoam fill may also be terminated with a vertical face on one or both sides. In such cases some form of protective casing should be added to the vertical face. Materials used for such purposes have been aluminum and steel sheets, concrete panels, wooden planks and sprayed concrete. In a landslide area on the Yamagata Expressway in Japan a 16 m high road structure was constructed with vertical walls on both sides, the same design was used to widen the road as shown in Fig. 4 [20, 21].

Here 10 cm thick sparsely reinforced concrete slabs were cast for every 3 m height of EPS block fill in order to bind the structure together and even out possible minor level differences when placing the blocks. Also, a form of sliding connections were introduced to allow for possible differential vertical movements.

When widening existing normal roads, it may also be advantageous to use Geofoam in the widened road structure in order to improve stability conditions and avoid differential settlements [22] between the old and the new road structure (Fig. 5).

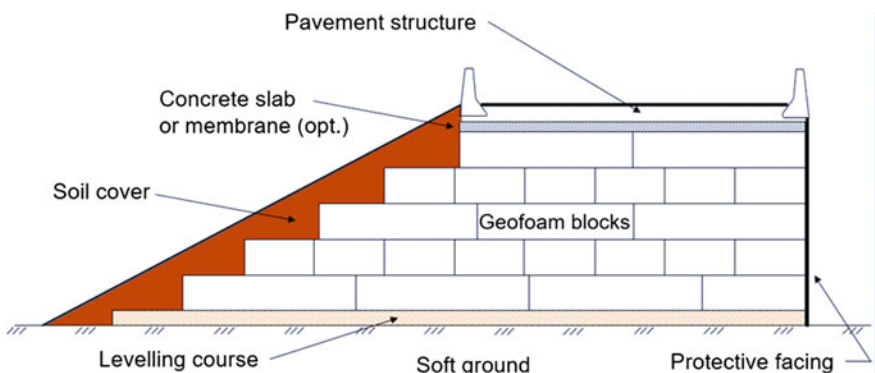


Fig. 3 Cross section of road embankment with geofoam blocks



Fig. 4 Yamagata Expressway, Japan with vertical side walls (EDO)

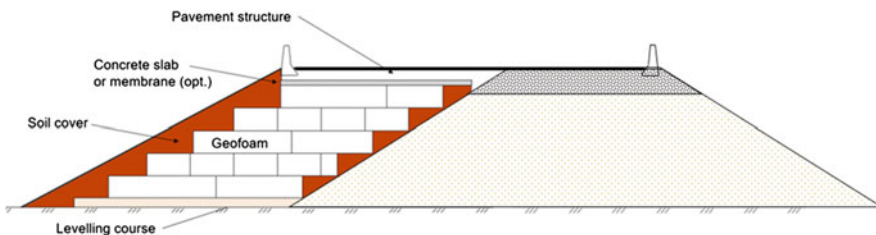


Fig. 5 Road widening application using geofoam blocks

When widening or constructing roads on steep side slopes, Geofoam blocks with vertical side termination may be a favourable solution (Fig. 6). On slopes, particularly where high fills are involved, the need for proper anchorage should then be analyzed separately. The anchorage should provide support for horizontal forces from soil pressure on the structure and vehicles hitting guard rails or side barriers.

On the Otari Road in Nagano Prefecture, Japan a 1.2 km road section was constructed (Fig. 7) [21]. The maximum height of the road structure was 17 m and volume of Geofoam blocks used 30,000 m³ (Fig. 5).

With a properly designed ballast layer and load distribution slab (if required) above Geofoam blocks of sufficient strength, the method may also be used for

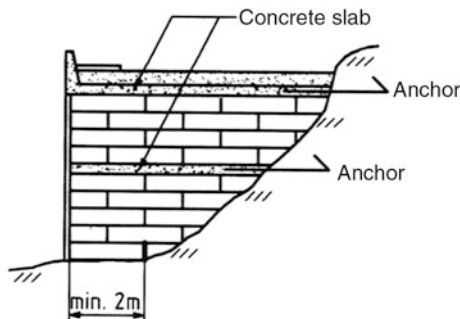


Fig. 6 Cross section of high embankment on slope (NPRA)

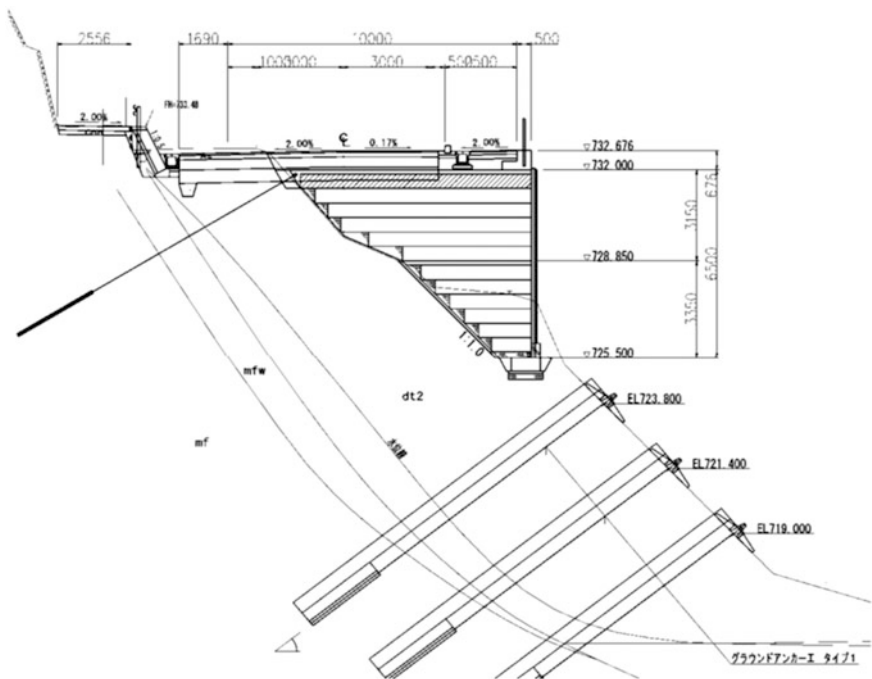


Fig. 7 Design cross section of Otari Road in Nagano Prefecture, Japan (EDO)

railroads and several such projects have been completed in Norway, the UK, Japan, U.S. and possibly in other countries.

The Utah Transit Authority (UTA) in Salt Lake City has constructed EPS bridge approach fills for its light-rail and commuter rail systems. The dynamic deflection performance of these systems under train loadings has been monitored [19]. Dynamic accelerations were obtained via accelerometer arrays placed on the rail sleepers for these systems. Dynamic deflections estimated from these measurements

based on a double integration of the acceleration data suggest that the dynamic deflections are acceptable and comparable to those measured on earthen embankment.

The same applies for airfields whether on taxiways or runways as it is only a question of making an adequate design in order for the structure to sustain the wheel loads from landing or taxiing aircrafts. The New Orleans Airport East/West runway rehabilitation project included the removal of existing damaged pavement and the construction of new taxiways. EPS geofoam was used under the new pavements to control settlement on the highly compressible and saturated subsoils and to prevent differential settlements at the intersection of new and existing pavements.

Geofoam blocks may also be used for stability improvement purposes in terrain with potential slide hazards and for slope failure mitigation in areas where slides have occurred (Fig. 8). In order to reduce the driving forces, here a volume of high density natural soil is replaced with Geofoam blocks. Proper drainage is also provided in order to prevent hydrostatic pressure building up within the soil/Geofoam structure. Recent studies were conducted to understand the behavior of slopes under seepage forces and corresponding remedial block configurations tested in a laboratory bench scale models [23–26].

Geofoam blocks may also be used as a compensating foundation for buildings in order to reduce the load on underlying compressible soils and minimize building settlement along with solving potential bearing capacity problems. At the building site existing soil is excavated and replaced by Geofoam blocks in order to reduce the net applied load to the soil by the new structure. If the amount of soil excavated equals the total load applied by the new structure, a fully compensated foundation is obtained, i.e. no increased load is applied to the subsoil by the structure.

Similarly, Geofoam blocks may also be used as a lightweight fill material for landscaping purposes. This may be particularly useful when creating undulating terrain features close to existing buildings where normal soil aggregate used for the

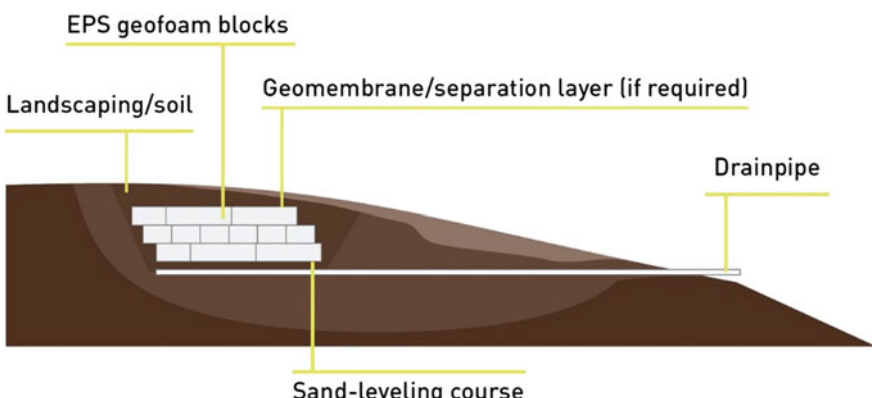


Fig. 8 Schematic drawing of geofoam block placement in a slide area [27]

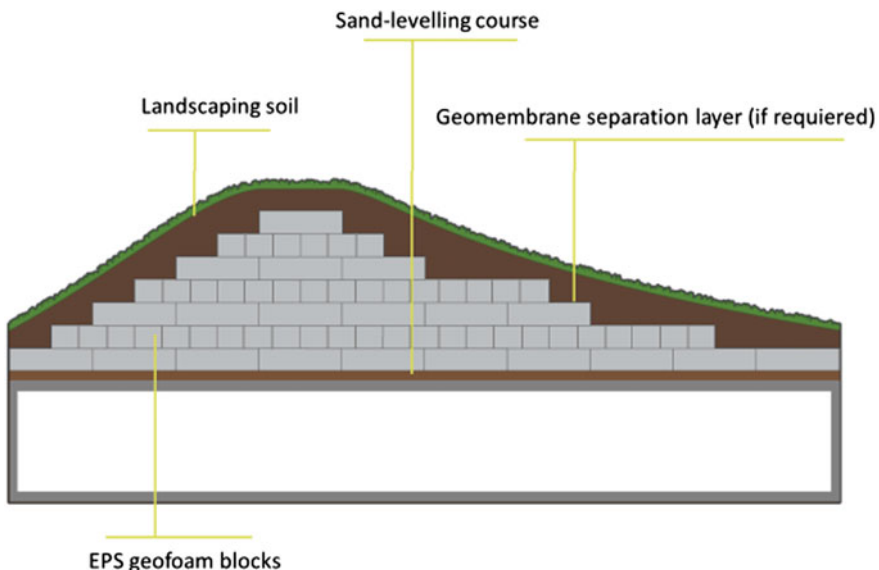


Fig. 9 Schematic drawing of vegetative roof on building [27]

same purpose could create settlement problems for the building foundations. Some examples of this application include creating roof gardens for urban buildings (Fig. 9). For the same reasons Geofoam blocks may also be used to construct sound barriers to protect roadside residents from noise pollution (Fig. 10).

When excessive settlements occur in levees and repair must be initiated to cope with expected flood levels, the use of Geofoam blocks may provide a favourable solution. If ordinary fill material is used to raise the embankment height, this will result in further subsidence. By replacing part of the embankment soil with Geofoam blocks, further subsidence may be halted. With the extremely low density of Geofoam, caution must, however, be observed to prevent the Geofoam blocks from becoming buoyant. The buoyancy potential must be considered based on expected flood levels and the volume of Geofoam blocks used and their position relative to the flood level. The uplift tendency may also be countered to some extent by providing anchorage (Fig. 11).

It is of course possible to utilise the buoyancy effect of Geofoam blocks directly for floating piers and similar harbour and marina arrangements. This effect has been taken advantage of for a long time, and in Vancouver, British Columbia, Canada Geofoam blocks are used to support a floating helicopter pad (Fig. 12).

A similar use of the buoyancy effect has been introduced in the Netherlands where a floating garden built on Geofoam blocks are seen on one of the canals in Amsterdam (Fig. 13).

Some special forms of Geofoam blocks have also been designed to accommodate rising water levels without introducing the full buoyancy forces that a solid Geofoam block would cause [28]. This is obtained by making hollow blocks with

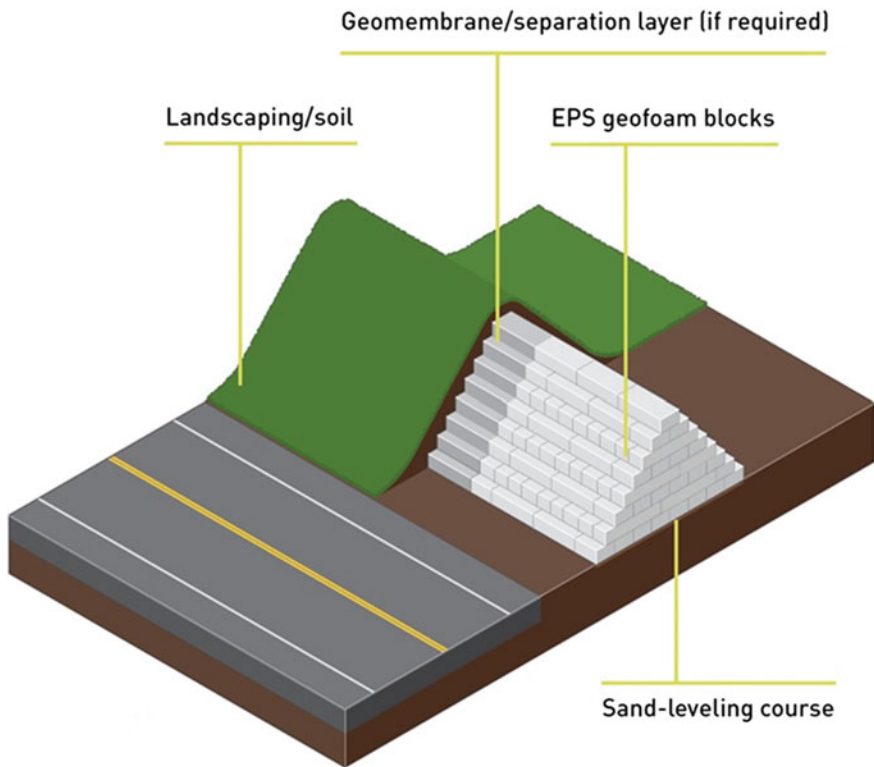


Fig. 10 Geofoam blocks used in noise barrier [27]

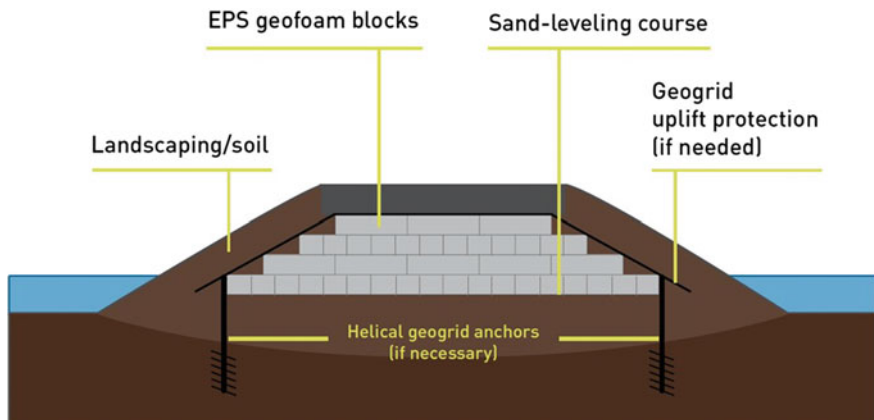


Fig. 11 Cross section showing levee repair using geofoam blocks [27]



Fig. 12 Floating helipad supported by geofoam blocks in Vancouver, Canada (www.mansonvilleplastics.com)



Fig. 13 Floating garden on one of the canals in Amsterdam, The Netherlands (T. Özer)

slits on the sides allowing water to enter without introducing the full buoyancy force of a solid block (Fig. 14).

Geofoam blocks may also be used to form tiered seating in locations such as auditoriums, movie theaters, gymnasiums and churches. The high compressive resistance and light weight of Geofoam make it well suited to both new construction and renovation projects. Stacked Geofoam blocks before a protective concrete layer is added and seats, bleachers and other attachments and finishes are installed to complete the project (Fig. 15).

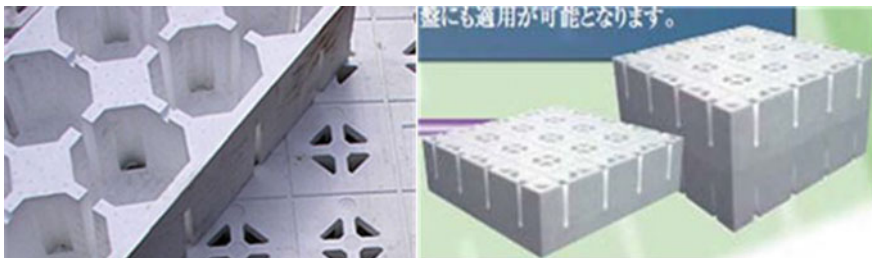


Fig. 14 Design of EPS block with reduced buoyancy effect (EDO)



Fig. 15 Stacked Geofoam blocks for seating arrangements (<http://blog.achfoam.com/?p=2455>)

2.2 Load Reduction

Particularly when encountering soft ground conditions with inferior bearing capacity but also in general when subsoil bearing capacity may be a problem due to heavy loads, Geofoam blocks may be used to improve both bearing capacity and settlement conditions. Since the material density of Geofoam blocks is much less than ordinary mineral soils, the load on the subsoil may be substantially reduced by replacing some amount of ordinary soil with EPS. This was the case for the first

application of Geofaom blocks in a roadfill in Norway in 1972. By balancing the loads removed by soil excavation with the loads applied to the subsoil by the completed structure, both satisfactory bearing capacity and settlement conditions may be achieved.

Depending on the structure loads and foundation area the compressive strength of the Geofoam blocks must be adjusted accordingly, but the difference in material density of various EPS strength qualities are small compared to the density of the mineral soil to be replaced.

In several projects, particularly in Europa and the US, this principle has also been applied in connection with the design of bridges where bridge abutments have been supported directly on Geofoam blocks. Such an example is shown where the foundations for a temporary Acrow type steel bridge is founded directly on some 5 m high Geofoam fills resting on soft and quick clay in Norway (Fig. 16) [29]. Similar solutions have also been applied for permanent concrete bridges (Fig. 17).

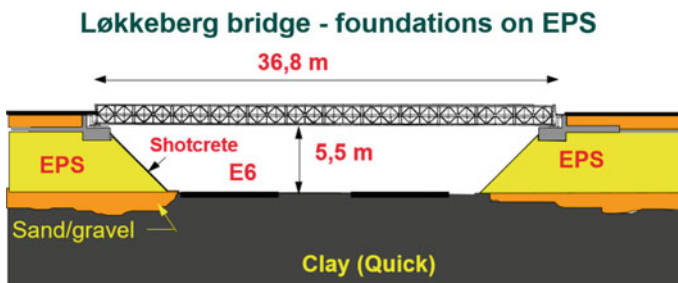


Fig. 16 Bridge abutment founded directly on geofoam blocks (NPRA)

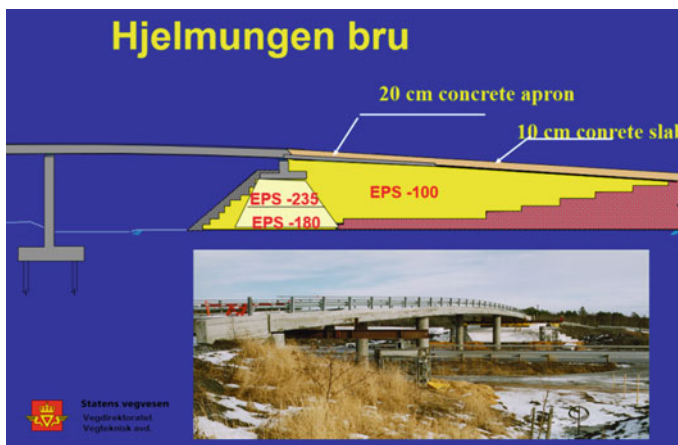
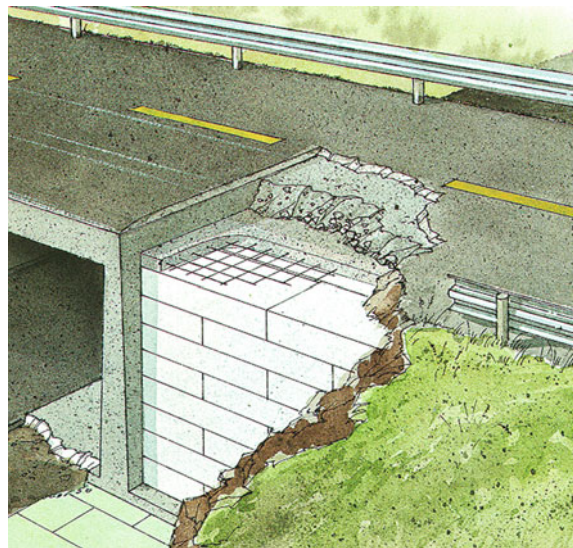


Fig. 17 Abutment for multispan concrete bridge founded directly on geofoam blocks with varying compressive strength (NPRA)

Fig. 18 Backfill of geofoam blocks against bridge abutment (NPRA)



Furthermore, since fills with geofoam blocks may be terminated with vertical walls, no or only minimal horizontal forces will be transmitted to any structure adjacent to or connecting to the fill. This effect will significantly simplify the design of bridge abutments and retaining walls related to accommodating horizontal forces (Fig. 18).

Another type of load reduction application associated with bridges is a simplified design (Fig. 19). The sheet piles may be driven from the river shores without polluting the water or interfering with fish activities. Scaffolding for casting the bridge deck is connected to the sheet piles or precast bridge deck slabs may be used.

Geofoam has been used to provide an alternative foundation system for replacing a single span steel girder bridge in Upstate New York [30]. The site is in a wide valley of deep soft sediments. The replaced bridge was supported on a shallow foundation and had settled excessively. The span and width of the replacement bridge was increased to provide more flow capacity and sidewalk. The precast concrete box girder replacement bridge and stub abutment system is heavier than the replaced bridge. Conventional deep pile foundations would have required end bearing at depths greater than 30 m. The alternative foundation system used for the replacement bridge consists of a sheet pile cell that surrounds each abutment foot print. Soil within the sheet pile cell enclosure was excavated and the water level was lowered by sump pumping. The volume of the excavated soil was replaced by EPS geofoam blocks to compensate for the weight of the bridge and foundation system (Fig. 20). The steel reinforcement for a 0.5 m load distribution cap and stub abutment over the geofoam backfill is welded to the top of the sheet pile enclosure. The precast concrete box girders rest on neoprene bearing pads over the stub abutments. While in service, the EPS geofoam blocks become fully submerged during high flood periods. The sheet pile wall friction resistance functions to

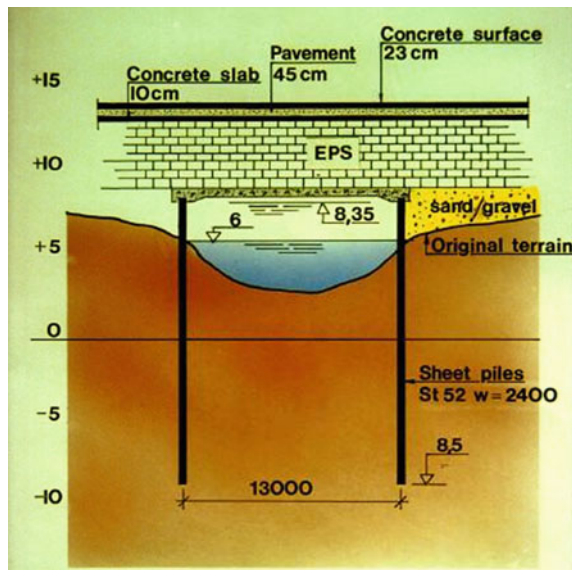


Fig. 19 Simplified bridge design (NPRA)



Fig. 20 Geofoam placement within the sheet pile cell (30)

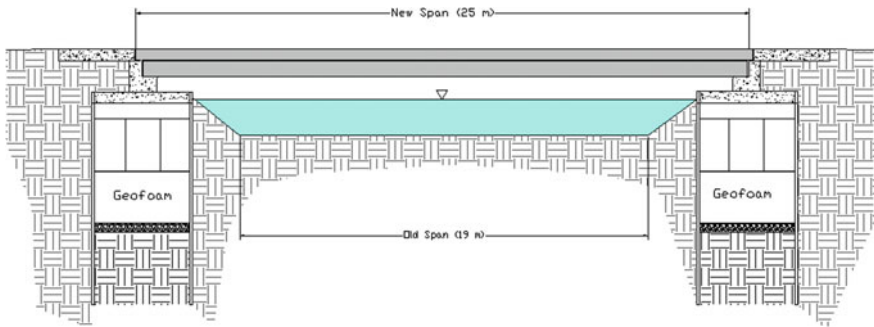


Fig. 21 Schematic section of the geofoam supported bridge (30)

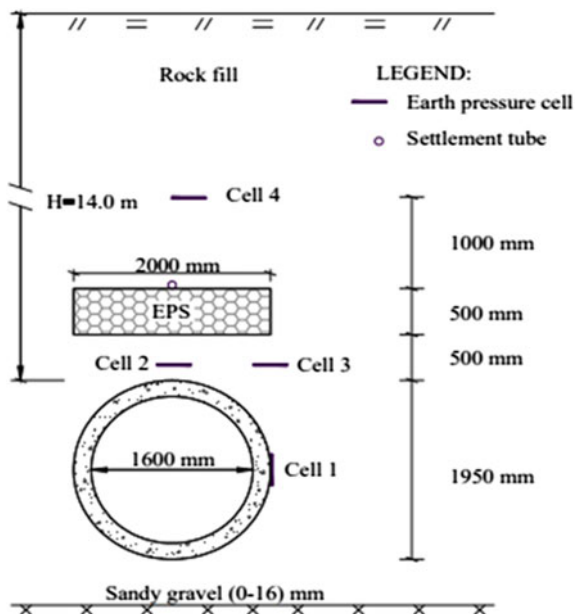
provide additional capacity to both downward loading and uplift due to buoyancy at low and high flood stages. The completed geofoam supported bridge (Fig. 21) is regularly inspected and continues to receive top rating.

The magnitude and distribution of earth pressure on buried culverts depend on the overburden thickness and the relative stiffness of culvert and soil with varying load distribution along the culvert perimeter. Normally the vertical pressure will be higher than the horizontal pressure. By introducing a compressible layer above the culvert, a more evenly distributed pressure system may be obtained around the culvert. This is a well-known method (often called the induced trench or imperfect ditch method) and various types of compressible materials have been applied for such purposes. EPS is a material well suited for this type of application as the stiffness of the EPS material and layer thickness may be selected to suit a particular project. As the embankment is constructed above the culvert, the EPS layer will deform creating arching effects in the soil above that will redistribute more vertical load to the side of the culvert and hence increase the horizontal pressure. Such effects have been monitored on many culvert projects proving theoretical effects (Fig. 22) [31].

For EPS fills where the blocks are subjected to lateral forces from behind the fill or from traffic and seismic loads, a similar effect by placing deformable EPS blocks against bridge abutments and non-yielding retaining walls, may be utilized to reduce lateral pressure against the wall or abutment [32–35].

For EPS fills with sufficient internal stability terminated in a vertical wall there is no need for a retaining wall as mentioned in Sect. 2.1, only some mechanical protection of the outer blocks. For bridge abutments it has also been demonstrated that leaving a small gap between a stable EPS fill and an abutment wall will prevent transmission of lateral forces on to the abutment from the EPS fill. Monitoring the abutment some 7 years after its completion showed that the EPS fill remained stable and that no measurable movement of EPS blocks had occurred [36].

Fig. 22 Example of monitoring pressure distribution on a culvert with a deforming EPS layer above (NPRA)



2.3 Energy Absorption

For protecting road users from avalanche hazards in mountainous areas avalanche sheds are sometimes constructed on road sections with frequent avalanche activities. Such sheds will normally have a cover of soil material on the shed roof to absorb some of the impact forces from falling rocks. In order to further reduce the impact loads, Geofoam blocks may be placed on the shed roof with a concrete slab and soil cover on top. When large boulders or rocks hit the structure, the EPS material will deform and absorb a major part of the dynamic energy thus substantially reducing the dynamic loads transferred to the shed (Fig. 23). This idea was first introduced and tested in Japan [37]. The method may also be applied for protecting other types of structures from dynamic impacts.

2.4 Seismic Effects on EPS Fills

From the start some concerns have been raised regarding the behavior and stability of EPS embankments subjected to seismic loads. This problem has been thoroughly addressed particularly in Japan [38] and the USA [39] both from a theoretical approach as well as in small- and full-scale experiments. This includes both the stability of normal EPS embankments, embankments on slopes and free-standing EPS structures terminated with vertical walls as well as fills adjacent to bridge abutments and retaining walls. Figure 24 shows a test setup of reduced scale



Fig. 23 Geofoam blocks applied for energy absorption on rock fall protection tunnel in Turkey (Courtesy of EPSDER, Turkey)

shaking table and Fig. 25 shows a test setup of a Geofoam structure on a large shaking table in Japan. The general picture is that the EPS material has a positive effect on the type of structures analysed during seismic loading and in Japan no special seismic design considerations are required for fills with heights less than 6 m and a height to breadth ratio <0.8 . For higher fills such considerations are recommended. Secondary seismic effects after an earthquake like tsunamis, landslides etc. may, however, damage EPS fills, but no serious damage was reported for EPS structures during the earthquake or the following tsunami effects from the 2011 Tohoku earthquake in Japan. During the 2016 Kumamoto earthquake large ground deformations occurred and an EPS embankment under construction deformed somewhat. The fill was, however, completed without adjustments and the finished road is in normal service.

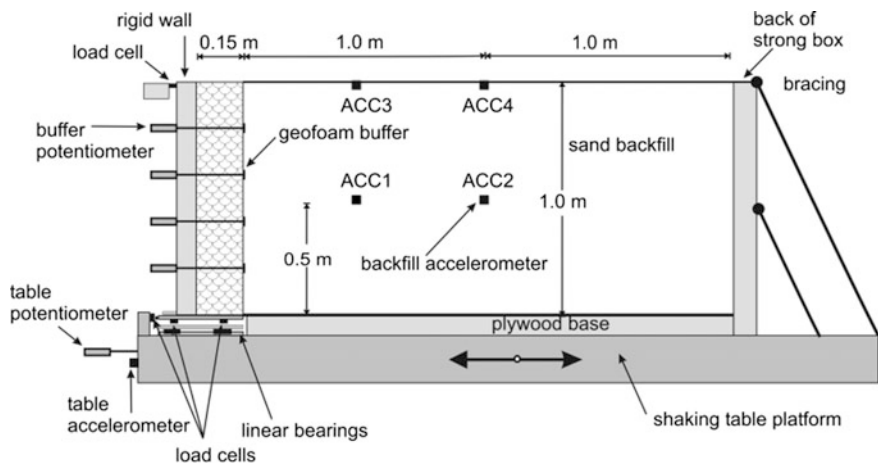


Fig. 24 Setup for shaking table test on geofoam block structure [32]



Fig. 25 Full scale seismic loading experiment on shaking table (EDO, Japan)

2.5 Speed and Ease of Construction

For various reasons some construction projects have to be completed within a minimum time span. With the light weight and relatively large volume per block Geofoam blocks may come in handy when construction speed is essential. This has proved the case in several projects [14].

When a high-speed rail service was to be established on the Manchester–Liverpool railway line this involved replacing an old steel bridge from 1899 with a new rail structure [40]. At the same time it was essential to keep the trains running with only a short brake allowed in the railway services for replacing the bridge. The bridge ran across a filled in river channel where various materials had been deposited over a long period of time. The construction method adapted was first to preload the subsoil with a 4.5 m high fill for a period of 9 months starting in 1997. The preload was then removed, and a Geofoam fill constructed up to a level just below the steel bridge with the bridge pillars still intact. Then the bridge was demolished, the height of the EPS fill increased to a level somewhat below the new track level and covered with a levelling layer of granular material. A precast concrete trough was then lifted on to the EPS fill. A HDPE liner, ballast material and rails were added on top of the concrete trough and the whole job was completed within 100 h from the bridge was removed until trains were running again (Fig. 26). The total volume of EPS blocks used with various densities, was 13,000 m³.

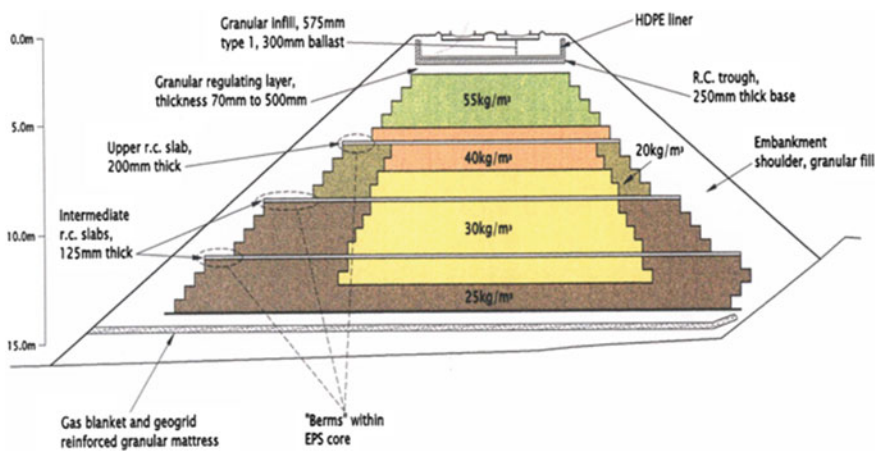


Fig. 26 Main components of EPS fill design for railway bridge replacement [40]

2.6 New Applications

2.6.1 Lightweight Culvert Structure

In Dutch road engineering practice, the arching principle is used to design a settlement-free tunnel construction integrated in an EPS embankment without a pile foundation (Figs. 27 and 28). The modular system of corrugated steel sheet elements fulfilled the specific project requirements such as a free space for cyclists and pedestrians, the available cover on the tunnel structure and the construction of the cover layers and pavement structure for the traffic load over the tunnel. In terms of both building costs and construction time reduction, the system offered advantages. The oval tunnel system is based on the load distribution by normal force along the “pressure points” in the steel shell construction. As an alternative to the standard



Fig. 27 Construction of corrugated steel tunnel in EPS fill (InfraDelft)



Fig. 28 Finished structure (InfraDelft)

design with compacted sand around the culvert, adequate side support is ensured by a light-weight foamed concrete enclosure combined with stronger EPS blocks. Such a tunnel construction is already in service under the new roundabout of the provincial road N222 near The Hague. There are no technical restrictions regarding either the profile or the traffic load over the considered tunnel system.

2.6.2 Seepage Mitigation

Geofoam blocks are used for slope stabilization in Japan and USA [41–44]. The design guideline for using geofoam blocks for slope stabilization and repair projects is based on the recommendation that geofoam slope system incorporate a drainage system for preventing water accumulation above the bottom of the geofoam block configuration [45]. However, the groundwater table may rise due to drainage malfunction. The behavior of geofoam blocks has been studied in Turkey using scaled physical slope experiments [23, 46]. Under the lights of this first study a geofoam block assemblage called this embankment type configuration where the backslope applies overburden along the geofoam block assemblage inside the slope (Fig. 29) was proposed [24]. It has been shown that this embankment type configuration could prevent both deep-seated failures of marginally stable sandy slopes subjected to seepage and hydrostatic sliding along the base of the geofoam block assemblage [24]. Further studies using geofoam blocks with internal drainage system showed that this would further improve the performance of slopes under seepage [25, 26]. However, the results of these laboratory studies can only be used for providing information about the basis to understand the prototype behavior of geofoam blocks in sandy slopes under seepage. It is recommended that the laboratory small scale 1-g model test results must be verified by an instrumented prototype model prior to implementing the recommended block assemblage in projects [22–26].

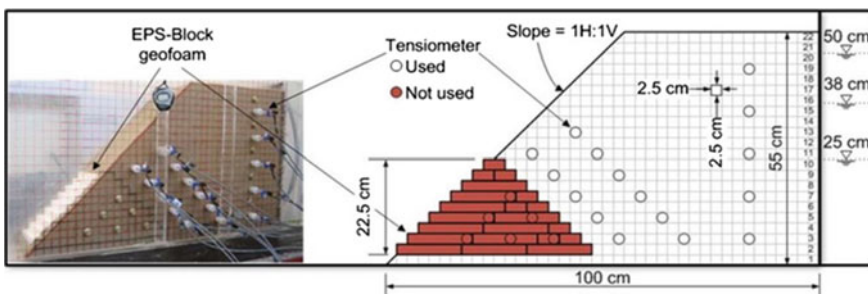


Fig. 29 Embankment type geofoam block configuration [24]

2.6.3 Interface Shear Strength

Internal stability analysis of geofoam highway embankments consists of hydrostatic sliding, transition due to wind and seismic stability [10]. The available shear resistance in between the geofoam blocks needs to be evaluated for seismic stability. If this resistance insufficient, additional resistance can be provided by shear key concept where continuous horizontal geofoam block planes are interrupted by installing half blocks periodically in the geofoam block assemblage [39]. In addition, adhesives can also be used to increase interface shear strength [47, 48]. Alternatively, a concept with interlocked geofoam blocks has been proposed [49] where the geofoam blocks have ledges and notches along their tops and bottoms, respectively. Therefore, when they are placed on top of each other, horizontal shear planes in between geofoam blocks are interrupted with interlocked configurations [49]. The interlocking mechanism will increase the interface shear strength of traditional geofoam block to geofoam block surface, and as the number of ledges and notches are increased, the interface shear strength of interlocked blocks approached to the internal shear strength of geofoam blocks [49]. Therefore, this interlocking mechanism can be a viable alternative for the geofoam embankments to be constructed in high seismic activity areas. However, due to the scale effect of the laboratory specimens, conducting large scale shear tests were recommended prior to using the interlocked concept in the field [49].

3 Material Specifications

When the first road project with EPS blocks was considered, the Norwegian Public Roads Administration (NPRA) decided to define the compressive strength of the EPS material at 5% strain when testing $50 \times 50 \times 50$ mm cubes in an unconfined compression test apparatus. With the use of EPS blocks for lightweight fill purposes adopted in many countries and the manufacturers showing a higher interest in such uses, more test methods have been introduced and a number of research projects have been carried out on this topic including dynamic loading. Different block shapes have also been tested (cubes and cylinders) with dimension varying from 50 mm to 100 mm and even full-size blocks. The tensile strength behavior of EPS geofoam has also been investigated [50] and found to depend on density. When strong fill materials with high strengths are required Indian investigations [51] show that expanded polystyrene-based geomaterial with fly ash can be used as a substitute for eps geofoam blocks.

This has resulted in both national and international standards being developed. Within the European Union (EU) a standard EN 14933 “Thermal insulation and light weight fill products for civil engineering applications—Factory made products of expanded polystyrene (EPS)—Specification” came into force in 2009 [52]. Here the strength of EPS material is defined at 10% strain tested on $50 \times 50 \times 50$ mm cubes, but requirements at 2 and 5% strain are added. Unit density is not set as a

requirement in this connection. Discussions are, however, ongoing regarding the size of specimens to be tested with the argument that larger samples will resemble the behavior of full size blocks more closely. In this connection and in order to harmonise requirements in EN 14933 with other CEN standards and Eurocodes the European Manufacturers of Expanded Polystyrene (EUMEPS) has set up a special task force to look into this matter.

The need for international standards is to harmonise material requirements to facilitate free trade and fair competition. The efforts within EU is a start in this direction, but at present most countries outside Europe adhere to local national standards but some also follow the European standard. Although national standards in general have similar requirements, a common international standard is not expected to materialize sometime soon.

4 Design Considerations

With the known properties of EPS material used for load carrying purposes, normal design procedures may be used for selecting a suitable quality of EPS material for the project in question. For road embankments a compressive strength of $\sigma = 100$ kPa corresponding to density of some $\rho = 20$ kg/m³ will normally be sufficient, but depending on the load situation other material qualities may be required.

For road fills involving Geofoam blocks, reduced loads are in most cases a key issue and in such projects a 10–20 cm sparsely reinforced (to prevent curing and temperature cracking) concrete slab is cast directly on top of the upper layer of Geofoam blocks for load distribution purposes. A minimum road base is then placed on top of the concrete slab before an asphalt topping or concrete pavement is added. In countries with below zero winter temperatures the base layer should have a minimum thickness (recommended 35 cm in Norway) in order to prevent black ice formation on the road surface during winter onset.

Since EPS material is soluble in petrol and other oil derivatives, some protective cover should be provided above the Geofoam blocks in case of a major oilspill. The load distributing concrete slab will act as a protective layer but in addition a protective geomembrane sheet (HDPE or similar) is commonly placed to cover the whole Geofoam structure. The membrane should have a thickness of at least 1.0 mm and be inert to petrol and other solving agents. So far no accidents involving damaged Geofoam blocks due to oilspill have been reported on a road in service and the risk for such incidents occurring is extremely low, but it is a scenario to be prepared for. Even if such an incident should occur, repair actions may easily be taken by replacing the damaged blocks.

In cases where maximum load reduction is not called for, a normal road base may be placed on top of the Geofoam blocks, but again as a precaution a protective geomembrane should be placed on the Geofoam surfaces. Other types of pavement structures may also be applied depending on the loads involved and the strength of the EPS blocks used.

For EPS fills with inclined side slopes, the Geofoam blocks should be covered by a soil layer on the side slopes above the geomembrane. A minimum cover thickness of 25 cm is recommended (Figs. 3 and 5).

For high Geofoam fills a lightly reinforced 10–20 cm thick concrete slab is usually added for every 3.5–4 m embankment height. This will bind the structure together and provide improved stability as well as evening out any minor height differences between blocks.

In order to avoid long term creep effects in the EPS structure, it is common practice only to utilise part of the short-term load capacity of the material in design procedures. For normal projects a long-term/short-term load ratio in the range of 0.3 is commonly applied. This procedure is expected to limit creep deformations to 2% over a period of 50 years. For transient loads a higher ratio may be applied. Also with improved manufacturing processes this may allow for higher ratios in the order of 0.40–0.45 to be used for permanent loads.

Although Geofoam blocks have a low unit density of $\rho = 20 \text{ kg/m}^3$ ($\gamma_d = 0.2 \text{ kN/m}^3$) when leaving the moulding form at the factory, some allowance should be made in design calculations for possible later changes when placed in the ground. For the first road fill in 1972 the NPRA adopted a design unit density of $\rho = 100 \text{ kg/m}^3$ ($\gamma_d = 1 \text{ kN/m}^3$). Based on later experience this design rule has later been changed to $\rho = 50 \text{ kg/m}^3$ ($\gamma_d = 0.5 \text{ kN/m}^3$) for Geofoam blocks placed in a dry position above the groundwater table while the design load for temporarily or permanently submerged blocks have been maintained at $\rho = 100 \text{ kg/m}^3$ ($\gamma_d = 1 \text{ kN/m}^3$). Similar design rules apply in other countries.

Submerged EPS blocks may become buoyant depending on the water level and the weight of the pavement structure on top of the blocks. The factor of safety against uplift must therefore be considered. Normally, EPS blocks are placed in a drained condition above the groundwater level. For buoyancy calculations a nominal density of $\rho = 20 \text{ kg/m}^3$ ($\gamma_d = 0.2 \text{ kN/m}^3$) should be applied if this is the material density of the EPS blocks used and the corresponding factor of safety against uplift should be $\gamma_m \geq 1.3$ based on the highest probable water level with a return period of 200 years. The factor of safety is calculated as the total weight of the fill divided by the occurring uplift force.

Since the EPS blocks may be considered as closed bodies where only minute amounts of water will enter when the blocks are suddenly submerged, the resulting buoyancy force per unit volume may be calculated as the difference between the unit density of EPS and the unit density of water, i.e.:

$$F_{\text{op}} = \gamma_{\text{EPS}} - \gamma_w = 0.2 - 9.8 = -9.6 \text{ kN/m}^3 \quad (1)$$

For the special blocks designed for reducing buoyancy forces as mentioned in Sect. 2, the buoyancy force calculation will be different.

The fill must have sufficient safety against uplift both during the construction stage and later.

In order to provide sufficient internal stability in fills on slopes, a minimum width of 2.0 m is generally required at the foot (Fig. 6). Also sufficient drainage

must be provided in order to prevent ponding of water and resulting horizontal forces, particularly on slopes. For high embankments, wind forces must also be considered, both during the construction stage and for the completed structure.

On slopes, particularly where high fills are involved, the need for proper anchorage should be analyzed separately. The anchorage should provide support for horizontal forces from vehicles hitting guard rails or side barriers and soil pressure on the structure.

When EPS is used as fill adjacent to and in contact with bridge abutments, retaining walls etc. the ratio between horizontal and vertical stress on the structure may be considered as $\sigma_h/\sigma_v = 0.1$. This implies that the ordinary fill material adjacent to the EPS fill is terminated with a stable slope so that no soil pressure is exerted on the EPS fill.

5 Construction Procedures

When the use of Geofoam blocks started, there was some concern regarding interface friction between blocks and possible block movements both during construction and later due to traffic forces. To eliminate such risks timber binders were used to bind the blocks together. The friction coefficient between adjacent blocks is, however, relatively high ($\mu = 0.7$) and it has been shown that when the fill is completed, the internal friction is sufficient to maintain a stable structure. In areas with seismic activities timber binders will, however, assist in preventing sliding of individual blocks. During construction high speed winds may create suction forces that can lift and shift individual blocks. In such cases timber binders or similar arrangement may be recommended. Gluing the blocks together is also a procedure that is known to have been applied.

EPS is a combustible material and in order to prevent fire accidents, a flame retarding agent [hexa-bromo-cyclo-dodecane (HBCDD), a brominated flame-retardant (BFR)] was for some period added to the EPS material in the production process. This practice has since been abandoned in Europe for environmental reasons as the HBCDD material is shown to accumulate in the ground, particularly near the production plants. When non-flame-retardant Geofoam blocks are used, the construction process and storage pile should be under constant surveillance on the construction site until the whole fill is covered, pavement placed on top and soil on side slopes (if relevant). When the structure is completely covered, fire hazards are eliminated.

5.1 Evenness and Tolerances

Before placing the first layer of blocks the ground surface should be prepared to form an even and level surface. A normal requirement may be that deviations in the

subsoil stratum from an even surface should be 10 mm or less measured with a 3 m straightedge. Blocks should not be placed on frozen subsoil.

When placing the EPS blocks, a continuous check should be kept to ensure that the evenness of the blocks is satisfactory in each layer. The importance of this factor increases with the height of the fill.

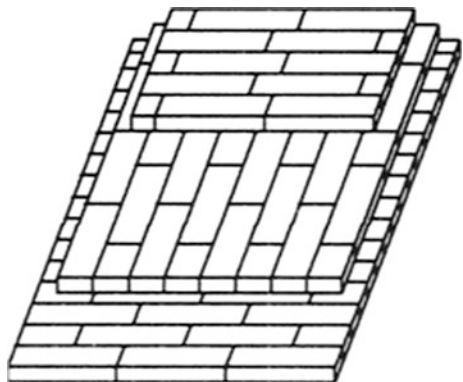
When more than one layer is applied, the EPS blocks in different layers should be placed with the longitudinal direction at right angles to each other and adjacent blocks in the same layer should be shifted about half a block length in relation to adjacent blocks in order to obtain an interlocked, stable structure and avoid continuous vertical joints running through the structure (Fig. 30). This is a very important part of the construction procedure

The different layers in an EPS fill should be parallel to the bearing courses. If the road surface is designed to have a two-way (roof type) cross fall, the EPS fill should still be placed in parallel layers. The specified cross fall may be achieved by adjusting the thickness of the pavement structure accordingly. End adjustments using EPS chips or thin boards (<10 cm thickness) should not occur.

For fills with normal side slopes of 1:1.5 or 1:2, the side slope of the EPS fill is often terminated with a side slope of 2:1. For very soft subsoils less steep side slopes may be considered in order to reduce loads on the subsoil and prevent excessive settlements. All types of fill material may be used on side slopes. The minimum thickness should be at least 0.25 m. After placing the protective membrane against the EPS side slopes, a geotextile cloth is often also added on top of the membrane before placing the soil cover.

In order to obtain a solid, homogeneous structure variations in block dimensions must be kept within certain limits. The shortest side of any block should at least be 0.5 m if not otherwise specified and the block length at least be 2.5 m. Block sides should be plane and at right angles to each other. Tolerance levels for given dimensions (length, width, height) is normally set to be within $\pm 1\%$ and block surfaces should not deviate from a plane surface with more than 5 mm measured with a 3 m straightedge. Differences in heights between adjacent blocks in the same

Fig. 30 Interlocking alignment of blocks in different layers (NPRA)



layer should not exceed 5 mm. Particular care should be taken if the blocks are delivered from different producers.

When placed in curves, small vertical gaps between blocks may occur. In such cases it is recommended to fill the gaps with LECA spheres (Light Expanded Clay Aggregate) of some other granular material.

5.2 Guard Rails

For road embankments above a certain height guard rails are normally required. For EPS fills guard rails may be anchored in the concrete slab (Fig. 31) the EPS blocks (if the slab design solution is used).

Guard rails may also be anchored by using a special arrangement (Fig. 32). If the concrete slab on top of the EPS is omitted, a similar arrangement may be used by reducing the width of the upper block layer by some 0.5 m replacing the EPS with ordinary fill materials instead.

Where EPS fills are used against bridge abutments, special concrete aprons may be installed in the transition zone between the EPS fill and bridge abutments or culverts to reduce settlement differences. The concrete apron may be 200 mm thick and 3–6 m long (in the direction of the road) cast with a high strength mix design. A joint should be provided between the apron and the concrete slab above the EPS blocks if a slab is used.

Construction of EPS fills may be performed during winter if the ground has been levelled and no frozen subsoil is present.

5.3 Quality Assurance

A producer of EPS blocks should at the latest, when a tender for delivery is opened, produce documents giving details of the quality assurance system applied in the

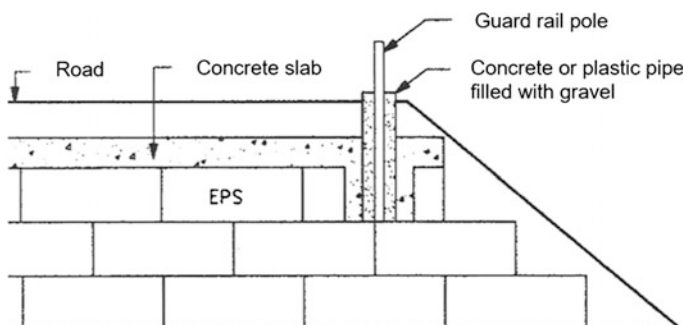


Fig. 31 Anchoring of guard rails (NPRA)

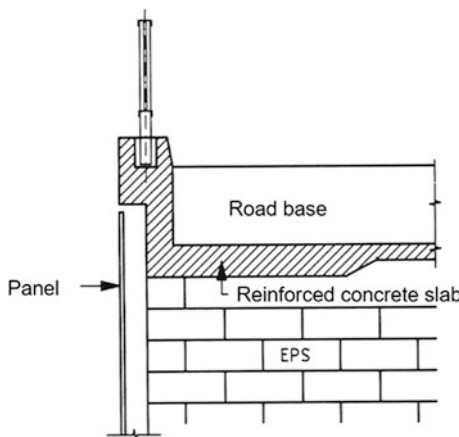


Fig. 32 Arrangement of guard rails for EPS fill with a vertical termination (NPRA)

production process. Quality certificates should be submitted for blocks delivered on site and detailed requirements for such documentation may be specified (i.e. like in EN 14933). Sampling should be performed by the authorities in charge of construction and the samples tested according to the specified quality control before the blocks are placed in the fill.

Selection of blocks for quality control should be made at random, but evenly distributed among any set of blocks. The frequency, when testing for material strength, may be as shown in Table 1. Sampling of test specimens may be performed as shown in Fig. 33. Block dimensions and evenness may be checked on one in every 25 blocks. Requirements regarding evenness and level of subsoil surface below the EPS may be checked in a cross-section profile for every 10 m of road.

For a specified EPS strength quality of $\sigma = 100$ kPa the average value for tested blocks should not be less than 100 kPa. The average value for individual blocks (minimum 6 samples) should not be less than 90 kPa and no single test result should be less than 80 kPa. This is a type of acceptance values that may be used.

Table 1 Frequency of control for compressive strength (NPRA)

Size of fill (m^3)	Number of blocks to be checked
<500	Minimum 3 blocks
500–1000	Minimum 5 blocks
>1000	Minimum 5 blocks pr. $1000 m^3$

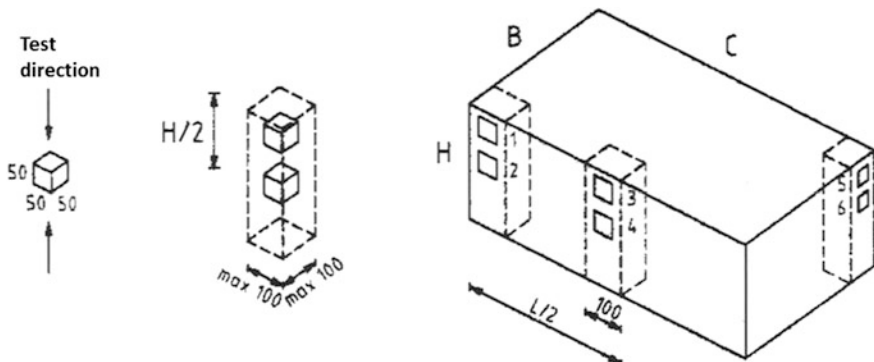


Fig. 33 Possible sample pattern for testing material strength (dimensions in mm) (NPRA)

6 Monitoring Programmes

Expanded polystyrene is a very stable compound chemically and no material decay should be expected when placed in the ground and protected according to the present design guidelines. Still, since the first road insulation project with EPS was performed in Norway in 1965 and the first EPS lightweight embankment was constructed in 1972, EPS embankments have been monitored for long term performance [29] along the lines followed for other lightweight fill materials used in road constructions. The monitoring programme has over a period of some 46 years focused on the following material properties:

- Material behaviour
 - Compressive strength
 - Water absorption
 - Decay
- Deformation
 - Total embankment deformation and deformation in EPS layers
 - Creep effects
- Stress distribution
- Reduced lateral pressure
- Bearing capacity.

Also laboratory and full scale tests have been performed related to stress distribution and deformations in the EPS material.

Measured values show that the material strength is maintained during the observation period and even a slight increase in strength has been indicated.

Observations of unit density furthermore show that the design unit weight of $\gamma_d = 0.5 \text{ kN/m}^3$ is not exceeded for embankments with EPS material placed above

the groundwater table. The corresponding water content is measured to below 1% by volume and no change is observed with time.

In blocks, which are periodically submerged, water contents of up to 4% by volume have been measured. In permanently submerged blocks measured water contents have reached values close to 10% by volume with some increase over the years. Further increases above 10% by volume are, however, not to be expected. For submerged fills the average density is therefore of the order of $\rho = 90\text{--}95 \text{ kg/m}^3$ after some 20 years in the ground. The water content decreases rapidly in blocks above the water table and show values for drained conditions only some 200 mm above the highest water level.

As expected excavated blocks from permanent and temporary structures show no visual sign of decay. Furthermore no indication of insect attacks have been observed and the EPS material has no nutritional value for either insects or animals. Rodents have, however, in one case been observed to have excavated their own small den for housing purposes. This had, however, not impaired the function of the EPS fill.

In EPS fills subjected to normal loads (weight of concrete slab and bearing course layers) deformations of the order of 1% of the fill height have been observed after the load has been applied. Even in fills supporting higher loads as shown in Figs. 16 and 17, deformations of the same order and with minute creep effects over time have been observed. Deformations and creep effects vary, however, somewhat for the different block layer.

Summing up, the overall results form the monitoring programme indicate that the EPS material behaves as expected and that the selected design parameters provide stable and satisfactory structures for long time performance [29].

Similar monitoring and research programmes performed in other countries show results along the same lines.

7 Failures

Of the several EPS projects now completed in many parts of the world, only a few known failures have been reported. Two failures are associated with water fluctuations and buoyancy forces. The other three are caused by fires.

On the 16th of October 1987 Northern Europe experienced exceptionally strong storms with high wind velocities and high rainfall intensities. Norway was also exposed to major floods, and in the Oslo area the first EPS fill built in 1972 floated off as did an adjacent section of motorway constructed some years later. What was wrong? Had the dangers of buoyancy forces not been considered? Yes, such calculations had been performed, but the highest possible flood level predicted at the design stage in 1972 was 0.85 m lower than the flood level that occurred in October 1987. It was therefore rainfall and flood level predictions in 1972 that were misleading.

Also the second failure reported from Thailand involved an unexpected high water level causing a completed road fill to be washed away. It should therefore be duly noted that the dangers of buoyancy forces should be carefully studied when considering the design of an EPS fill. Often soft subsoils are located in lowland areas subjected to flooding. In such cases accurate predictions of the highest possible water level are essential to obtain a safe and lasting road structure.

An incident is also reported from Crayford near London, England in 2016 where 16 cars were damaged in an underground carport when a 24-in. pipe burst and flooded the carport. The EPS boards used under the parking level in this case, became buoyant and the car roofs crashed against the ceiling of the carport. The flooding was of course very unfortunate and unexpected.

Ordinary polystyrene is a combustible material and will burn when set on fire. For this reason some precautions should be taken when constructing EPS fills using normal quality material as described in Sect. 5. Such precautions may include fencing in any stockpiles at the construction site and provide guards round the clock, or place the blocks directly in the fill when they arrive on site, working round the clock if necessary. However, once the EPS is covered by the pavement material on top, and soil on the slopes, there will not be sufficient oxygen available to sustain a fire.

Two failures due to fires have occurred in Norway, and both were caused by welding activities on bridge abutments adjacent to EPS fills during the construction phase. In the first case 1500 m³ of EPS were transformed into black smoke in a matter of some 10 min. The concrete bridge abutment was also damaged due to the heat developed with concrete spalling from the reinforcing bars (Fig. 34). Since the fire was initiated by sparks from welding activities on the bridge, the contractor responsible for the welding had both to repair the bridge abutment and replace the EPS fill at his own expense. A similar incident occurred in 1995 and again the repair costs had to be covered by the contractor responsible for the welding activities. The fire potential should therefore not be overlooked.

8 Reuse of EPS

When the first EPS fill in Norway at Flom bridge floated up in 1987 as described in Sect. 7, there was at the same time an incident in downtown Oslo where a sheet pile wall, for a deep excavation next to a road off ramp, was on the verge of collapsing. This required a rapid temporary removal of the off ramp, but since the ramp served a busy traffic intersection, it also needed to be quickly repaired. At the time in question block manufacturer could not supply new blocks as quickly as required. Instead the blocks that was removed from the Flom bridge area, was reused to quickly repair the off ramp in downtown Oslo.

In 2006 two embankments on Euroroad 6 in the southern part of Norway (Løkkeberg Bridge Fig. 16 and Hjelmungen Bridge Fig. 17) was removed partly due to widening but also due to changes in the alignment of E6. These blocks were



Fig. 34 Bridge abutment damaged by EPS blocks put on fire (NPRA)

also examined and checked as part of the monitoring programme and it was decided to reuse more than 5000 m^3 EPS blocks (Fig. 35) on other EPS embankments connected to the E6 project. Some 17 years after the blocks were first placed, test data show results well above that of a normal EPS quality (average value of $\sigma = 104.6 \text{ kPa}$ for $\rho = 20 \text{ kg/m}^3$ material).

The Carousel Shopping Mall in Syracuse NY was constructed in 1989 using $28,000 \text{ m}^3$ of EPS geofoam blocks to control perimeter settlements of a large mat foundation. After four years of service expansion of the mall was required and geofoam blocks along 100 m of the foundation wall were removed. All of the

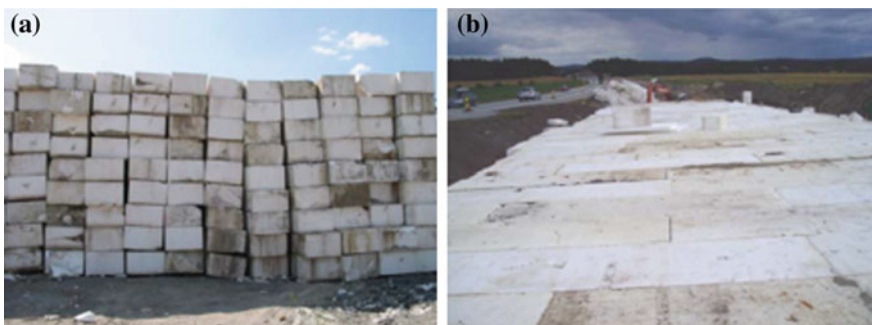


Fig. 35 **a** Stockpile of EPS from Løkkeberg Bridge. **b** Reuse of EPS blocks from Løkkeberg Bridge (NPRA)

exhumed blocks, except ones damaged in the process of recovery, were in good condition and were reused for the expansion construction. The performance of the reused EPS blocks has been satisfactory over more than 20 years.

The major volume of EPS material worldwide is produced for packaging and insulating purposes and this has to some extent become an environmental problem since packaging use is only temporary with a large volume of discarded material accumulating. To counter this effect collecting systems have been established in many countries and the manufacturers are now adding some amount of discarded EPS material into the production of new Geofoam blocks. With a recycling content of some 20% at present this may cause some greater variation in material quality of the finished product.

9 Conclusions

All knowledge gained from research activities involving both lab tests and full scale monitoring programmes as well as experiences from construction activities, confirm that the use of Geofoam blocks in civil engineering projects may provide satisfactory solutions. Whether Geofoam blocks are to be considered favourable on a certain project, will depend on many factors like local technical conditions, economy and construction time allowed. With the number of new countries adopting the method and with the increasing number of projects being completed, it will not come as a surprise if such use of Geofoam blocks will escalate further. New application forms may also well be introduced increasing the use even further.

So stick to the motto:

Be bright,
think light and
do it right.

References

1. Alfheim S, Flaate K, Refsdal, G et al (2011) The first EPS geoblock road embankment—1972. Paper presented at the 4th international conference on geofoam blocks in construction applications—EPS 2011, Lillestrøm, Norway, 6–8 June 2011
2. Norwegian Road Research Laboratory (NRRL) (1987) Plastic Foam in Road Embankments, Meddelelse nr. 61, Oslo
3. EPS Development Organization (EDO) (1996) Proceedings of international symposium on EPS construction method, Tokyo
4. Proceedings of the 3rd International Conference on Geofoam (2001), Salt Lake City, USA, 10–12 Dec 2001
5. Proceedings of the 4th International Conference on Geofoam blocks in Construction Applications—EPS 2011, Lillestrøm, Norway, 6–8 June 2011

6. Özer AT, Danyıldız E, Akinay E et al (2017) Using geofoam blocks to construct roadway embankments over buried utility corridors: a case study. Paper presented at 7th national geosynthetics conference G7 2017, İstanbul, Turkey, 11–12 May 2017 (In Turkish)
7. Özer AT, Akinay E (2017) Short term performance evaluation of geofoam block embankment using field instrumentations. In: 7th geotechnics symposium, İstanbul, Turkey, 22–24 November
8. Beinbrech G, Hillmann R (1997) EPS in road construction—current situation in Germany. *Geotext Geomembr* 15(1–3):39–57
9. Norwegian Road Research Laboratory (NRRL) (1992) Use of expanded polystyrene in road embankments—design, construction and quality assurance. Public Roads Administration, Oslo, Norway
10. Stark TD, Arellano D, Horvath JS et al (2004) Guideline and recommended standard for geofoam applications in highway embankments. NCHRP Report 529, Transportation Research Board, Washington, D.C
11. Duškov M, Nijhuis E (2011) Lightweight road embankments for the crossover of the N207 over the railway Alphen A/D Rijn-Gouda. Paper presented at the 4th international conference on geofoam blocks in construction applications, Lillestrøm, Norway, 6–8 June 2011
12. Farnsworth CB, Bartlett SF, Negussey D, Stuedlein AW (2008) Rapid construction and settlement behavior of embankment systems on soft foundation soil. *J Geotech Geoenviron* 134(3):289–301
13. Herle V (2011) Design and monitoring of EPS embankment on D1 near Ivanovice in the Czech Republic. Paper presented at the 4th international conference on geofoam blocks in construction applications, Lillestrøm, Norway, 6–8 June 2011
14. Kubota T (2011) Case history of EDO-EPS method in Japan. Paper presented at the 4th international conference on geofoam blocks in construction applications, Lillestrøm, Norway, 6–8 June 2011
15. Papacharalampous G, Sotiropoulos E (2011) First time application of expanded polystyrene in highway projects in Greece. Paper presented at the 4th international conference on geofoam blocks in construction applications, Lillestrøm, Norway, 6–8 June 2011
16. Spasojević S, Mitrović P, Vučanić V et al (2011) The application of EPS in geotechnical practice: a case study from Serbia. Paper presented at the 4th international conference on geofoam blocks in construction applications, Lillestrøm, Norway, 6–8 June 2011
17. Youwai S, Kongkitkul W, Sripobink T et al (2011) Application of EPS for remedial work of bridge bearing unit on Bangkok Soft Clay: A case study. Paper presented at the 4th international conference on geofoam blocks in construction applications, Lillestrøm, Norway, 6–8 June 2011
18. O'Brian AS (2001) Design and construction of the UK's first polystyrene embankment for railway use. Paper presented at the 3rd international conference on geofoam blocks in construction applications, Salt Lake City, USA, 10–12 December 2001
19. Neupane R (2015) Expanded polystyrene geofoam embankment for support of railways and bridges. Ph.D Dissertation, University of Utah, SLC, UT, USA
20. Kawashima Y, Atsushi, N, Kawagishi Y et al (2001) Construction of high eps embankment in heavy snowfall region. Paper presented at the 3rd international conference on EPS geofoam blocks in construction applications, Salt Lake City, USA, 10–12 Dec 2001
21. Aunaas K (2011) Recent impressions from EPS projects in Japan. Paper presented at the 4th international conference on EPS geofoam blocks in construction applications—EPS 2011, Lillestrøm, Norway, 6–8 June 2011
22. Özer AT (2016) Laboratory study on the use of EPS-block geofoam for embankment widening. *Geosynth Int* 23(2):71–85
23. Akay O, Özer AT, Fox GA et al (2013) Behavior of sandy slopes remediated by EPS-block geofoam under seepage flow. *Geotext Geomembr* 37:81–98
24. Özer AT, Akay O, Fox GA et al (2014) A new method for remediation of sandy slopes susceptible to seepage flow using EPS-block geofoam. *Geotext Geomembr* 42(2):166–180
25. Akay O, Özer AT, Fox GA (2014) Assessment of EPS block geofoam with internal drainage for sandy slopes subjected to seepage flow. *Geosynth Int* 21(6):364–376

26. Akay O (2016) Slope stabilisation using EPS block geofoam with internal drainage system. *Geosynth Int* 23(1):9–22
27. EPS Industry Alliance. Expanded polystyrene (EPS) geofoam applications and technical data. Crofton, MD, USA
28. Shinntani M (2011) Embankment constructions applying buoyancy-resistant EDO-EPS blocks. Paper presented at the 4th international conference on EPS geofoam blocks in construction applications—EPS 2011, Lillestrøm, Norway, 6–8 June 2011
29. Aabøe R, Frydenlund TE (2011) 40 years of experience with the use of EPS geofoam blocks in road construction. Paper presented at the 4th international conference on geofoam blocks in construction applications, Lillestrøm, Norway, 6–8 June 2011
30. Stuedlein A, Negussey D (2013) Use of EPS geofoam for support of a bridge. Paper presented at geo-congress 2013: Honoring Robert D. Holtz II, sound geotechnical research to practice, San Diego, California, USA, 3–7 Mar 2013
31. Vaslestad J, Murad SS, Johansen TH et al (2011) Load reduction and arching on buried rigid culverts using EPS. Paper presented at the 4th international conference on EPS geofoam blocks in construction applications, Lillestrøm, Norway, 6–8 June 2011
32. Zarnani S, Bathurst RJ (2008) Numerical modeling of EPS seismic buffer shaking table test. *Geotext Geomembr* 26:371–383
33. Ertugrul OL, Trandafir AC (2011) Reduction of lateral earth forces acting on rigid nonyielding retaining walls by EPS geofoam inclusions. *J Mater Civil Eng* 23(12):1711–1718
34. Athanopoulos-Zekkos A, Lamonte K, Athanopoulos GA (2012) Use of EPS compressible inclusions for reducing the earthquake effects on yielding earth retaining structures. *Soil Dyn Earthq Eng* 41:59–71
35. AbdelSalam SS, Azzam SA (2016) Reduction of lateral pressures on retaining walls using geofoam inclusion. *Geosynth Int* 23(6):395–407
36. Aabøe R (1985) 13 years of experience with expanded polystyrene as a lightweight fill material in road embankments. Paper presented at the 1st international conference on EPS geofoam blocks in construction applications, Oslo, Norway, 22 June 1985
37. Konno H, Nakono O, Kishi N et al (2001) A practical design method of three-layered absorbing system. Paper presented at the 3rd international conference on EPS geofoam blocks in construction applications, Salt Lake City, USA, 10–12 Dec 2001
38. Tsukamoto H (2011) History of R&D and design code for EDO-EPS method in Japan. Paper presented at the 4th international conference on EPS geofoam blocks in construction applications, Lillestrøm, Norway, 6–8 June 2011
39. Bartlett SF, Lawton EC (2008) Evaluating the seismic stability and performance of freestanding geofoam embankment. Paper presented at the 6th National Seismic conference on Bridges, Charleston, South Carolina, USA
40. O'Brien AS (2001) Design and construction of the UK's first polystyrene embankment for railway use. Paper presented at the 3rd international conference on EPS geofoam blocks in construction applications, Salt Lake City, USA, 9–11 Dec 2001
41. Mann G, Stark TD (2007) Slope stabilization using geofoam. Paper presented at the proceedings of Geo-Denver 2007: New Peaks in Geotechnics, GSP 161 Embankments, Dams, and Slopes, ASCE, 18–21 Feb 2007
42. Tsukamoto H (1996) Slope stabilization by the EPS method and its applications. Paper presented at the international symposium on EPS construction method (EPS Tokyo '96), EPS construction method development organization, Tokyo, Japan, pp 362–380
43. Reuter G, Rutz J (2000) A lightweight solution for landslide stabilization. *Geotech Fabr Rep* 18(7):42–43
44. Reuter GR (2001). Use of geofoam for landslide stabilization-CTH "A", Bayfield County, Wisconsin. Paper presented at the 3rd international conference on geofoam blocks in construction applications, Salt Lake City, USA, 10–12 Dec 2001
45. Arellano D, Stark TD, Horvath JS et al (2011) Guidelines for geofoam applications in slope stability projects: final report. NCHRP Project No. 24-11(02), Transportation Research Board, Washington, D.C., USA

46. Akay O, Özer AT, Fox GA (2012) Experimental investigation of failure mechanism of expanded polystyrene block geofoam slope system under seepage. Paper presented at the 5 European geosynthetics congress, EuroGeo5, 16–19 of September, Valencia, Spain
47. Amini ZA (2014) Dynamic characteristics and seismic stability of expanded polystyrene geofoam embankments. Ph.D. Dissertation. University of Utah, Salt Lake City, Utah
48. Barrett JC, Valsangkar AJ (2009) Effectiveness of connectors in geofoam block construction. Geotext Geomembr 27(3):211–216
49. Özer AT, Akay O (2016) Interface shear strength characteristics of interlocked EPS-block geofoam. J Mater Civil Eng 28(4). [https://doi.org/10.1061/\(ASCE\)MT.1943-5533.0001418](https://doi.org/10.1061/(ASCE)MT.1943-5533.0001418)
50. Mandal JN (2017) Geosynthetics engineering: in theory and practice. Research Publishing Services, Singapore, p 1352
51. Padade AH, Mandal JN (2014) Expanded polystyrene-based geomaterial with fly ash. Int J Geomechanics ASCE 14(6):06014013
52. Tepper H (2011) EU product standard for eps and performance requirements. Paper presented at the 4th international conference on EPS geofoam blocks in construction applications, Lillestrøm, Norway, 6–8 June 2011

Part II

Construction Applications

Dutch A4all Tramway EPS Embankment with Vertical Sides



Milan Duškov and Johan de Jongh

Abstract New section of the motorway A4 in the urban area between Vlaardingen and Schiedam is constructed in a concrete tunnel realized on ground level and covered by soil for a minimal environment impact. This new A4 route crossed the existing tram tracks. The construction of the tunnel with belonging embankments resulted in a 6 m high position of the tramway overpass. Despite low bearing capacity of the local subsoil the strict settlement requirements were valid for the ≥ 180 m long embankments on both sides of the motorway tunnel. Additionally complicating aspect was the realization period of only twelve weeks. Also the inconvenience to local residents living in surrounding large apartment buildings had to be minimized. Therefore, almost entire embankment length has been realized using 22,000 m³ EPS geofoam blocks. Applied embankment cross section design with vertical sides without slopes made it possible to realise the cross sections in two phases. Firstly, the northern cross section half with a pavement structure at the top was completed. Otherwise the original tram line could not stay in service during time of construction and the deadline of twelve weeks could not be met. These twelve weeks were necessary to complete the embankment cross section with the southern half. The new tram tracks are assembled at the top of it. The applied design approach for a phased realization of the 20 m wide lightweight embankment cross section is unique for Dutch engineering practice.

Keywords Lightweight geofoam fill · EPS embankment with vertical sides
Tramway embankment

M. Duškov (✉)
InfraDelft, Delft, The Netherlands
e-mail: milan.duskov@infradelft.nl

J. de Jongh
Heijmans, Rosmalen, The Netherlands

1 Introduction

In the urban area between Vlaardingen and Schiedam (nearby Rotterdam) a new section of the motorway A4 was built in a concrete tunnel realized on a ground level and covered by soil. This costly approach was chosen in order to minimize environmental impact of the motorway. Consequently, a new tramway overpass became necessary since a level crossing was not possible any more. The construction of the land tunnel with belonging embankments resulted in a 6 m high position of the tramway overpass. Due to this altitude difference, a total of 400 m long combined tramway and road embankments were built on either side of the land tunnel. Those embankment lengths were necessary in order to raise the level of the tramway to the correct grade. In the terms of bearing capacity the embankments had to provide adequate support not only for the layers of base and surface courses that make up the tramway but also for a pavement structure suitable for heavy freight traffic in the event of a disaster. The pavement structure belongs to the road parallel to the tramway path usually in serve as a cycle path.

Despite the on-site thick compressible soil layers and the lack of preloading for proper consolidation, only negligible settlements of the new tramway track were acceptable. The strict set-up requirements represented a drastic limitation of design freedom. This actually required a settlement-free and maintenance-free solution scenario. In addition, the cost aspects obviously weighed heavily, and the tram line, excluding the 12-week out of service summer schedule, had to continue to function normally. The commissioner also demanded to minimize the inconvenience caused by construction activities for the inhabitants of the neighbouring apartment buildings. The tram line embankments cross the urban area with high buildings located right next to the route. These complex boundary conditions dictated the application of the ingenious design methodology and a proper realization approach for the new tramway track embankments.

2 Situation Description Including Subsoil Profile

In order to gain a complete insight into the local soil profiles, cone penetration tests and drillings have taken place along the A4 route including the intersection site. An approximately 10 m thick compressible package of peat and clay layers with the underlying Pleistocene sand was found along the tramway route. In view of a total length of approximately 400 m of the designed lightweight embankments, for each representative cross section the nearest CPT results are implemented in their Plaxis models. No preloading sand fill was placed to accelerate primary consolidation on both sides of the motorway tunnel.

The original tramway track was almost at ground level between NAP -1.3 m and NAP +1.6 m. NAP is Dutch abbreviation for average sea level. The tramway viaduct at the site of the land tunnel reached the level at NAP +5.4 m and that

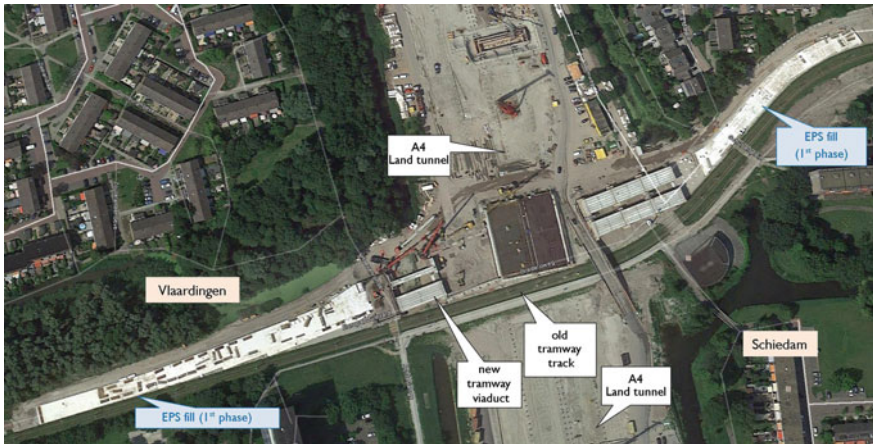


Fig. 1 View from above of the lightweight EPS fills under construction of the intersection of the tramway and the A4 route

height difference had to be bridged with adequate embankments without causing significant settlements. The slope of the tram track has an angle of 3.1% (=1: 32.5) on both sides. As a result, the ramps are relatively long, about 175 m in the Schiedam area and about 230 m on the western side. How the route is adjusted along the existing tramway can be seen in Fig. 1. At that stage the old tramway is still in service despite the parallel located EPS fills belonging to the cycle path.

The consequence of creating a space for the parallel cycle path was the width doubling of both the embankments and the tramway viaducts. Even by means of using the EPS-geofoam blocks it was impossible to realize 20 m wide, up to 6 high and 400 m long embankments during only 12 weeks. The solution was found to prolong the time in service of the old tramway by constructing first 50% of the embankment cross section under the cycle path without slopes. Due to the proper design which included vertical sides instead of slopes the original tram track could stay in service and the construction of the parallel lightweight embankment could be continued without problems.

3 Cross Sections of Lightweight Embankments

Figure 2 illustrates schematically the whole cross section of the lightweight embankment west of the motorway A4. As shown in Fig. 2, the EPS package has vertical sides. As mentioned above firstly the cross section part under the cycle path was realized. The pavement structure of the cycle path is designed for heavy trucks to be used in case of calamities. It means that the cycle path does not differ from a normal road structure in terms of bearing capacity. A cement-bonded layer at the

top of EPS ensures both adequate load distribution under traffic loads and vertical support during compaction of higher unbound road base layers in the construction phase. In addition, according to the instructions given by the client, (green) steep walls are drawn for esthetical reasons, but those provide no horizontal support to the EPS embankment.

Convincing the authorities involved (the Rotterdamse Elektrische Tram—RET is the main public transport operator in Rotterdam, the municipalities of Schiedam and Vlaardingen and Dutch Rijkswaterstaat—RWS) that relatively heavy trams with associated axle loads can drive approximately 6 m above ground on top of the EPS fills with an elastic modulus of ≤ 10 MPa, required extensive model analysis. In addition, the sides of the phased realized embankments are virtually vertical. In this scope, *inter alia*, parameter analyzes were made with interface elements to investigate the friction between the EPS blocks/sublayers and to ensure adequate tolerances. All kinds of sometimes far-reaching scenarios have been elaborated with regard to possible load patterns, subsoil behaviour and covering side constructions. Also detailed solutions for rainwater drainage, cables, masts foundations and transition structures required attention. The project license has only been granted on the basis of detailed explanations.

The advanced Soft Soil Creep and Hardening-Soil models were applied for the Plaxis calculations. The iterative approach involved the use of step-by-step changes in the models per selected scenario which was influenced by interaction with the client. All representative cross profiles were modeled were only after the iteration process resulted in a high degree of certainty about the contours of the design solution. The resulting settlements are illustrated in Fig. 3.

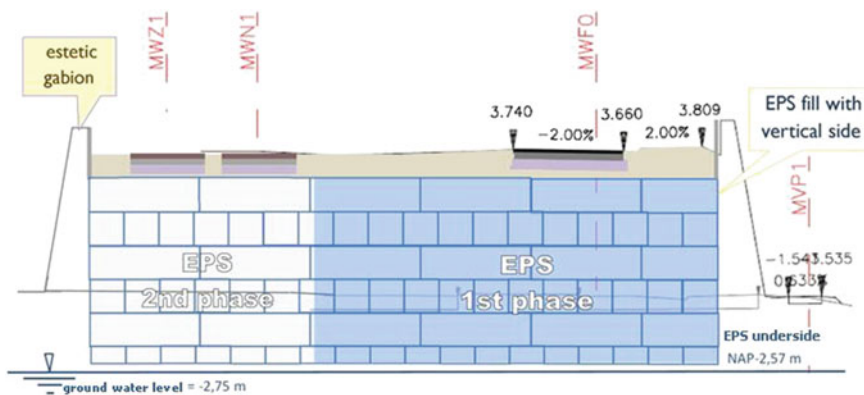


Fig. 2 Characteristic cross section of the lightweight embankment including the tram track west of the A4 land tunnel with schematically indicated EPS package

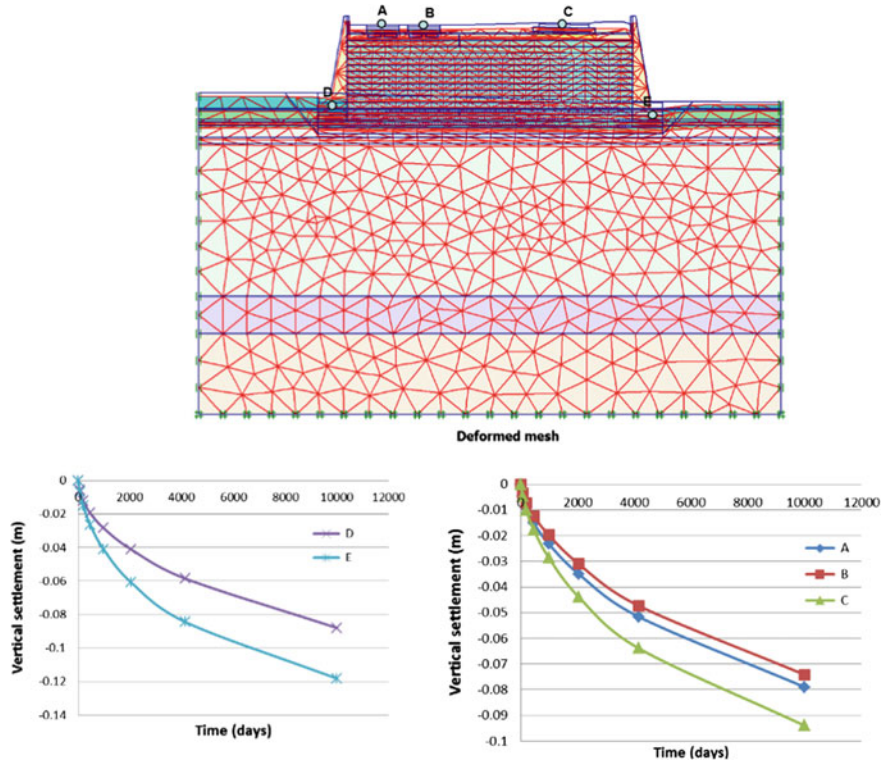


Fig. 3 Deformed Plaxis model of a cross section of the A4-tramway embankment with a relatively thick upper structure on top of a 20 m wide and 6.5 m thick EPS fill with vertical sides and Plaxis results for the settlements

4 Realization

Regarding minimization of the impact of contraction works for the residents, it was a proper choice to implement largely the lightweight EPS fills. The manual stacking of EPS blocks is completely silent and the mechanical supply only causes usual traffic noise. As part of reducing the total load on compressive soil layers, the top soil layer is excavated without further influence on the local situation. The upper ground layer has been replaced by the lightweight embankments without significant additional load on the subsoil. Therefore the settlements in the adjacent area were by definition excluded. In other words, despite the compressible subsoil, the chosen design methodology excluded any significant impact on the neighboring objects. The adjacent old tram track on the ground level could thus remain in service until the last moment. As a result, it was possible to autonomously realize one half of the embankment cross section for the cycle path/road road construction.



Fig. 4 The first autonomously completed embankments cross section part for the bicycle cycle path/road construction over the future motorway A4

Regarding the completion of the tramway embankment part, the RET deadline period of 12 weeks has been strictly taken into account. The construction time with the EPS geofoam blocks actually depends on the delivery logistics. As mentioned before, this construction time was additionally shortened by first realizing the entire cycle path embankment cross section part as illustrated in Fig. 4.

From the aesthetic point of view, decorative gabions are placed along the vertical sides without supporting the EPS fills of other constructive contribution. That was a choice of involved architects and made only more complicated for the designers. “The eye also wants something” is understandable credo, but this choice did lead to undesirable additional line load on the subsoil along the embankments. Technically, EPS geofoam sides could be covered much cheaper and without significant additional loading. Longer than half a year there was only a membrane cover over the sides as shown in Figs. 5 and 6.

5 Extra Benefits Due to Applied Design Methodology

In case of the EPS embankments their slopes are functionally not necessary. Thanks to sufficient friction between EPS-blocks combined with low Poisson’s ratio of this material enough stability of properly designed lightweight embankments with vertical sides is guaranteed. Such a design implicated following additional advantages over traditional embankments with slopes: lower construction costs (by the use of less EPS geofoam and less ground area), less space needed, phased construction and shorter construction time, no settlement directly along the EPS fills and no additional load on the underground infrastructure directly along the route. However, this new design solution requires specific expertise.

The cause oriented design methodology was aimed at excluding/preventing additional loading on compressible subsoil layers after completion of the tramway



Fig. 5 The two-stage realization for the cycle path/calamity road on one side and the tramway over the A4 on the other



Fig. 6 The EPS fill (covered temporarily only with a membrane) with virtually vertical sides



Fig. 7 Evaluation photos prove that no settlement differences have occurred after four year in service of the lightweight embankments with the tramway tracks and the cycle path/calamity road construction

embankments. By avoiding triggering the consolidation process, the maintenance in the future are practically marginalized. A visual inspection of the project site confirms that lightweight embankments built-up with EPS blocks, if properly designed and realized, are virtually maintenance-free. No settlements differences are noticeable at the connection points more than three year after the opening of the tramway embankments as shown in Fig. 7.

Geofoam Eps Used in Bridge Abutment, E18 Farris Bridge



Jan Vaslestad, Jørn Einar Liveroed, Tseday Damtew, Staale Singstad
and Dag Loevstad

Abstract Norwegian Public Roads Administration is building Farris Bridge on European road 18 in Larvik. The total length of the Farris Bridge is 570 m. EPS Geofoam is used in the bridge abutments. Ordinary stone embankments as bridge abutments would have created large settlements. Use of EPS Geofoam is also a very economical alternative compared to a piled embankment inside the abutment. The total volume of EPS in the bridge abutments is 11,000 m³, with 4000 m³ in abutment east and 7000 m³ in abutment west. The quality of EPS used is mainly with strength 180 kPa. In some highly stressed zones of the embankments, the strength of EPS is 300 kPa. Result of testing for quality control is included in the article.

Keywords EPS embankment · EPS abutment · Farris bridge · EPS abutments

1 Introduction

The southern regional road department of Norwegian Public Roads Administration (NPRA) has been constructing a bridge over a lake called Farrisvannet in Larvik. The bridge, called Farris Bridge, extends over a span of 570 m including via ducts at the west and east side of the bridge (Fig. 1).

2 EPS Geofoam Blocks in the Project

The abutment at the east side of the bridge was to be founded on a soft clay soil deposit with a low bearing capacity. The project evaluated different mitigations to alleviate the bearing capacity problem of the underlying soil. Among others,

J. Vaslestad (✉) · J. E. Liveroed · T. Damtew · S. Singstad · D. Loevstad
Norwegian Public Roads Adminstration, Oslo, Norway
e-mail: jan.vaslestad@vegesen.no



Fig. 1 Overview of Farris bridge

foundation on piles were considered, but the use of EPS geofoam was favored because it was found to be the most cost effective geotechnical solution for the project [1]. EPS geofoam blocks were therefore used to make up the filling inside the abutment.

EPS geofoam was also used in the road embankment just behind the abutment for the same reason of low bearing capacity of the underlying soil and to secure a smooth transition between the road embankment and the bridge.

The abutment at the west side was also constructed with the use of EPS geofoam to reduce settlement, to reduce lateral pressure on the wing walls and to satisfy esthetic requirements. If crushed stone were to be used as a filling, it would have resulted in large settlements and heavy wing walls.

The total volume of geofoam used in the east and west abutments of the Farris Bridge is approximately 11,000 m³. The east side abutment had 3300 m³ geofoam filling and the west side had 7700 m³ (Fig. 2).

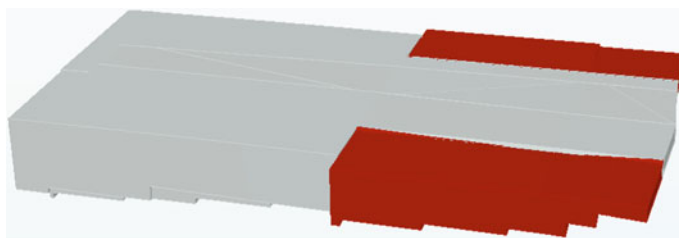


Fig. 2 Typical 3D-model of EPS geofoam filling at the west abutment. The red part is EPS blocks with compressive strength 300 kN/m² and the grey part is EPS blocks with compressive strength 180 kN/m²

3 Construction of the Geofoam Filling

The geofoam blocks that have been used in the project were delivered as full size blocks. The contractor at the project had little experience with the use of geofoam blocks and hence ordered these large blocks instead of the usual block size ($2420 \times 1220 \times 500$ mm) as suggested on NPRA's guidelines [4]. The large blocks were heavy for hand lifting and two to three people were needed to place them in place even with the use of lifts. This resulted in longer installation time (Fig. 3).

Later, the contractor ordered the usual standard size EPS geofoam blocks for the last few deliveries.

EPS geofoam blocks with compressive strength of 180 kN/m^2 at 5% deformation constituted large part of the filling. Blocks with higher strength were also used at selected sections and these had a strength of 300 kN/m^2 at 5% deformation.

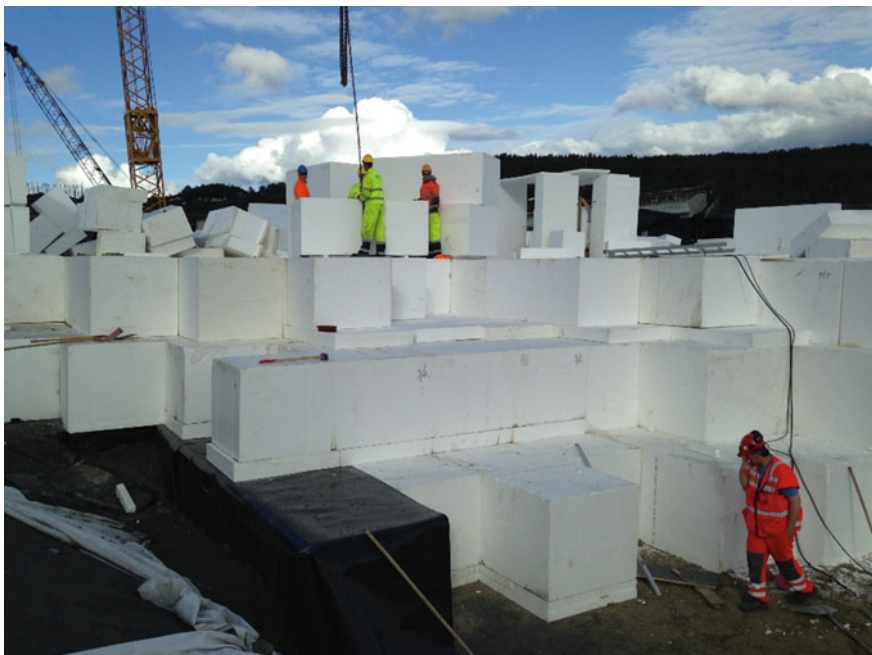


Fig. 3 Placing the EPS geofoam blocks at the construction site

4 Challenges at Construction Site

4.1 Fitting the EPS Geofoam Fill

Crossfall for the bridge is 7.5% and hence presented a challenge in placing the geofoam blocks to fulfill the crossfall requirement. The requirement was met by leveling of the roadbed. The subgrade had to be shaped with 7.5% inclination. This has resulted in extensive follow up during construction of the EPS geofoam filling during fitting the blocks at the boundary with the wing walls and at the foundation level. Fitting the EPS geofoam blocks against the wing walls took the major part of the construction period for the EPS filling (Fig. 4).

4.2 EPS Geofoam and Surface Water

Another challenge during construction was how to handle surface water at the construction site. The client has experienced an uplift of the EPS filling at the west side during the construction period. In order to mitigate the problem, temporary drainage systems were installed. The drainage system helped to get rid of the surface water away from the EPS filling. The client decided to keep the drainage system until the EPS filling was surcharged by the approach slab of the bridge. Potential buoyancy was designed according to NPRA guidelines [2].



Fig. 4 Crossfall of 7.5% for the roadbed and storage of geofoam blocks at the construction site



Fig. 5 Cutting the EPS geofoam blocks with hot wire apparatus at the construction site

4.3 *Sizing of the EPS Geofoam Blocks*

Under placement of the geofoam blocks, adjustment to their size was done by the use of hot wire. The method was easy to perform at the construction site and resulted in clean cuts of the blocks. Usage of hot wire also minimized the waste material which would have been spread and difficult to contain at the construction site and hence little environmental impact for the surrounding area (Fig. 5).

At the end of the EPS filling of the abutment, the filling was constructed such that it will be easy to continue with a new EPS filling of the road embankment behind the bridge abutment (Fig. 6).

5 Delivery Control

The client of the project, NPRA, has performed delivery control at the construction site. The delivery control includes follow up of proper labelling and spot tests of the EPS geofoam blocks.

EPS geofoam blocks delivered at the start of the project did not have proper labelling and lacked labels such as block number, production date and strength and deformation values. The contractor later ratified the lack of labelling at the request of the client. Due to the lack of labelling of the production date of the blocks, the contractor agreed that the delivered blocks had been stored for 10 days before installation.



Fig. 6 EPS filling at the end part of the abutment filling—ready to be connected to the next EPS filling

Spot test were performed on samples collected at the construction site [3]. The spot tests were done at the NPRA's laboratory and the large size of the blocks presented some challenges with respect to cutting out test samples at the laboratory.

The Figs. 7 and 8 present samples of summary of spot tests. The results were inside the allowable range even if some of the results were close to required lowest values.

Abutment axis 10					
Sample No.	Compressive Strength	Block No.	Average Singel block Required > 90%	Lowest singel test Required > 80%	
2130252-070	171,10	116	171	158,50	
2130252-071	188,40	126	188	176,20	
2130252-074	177,80	862	178	172,90	
2130252-075	172,50	861	173	163,80	
2130252-076	194,90	838	195	187,80	
2130252-077	168,90	763	169	158,90	
2130252-078	170,30	764	170	158,90	
labprøve1	194,00	1	194	182,00	
labprøve2	188,20	331	188	189,00	
labprøv	189,50	292	190	176,00	
Average Strength (kN/m ²)		181,56			
Required Strength (kN/m ²)		180	-	162	144

Fig. 7 Spot test results of EPS 180 blocks used in the abutment at the west side

Abutment axis 10					
Sample No.	Compressive Strength	Block No.	Average Singel block Required > 90%	Lowest singel test Required > 80%	
2130252-079	302,80	252	303	276,30	
2130252-080	268,50	251	269	256,50	
2130252-081	319,30		319	312,60	
2130252-082	305,90		306	299,10	
2130252-083	303,30	196739	303	299,30	
labprøve	317,50		318	312,00	
labprøve	322,30		322	315,00	
Average Strength (kN/m ²)	305,66				
Required Strength (kN/m ²)	300	-	270	240	

Fig. 8 Spot test results of EPS 300 blocks used in the abutment at the west side

References

1. Aabøe R (2011) 40 years of experience with the use of EPS geofoam blocks in road construction. Paper presented at the 4th international conference on geofoam blocks in construction applications, Lillestrøm, Norway, 6–8 June 2011
2. Statens vegvesen (2005) Vegbygging, Handbok N200, Vegdirektoratet, Oslo 2005. <http://www.vegvesen.no/Fag/Publikasjoner/Handboker>
3. Statens vegvesen (2014) Vegdirektoratet Handbok V220, Geoteknikk i vegbygging, 2014. <http://www.vegvesen.no/Fag/Publikasjoner/Handboker>
4. Statens vegvesen (2014) Vegdirektoratet Handbok V221, Grunnforsterkning, Fyllinger og Skråninger, 2014. <http://www.vegvesen.no/Fag/Publikasjoner/Handboker>

EPS Geofoam Used in E16 Sandvika–Wøyen



Ermias Hailu Mijena

Abstract The Norwegian Public Roads Administration is building a new four lane motorway between Sandvika and Wøyen. The construction involves development of new intersections with a planned terrain elevation of up to 7 m, in areas with soft clay. This is challenging with respect to ground stability and settlements. Especially since the existing road, that was built in the 1980s, has already experienced settlements of 1.5–2 m. The designed solution has therefore involved extensive use of EPS in combination with granulated foam glass. In total 3 EPS-fill will be constructed during the project and one of them is placed on lime/cement reinforced ground. The most comprehensive fill will have a volume of approx. 11,000 and 27,000 m³ for the project in total. The compressive strength of the EPS is 100 kPa.

Keywords Design-construction • Embankment • EPS geofoam
Stability • Settlement

1 Introduction

EPS has been used in road filling over soft soils in Norway since 1972 [1]. It is used to reduce lateral loading on retaining structures, as soft soils remediation, for slope stabilization, to reduce the load on buried pipes etc.

The soil condition in the project area is predominantly a highly compressible soft clay. Therefore, control of settlement and stability of the area is crucial. Thus, various ground improvement methods such as lime cement columns, piling and lightweight fills with EPS geofoam and foam glass were implemented during construction of the embankments.

There exists three lightweight fills with EPS blocks at different locations in the project. In this paper, it will specifically be discussed about the two largest lightweight fills (L1 and L3). Lightweight fill L1 comprises of about 11,000 m³ EPS

E. H. Mijena (✉)

Norwegian Public Roads Adminstration (NPRA), Oslo, Norway
e-mail: ermias.mijena@vegvesen.no

blocks. Lightweight fill L3 comprises of about 27,000 m³ EPS blocks and 22,000 m³ of foam glass. The supplier of the blocks is Brødr. Sunde AS EPS geofoam is available in various densities and compressive strength. The blocks, which were used in this project, have a compressive strength of 100 kPa (at 5% strain) and a density of 19 kg/m³. The dimension of the block is 0.5 m high, 1.2 m wide and 2.4 m long. The dry unit weight of the block is 0.5 kN/m³ and the saturated unit weight is 1.0 kN/m³.

2 The Project Description

E16 is the main artery between Oslo and Bergen. The project is located 18 km from Oslo central railway station. It is as part of the plan to build a new four lane motorway from Sandvika to Skaret. The project planning and design is divided into three phases: The first phase, Wøyen–Bjerrum, construction completed and opened for traffic in 2009. The second phase, Sandvika–Wøyen, is currently under construction, and the third phase, Bjerrum–Skaret, is still on the design phase.

The route E16 Sandvika–Wøyen is about 3.5 km long. The design of the project was done by Aas-Jakobsen AS with Geovita AS as a geotechnical consultant. The construction of the project is divided into two contracts. The first contract, Bjørnegård tunnel, is stretching from Sandvika to Bærumsveien (Rud) and comprises construction of about 2.3 km long motorway tunnel. The second contract is stretching from Rud to Vøyenenga and includes the construction of about 1.6 km long motorway. The project will be finalized in summer 2019 (Figs. 1 and 2).

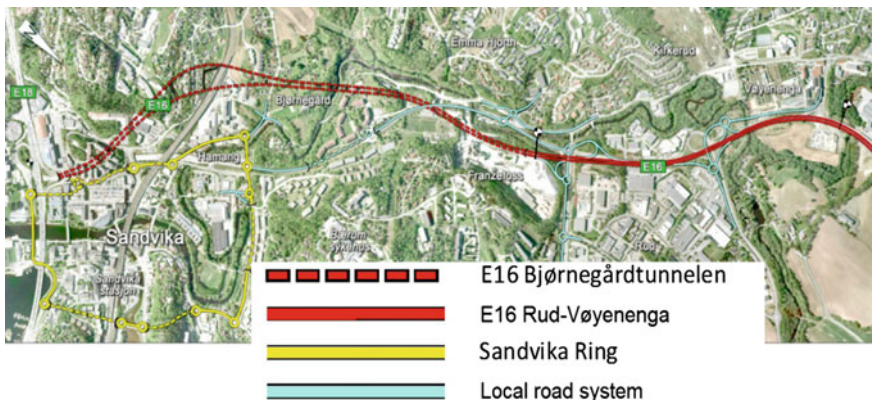


Fig. 1 Overview of E16 Sandvika–Wøyen

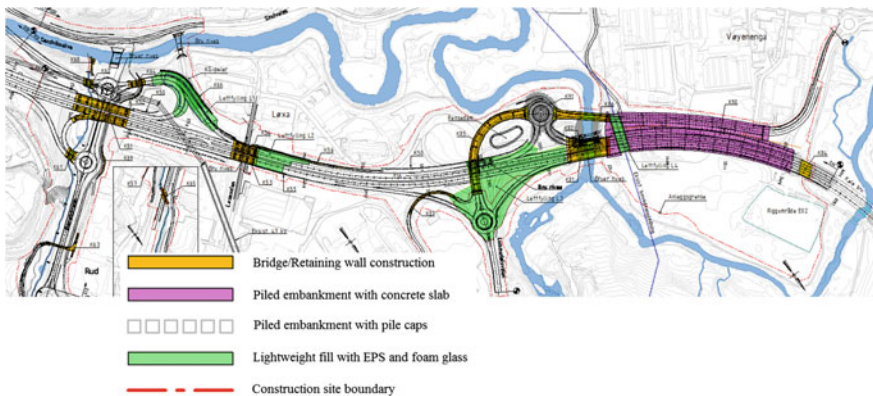


Fig. 2 Overview of E16 Rud–Vøyenenga

3 Lightweight Fill L1

3.1 Soil Conditions

An extensive ground investigation have been performed in the area. Based on the soil sample taken from two boreholes in the area and result from the CPTU, the soil condition at the area is a top layer of dry crust over a clay with organic content. Deeper 1–2 m thick layer of sensitive soft clay with underlying layer of normally consolidated soft clay is found. A till layer of varying thickness overlies the bedrock. To the south east of the exit ramp, there exists outcropping bedrock. The rock dips towards the west, and at the new roundabout, the rock is found at depths up to 10–16 m. The existing exit ramp lies up to 3–4 m high filling over the natural ground surface.

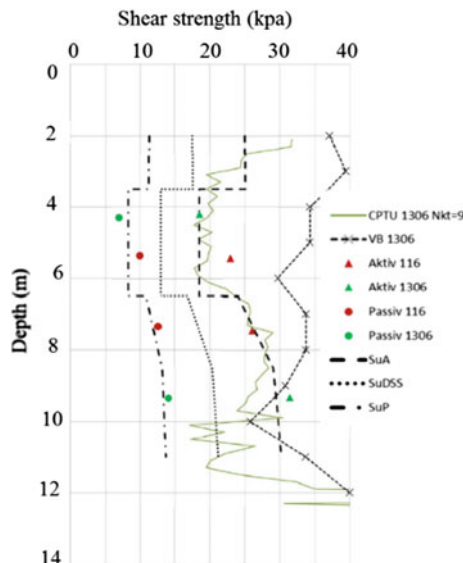
Two pore pressure measurements were installed by Norwegian Geotechnical Institute (NGI) at two different depths: 4 and 8 m. The pore pressure measurements indicate pore pressure value the same as hydrostatic pore water pressure distribution with the ground water table (GWT) at elevation +21.3, i.e. about 1 m below the surface.

3.2 Design Parameters

Soil geotechnical parameters were determined from a series of in situ and laboratory tests. The in situ tests included total sounding (TOT), rotary pressure sounding (DRT), cone penetration tests (CPTU), vane shear test and pore pressure measurement. Laboratory tests include soil classifications, oedometer and triaxial tests. A summary of the design parameters for the clay, which were used in the design,

Table 1 Material parameters for clay [3]

Layer	Depth (m)	Friction angle ($^{\circ}$)	Attraction (kPa)	Unit weight (kN/m^3)	Modulus number
Clay 1	2–6.5	26	15	17–17.5	11
Clay 2	6.5–8.5	34	5	17.5	14
Clay 3	8.5–11	26	5	18.0	14

**Fig. 3** Undrained shear strength profile [3]

are presented in Table 1. According to the Norwegian way, attraction (a) = cohesion (c). $\tan \phi$. A modulus number (m) [2] is the slope of the straight-line part of the graph tangent constrained modulus, M vs. vertical effective stress (σ'_v). The undrained shear strength profile, which was used in the design, is shown in Fig. 3.

3.3 Design Rules

The following design codes were followed during the stability analysis:

- NS-EN 1997-1:2004 + NA:2008, Eurocode 7, Geotechnical design
- NPRA Handbook V220.

Based on the project preconditions, the fill was set to Geotechnical category 2. In addition, since the new fill is higher than the existing fill and there exists a layer of soft and sensitive clay, the fill was placed in a consequence class 3. Therefore, an independent or third party control was required in addition to internal or agency control.

The partial factor was set to 1.5 for both undrained and drained analysis. According to Eurocode 3 Table NA.A1.2.(C) the load factor was set to 1.3. According to NPRA handbook V220, it was used a characteristics traffic load of 10 kPa and a terrain load of 5 kPa. According to Eurocode 8.5 NA.3.1(3), in the application of seismic load, a factor of safety FOS = 1.4 and FOS = 1.25 is required for undrained and drained analysis respectively.

3.4 Stability Analysis

The stability analysis was done by a geotechnical consulting company, Geovita AS at three profiles namely, profile 5, 8 and 11. Slide, a software that applies limit equilibrium method, and Plaxis 2D, a FEM program, were used to determine the factor of safety (FOS) against stability. The design height of the fill is up to 7.5 m high. The addition of a normal fill to the existing ground would trigger stability

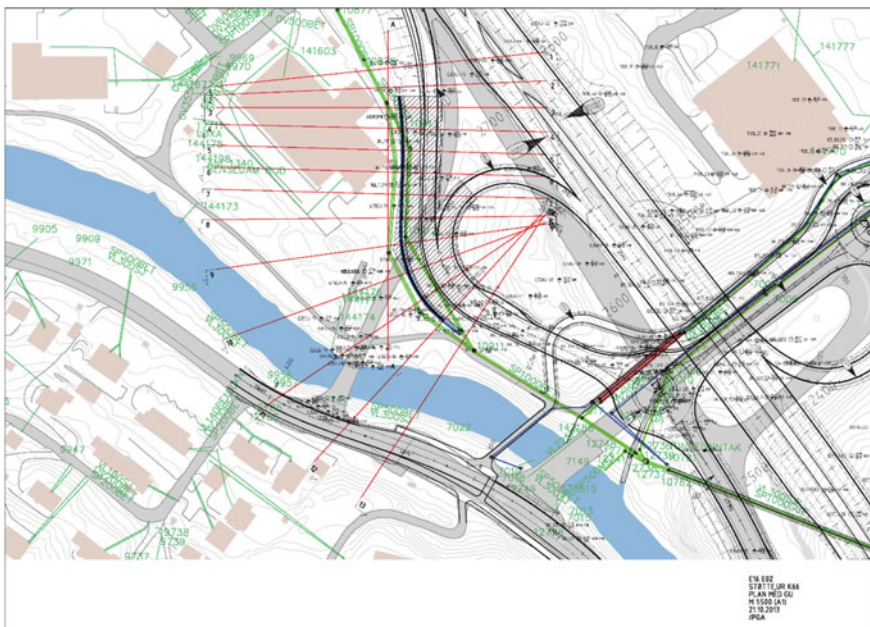


Fig. 4 Profiles considered for stability analysis

problem and post construction settlement. Therefore, the analysis was done by considering lightweight fill with EPS. Figure 4 shows profiles considered for stability analysis.

3.4.1 Profile 5

At profile 5, stability analysis was done by both Slide and Plaxis 2D. Both undrained and drained analysis were performed. In addition, drained and undrained analysis with considering seismic load. A pseudostatic inertial force is applied and the magnitude of the force according to EC8 is:

$$F_H = 0.5 \cdot \alpha \cdot S \cdot W \quad (1)$$

$$\alpha = a_g/g \quad (2)$$

$$a_g = \gamma_I \cdot a_g R = \gamma_I \cdot 0.8 \cdot a_g \text{ 40 Hz} \quad (3)$$

$$F_V = \pm 0.33 \cdot F_H \quad (4)$$

where:

W is the weight of the sliding mass

a_g is the design ground acceleration for type A ground

$a_g R$ is the reference peak ground acceleration for type A ground

g is acceleration of gravity

γ_I is importance factor

S is soil factor.

The design values of the seismic inertia forces used in slope stability analysis of the embankment are: $F_H = 0.045 W$ and $F_V = \pm 0.015 W$. The effect of vertical pseudostatic force on sliding mass is ignored as it has very little effect on slope stability.

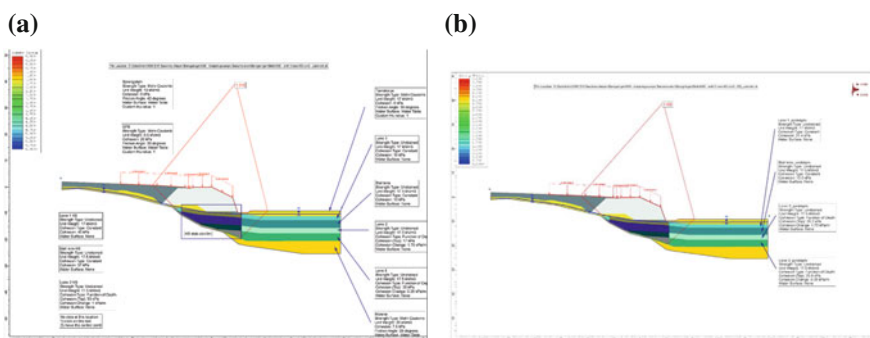


Fig. 5 Undrained stability analyses using Slide **a** without considering seismic load (FOS = 1.518). **b** With considering seismic load (FOS = 1.430)

Based on the result from the analysis, use of only EPS blocks in the embankment has shown inadequate factor of safety against stability. Therefore, it was decided to use double ribs lime-cement columns with 1 m width and c/c 3 m. Some of the results from stability analysis are shown in Fig. 5.

3.4.2 Profile 8 and 11

Since the results found from Slide in profile 5 is conservative, stability analysis at profile 8 and 11 were done only by use of Slide software. At profile 8, the factor of safety achieved considering EPS fill without lime cement stabilization is insufficient. However, the use of both lime cement stabilization and EPS gave a factor of safety 1.7 and 1.5 for undrained analysis without considering seismic load and with considering seismic load respectively. A factor of safety 2.6 has been achieved for drained analysis.

At profile 11, using only EPS fill has shown a factor of safety about 1.9 in both undrained and drained conditions, which is above the requirement. Therefore, there was no need for lime cement stabilization at this location.

3.5 *Buoyancy/Uplift Analysis*

Lightweight fill L1 lies adjacent to the river Sandvikselva. Since EPS blocks are super lightweight, they are highly susceptible to floatation. Therefore, it is crucial to perform buoyance analysis. According to the NPRA handbook, the factor of safety against buoyance/uplift is 1.3. A 200-years flood level was considered for the analysis and adequate safety factor against uplift was achieved.

3.6 *Construction and Quality Control*

Existing fill material was first removed and then the soft clay was stabilized with double ribs dia. 600 mm lime cement columns. The columns end on the rock or till layer. Due to the presence of pre-existing water line in the area, the lime cement columns stabilization was performed in two phases. First, the area with in the blue line shown in Fig. 6a was stabilized and then the new water and sewer line was constructed and after that the old water and sewer line was removed. Finally, the rest of the area was stabilized.

After stabilization was completed, the area was excavated to the right level and Class 3 geotextile was laid and then a sand-levelling course of 100 mm thickness was laid. Finally, a geomembrane of thickness 1 mm was then placed over the level base prior to placing the EPS blocks. EPS blocks should not be placed over a frozen soil.

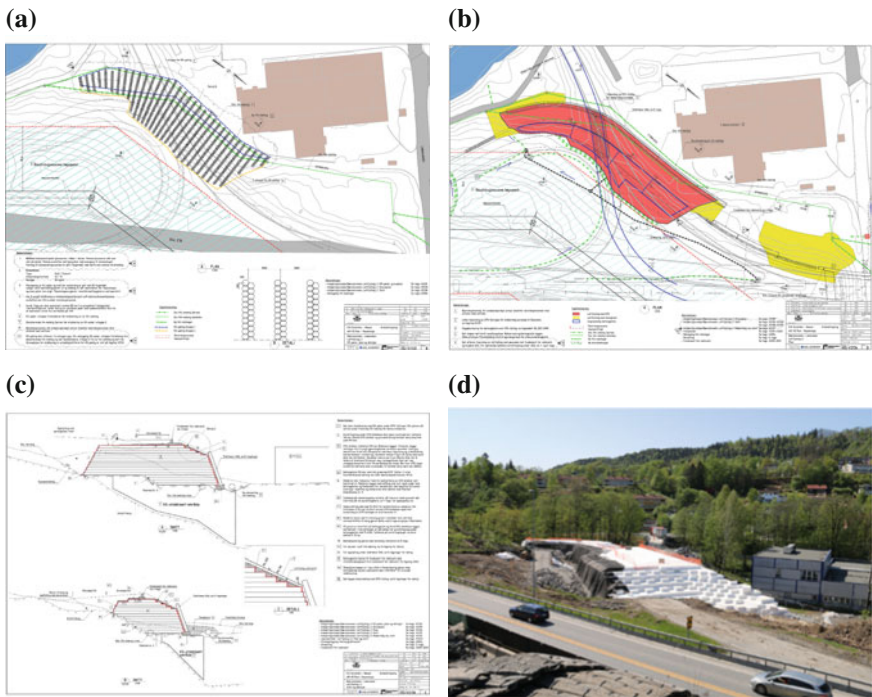


Fig. 6 **a** Lime cement stabilization at L1, **b** plan drawing of L1 (EPS, red and foam glass, yellow), **c** profile A, B and C at L1, **d** overview picture at L1. *Photo Maria Kristiansen, Geovita AS*

The fills should be constructed so that blocks fit together tightly and in such a way to avoid continuous vertical discontinuities. Block layout and placement should be in accordance with the guideline (NPRA, Handbook V221). According to the guideline, gap between adjacent blocks, which is less than 3 cm, is tolerated. Gaps between 3 and 5 cm should be filled with sand and if the gap exceeds 5 cm, it is not acceptable. The existence of gaps will create stress concentration in the area of contacts. Excessive immediate strains and large creep strains may result from such gaps. The resulting overall settlement may result in unsatisfactory situations such as decreasing the lifetime of a pavement structure [4]. The area between the cut/natural slope and EPS block was also filled with sand.

The EPS fill is up to 8 m high and a total volume of about 11,000 m³ was constructed. Figure 6d shows overview of the fill. Bulldogs were used to hinder horizontal movement of blocks during construction period. Bulldogs are mechanical connectors used to provide additional interface resistance. Towards the west and north west side of the exit ramp, a gravity retaining wall with 3 V:1H inclination, was constructed. The function of the wall is to prevent the blocks from possible future fire risk and to incorporate aesthetic value.

After the fill was in place, it was covered with a geomembrane and Class 3 geotextile. The purpose of the geomembrane is to protect the fill from possible

accidental contact with gasoline and other petroleum products. The geotextile protects the geomembrane from damage. It was used a crushed rock (22/120) as a cover over the EPS fill and in this case the geomembrane have to be protected with smaller fraction of crushed rock (0/63) before filling with larger fractions.

The blue boundary in Fig. 6b shows the limit of the concrete slab. The purpose of the concrete slab is to distribute the traffic load to a desirable level. The slab was casted directly over the EPS fill covered with geomembrane and geotextile. The thickness of the slab is 150 mm and increasing locally to 200 mm. The quality of the concrete which was used is B35 (characteristic cylinder strength of 35 MPa).

The project involved some challenges with respect to place constrains for construction equipment to move freely. There was some challenge in the winter as well regarding snow and ice accumulated on the blocks. Salt had been used to remove the ice. The salt was removed together with the ice. The salt has no short term or long term effect on the blocks. When it was snowing, the fill used to be covered with some sheet so that the snow could easily be removed. Since the geomembrane is not flexible material, it was also a challenge putting it on the steps at the slope. Risk of fire should be eliminated during the construction activity. For instance, fire from welding equipment.

To reduce settlement, it was recommended to excavate 1.5 m below the existing terrain for compensated filling. In addition, to minimize the settlement in the transition zone between the EPS fill and normal fill, it was recommended to use foam glass (see yellow colour in Fig. 6b). The foam glass is also a lightweight fill material with unit weight 3.5 kN/m³ and that makes it helpful to use it in the transition zone to reduce differential settlement.

The supplier have to test the EPS blocks before shipping to the project site. They should send documentation about the product to the client. They also send the results from testing (density, compression etc.). In addition, NPRA also test some random samples. The evenness of the blocks have to be checked on the field as well.

According to the Norwegian guidelines, the following quality control criterial should be fulfilled [5].

Table 2 A test result of compressive strength and density of EPS block which was used at L3
Source NPRA laboratory

Cube number	Mass (g)	Length (cm)	Width (cm)	Height (cm)	Volume (cm ³)	Surface area (cm ²)	Density (Kg/m ³)	Compressive strength at 5% def. (kN/m ²)
1	2.65	5.00	5.00	5.00	125.0	25.0	21.2	99.7
2	2.72	5.00	5.00	5.00	125.0	25.0	21.8	101.7
3	2.96	4.95	5.00	5.00	123.8	24.8	23.9	105.6
4	2.91	5.00	5.00	5.00	125.0	25.0	23.3	104.7
5	3.13	4.95	5.00	5.00	123.8	24.8	25.3	110.0
6	2.97	5.00	5.00	5.00	125.0	25.0	23.8	110.2
						Average	23.2	105.3

- The blocks should be a minimum of 3 weeks old before they are used for stabilizing.
- The average compressive strength for a single block (6 tests) should not be less than 90 kPa and no single measurement should be less than 80 kPa (Table 2).
- The blocks should meet the density requirement
- Blocks should be smooth and flat on all surfaces.
- The allowed deviation from design level is ± 50 mm. The level difference between two adjacent blocks should be less than 5 mm. Unevenness should be maximum 5 mm measured over 3.0 m.
- To hinder horizontal movement of blocks during construction, the blocks should be anchored by two pcs. dia. 95 mm bulldog per block.
- The minimum soil cover on the side slopes is 0.25 m and the allowed deviation from this is ± 0.15 m.

4 Lightweight Fill L3

4.1 Soil Conditions

As shown in Fig. 7 an extensive ground investigation have been performed in the area. Based on the results obtained from field and laboratory tests, the area consists

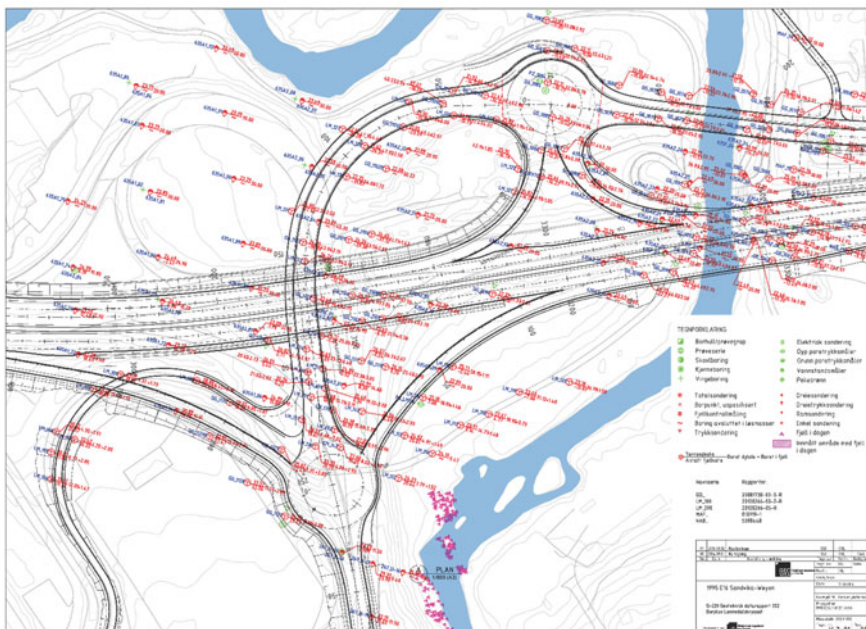


Fig. 7 Plan drawing showing boreholes

of 2 m thick existing fill layer over a layer of dry crust. Further a clay layer with dry crust effect underlain by soft/middle stiff clay. The rock lies mainly 5–15 m under the terrain and it dips steeply from the roundabout towards E16. The soil consists of much of silt layer and some shell remains.

Two pore pressure measurements were installed at two different depths: 4 and 8 m. The result has shown hydrostatic pore water pressure distribution with the ground water table at elevation +22, i.e. about 2 m below the surface.

4.2 Design Rules

The embankment, to be constructed, is extensive. In addition to this, there exists a soft sensitive clay in the area. Based on this fact and Eurocode 7, the fill was set to Geotechnical category 3 and consequence class 3, which suggests an independent or third party control in addition to the internal or agency control. The partial factor in this case was set to 1.6 for both undrained and drained analysis.

4.3 Design Parameters

A summary of the design parameters for the clay, which were used in the analysis, are presented in Table 3.

4.4 Stability Analysis

The maximum lightweight fill in the area is 7.5 m. For the stability analysis, Geovia AS used GeoSuite, a software that applies limit equilibrium method, to determine the factor of safety (FOS) against stability. As shown in the Fig. 8a, stability analysis were done at five profiles (A–A, B–B, C–C, D–D and E–E). The following phases of the project were considered during the analysis.

- Pre-excavation stability of the area
- Post-excavation stability of the area
- Stability of the area after filling with lightweight fill (both drained and undrained analysis)
- Stability of the area after filling with lightweight fill with considering seismic load (both drained and undrained analysis).

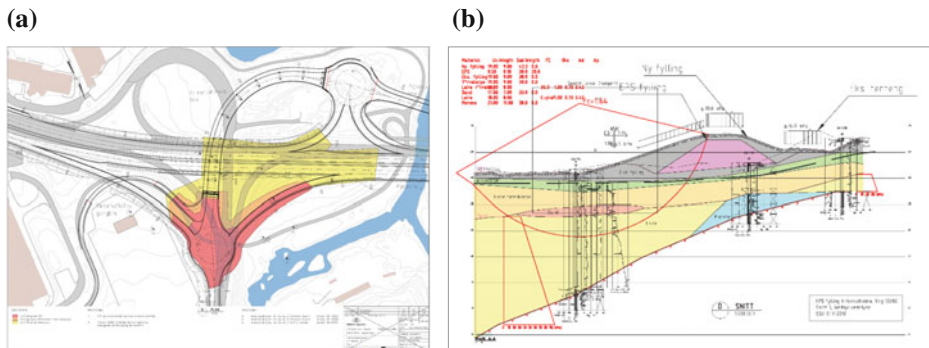


Fig. 8 **a** Plan drawing of L3 showing profiles considered in stability analysis (EPS, red and orange and Foam glass, yellow), **b** undrained Stability analysis result at profile D by considering seismic load (FOS = 1.64)

Table 3 Material parameters for clay [6, 7]

Layer	Friction angle ($^{\circ}$)	Attraction (kPa)	Unit weight (kN/m^3)
Clay with dry crust effect	30	3	18
Soft clay	26	0	18

To avoid/reduce road settlement, it was recommended to excavate 1.5 m below the existing terrain for compensated road filling. Stability analysis at profile A–A, B–B, C–C and D–D have shown sufficient factor of safety. However, at profile E–E, stability analysis of post excavation has shown low factor of safety (FOS = 1.32). Therefore, one must carefully supervise the inclination of the slope during the excavation work for E16 after the fill for the exit road from E16 is constructed. Figure 8b shows stability result at profile D–D.

4.5 Buoyancy/Uplift Analysis

Similar to L1, lightweight fill L3 lies adjacent to the river Sandvikselva, but relatively on a lower elevation. According to the map from Norwegian Water Resources and Energy Directorate (NVE), the 200-years flood level lies +24.8. Buoyancy analysis has shown sufficient factor of safety against uplift ($\gamma > 1.3$).

4.6 Construction

Soil excavation work had been started from the roundabout towards E16. Unlike in L1, where the EPS fill lies on a lime cement stabilized ground, here the fill lies

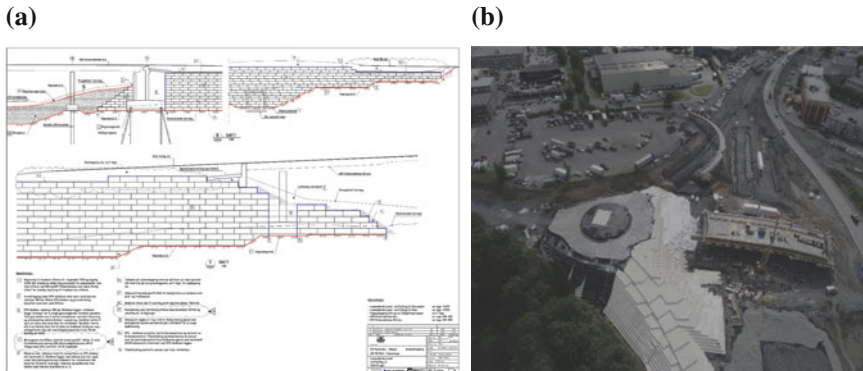


Fig. 9 **a** Profiles towards the bridges, **b** aerial drone photo of L3. *Photo Scan survey AS*

directly on top of the soft clay. As shown in Fig. 9, the fill is an abutment to the bridge crossing E16 at one end and also an abutment to the walkway bridge at the other end. Thus, this will be helpful in minimizing settlement between the approach embankments and the bridge decks. The construction procedure of the fill is the same as L1.

The blue boundary in Fig. 8a is the limit of the concrete slab. The blocks delivered to the construction site should be stored properly. Care should be taken in terms of safety.

The construction challenges are mostly similar to that of L1 as well. It had been observed that the blocks had turned to yellow colour due to exposure to ultraviolet light during the summer season and it is perfectly fine to use the blocks in the fill.

5 Conclusions

Stability analysis at L1 using only EPS fill in the embankment has shown insufficient factor of safety. Therefore, the area was first stabilized with lime cement columns before filling with EPS. Unlike at L1, stability analysis at L3 using only EPS in the road filling has shown sufficient factor of safety against stability. To minimize settlement in both Lightweight fill L1 and L3, it was recommended to excavate 1.5 m below the existing terrain for compensated road filling. In addition, to minimize settlement between the EPS fill and normal road fill (in the transition zone), it was recommended to use foam glass.

A thorough inspection of the embankment during construction is crucial. Overall, the lightweight fill in both places are safe with regard to settlement and stability concerns.

References

1. Aabøe R (2011) 40 years of experience with the use of EPS geofoam blocks in road construction. Paper presented at the 4th international conference on geofoam blocks in construction applications, Lillestrøm, Norway, 6–8 June 2011
2. Janbu N (1963) Soil compressibility as determined by oedometer and triaxial tests. Europäischen Baugrundtagung 1963, Wiesbaden. Published also in Bulletin, Geotechnical Division, Norwegian Institute of Technology
3. Geovita AS/Aas-Jakobsen AS (2015) G-201-E02 Avkjøringsrampe Bærumsveien stabilitetsberegninger
4. Negussey D, Elragi A (2000) “EPS geofoam, an overview” internal report AE1-00. Geofoam Research Center, Syracuse University, Syracuse, NY
5. Norwegian Public Roads Administration (NPRA) (2015) Prosesskode for Enterprise E02 Rud-Vøyenenga
6. Geovita AS/Aas-Jakobsen AS (2014a) G-220-E02 Geoteknisk data rapport
7. Geovita AS/Aas-Jakobsen AS (2014b) G-203-E02 Lettfylling Lommedalskrysset stabilitet og setninger

First Geofoam Roadway Embankment Application in Turkey



Abdullah Tolga Özer and Emre Akinay

Abstract The first geofoam block roadway embankment application in Turkey was completed in April 2017 in Acibadem, Istanbul. Geofoam technology was selected to construct the roadway embankment on a site where two 2.2 m diameter water mains are located 3.8–5.6 m below the foundation of the embankment. Geofoam blocks not only prevented the relocation cost of this infrastructure in a very complex urban setting in terms of buried utility corridors, but also prevented possible structural damage to the mains if conventional earth fill was used to construct the embankment. In addition, water service was not interrupted during the construction. The project background, design considerations, and construction sequence is presented. In order to monitor the performance of the embankment, a field instrumentation array comprised of extensometers was installed in the foundation soil, bedding sand, geofoam block assemblage, and under the load distribution slab. Instrumentation details and monitoring results over a period of ten months is discussed, and long-term performance projections were evaluated using short-term performance data.

Keywords EPS-block geofoam · Geofoam embankment · Instrumentation Field monitoring · Settlement plate

1 Introduction

Construction of highway embankments over soft soil sites using expanded polystyrene (EPS) block (geofoam block) to mitigate consolidation settlement is a mature technology and has been implemented by various countries around the world [1–13]. In addition, geofoam technology provides a unique solution for

A. T. Özer (✉)
Okan University, Istanbul, Turkey
e-mail: tolga.ozер@okan.edu.tr

E. Akinay
Austrotherm Turkey, Istanbul, Turkey

embankments constructed over buried utility corridors [14]. Utilizing geofoam technology can help prevent possible structural damage of buried utilities when compared to embankments constructed using conventional compacted earthen fill.

The first geofoam block roadway embankment construction in Turkey was completed recently in April 2017 in Acıbadem, İstanbul (Fig. 1). The project site is located at the northwest corner of the Highway 01 and D100 motorway intersection, and south of Akasya Shopping Mall (Fig. 1). The geofoam embankment was constructed for a roadway to divert a portion of the traffic on Harem Exit of Uzunçayır Exit of Highway 01 towards the Acıbadem district, to alleviate some of the merging traffic onto the D100 motorway [15].

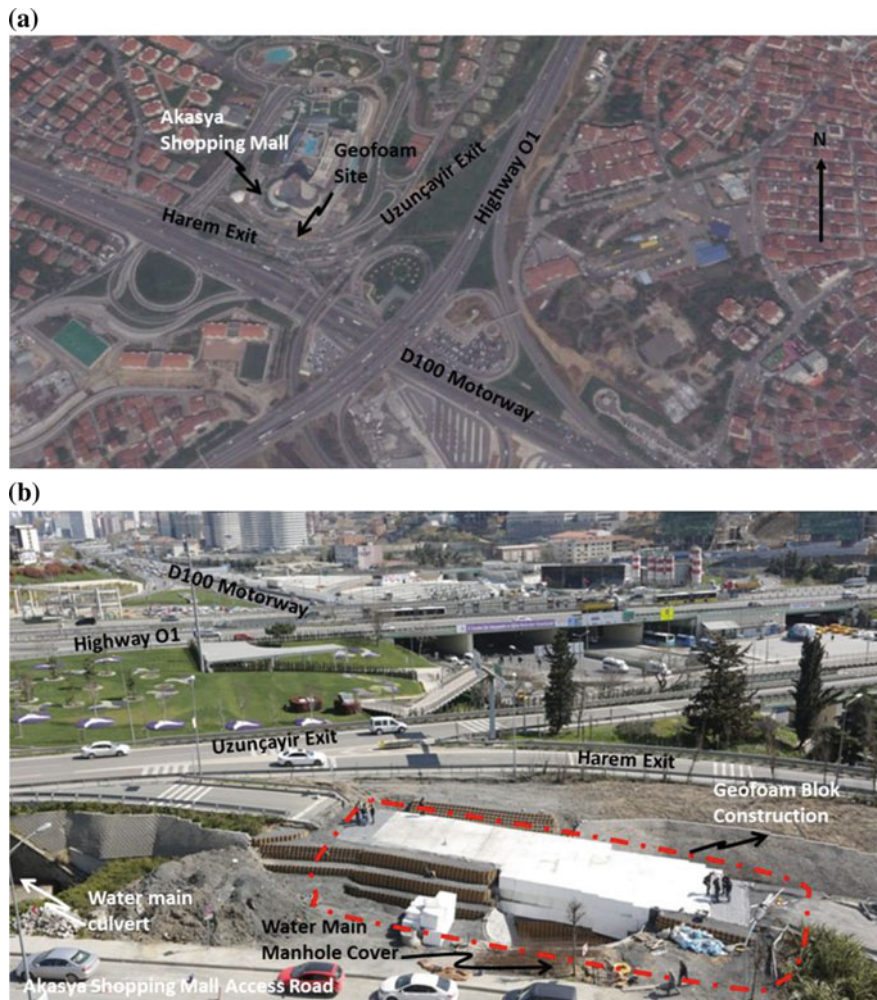


Fig. 1 Site location map **a** aerial view of the site location, Acıbadem, İstanbul, **b** geofoam block construction area

The site is not only located in a densely populated area but it is also located next to one of the busiest main highways in Istanbul. In addition, there are many buried-utility corridors located in the vicinity. Two 2.2 m diameter water mains, crossing under Highway 01's Uzunçayır Exit in a concrete box culvert, run parallel to the D100 motorway along the north side of the Harem Exit. These water mains are located approximately 3.8–5.6 m below the foundation level of the proposed embankment (Fig. 2). Any structural damage to these water lines during construction would cause significant utility service interruption, and inconvenience to the residents. Relocating these water mains in this urban environment would not only be a complex task, it would also cause significant delays in the project completion time.

Therefore, geofoam blocks were selected as a viable solution to construct the portion of the exit-diversion embankment over the water mains (Figs. 1 and 2). Approximately 720 m³ of geofoam blocks was used.

Construction details [15], and the details of the instrumentation program [16], of this first geofoam-embankment application in Turkey have been published in proceedings of local conferences. In order to monitor the performance of the geofoam embankment, extensometers were installed. In this study, monitoring results since the beginning of construction is discussed. Projected long-term performance, including geofoam creep, is evaluated using short-term post-construction performance data. Also, the behavior of the geofoam embankment under working stresses was compared with well-documented I-15 embankment data [14].



Fig. 2 Approximate locations of water mains [16]

2 Materials and Design

Several countries have adopted design guidelines for geofoam highway embankments [4, 17, 18]. Guideline and Recommended Standard for Geofoam Applications in Highway Embankments, published by the National Cooperative Highway Research Program (NCHRP), was adopted for this project [4].

Both external and internal stability evaluations were performed according to the NCHRP guideline. The total vertical stress applied on top of the geofoam block assemblage, beneath the pavement system, composed of dead loads (gravity stresses due to the pavement system, σ_{DL}) and traffic loads (live loads or transient loading, σ_{LL}). The NCHRP guideline recommends a factor of safety (FS) of 1.2 for load bearing analysis since σ_{LL} is the main component of the total stress, not σ_{DL} [4]. Therefore, the minimum required elastic-limit stress of geofoam blocks (stress corresponding %1 strain, σ_e) under the total stress ($\sigma_{total} = \sigma_{DL} + \sigma_{LL}$) needs to be higher than the factored total vertical stress ($\sigma_e > FS \times \sigma_{total}$) [4].

Based on this criterion, geofoam block with a nominal density of 22 kg/m^3 (EPS22 according to ASTM D6817 [19]) was selected for the geofoam row directly beneath the pavement system. Even though the applied vertical stresses dissipate (calculated by 1 horizontal: 2 vertical method) through the depth of the embankment, EPS 22 was conservatively used throughout the entire project (Fig. 3). 1 m high, 1.2 m wide and 2.5 m long blocks were used to construct the 3 m high geofoam embankment (Fig. 3). The total thickness of pavement layer is 61 cm. Sloped sides of the embankment were protected against possible chemical attack with geomembrane, and also covered with geocells filled with topsoil for vegetation growth (Figs. 3 and 4). Vertical sides of the embankment were sealed with shotcrete (Fig. 3).

A total of four $50 \text{ mm} \times 50 \text{ mm} \times 50 \text{ mm}$ -size geofoam samples were collected from four different blocks shipped to the site on different days, and

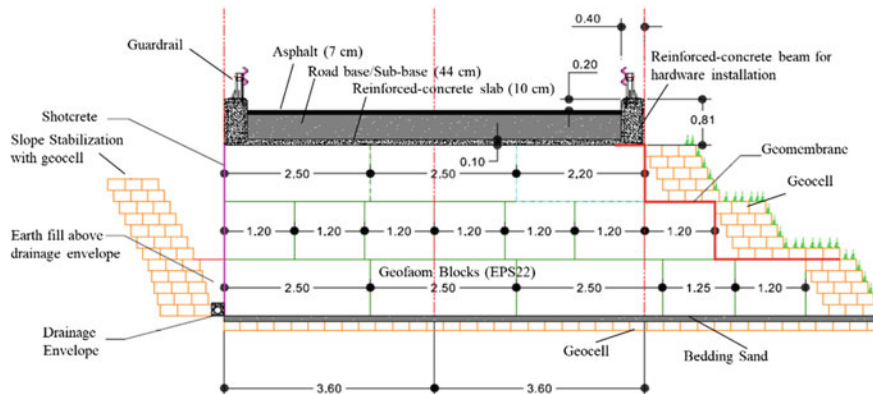


Fig. 3 Typical cross-section of geofoam roadway embankment



Fig. 4 Geomembrane protection and geocell application at the sloped section of the geofoam embankment

compressive strength tests were performed according to ASTM D1621 [20]. Test results were summarized and compared with ASTM D6817 minimum required values (Table 1). Physical and mechanical properties of blocks shipped from different batches showed uniformity in the molding process (Table 1).

The construction of geofoam embankments generally follows a well-established and straightforward process. The traditional construction sequence involves placing bedding sand over the foundation, assembling the blocks according to the block placement plan, and constructing the load distribution slab and the pavement system (base and sub-base material and coating) [4]. This same process was also

Table 1 Mechanical properties of the geofoam blocks used in the project [15, 16]

Property	Laboratory test values, minimum–maximum (average, standard deviation)	ASTM D6817 [19] definition	ASTM D6817 [19] minimum required values
γ (kN/m ³)	20.9–22.1 (21.6, 0.39)	EPS22	21.6
σ_1 (kPa)	50.0–54.3 (52.1, 1.74)		50
σ_5 (kPa)	113.3–118.1 (115.4, 1.94)		115
σ_{10} (kPa)	128.8–132.5 (130.2, 1.56)		135
E_i (MPa)	4.9–5.5 (5.2, 0.2)		—

ASTM American Society for Testing and Materials

γ apparent density

σ_1 , σ_5 , σ_{10} compressive strength at 1, 5 and 10% strain, respectively

E_i initial Young's modulus

followed in this first application in Turkey, and is discussed in detail in previous papers [15, 16]. Even though there are no bearing-capacity or settlement concerns, the project owner elected to apply geocell at the foundation level on this project (Fig. 3).

Sloped sections are traditionally protected with geomembrane and covered with topsoil [4]. In this application, instead of placing topsoil directly over the geomembrane, geocell application was preferred by the owner (Fig. 4).

3 Instrumentation and Short-Term Monitoring

Magnet extensometers have been used successfully in monitoring the performance of geofoam embankments [14]. Therefore, to monitor the performance of the geofoam embankment, a field instrumentation array, which composed of extensometers, was installed in this first application in Turkey. The magnet-extensometer array for the geofoam embankment consisted of a total of five plate magnets and a datum magnet (Fig. 5). Each square magnet plate has 305 mm sides and is 12.5 mm thick with a 60 mm thick annular magnet collar with an inside opening of 33.5 mm (Fig. 5). A schedule 40 PVC access pipe, which enables the annular opening of the magnet to slide through to the desired level, was used. The datum magnet consists of a 60 mm thick collar with a 33.5 mm inside opening, which was directly fixed to the riser pipe by set screws. The datum magnet was installed approximately 50 cm below the foundation in the natural ground and served as a reference point. Plate #1 is located on the foundation, beneath the geocell

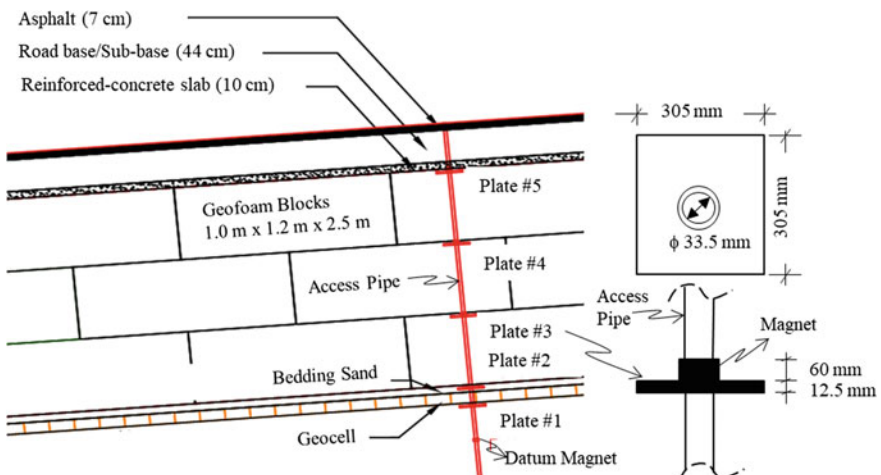


Fig. 5 Layout of the plate-magnet array for long-term settlement monitoring of the geofoam embankment

application at the foundation level. Plate #2 is located within the bedding sand. Plate #3 and Plate #4 are located at the interface of the first and second rows of geofoam blocks and second and third rows of geofoam blocks, respectively. Plate #5 was installed at the interface between the top row of geofoam blocks and the reinforced-concrete load-distribution slab. Therefore, plastic sheeting was placed over the top of Plate #5 to break the bond between the concrete and the plate, so that the plate can freely move along the riser pipe as the blocks settle. During the installation of the pipe and plates, ultimate care was taken so as to install the plates parallel to the road surface plane.

A magnet probe, connected to a graduated cable (with 1 mm graduations) which is wrapped on a reel with a built-in buzzer to detect the position of the magnets, was lowered into the access pipe until the probe reached the bottom of the access pipe. Then the probe was gradually raised until the buzzer sounded, and then was continued to be slowly raised until the buzzer sounded a second time, which indicated the exact location of the magnet. The position from the top of the riser pipe is then recorded using the graduated cable. Upon recording the position of this first magnet, the probe was continued to be raised to the next magnet, and again the location was recorded at the second buzzer sound. This process was repeated for all of the magnets. The differences between each set of readings indicates the settlement. Readings are repeatable to ± 3 mm [14].

Observed settlements at the magnet plate locations (Fig. 5), both during and after construction, were recorded (Fig. 6). Since there was no settlement recorded both in

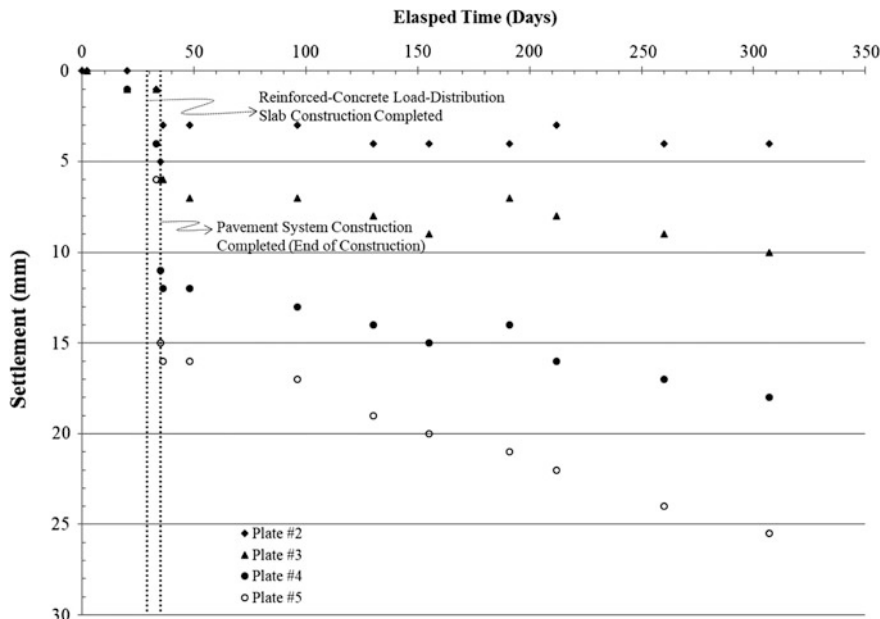


Fig. 6 Cumulative construction and post-construction settlements

the datum magnet and Plate #1, they are not shown in Fig. 6. Therefore, all the deformation recordings were referenced to the base plate (Plate #1).

Settlements ranging from 1 to 3 mm per instrumented row of blocks were observed after placement of the reinforced-concrete load-distribution slab which casted 33 days after the beginning of construction (Fig. 6). The total settlement after the placement of the reinforced-concrete load-distribution slab was 6 mm (Fig. 6). Since all the deformation recordings were referenced to the base plate (Plate #1), the recordings of Plate #5 represent the cumulative settlement of the geofoam blocks plus the bedding sand (Fig. 6). The total settlement reached 16 mm (Plate #5) when the pavement system components (sub-base and asphalt) were completed (end of construction), which includes a total of 3 mm of settlement (seating) at the bedding sand (Plate #2).

The cumulative settlement of 16 mm at the end of construction, which includes gap closure, seating at the base, and geofoam block deformations, was about 0.55% of the embankment height (Fig. 7). The measured end of construction strain is less than the elastic limit strain (Fig. 7). This can be attributed to selecting all the block densities (EPS 22) conservatively based on the factored total stresses at the base of the pavement system. Even when considering the total strain from the beginning of construction to the end of post-construction data collected thus far, approximately 0.85%, the measured strain is less than elastic limit strain (Fig. 7).

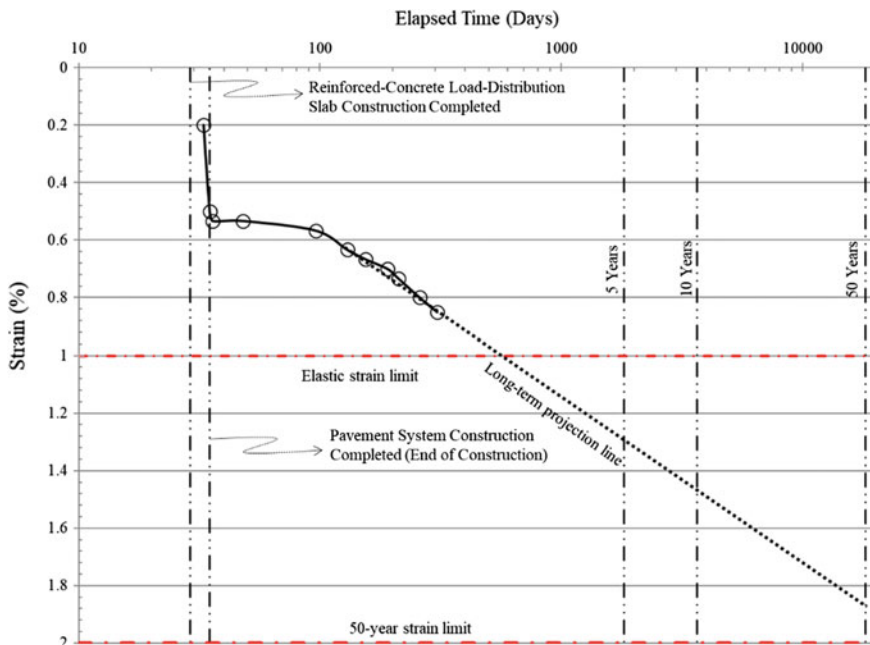


Fig. 7 Cumulative geofoam-block strain

So far, the post-construction data collected covers a period of 270 days since opening the roadway to traffic. Since the opening of traffic, the total post construction strain is about 0.3% (Fig. 7). Based on the data collected, the trend of post construction settlements will most likely be less than the total post construction deformation limit of 2% strain (1% allowable construction strain plus 1% allowable long-term creep at 50 years). The post-construction monitoring program will continue to collect recordings from the settlement array (one reading per month), which will decrease the sensitivity of the post-construction creep estimation.

This settlement performance data is based on an instrumentation array similar to that of the well-documented I-15 embankment performance [14]. The I-15 settlement criteria were established as 1% strain at the end of construction, and up to 2% total strain over the post-construction period of 50 years [14].

The I-15 data showed that the total strain condition has been met under the designed pavement-system loading, and the expected creep for post construction is less than 1.0% [14]. The I-15 criteria for both the short- and long-term conditions are shown in Fig. 7 with red dashed lines. Similar to the I-15 performance data, if the current strain trend continues, the projected total post-construction strain will be on the order of 1.2 and 1.5% at the end of 10 and 50 years, respectively (Fig. 7).

4 Summary and Conclusions

The very first geofoam embankment in Turkey has been constructed, opening to traffic in April 2017. The use of geofoam blocks averted the costly relocation of water mains, and the project was completed without any interruption of the water services. Using collected performance data, projected long-term settlement performance indicates total strains will remain within allowable limits.

Construction of this well-documented and monitored first geofoam embankment provided a leading example, and showed the possibilities of using geofoam technology to solve challenging tasks to local transportation officials, contractors, designers and the EPS society.

Acknowledgements The first geofoam embankment application in Turkey would not have been possible without the collaborative efforts of many different entities. The authors acknowledge the contribution of Akiş Real Estate Investment Trust, Sinpas Construction, Aderenza Construction, HDS Engineering, MOVEA Engineering with Geosynthetics, and Austrotherm Turkey.

References

- Thompson DJ, Walker A, Radley RJ et al (1995) Design and construction of expanded polystyrene embankments. Practical design and methods as used in the United Kingdom. Const Build Mater 9(6):403–411

2. Beinbrech G, Hillmann R (1997) EPS in road construction—current situation in Germany. *Geotext Geomembr* 15(1–3):39–57
3. Perrier H (1997) Ultra light cellular structure—French approach. *Geotext Geomembr* 15(1–3):59–76
4. Stark TD, Arellano D, Horvath JS et al (2004) Guideline and recommended standard for geofoam applications in highway embankments. NCHRP Report 529. Transportation Research Board, Washington, D.C.
5. Bartlett S, Negussey D, Kimble M et al (2000) Use of geofoam as super-lightweight fill for I-15 reconstruction. Paper presented at the Transportation Research Record 1736. Transportation Research Board, Washington, D.C.
6. Horvath JS (2010) Emerging trends in failures involving EPS-block geofoam fills. *J Perform Const Fac* 24(4). [https://doi.org/10.1061/\(asce\)cf.1943-5509.0000114](https://doi.org/10.1061/(asce)cf.1943-5509.0000114)
7. Aabøe R (2011) 40 years of experience with the use of EPS geofoam blocks in road construction. Paper presented at the 4th international conference on geofoam blocks in construction applications, Lillestrøm, Norway, 6–8 June 2011
8. Duškov M, Nijhuis E (2011) Lightweight road embankments for the crossover of the N207 over the railway Alphen A/D Rijn-Gouda. Paper presented at the 4th international conference on geofoam blocks in construction applications, Lillestrøm, Norway, 6–8 June 2011
9. Herle V (2011) Design and monitoring of EPS embankment on D1 near Ivanovice in the Czech Republic. Paper presented at the 4th international conference on geofoam blocks in construction applications, Lillestrøm, Norway, 6–8 June 2011
10. Kubota T (2011) Case history of EDO-EPS method in Japan. Paper presented at the 4th international conference on geofoam blocks in construction applications, Lillestrøm, Norway, 6–8 June 2011
11. Papacharalampous G, Sotiropoulos E (2011) First time application of expanded polystyrene in highway projects in Greece. Paper presented at the 4th international conference on geofoam blocks in construction applications, Lillestrøm, Norway, 6–8 June 2011
12. Spasojević S, Mitrović P, Vučanić V et al (2011) The application of EPS in geotechnical practice: a case study from Serbia. Paper presented at the 4th international conference on geofoam blocks in construction applications, Lillestrøm, Norway, 6–8 June 2011
13. Youwai S, Kongkitkul W, Sripobink T et al (2011) Application of EPS for remedial work of bridge bearing unit on Bangkok soft clay: a case study. Paper presented at the 4th international conference on geofoam blocks in construction applications, Lillestrøm, Norway, 6–8 June 2011
14. Farnsworth CB, Bartlett SF, Negussey D, Stuedlein AW (2008) Rapid construction and settlement behavior of embankment systems on soft foundation soil. *J Geotech Geoenviron* 134(3):289–301
15. Özer AT, Danyıldız E, Akınay E et al (2017) Using geofoam blocks to construct roadway embankments over buried utility corridors: a case study. Paper presented at 7th national geosynthetics conference G7 2017, İstanbul, Turkey, 11–12 May 2017 (in Turkish)
16. Özer AT, Akınay E (2017) Short term performance evaluation of geofoam block embankment using field instrumentations. Paper submitted to 7th geotechnics symposium, İstanbul, Turkey, 22–24 November, under review (in Turkish)
17. Norwegian Road Research Laboratory (NRRL) (1992) Use of expanded polystyrene in road embankments—design, construction and quality assurance. Public Roads Administration, Oslo, Norway
18. European Manufacturers of Expanded Polystyrene (EUMEPS) (2014) EPS white book, EUMEPS background information on standardisation of EPS. Version: 15/10/2014
19. ASTM (2015) Standard specification for rigid cellular polystyrene geofoam. ASTM D6817, West Conshohocken, PA
20. ASTM (2010) Standard test method for compressive properties of rigid cellular plastics. ASTM D1621, West Conshohocken, PA

Dutch A76 Highway Widening Using EPS Embankment with a Vertical Side



Milan Duškov, Martin den Uil and Michaël Fütterer

Abstract This article concerns the A76 highway widening (near the Kerensheide junction) using a lightweight fill with a vertical embankment. The A76 highway section (widened from 2 × 2 to 2 × 4 lanes) lies 4 m above a truncated slope and is situated between two concrete structures. The design of the fill should not decrease the stability of the current slope (with a high retaining wall at the toe of the slope) and had simultaneously to create sufficient space for the planned highway widening. In addition, the fill should have no influence on a crossing high-pressure gas pipe. The daily traffic load amounts to about 8600 trucks. These complex conditions have led to an extension of the highway cross section realized with EPS blocks with a vertical embankment; a first in the Dutch engineering practice. The EPS geofoam blocks were piled up 4 m above ground level and 2 m bellow the slope line. The performed parameter study confirmed that the friction between the EPS-blocks in combination with a low Poisson's ratio is sufficient to provide stability. No side support is needed to secure the slope stability after the completion of the highway A76 widening. Although the applied design method requires specific expertise, this design offers multiple advantages such as saving both space and costs, stability increase and a very short construction time.

Keywords Project case · Lightweight embankment · Highway widening
Vertical embankment side · Crossing gas pipe

M. Duškov (✉)

InfraDelft, Delft, The Netherlands
e-mail: milan.duskov@infradelft.nl

M. den Uil

Movares, Utrecht, The Netherlands

M. Fütterer

Heijmans, Rosmalen, The Netherlands

1 Introduction

That a complex assignment can allow for a good result, is illustrated by the highway widening of the A76 at the junction Kerensheide, across the industrial site Chemelot in Geleen (in the southeast of the Netherlands) that was realized in mid-2012 by contractor Heijmans. There was actually no space available between the successive engineered structures. In the existing situation, the embankment had already been shortened and supported with a long retaining wall. In addition, the highway widening could not have any impact on the existing high-pressure gas pipeline. Because a conventional solution such as an anchored sheet pile wall would increase the loads on the existing structures and the gas pipeline to an unacceptable level, the solution had to be found in a construction with limited weight and reduced footprint. A 6.5 m thick lightweight embankment with a vertical side provides enough space for the new traffic lanes without affecting slope stability or additional loads on the existing gas pipe.

2 Situation Description and Implementation Aspects

For the planned highway extension of the A76 that lies between an existing tunnel for pipes (KW16) and the new viaduct above the railway line Sittard-Maastricht (KW17), it appeared not possible to connect the new extension to the existing retaining wall of the tunnel under a natural slope. The current situation is shown in Fig. 1 (top view). Because of the existing retaining wall and the cable and pipes layout, it was not possible to apply a conventional solution such as an anchored sheet-pile wall. Demolition of the existing retaining wall could lead to considerable hazards for the existing pipes and business processes at Chemelot. The solution had to be sought in a construction with limited weight and that at the same time would take little space. In addition, the relevant section of road should be built in a tight time frame of 6 months in order to be ready for opening. In addition to the EPS structure, several other structures were to be built before the final road construction could be constructed.

The highway section is located in an area with a low ground water level. Therefore buoyancy doesn't appear to be a concern at this site. Furthermore, due to the local climate conditions in the southeast of the Netherlands differential freezing has not been considered as a critical design issue.

3 Design of the EPS Construction Including Stability Shortened Slope

The design methodology for lightweight embankments is widely analyzed and matured. In practice, one of the underexposed aspect concerns the introduction of resulting horizontal stresses caused by friction between the EPS blocks in the

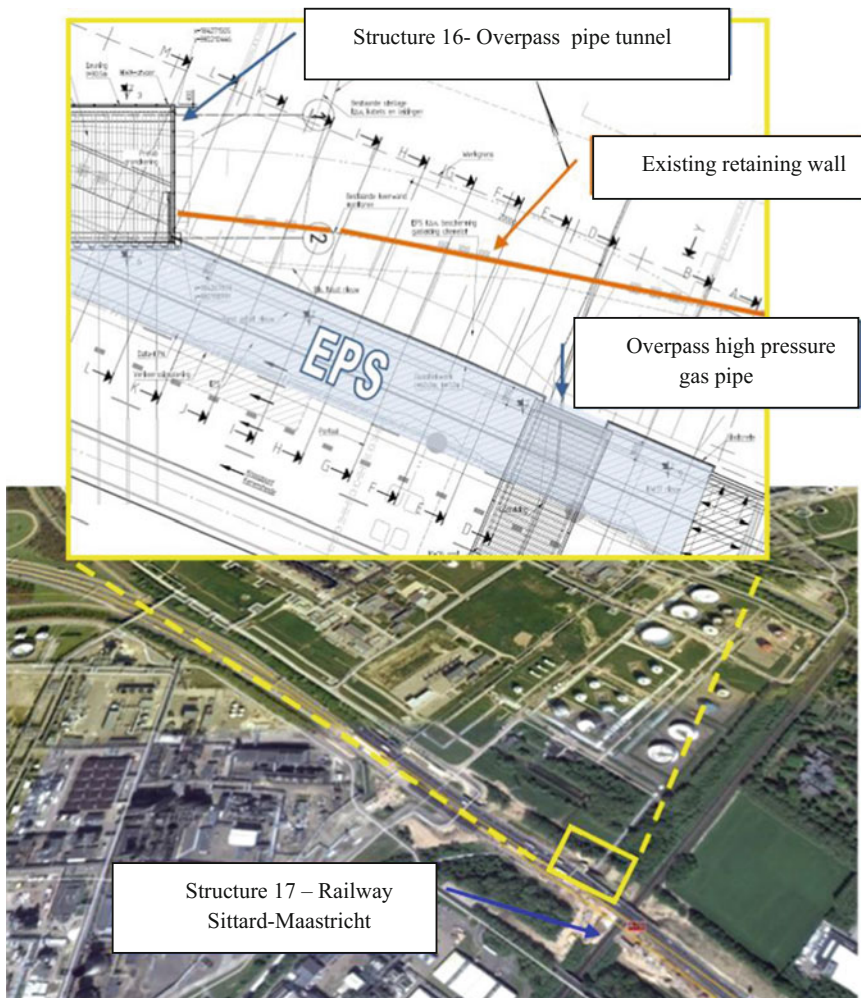


Fig. 1 Satellite image of the A76 near the A2 Kerensheide junction with the highway and layout plan with the 60 m long lightweight highway section. The EPS is highlighted and the existing retaining wall indicated with a thick line. The road section is located between two engineered structures; at the west KW16 above the tunnel of the mining tracks; at the east KW17. The overpass of the gas pipeline is also visible

different layers. The question for both the contractor and the client was namely to which extent should the structure be regarded as an earth-retaining structure and how could it be proven that the structure made up of stacked up blocks would be sufficiently stable. In other words: how can be shown that the loosely stacked up EPS blocks would not shift under any given load combination.

Through a parametric study, it has been verified within which range the elasticity modulus and the friction coefficient of EPS should lie in order to be able to bear the usual load combinations applied on retaining structures.

Several relatively complex models of the embankment including interface elements (making thankful use of the expertise of Dr. Liu Xueyan) were calculated using Plaxis 2D (Fig. 2). The resulting vertical and horizontal stresses are shown in Figs. 3 and 4. The conclusion to this parameter study was that the EPS construction was found to have sufficient stability under all load conditions.

The purpose of the additional Plaxis calculations was not to check more realistic scenarios with respect to the already reported outcomes. On the contrary, the client wanted to gain more insight into the robustness of the lightweight construction under theoretical high loads and unrepresentative low values for the E-modulus/friction coefficient. In that context, the vertical loads imposed as a result of increased traffic amounted to 30 kN/m^2 . (Actually, this value is unrealistically high for traffic load and means in practice >10 tons per linear meter on all traffic lanes). The elasticity modulus of the concrete layer was reduced to 10,000 MPa. Finally, the friction coefficient was reduced to unrealistically low levels.

Because the EPS blocks are placed approximately 2.5 m below the original slope line, the road widening has not resulted in additional burden on the existing retaining wall. Additional vertical effective stress—and thus settlement of the ground—are avoided and therefore the construction can be described as a neutral construction. The existing gas pipeline will therefore undergo no deformation. The design also meets the requirements with respect to residual settlements (absolute and differential settlements in the cross section) of the road widening, which was shortly after construction opened to traffic.

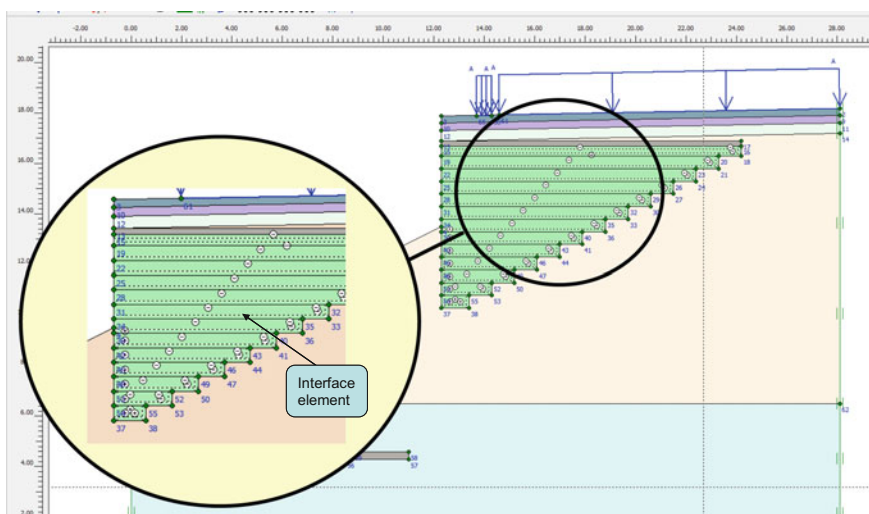


Fig. 2 Plaxis-model of a transverse section of the A76 with visible interface elements between the EPS-layers for the control of friction effects on the constructive behaviour; in order to meet with the requirements of Dutch Rijkswaterstaat—RWS

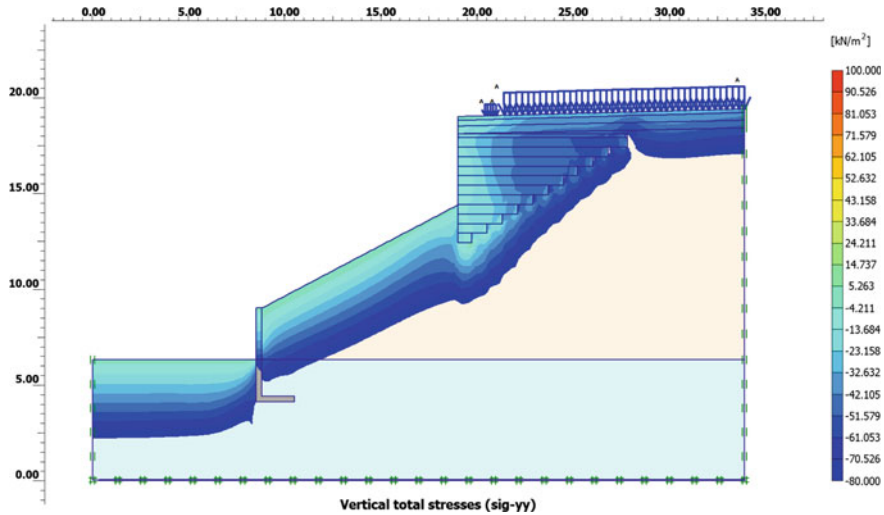


Fig. 3 Vertical stresses in a characteristic cross section caused by the own weight of the pavement layers and the barrier plus uniform vertical load of 30 kN/m^2 on the road surface

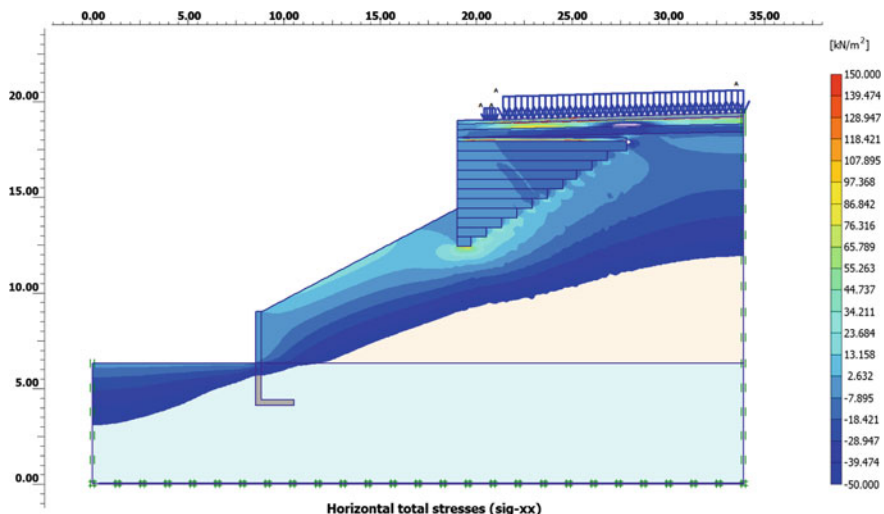


Fig. 4 Horizontal stresses in a characteristic cross section caused by the own weight of the pavement layers and the barrier plus uniform vertical load of 30 kN/m^2 on the road surface

The elevation of the top of the existing asphalt of the A76 is around NAP +79.5 m and the ground at the foot of the embankment at about NAP +66.5 m. In order to properly map the local ground profile is a geotechnical survey conducted in the form of CPT's, core-drilling and laboratory tests on soil samples. The natural ground



Fig. 5 The highway widening of the A76 with the not yet covered EPS side; The EPS bulk is piled up 4 m above the slope line; the truncated slope is supported by an existing retaining wall. The new concrete wall in the foreground has only a shielding function for the EPS construction in case of calamities from the Chemelot terrain

next road embankment consists of sand and loamy sand, this from ground level down to a greater depth (Fig. 5).

To address the stability aspects of the EPS and road construction, two controls have been carried out: control of the possible emergence of a potential slip plane immediately below the EPS construction; known as the shallow slip plane (just along the top of the existing retaining wall); and control of the possible emergence of a potential slip plane entirely under the existing retaining wall; known as the deep slip plane. The slip plane calculations were performed with the software MStab from Deltares Systems and then verified with Plaxis. It has been established that the safety against sliding of the structure, including the traffic load, complies with the requirements of the client, Rijkswaterstaat (Dutch Department of Public Works) and the prevailing standards.

4 Savings and Additional Benefits

Because some EPS slopes proved to be constructively unnecessary (Fig. 6), this design provides additional advantages over designs using traditional fill materials such as: lower construction costs (by reducing the volume of EPS and less land expropriation), smaller space requirements, shorter construction time, no top load/settlement directly along the embankment and no additional load on the underground infrastructure directly along the route. However, this new design solution requires specific expertise.



Fig. 6 Constructively unnecessary embankments made from EPS blocks: sections between the lines (reference: highway N207)

5 Conclusions

It has been proved that building a highway widening with a vertical embankment using EPS blocks is possible. As a result, the widened section can be realized without increasing the ground stresses so that post settlements can be minimized, and the existing structures require no adjustments. The mathematical fundament for the design required particular attention to the necessary range of the friction coefficient. This analysis of the coefficient of friction should also be given due consideration in future projects.

By using EPS blocks, infrastructural embankments and extensions can now be achieved cheaply and quickly without unnecessary embankment slopes. The proof of this is to be found in Limburg, in the southeast of the Netherlands.

References

1. Negussey D (2000) An investigation of geofoam interface strength behavior, Geofoam Research Center Syracuse University. Paper presented at the Soft Ground Technology Conference, Noordwijkhout, Netherlands, May 2000
2. Duškov M (1997) EPS as light-weight sub-base material in pavement structures. Ph.D. Thesis, Delft University of Technology, Delft, Netherlands, 251 p

Dutch N201 Road Embankment with EPS Geofoam



Milan Duškov and Wim Erkelens

Abstract The new section of the provincial road N201 between the Amstel aqueduct (founded on piles) and a junction near Uithoorn characterizes a 200 m long lightweight road embankment which is necessary because of local settlement sensible subsoil. In total 14,000 m³ EPS is built-in in this up to 4.1 m high embankment despite applied preloading and partial weak subsoil replacement. In the scope of the designing process the subsoil parameters for the Plaxis models were adjusted on the basis of the monitoring results. In this way the road embankment design was optimized regarding both the structural and the settlement behaviour. However, visual inspections carried out by the supervision team of the province North Holland in combination with quality controls in laboratories during the construction process pointed out serious shortcomings of delivered materials and the construction work. Therefore the design had to be adjusted twice to guarantee the design life of the lightweight road structure and to minimize the settlements. Specialized technical assistance was necessary to ensure timely and effective checks needed and to prescribe appropriate compensatory measures. Obviously, contractors often underestimate the consequences of the use of EPS in engineering practice and the differences between geofoam blocks and other conventional embankment materials.

Keywords Project case · Lightweight road embankment · EPS quality control
Redesign during construction

M. Duškov (✉)
InfraDelft, Delft, The Netherlands
e-mail: milan.duskov@infradelft.nl

W. Erkelens
Province of North-Holland, Haarlem, The Netherlands

1 Introduction

As part of the implementation of the Masteplan N201+, a part of the provincial road N201 was relocated near Uithoorn, on the border between the provinces of North Holland and Utrecht. This new road section includes an aqueduct under the Amstel River. Due to local subsoil compressibility related problems and the necessary high altitude of the aqueduct highest part (which serves as a defense against flooding), a 200 m long lightweight road embankment was realized adjacent the concrete aqueduct access road on pile foundation. The maximum altitude difference was 4.12 m in relation to the ground level. This paper describes the boundary conditions, quality controls and redesign aspects during construction. The adaptations of the pavement structure design was twice necessary to guaranty the design life of the road construction.

2 Situation, Subsoil Profile and Design Premise

The subsoil of the local polder landscape is compressible and settlement-sensitive due to the presence of soft clay and peat layers as in Fig. 1 illustrated. Such unfavorable subsoil conditions were problematical for the construction of a more than 4 m high road embankment at the site. The subsoil bearing capacity was slightly improved by applying multiple sand layers as preloading. However, the original embankment design by means of a traditional preload could not prevent undesirable significant influence on the nearby objects during construction activities. The necessary height of the sand preloads could therefore not be realized without negative consequences over the entire length of 200 m of the relevant road section. Even local subsoil improvement by digging out the upper peat layer was not a satisfactory solution. A cause-oriented lightweight design in accordance with the principle of minimum additional embankment own weight proved to be necessary for adequate settlement reduction/minimization. The considered road embankment has been since May 2014 in service and connects without thresholds to both the northwest concrete overpass and the south-eastern aqueduct.

The design analysis involved both the constructive and settlement aspects of the relevant lightweight road embankment (consisting of 14,000 m³ EPS geofoam blocks, 25 kg/m³) and the belonging pavement structure. Thanks to the applied fill of ultra lightweight EPS blocks, vertical load on the subsoil layers and thereby the effect on the neighboring greenhouse complex could be minimized. The design of the lightweight elevation optimally took into account all relevant specific aspects. “Optimum” refers here to the required design life, allowable settlements, maximum stress values and dimensions of the EPS fill (Fig. 2).

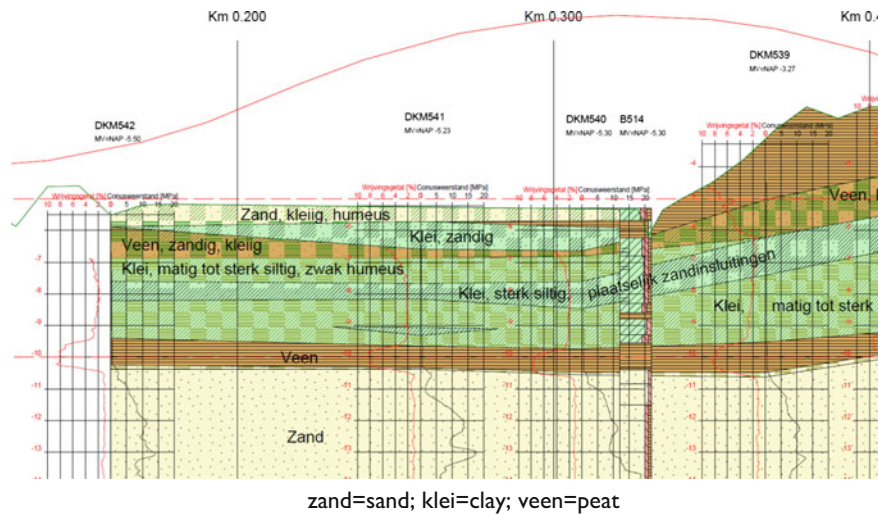


Fig. 1 Local subsoil profile based on probe results along the N201 route with clear distinction between the lower area and the upper polder near the Amstel River



Fig. 2 Lightweight embankment of the provincial road N201 nearby Uithoorn and the aqueduct under the Amstel River under construction

3 Terms of Reference

The project terms of reference for the N201 lightweight embankment construction set by the province of North Holland were determined mainly by (a) local altitude differences between design road surface and the ground level, (b) the necessary pavement layer thicknesses, (c) pre-loading in the past and (d) cost-effectiveness of the design (without consequences for durability, settlement behaviour and embankment

stability). For example, the maximum permissible residual settlement determined by the province was 10 cm in the middle road section after 30 years to limit road users discomfort. Nearby concrete road parts founded on piles only negligible settlements were permitted. Also, no permanent deformation or damage of the road construction during the design life was aloud.

The traffic intensity of medium and heavy motor vehicles amounted to approximately 2300 vehicles a day in both directions for this part of the new N201 road section. The growth rate of the increase in traffic intensity has been set at 1.5% per year until 2034 when the lifetime of the pavement structure ends contractually.

4 Plaxis Modelling

The preload (sand) thicknesses have not been uniform along the entire N201 road section route. However, vertical drains have been drilled everywhere. The sand thickness reached a local height of 3.5 m. The effects of different preloads and the use of vertical drainages were determined by two-dimensional Plaxis models. This finite element-based program made it possible to quantify the actual effects of such consolidation acceleration measures for different thicknesses/lengths/widths of EPS sublayers. Such insights resulted in a minimization of the total amount of EPS and thus a cost reduction. Also, different types EPS and roadbase layers could be checked regarding calculated stress values and settlements (Figs. 3 and 4).

5 Supervision During Realization

For an optimal construction supervision, the province of Noord-Holland made use of specific experience/expertise of InfraDelft. The supervision team was thus in position to monitor effectively delivered EPS blocks as well as pavement material quality. The quality control focus was on delivered material specifications, real material properties, exact volumes, compaction degrees and layer thickness control. For the checking of real EPS and foamed concrete characteristics, on behalf of the province North Holland the certified inspection institutes carried out mechanical tests on selected material samples. For example, mechanical testing on drilled EPS cores was the only way to determine its actual compressive strength and modulus of elasticity. In addition to timely and adequate controls, the specialized technical assistance provided the necessary compensatory measures when considered necessary during realization. In this way, the province of North-Holland was able to anticipate and adjust the design during road construction, so that the final result guaranteed the intended sustainability and the required settlement behaviour (Fig. 5).

The control calculations of buoyancy forces also confirmed safety factor values higher than required minimum factor (=1.1) in all relevant cross sections of the

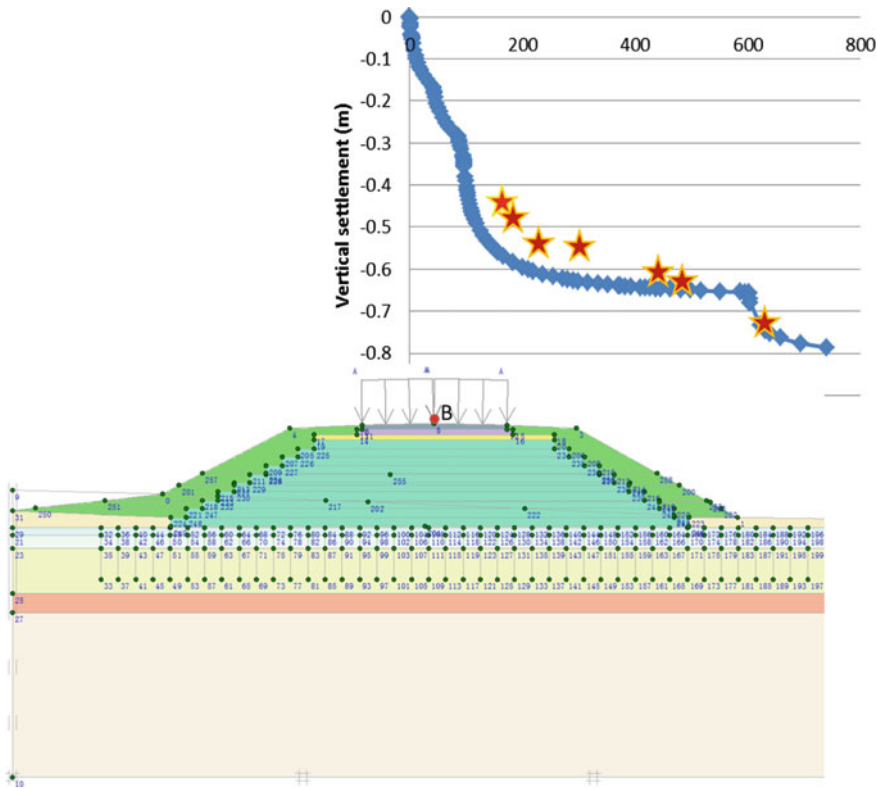


Fig. 3 Measured (by means of settlements rods) versus calculated (by means of Plaxis model) settlement progression in time due to preloading along the N201 road route

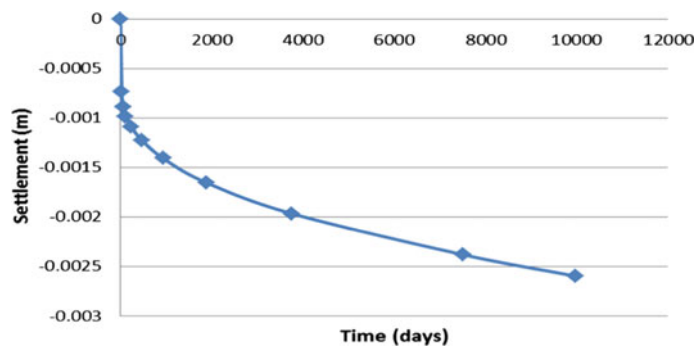


Fig. 4 Calculated settlements for a period of 30 years by means of the Plaxis model of a representative N201 road construction cross section

Fig. 5 Visible EPS fill belonging to the lightweight N201 road embankment nearby the aqueduct



N201 road embankment. However, for absolute certainty, additional ground monitoring wells were placed near the aqueduct. Obviously there was absolute clarity about the local groundwater level needed because of unacceptable consequences if buoyancy forces would have caused problems. During the construction phase, the pump draining was also implemented in lower route sections.

6 Problematical Realization Aspects and Redesigning

Sometimes (functionally unnecessary) additional treatments, such as the gluing of successive EPS sublayers, result in complications. Glued blocks made it difficult to move those during the stacking-up process without causing damage. Another issue was the transport of building materials over the EPS fill without any protection. Once locally overloaded EPS (consequently damaged cell structure) has less good mechanical behaviour than assumed for the design. Fortunately, it happened on a limited scale below the middle of the road where no traffic load occurred. All in all, the risk of those shortcomings for an inadequate final result was considered to be practically negligible.

6.1 Redesign Due to Inadequate EPS

The delivered EPS blocks turned out to be an issue of importance. As mentioned above, for control purposes, certified inspection institutes tested selected samples. The results show that the weak blocks had up to 20% lower (average) stiffness than the minimum required values. “Average” meant also lower minimum stiffness values (-25%) were measured on some samples. The amount of weak EPS blocks supplied has been significant. Furthermore, block widths varied between 1250 and

1270 mm. As a consequence, unwanted local 4 cm wide open joints occurred during the stacking-up of the EPS blocks. This was undesirable due to lack of support at the bottom for the next upper layer. In view of the magnitude of the identified shortcomings and the estimated possible impact on the final result, the review of the design was considered necessary to anticipate the observed deviations. The design in realization had to be revised mainly because a part of the EPS blocks delivered did not meet the design requirements in terms of constructive behaviour. The design adjustments had to guarantee both the proper design life and the settlement behaviour of the lightweight road construction under consideration in the current situation.

In order to compensate for the identified serious shortcomings, the pavement structure has been redesigned based on iterative calculations. The redesign pavement concerned the roadbase at the top of the EPS fill. The changes in asphalt and granulate thickness could be avoided. In order to deal with the weaker delivered type EPS than originally advised, the 0.3 m thick layer of foamed concrete was adjusted. An identical thick but stronger layer of heavier SB700 (dry bulk mass 700 kg/m³) guaranteed sufficient load distribution. In this way, the stress values caused by heavy trucks were sufficiently reduced for the actual weaker EPS type and the delivery problem was adequately solved.

For the dimensioning of flexible pavement structure with an asphalt surface, the linearly elastic multi-layer programs CARE of Dutch Rijkswaterstaat and BISAR of the Delft University of Technology have been used. Flexible pavement designs are based on the expected numbers of standard axle load repetitions. This determines the thicknesses of asphalt and foundation layers at the top of the EPS fill based on the prescribed fatigue curves. The horizontal strain level at the bottom of the asphalt layer is the benchmark design criterion combined with the vertical strain values at the top of the EPS package. The resulting strain values must ensure durability of ≥ 20 years of the asphalt top layers for the accumulated traffic load in accordance with the fatigue ratio. In addition, the results had to indicate sufficient load distribution above the EPS layer. The calculated vertical strain value at the top of the EPS had to remain within the prescribed linear elastic limit also under maximum axle loads increased with the own weight of the pavement layers.

6.2 Redesign Due to Inadequate Foamed Concrete

Unfortunately, the realization in progress had to be stopped for the second time by the supervision team of the province of North Holland because the foamed concrete did not comply with the material specifications in accordance with the redesign report. The applied foamed concrete had significantly lower both compressive strength and modulus of elasticity than prescribed. Therefore its constructive behaviour did not comply with the material characteristics according the program of requirements. Actually, identified variations in mechanical properties in the foamed concrete layer were found to be very high, potentially causing local weak spots

everywhere. The proposed design life was no longer achievable with the poured foamed concrete without extensive recovery measures.

Confronted with findings, the province of North Holland preferred complete removal of the inadequate foamed concrete layer and replacing it according to the specifications. To revise the design for the second time is highly unusual and the relevant road section could not be finished on time any more. However, the removal of directly at the top of the EPS fill hardened foamed concrete was found to be practically impossible without (too) high risks. In accordance with the submitted recovery plan, the contractor wanted to use a hydraulic sledge hammer. In that case resulting stress values would inevitably lead to significant plastic deformations in the underlying EPS fill.

At last, based on the additional calculations the adjustment of the roadbase turned out to offer the best pragmatic solution. The supervision team of the province North Holland and the contractor agreed finally about this approach instead of highly risky removal of the inadequate foamed concrete layer. The unbound foundation layer thickness was reduced to 0.2 m and a 0.1 m thick concrete layer was poured on top of the already hardened foamed concrete layer. In this way, the stress values within the EPS fill were sufficiently reduced and no problems were expected either during realization of work or in-use phase of the N201 road embankment (Fig. 6).

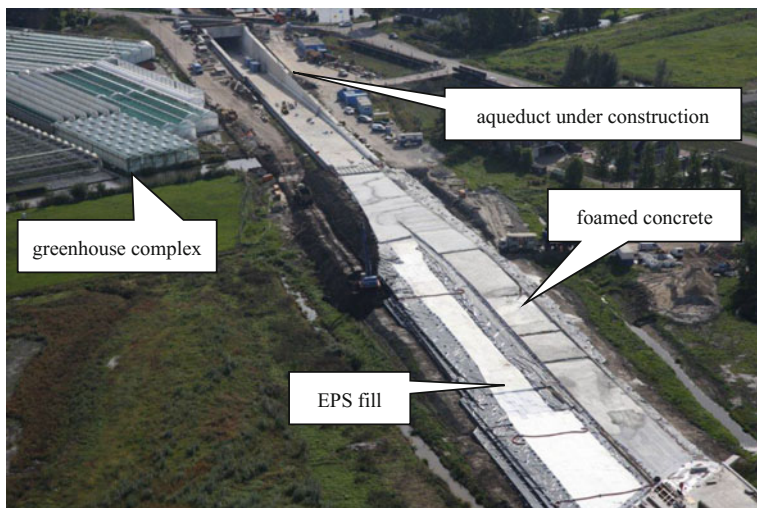


Fig. 6 Aerial view of the N201 road embankment with visible EPS fill and still unfinished foamed concrete layer

7 Recommendation

If a relatively large volume of EPS geofoam is implemented, the quality control based on the delivery documentation is insufficient. Actually, the supervision team of the province North Holland had to hire a specialized technical assistance and organize auditing tests by certified inspection institutes for control purposes. Due to the specific nature of the construction of EPS fills, the expert assistance is recommended. Such specialized assistance is intended for design revision when necessary.

References

1. CUR (1995) Werken met schuimbeton – Eigenschappen en toepassingen, CUR publicatie 181. Gouda, Netherlands
2. Duškov M (1997) EPS as light-weight sub-base material in pavement structures. Ph.D. Thesis, Delft University of Technology, Delft, Netherlands, 251 p

Post-use Examination of EPS Block Characteristics: Finnish Case Histories



Gowthaman Sinnathamby, Leena Korkiala-Tanttu
and Henry Gustavsson

Abstract Since its introduction as a lightweight fill in the 1980s, EPS has been used in a number of test highway embankments across Finland. This paper presents the experiences in using EPS blocks as structural element in two lightweight road/highway embankment sites in Finland. These embankments were built on soft soil deposits and therefore, the EPS was introduced to improve the bearing capacity of the ground and to subsequently reduce settlement. Once the use was ceased, the EPS blocks were retrieved from the embankments and tested for their water absorption characteristics and mechanical properties. These properties were then compared with their original properties and other relevant local standards in order to assess their potential reusability. The test results revealed that the retrieved EPS blocks still fulfilled the mechanical requirements of the Finnish guidelines after being in contact with the ground for over 14 years. One of the primary goals of this study was to increase the competitiveness of EPS in civil engineering applications and to encourage the reuse of EPS in other civil engineering applications in Finland. The information presented in this paper is intended to provide an understanding of the performance of EPS blocks in lightweight fill applications. It may also assist engineers in design and construction methods of similar EPS applications, and the potential reusability of such used EPS blocks in various other applications.

Keywords EPS · Lightweight fill · Ground improvement · Recycling
Sustainable construction · Circular economy

1 Introduction

Expanded polystyrene (EPS) is a geofoam that is commonly used in various civil engineering applications ranging from building insulation to ground improvement-settlement prevention in road construction. EPS road structures not only address the

G. Sinnathamby · L. Korkiala-Tanttu (✉) · H. Gustavsson
Department of Civil Engineering, Aalto University, Espoo, Finland
e-mail: leena.korkiala-tanttu@aalto.fi

technical challenges in soft soil construction but also accelerates the construction process, thus adding socioeconomic benefits especially in urban settings.

Norway has become the first country to introduce EPS blocks as lightweight fill in road embankments almost 45 years ago (1972—Norwegian Public Road Authorities) [3]. Since then, the use of EPS as lightweight fill in road construction has widespread across the globe and is currently being used in countries like Canada, France, Germany, UK, USA, Sweden, Japan, New Zealand, The Netherlands and Finland.

Between 1999 and 2000, a number of EPS lightweight embankment pilot studies were conducted in Finland. The primary objectives of these studies were to develop and specify design procedures for EPS lightweight embankments and to increase the competitiveness of EPS in the construction industry as a substitute lightweight fill [4]. Construction feasibility and performance of these EPS lightweight embankments were also assessed.

Findings from two of the EPS lightweight embankment sites located in Muurla/Salo and Jupperi/Espoo are discussed in this article. Of these two sites, Muurla was a highway and Jupperi was a street.

Over the years, various in situ and laboratory studies were conducted in order to study the mechanical and water absorption characteristics, and the potential reusability of the used EPS blocks from these sites. Assessing and understanding the overall performance of the EPS blocks was another objective. This paper presents the overall experience in using EPS blocks as lightweight fill in test embankment sites in Finland. Technical details from these test sites will be reported separately in a journal article.

2 Muurla EPS Lightweight Embankment

The Muurla EPS lightweight test embankment was located near Salo. The 170 m long test section was part of a temporary road connection of highway E18 and was in operation from 2003 to 2008 with the design service life of 10 years. The thickness of the EPS embankment varied between 500 and 1000 mm and the width was approximately 18 m. A steel grid was mounted to the subbase layer over a 80 m long-section in order to increase the stiffness of the upper part of the pavement. The base layer was a 180 mm thick cement stabilized layer. The subsoil was a clay deposit (normally consolidated or slightly over consolidated with undrained shear strength of 9–20 kPa) with varying thickness of 14.5–16.5 m. The top 0.8–1.7 m was dry crust. Preliminary calculations showed that the factor of safety (FOS) at this location was below the required level of 1.5 with a minimum FOS of 1.3. Therefore, a lightweight embankment was proposed which with the partial reduction of embankment weight, increased the FOS to 1.9 [7].

2.1 Site History

The construction of the Muurla temporary road connection was done between 2001 and 2002, and was opened for public use in 2003. After 4.5 years of use, the temporary road access was closed during midsummer 2008, but was dismantled only in 2016. The EPS blocks were about 6 years old when the operation was ceased in 2008. A measurement and sampling programme was conducted in order to investigate the performance of the EPS-blocks and the overall embankment when the operation was ceased and the findings are reported in Kivikoski and Juvankoski [6]. The latest investigation was conducted when the embankment was dismantled in 2016. One of the aims of the Muurla lightweight EPS test embankment was to study how an EPS embankment without a concrete plate performs under heavy traffic loading. Developing better design methods and guidelines of EPS embankments was another objective [8].

2.2 Site Location and Design of the Embankment

The Muurla EPS embankment site was on the connection road to the new highway E18 (Fig. 1) from the existing Helsinki-Turku highway 110. The EPS section of the embankment was installed between chainage 1180 and 1350, a total length of 170 m (Fig. 2). The steel grid section was located between chainage 1260 and 1350, over a length of 90 m [8].

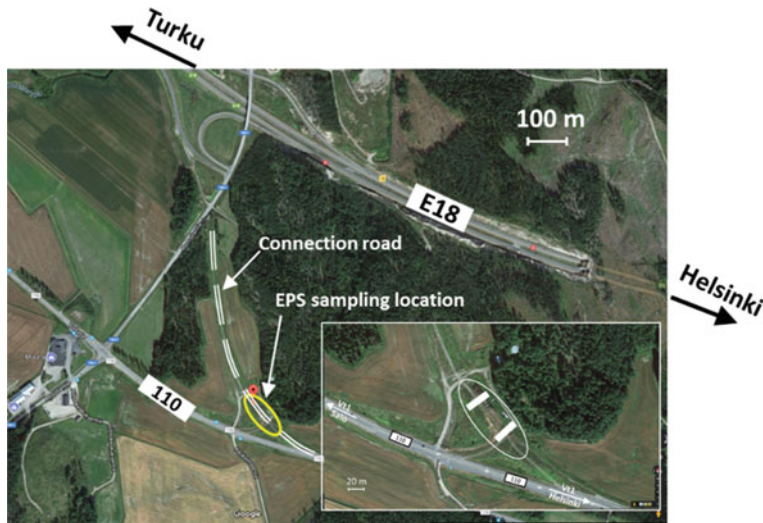


Fig. 1 Site location of Muurla EPS-test embankment and sampling location of EPS test specimens (Source Googlemaps)

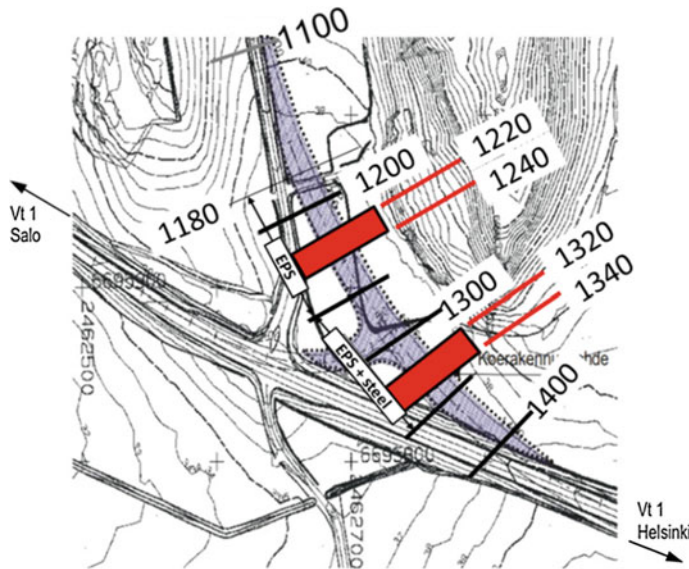


Fig. 2 Sampling location (chainage) of EPS test specimen (Modified from [7])

EPS blocks with sizes $0.5 \times 1.2 \times 3.0$ m ($T \times W \times L$) and $0.25 \times 1.2 \times 3.0$ m were used in different combinations in order to achieve the required thickness and they were placed on top of a levelled sand layer (Fig. 3). The blocks were anchored together with steel barbed connector plates. The EPS blocks were then covered with a 0.2 mm thick plastic sheet. An overlaying geotextile (SP4) layer protected these plastic sheets. Crushed rock with grain size of 0–16 mm was placed on top of the EPS blocks with varied thickness between 0 and 300 mm, depending on the requirement of the final road surface profile.

A minimum of 700 mm thick granular layer was placed on top of EPS in order to prevent skidding on the road surface during winter months. A 150 mm thick stabilized composite crushed rock layer was used in the upper part of the base layer

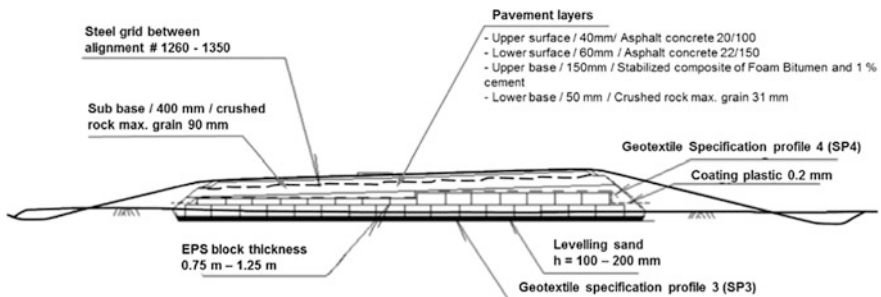


Fig. 3 Sectional view of the EPS-test embankment [7]

for stiffening the upper part of the structure [8]. Detailed information on the construction methods and stages of construction are well documented in earlier publications [8].

2.3 Observations and Lessons Learnt

Overall, the Muurla EPS pavement demonstrated that a stable lightweight pavement for a temporary road with high volume traffic can be constructed using EPS-blocks, without a concrete plate but instead stiff layers above EPS, such as a cement stabilized base layer in this case. For longer service life, a more stiff pavement layer or concrete plate would be needed. This kind of EPS lightweight embankment may be even more economically applied for low-volume pavements such as rural roads, streets, parkings etc. The applicability of EPS as a lightweight fill in pavements has been technically proved, as well as the design methods have been tested.

2.3.1 Dismantling and Observations

The dismantling of the Muurla EPS-test embankment was done in 2016 (Fig. 4a, b). The retrieved EPS blocks from the Muurla embankment were installed in noise-barrier composite structure on the sides of Ring Road I in Konala, Helsinki. Several in situ and laboratory performance assessments were conducted on the used EPS blocks after a ground contact of around 14 years.

The primary objective of the performance assessments was to evaluate the recyclability of the used EPS blocks and their long-term performance in an EPS lightweight embankment. This intends to enhance the knowledge of EPS-embankments and eventually leads to better design methods and construction practices.

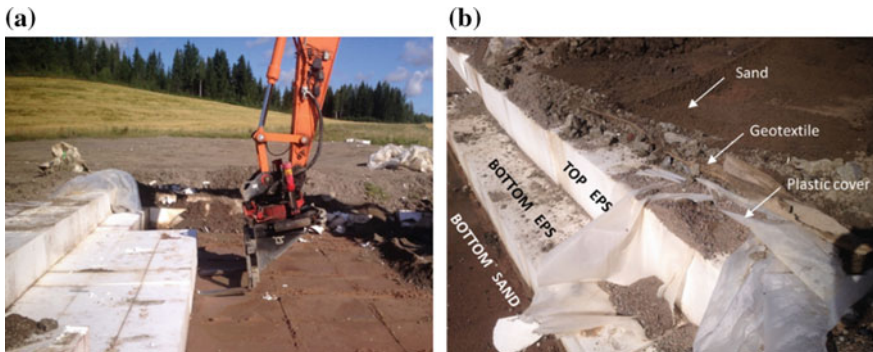


Fig. 4 Pictures from the Muurla EPS embankment: **a** removal of EPS blocks for reuse and, **b** in situ conditions of the EPS test embankment

Performance assessment involved a number of in situ observations, field measurements and various laboratory tests.

In situ straight edge profile of the upper EPS block surface as well as the rutting of the EPS blocks were measured during dismantling of the embankment. Moisture content and mechanical properties (compressive strength) of the EPS blocks were measured at the laboratory from collected EPS specimen. Test results were then compared with previous results reported by other researchers (e.g. [6]).

2.3.2 The Lightweight Pavement

In general, the EPS lightweight pavement in Muurula performed well during the operational period. The measured differential settlements varied between 20 mm and 160 mm, but in general it was within the estimated settlement of 140 mm (Fig. 5) [6, 7]. According to the Finnish Transport Agency's guidelines, the maximum permissible settlement on a motorway with a speed of 120 km/h is 300 mm during a 50-year period [2]. However, this permissible settlement value may be reached during a short design life for a temporary structure, similar to the one in Muurula. Thus, it can be concluded that the temporary EPS road structure in Muurula performed relatively well against settlement.

Overall, the EPS-layers preserved their elasticity and original thickness. Thus, the influence of plastic irreversible deformation on pavement surface was minor. As stated in a previous investigation [6], the main damages were caused by the stabilised layer which had reduced thickness from the designed value during construction on the “EPS+steelmesh reinforcement” section. Further, the EPS-lightweight fill proved to

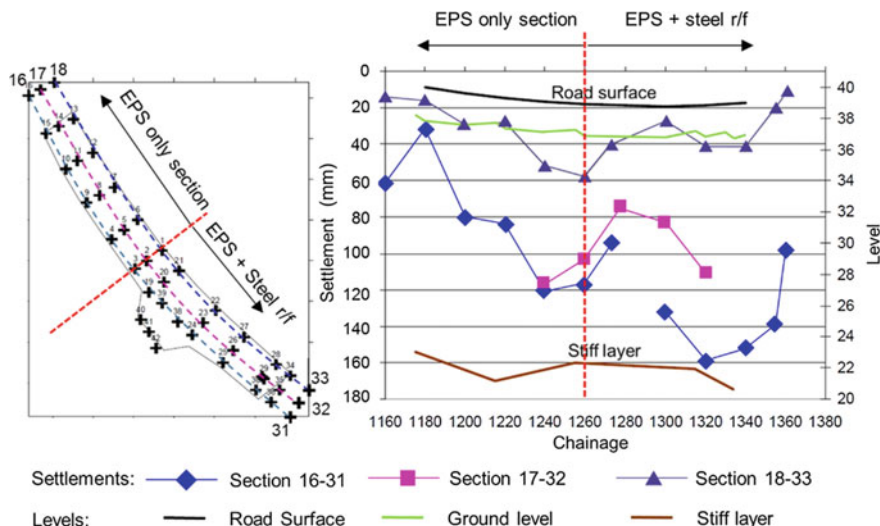


Fig. 5 Measure settlement profile during 2008 [6]

be comparable with adjoined reference pavement as well as the transient structure containing LECA (Lightweight Expanded Clay Aggregate).

2.3.3 The EPS Blocks

Heavy machinery, a flat-bladed forklift that was attached to the excavator, was used to dismantle the embankment (Fig. 4a). In general, the EPS blocks were handled well and retrieved with minor damages; however, trained professionals and cautious handling of removal and transport would reduce the amount of damaged EPS blocks further. The working tools and methods for dismantling old EPS structures should be developed in order to minimize the deterioration and damage to the EPS blocks. The disposal of EPS-waste into landfills should be prevented, because EPS will stay in the environment for prolong periods of time.

The tested retrieved-EPS blocks, after being used as a light-weight fill, still satisfied the minimum compressive strength requirement. They also exhibited a very low moisture pick up despite the fact that the groundwater fluctuated significantly in certain locations. The maximum observed volumetric water content was around 7% (this particular EPS was partially submerged under the water table for a certain period). This amount of water can be considered insignificant for a light-weight fill. Further, this low moisture pickup value has no practical influence on insulation properties of frost protection applications in roads and railway embankments. Similar trend was also observed at the Jupperi/Espoo site.

The mechanical properties of investigated EPS blocks proved to be similar to that of the parent product. Thus, the used EPS blocks could be reused, in principle, in similar applications to the original product; i.e. as part of fills, frost protection etc, if the blocks are intact and undamaged. However, the retrieved blocks that underwent alteration in their shapes are no longer suitable for lightweight fill applications and maybe used in secondary applications. Of those EPS blocks retrieved from Muurla site and subsequently transported to the noise barrier site in RingRoad I, at least 99% of EPS was reused in construction and only a small amount of spall and otherwise cut-out pieces of EPS were disposed as construction waste and delivered to a landfill.

3 Jupperi EPS Lightweight Embankment

The Jupperi EPS-lightweight road embankment was located at the intersection of Pitkäjärventie and Riihiniityntie/Tamnipääntie (formerly Jupperintie), near the Espoo–Vantaa border (Fig. 6). The site was located on a peat area, thus an EPS-lightweight road embankment was introduced to increase bearing capacity of the ground and to reduce settlements. Full-scale EPS blocks with dimensions of $0.25 \times 1.0 \times 3.0$ m were used on this site.

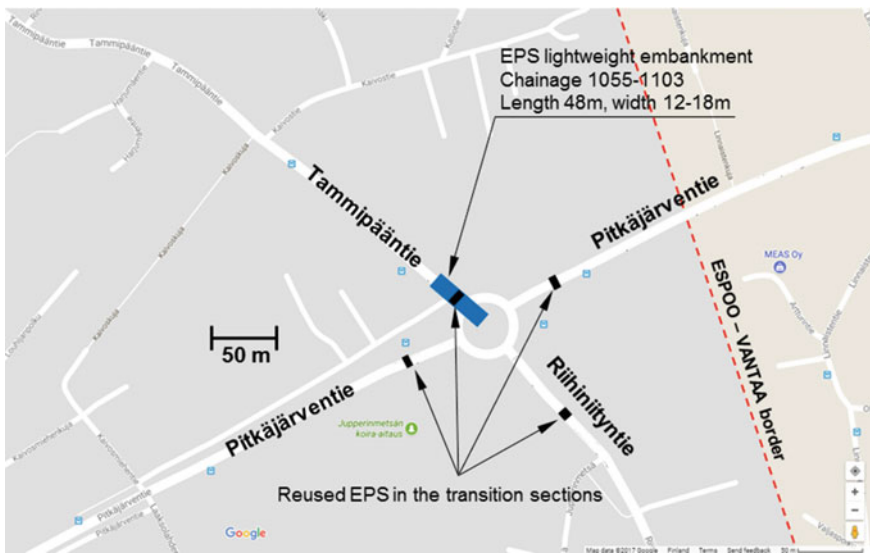


Fig. 6 Location of the original Jupperi EPS lightweight embankment and the location of reused EPS blocks in transition sections after the construction of a roundabout (*Source Googlemaps, taken on 15.06.2017 at 14:25 EEST*)

This EPS road section stretched over a length of 48 m between chainage 1055 and 1103. The plans and design of the embankment were made in 1992 and the construction was completed in 1996. After nearly 16 years, in 2012, a roundabout at this location replaced the existing intersection. The old EPS-structure was dismantled and the area was stabilised by mass and column stabilisation (Fig. 6). Recovered EPS blocks were then used in the transitional section between the aforementioned mass-column stabilised road section and the normal section (Fig. 6).

3.1 Site History

The proposed site was located on a 0–3.5 m thick peat layer with water content of 500–1000%. Anticipating significant settlement over the years in the peat layer, EPS-blocks were incorporated in the pavement design for settlement mitigation. Underneath the peat, there was a clay layer with a thickness of around 0–4 m. Moraine and silt layers were found underneath the clay layer. The groundwater table was at 0–1.5 m below the top surface of the peat layer. EPS-blocks with density of 20 kg/m³ were used as the lightweight fill at this embankment site. The density was tested randomly, at least one piece per batch, and the value of a single block should not exceed the required density by more than 10%. The compressive strength of the EPS blocks was at least 90 kPa at 5% compression. A geotextile (class IV) was

installed on top of the EPS blocks, on which a minimum of 300 mm thick crushed aggregates (0–32 mm) and 370 mm thick crushed aggregates (0–64 mm) and a 130 mm thick bonding layer were placed. A profiled steel sheet layer laid the platform at the bottom of the excavation on which a levelling granular layer was placed (Fig. 7).

3.2 Observations and Lessons Learnt

Two $0.25 \times 1.0 \times 3.0$ m EPS-blocks (one upper and one lower blocks from the same location) were collected from the site during removal and were tested for change in dimensions (density), volumetric water content, compressive strength and thermal conductivity. The designed bottom level of the EPS-blocks was at +33.18. The groundwater table at the time of the removal was at +32.90 (i.e. 280 mm below the bottom surface of EPS) while the groundwater fluctuated between +33.27 and +34.00 with an average groundwater level of +33.65 during 2008–2011, thus indicating that the EPS blocks were partially submerged during the operational period of the embankment.

In general, the examined EPS blocks after 16 years of ground contact continued to meet the requirements and performed well as a lightweight fill. Notably, the upper layer of EPS blocks suffered rutting and damages, thus did not fulfil the thickness requirement for reuse in similar applications. The average thickness of the upper EPS block was 240 mm, which was lower than the allowed tolerance of 250 ± 3 mm. The average thickness of the lower EPS block was 247 mm, just fulfilling the allowed tolerance for thickness.

The measured volumetric water content of EPS blocks ranged between 0.05 and 1.34% (avg. 0.54%), exhibiting a very low water absorption characteristic. The average wet and dry density of the EPS blocks were 26.2 and 20.8 kg/m^3 ,

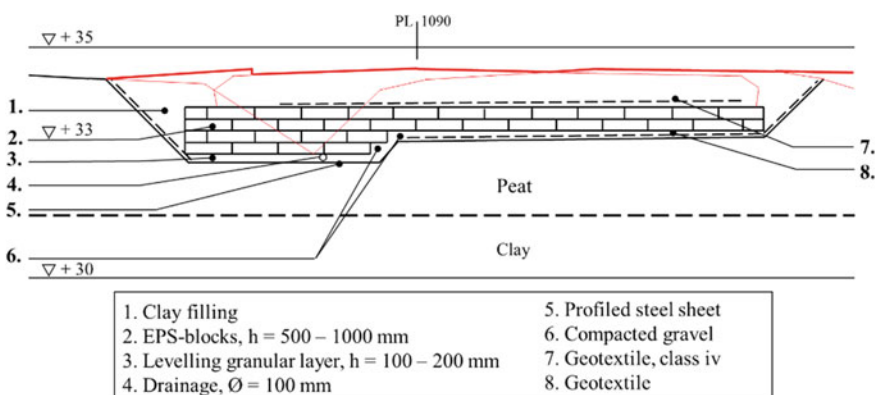


Fig. 7 Cross section of the Jupperi EPS-lightweight embankment [1]

respectively. Thus, the tested EPS blocks satisfied the required minimum dry density of 20 kg/m³ (+10%).

The average compressive strength σ_5 (corresponding to 5% compression) of the tested EPS specimen was around 125 kPa, satisfying the minimum required compressive strength of 90 kPa. The EPS blocks recovered from the Jupperi lightweight embankment were reused later in the transition zone of the newly constructed road section at the same location where a mass and column stabilised road section meets the non-stabilized pavement section (Fig. 6).

4 Conclusions

The following conclusions can be drawn from the experience in using EPS as lightweight fill material in both road embankment sites discussed in this paper.

- Overall, the EPS embankments performed well during their designed life. The post use investigations of the used EPS blocks indicated that the retrieved blocks still fulfill most of the design criteria to be used as a lightweight fill. However, the retrieved blocks that underwent alteration in their shapes are no longer suitable for lightweight fill applications and maybe used in secondary applications.
- Significant data, knowledge and experience in terms of design and construction of EPS light-weight embankments have been gathered from the test embankments in Finland. Reusability aspects of the used EPS have been satisfactory and it is recommended to increase the reuse of used EPS in secondary applications for economic and sustainable engineering practice.
- The dimensions and straight edge profile of the surface of the upper layer blocks have somewhat altered during the years and some EPS blocks do not fulfil all General Quality Requirement for Infrastructure [5] requirements. It is assumed that these deformations were not traffic induced but possibly due to the movement of heavy construction machinery during construction and/or removal periods.
- The EPS blocks performed well against water absorption. The water content of EPS material when in contact with soil could increase over the years especially, if it is in direct contact with groundwater. However, the observed water contents were very low, especially in the lower blocks, with an average of around 1% (by vol) and a maximum of around 7% (by vol). The upper blocks were almost dry with an average water content of 0.5%. These values are insignificant considering the length of the period of ground contact.
- The compressive strength of the tested EPS specimen remained satisfactory, fulfilling the requirements.
- The experience of reusing EPS blocks was satisfactory and reuse in similar applications is also recommended in other sites. Attention should be paid when removing and handling the EPS blocks with heavy machinery as they tend to damage the blocks close to the edges.

Acknowledgements This study was funded by the Finnish Transport Agency (Liikennevirasto), Finnish EPS Industry and ThermoSol Oy.

References

1. City of Espoo (1995) Jupperi road ground improvement map chainage, pp 1025–1103. Map No: 4469/8
2. Finnish Transport Agency (2012) Geotechnical Design of Roads (Tien geotekninen suunnittelu-Liikennevirasto) p 24 (in Finnish). https://julkaisut.liikennevirasto.fi/pdf3/lo_2012-10_tien_geotekninen_web.pdf. Accessed 21 Dec 2017
3. Frydenlund TE, Aabøe R (2001) Long term performance and durability of EPS as a lightweight filling material. In: 3rd conference international EPS Geofoam 2001
4. InfraRYL (2010) General quality requirements for infrastructure Part 1: routes and regions (in Finnish: InfraRYL2010- Infrarakentamisen yleiset laatuvaatimukset Osa1- Väylät ja alueet), p 261
5. Kivikoski H, Juvankoski M (2008) EPS test embankment in Muurula, light weight structure Studies/EPS-koeterakerinne Muurlassa, Kevennerakennetutkimukset, VTT report, VTT-S-09017-08 (in Finnish). www.epseriste.fi/doc/Loppurap_RTE50-IR-14_2003.pdf
6. Korkiala-Tanttu L (2003) The design of Muurula EPS test embankment, VTT internal report, 6.2.2003 (in Finnish)
7. Korkiala-Tanttu L, Juvankoski M, Kivikoski H (2011) Proceedings of the 4th international conference on the use of Geofoam blocks in construction applications, 6–8 June 2011. Oslo 2011. The Norwegian Public Roads Administration
8. Saarelainen S (2003) Paksun EPS kerroksen kuormituskestävyys. Final report of EPStress program, VTT internal report RTE50-IR-14/2003, VTT, (in Finnish). http://www.eps-eriste.fi/doc/Loppurap_RTE50-IR-14_2003.pdf

Analysis of Crack and Differential Settlement on Pavement in EPS After Highway Opening



Yongchai Chang and Nagyoung Kim

Abstract The lateral movement of abutment has induced significant problems in the terms of either construction and management since 1990 in South Korea. The research related to this issue has been also paid wide attention. In order to overcome these problems, modified lateral float, sand compaction method (SCP), and pile-slab method have been developed. Especially, the EPS was extensively used in the soft ground to either prevent or mitigate the lateral movement. Although the EPS is surely effective on reducing lateral movement of abutment and load during the construction, cracks and deterioration may be found on the pavement in the EPS section after opening the road. In this study, structural performance test and eye investigation of drilling cores from the site where the EPS was widely applied were conducted and analyzed.

Keywords Sand compaction method (SCP) • Falling weight deflectometer (FWD) test • Lateral movement of abutment

1 Introduction

This study conducted site investigation on the pavement in service where the EPS was used. According to the eye investigation on cored sample, crack grew to 10 cm from the surface, not reaching the bottom of base yet. Transverse and longitudinal crack were found in both lanes at the beginning of backfilling. Fatigue crack and patching work was also found in the traffic direction. In order to examine the causes of crack found in the site, crack depth from the cored samples was measured and Falling Weight Deflectometer (FWD) test was performed on both the EPS section and non-EPS section and comparison was made.

Y. Chang (✉)
Mokpo National Maritime University, Mokpo, Korea
e-mail: geo@mmu.ac.kr

N. Kim
Korea Expressway Corporation, Gimcheon, South Korea

2 Cored Sample Analysis on EPS Section

Figure 1 shows the cracks on the pavement in service where the EPS was used. As seen in the figure, the cracks are widely spread and core was drilled on these areas to measure how deep the crack propagated as seen in Fig. 2. As measured, the crack was 8–10 cm in depth, which is limited to the asphalt layer. The top-down crack generally occurs due to the repeated traffic loading such as fatigue crack unlike to the bottom up crack caused by the structural matter of pavement.

3 Analysis of FWD on EPS Section

FWD test was performed on both EPS section and non-EPS section and the deflections were compared. The FWD tested on total of four pavement sections; approach slab of EPS section, EPS section, border of EPS and non-EPS section, non-EPS section. The results are presented in Table 1.

Fig. 1 Cracks on the pavement above EPS



Fig. 2 Drilled cores on the cracked pavement above EPS



Table 1 Mechanical properties of EPS19 geofoam blocks [1]

Location	Load (kN)	Deflection (μm)						
		Distance (cm)						
		0	30	60	90	120	150	180
Approach slab of EPS section	579	281	242	221	198	179	160	141
	840	409	364	334	308	278	254	232
	1120	531	472	435	400	365	333	304
EPS section	561	449	378	315	268	237	206	176
	823	689	600	515	454	408	371	331
	1097	851	730	625	547	489	438	384
Border of EPS and non-EPS section	578	363	305	247	206	163	126	96
	836	522	438	365	300	237	185	144
	1111	680	571	478	394	313	245	192
Non-EPS section	577	160	123	92	68	48	35	27
	846	242	185	140	103	75	54	40
	1131	323	250	189	142	104	75	57

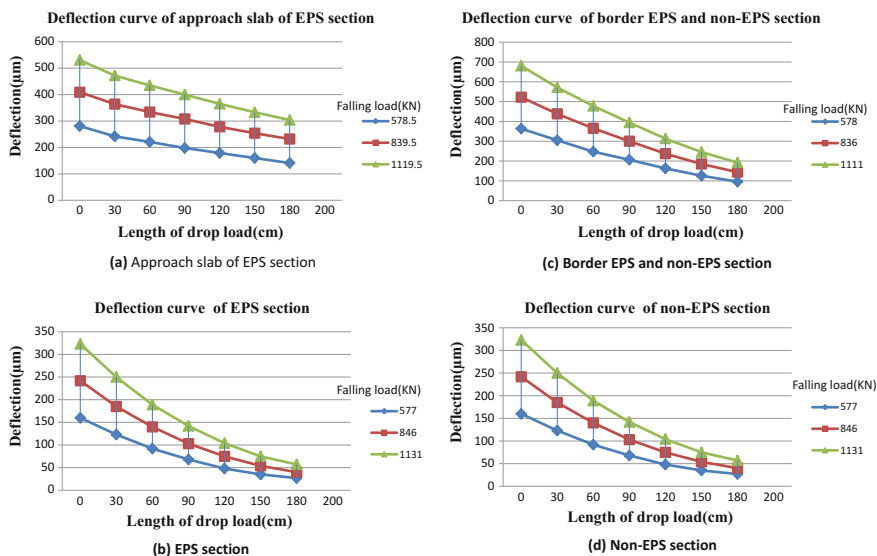
**Fig. 3** Deflection curves from FWD tests

Figure 3 presents the deflection curves responded to the drop load of FWD; (a) approach slab of EPS section; (b) EPS section; (c) border of EPS and non-EPS section; and (d) non-EPS section. As shown, the magnitude of deflection is EPS section, border of EPS and non-EPS section, approach slab of EPS section and non-EPS section in high order. The deflection of EPS section at a specific location

is three times higher than that of non-EPS section. This may be the fact that higher vibration from traffic load be generated on the pavement above EPS section. Additionally, the deflection of border of ESP and non EPS section is about 2–2.5 times higher than that of non-EPS section. It can be said that the presence of EPS make a significant difference on the pavement deflection. As a result, asphalt pavement above EPS is highly prone to undergo fatigue cracks relatively compared to the non-EPS section.

4 Conclusion

Based on investigation of cored samples from the cracked pavement and FWD test results, the conclusions of this study on the effect of EPS can be drawn as follows.

1. The cracks on the pavement in service above EPS occurred due to the repeated traffic loading such as fatigue cracks based on the cored sample investigation.
2. The deflection of EPS section is three times higher than that of non-EPS section.
3. The fatigue crack may occur on asphalt pavement constructed above EPS, because the EPS creates higher vibration load from the traffic relatively compared to the non-EPS (general ground).
4. The reconstruction may be needed in EPS section using a high resistance material to plastic deformation and fatigue crack.

References

1. Chang YC (1994) A case study on EPS construction method at Se-Chang J/C in Korea. In: International symposium on the application of EPS form for embankment construction/June. Seoul, Korea
2. Chang YC (1995) A study on EPS construction method. Korea Highway Corporation
3. Chang YC (1996) The numerical analysis and field measurement of EPS embankment. In: International symposium on EPS construction method (EPS Tokyo 96)
4. Frydenlund TE (1986) Expanded polystyrene—a lighter way across soft ground. In: International report
5. Korea Expressway Corporation (2002) The report of Seohaean expressway, Korea
6. NRRL (1984) The use of plastic foam in road embankments. Norwegian Road Research Laboratory, Int report no 1191

Load Reduction on Buried Rigid Culverts, Instrumented Case Histories and Numerical Modeling



Jan Vaslestad and Murad Sani Sayd

Abstract Three instrumented full-scale tests using geofoam (expanded polystyrene) for load reduction on buried rigid culverts are described. The culverts were built and instrumented during the period 1988–1992. The method involves installing a compressible inclusion (EPS Geofoam) above rigid culverts in order to reduce the vertical earth pressure. The first instrumented culvert is a concrete pipe with diameter 1.95 m beneath a 14 m high rock-fill embankment. The second full-scale test is a concrete pipe with diameter 1.71 m beneath a 15 m high rock-fill embankment. The third instrumented structure is a concrete box culvert with width 2.0 m beneath 11 m of silty clay. The long-term observations of earth pressure and deformation are presented, and compared with a simplified design method and finite element modelling using the finite element program, Plaxis 2D for the box culvert. The instrumentation consisted of hydraulic earth pressure cells, deformation and temperature measurements. The use of geofoam effectively reduces the vertical earth pressure, and long-term observations shows that the earth pressure is reduced to less than 30% of the calculated overburden in case of granular fill. Whereas the earth pressure is reduced to less than 50% of the calculated overburden in case of silty clay fill. The long term observations of earth pressure and deformation for more than 25 years show that the method using geofoam is stable over time. The last measurements were taken in 2015. The results from the numerical modelling are in agreement with the field measurements.

Keywords Load reduction · Arching · EPS-Geofoam · Instrumentation
Numerical modeling · Buried culverts

J. Vaslestad (✉)

Norwegian Public Roads Authority, Norwegian University of Life Science,
Oslo, Norway

e-mail: jan.vaslestad@vegvesen.no

M. S. Sayd

Norwegian Public Roads Authority, Oslo, Norway
e-mail: murad.sayd@vegvesen.no

1 Introduction

The problem of earth pressure on buried structures has a great practical importance in constructing embankments over pipes and culverts. The earth pressure on deeply buried culverts is significantly affected by arching. Both the magnitude and distribution of earth pressure on buried culverts are known to depend on the relative stiffness of the culvert and the soil. The vertical earth pressure on a rigid culvert is greater than the calculated overburden pressure above the structure, which, result in a negative arching effect. The so-called induced trench method (also called imperfect ditch) involves installing a compressible layer above the rigid culvert. As the embankment is constructed, the soft zone compresses more than the surrounding fill, and thus induces positive arching above the culvert.

Expanded Polystyrene (EPS) geofoam blocks have been used for load reduction on buried rigid pipes under high fill since 1988 in Norway. The deformation in the EPS geofoam provides a mobilization of shear strength in the fill and reduces the expected vertical earth pressure. The properties of soil-structure interaction in the buried culverts highly depend on the mechanical properties of the backfill material and the stiffness of the compressible material, the expanded polystyrene (EPS) geofoam in this case. A better understanding of the arching effect of EPS on buried culvers has been obtained from a field-based study using full-scale test measurements and recently by means of finite element modelling. Terzaghi [5] stated that the amount of arching can only be obtained by direct measurement under field conditions. The instrumented field installations presented in this paper were built in Norway in the period between 1988 and 1992 [7, 8]. Three long-term measurements (two concrete pipes with granular fill and one cast in place box culvert with silty clay backfill) of deformation and earth pressure on buried concrete pipes were carried out using hydraulic pressure cells.

In the later years, this method using geofoam to reduce earth pressure have also been used on concrete culverts below high fills in China, Yang and Yongxing [9], Zhang et al. [10] and McAfee and Valsangkar [3].

2 Instrumented Case Histories

Three long-term measurements of deformation and earth pressure on buried concrete pipes were carried out using hydraulic pressure cells. The field installations were carried out during the period 1988–1992. To measure the vertical and horizontal earth pressures around the concrete pipe, hydraulic pressure measuring cells has been installed. Geometrical arrangements and registered results are presented below for each case. Standard expanded polystyrene (EPS) blocks $0.5 \times 1.0 \times 2.0$ m were used as a compressible layer to create positive arching. The compressive strength of the EPS block was 100 kPa and density 20 kg/m^3 .

2.1 Field Installation—Eidanger, (1988)

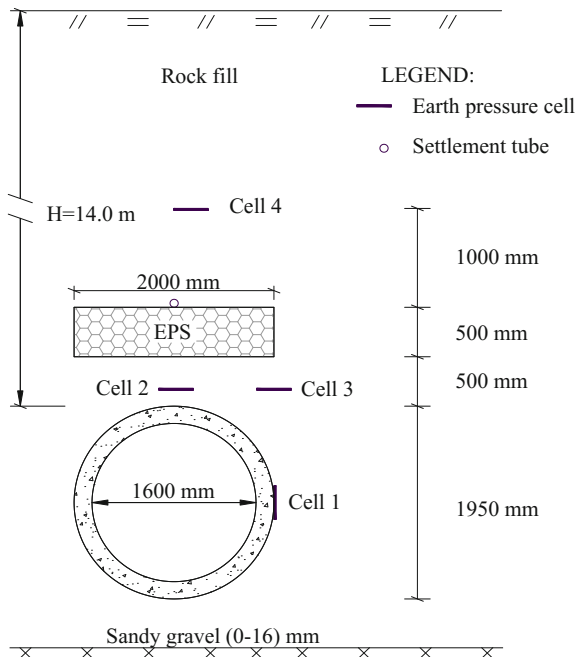
The first field installation built in 1988 is a concrete pipe with outer diameter 1.95 m beneath a 14 m high rock-fill embankment. The geometry of the instrumented cross section with the extent of backfill zone is shown in Fig. 1. The pipe was placed after the in situ soil was excavated to about 0.5 m below the culvert elevation, down to bedrock, and replaced by 0–16 mm sandy gravel.

The same material (0–16 mm sandy gravel) was used for backfill, with a compaction requirement of 97% Standard Proctor.

The backfill extended 1 m out from the springline and 0.5 m over the top of the pipe. The remaining fill in the embankment is rock-fill that was placed in 3 m thick layers, and compacted to 95–97% Standard Proctor.

The construction began in August 1988 and was completed in June 1989. Results from the registered vertical pressures on cell 2, are shown in the Fig. 2. The earth pressure on cell 2 increased to 72 kPa in September 1988 when the fill height was 8.3 m. Further increase of fill height to 13.7 m did not increase the earth pressure. In the period between January 1996 and January 2008, the earth pressure on the top of the pipe was registered as relatively constant around 66–68 kPa, which is 25% of the calculated overburden pressure. The registered vertical compression of the EPS geofoam is also shown in Fig. 2. The vertical deformation stabilises around 140 mm. The result showed no further increase after almost 12 years of measurements. The measured deformation is 28% of the initial thickness of the EPS block.

Fig. 1 Locations of pressure cells and EPS geofoam above the pipe



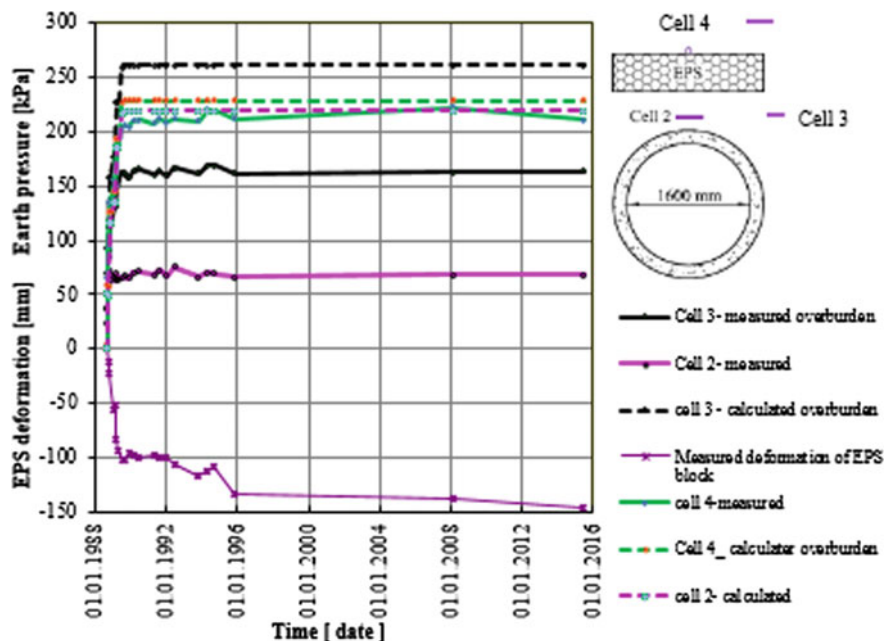


Fig. 2 Vertical overburden pressures and deformation of EPS geofoam block

2.2 Field Installation—Hallumsdalén, 1989

A cast-in-place box culvert was also instrumented to monitor the long-term performance of the culvert as shown in Fig. 3. It is a continuous culvert having a total length of 385 m and is crossing a valley beneath an embankment of compacted dry crust clay up to 23 m in height. The subsoil consists of over consolidated silty clay with water content 25–30% and undrained shear strength 35–70 kPa.

To investigate the time effects on the earth pressure in the cohesive fill in the imperfect ditch method, expanded polystyrene was placed above the culvert in a length of 20 m. The instrumented section of the culvert is situated in the counter fill that is built up with silty clay with unit weight, $\gamma = 20 \text{ kN/m}^3$. The EPS block was placed above the culvert as shown in Fig. 3. This section (case a, in Fig. 3) was instrumented with two hydraulic earth pressure cells of the Gletz type, cells 1 and 2. The deformation of the EPS was measured using a settlement plate. To compare the earth pressure on the imperfect ditch section with a conventional section, one earth pressure cell was placed above the culvert in a cross-section without EPS, cell 3, see Fig. 3. The construction of the embankment began in July 1989 and was completed in February 1990. At completion of the fill, the fill height was 10.8 m above the cell level with overburden pressure 206 kPa. The measured earth pressure was 132 kPa at this fill height, which is 63% of the calculated overburden pressure.

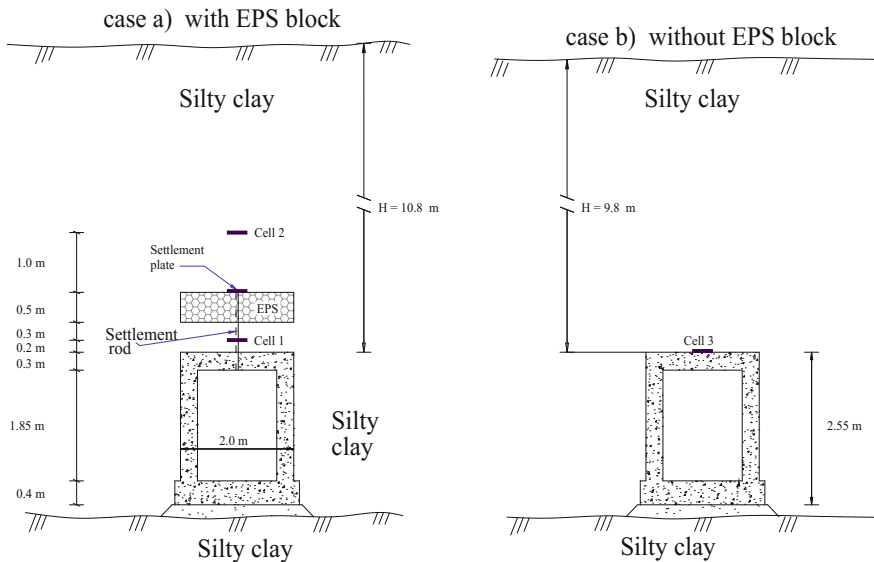


Fig. 3 Locations of pressure cells and EPS geofoam above the culvert

The earth pressure decreased to 123 kPa in April 1991. The pressure further decreased to 88 kPa in December 1991. This is possibly due to stability problems and movements in the counter fills that occurred in April 1991. The earth pressure stabilised around 100 kPa in 1993. The last measurement carried out in June 2015 showed a value around 94 kPa. This is about 48% of the calculated overburden pressure. However, the vertical earth pressure measured with cell 3, which is located on top of the culvert in a section without EPS, shows the reverse as shown in Fig. 4. At completion of the fill in February 1990, the fill height above the culvert was 9.8 m. Thus, the calculated overburden is 196 kPa. The registered earth pressure was 244 kPa, which is 124% of the calculated overburden. Based on extensive finite element modelling, Tadros et al. [4] proposed an expression for calculating the earth pressure on concrete box culverts. For silty clay soil, this expression gives an earth pressure value of 1.17 times the overburden on top of the culvert. The registered earth pressure in July 2007 and June 2015 is 245 and 254 kPa respectively.

The measured deformation of the EPS was 60 mm at an overburden of 100 kPa, which corresponds to the compressive strength of the EPS. The deformation was then 220 mm at completion of the fill, when the overburden was 196 kPa. For the next four years, the deformation gradually increased to 250 mm, which is 50% of the initial thickness of the EPS. The last two measurement performed in July 2007 and June 2015 show an increase to 269 and 275 mm deformation respectively, which is 54 and 55% of the initial thickness. This shows that the deformation of the EPS in cohesive fill is greater than in granular fills. The observed settlement of the culvert was between 70 and 110 mm in the instrumented sections for the observation period.

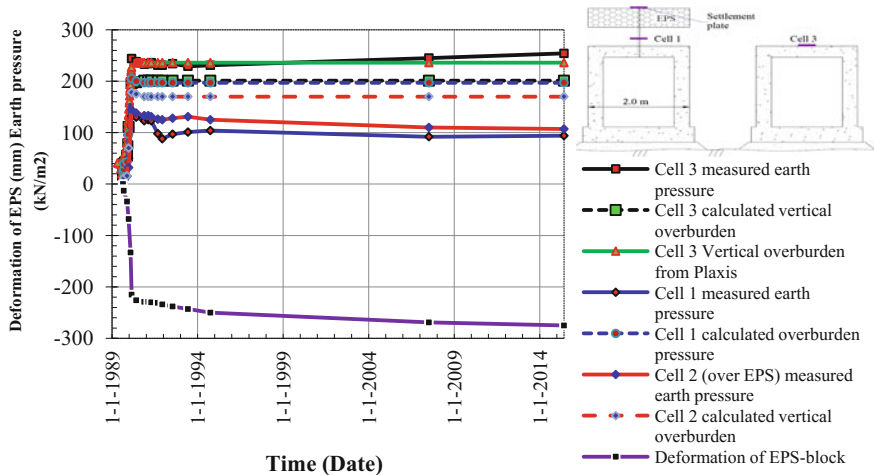


Fig. 4 Vertical overburden pressures and deformation of EPS geofoam

2.2.1 Numerical Modeling

The finite element program, Plaxis 2D [1], is used to further study the vertical overburden pressure distribution over these two sections of the culvert. The model is performed both for culvert with and without EPS-block. The construction is modelled following the real construction stages and the pressure and deformation points are placed fairly near the pressure cells and settlement sensors. The results are reasonably comparable and can help for better understanding the arching effect of EPS Geofoam on buried culverts.

The effect of the width of the compressible layer, EPS Geofoam, is also studied by varying the width of EPS block. As shown in Figs. 6 and 7, the width of compressible layer has some effect of reducing the vertical pressure on buried pipes.

For the width of EPS block equal to the width of the culvert, the vertical pressure at mid span is 109 kPa and the maximum pressure at the edge of the culvert is 234 kPa. However, for the width of EPS block extended by 50 cm, both sides beyond the width of the culvert, the vertical pressure at mid span is 127 and 203 kPa at the edges of the culvert (see Fig. 6).

The vertical pressure across the geofoam block is shown in Fig. 7. At the center of the EPS block, the vertical pressure is 107 kPa and is about 62 kPa at the edge for the width of compressible layer equal to the width of the culvert. The corresponding vertical pressures are 129 and 64 kPa at the center and edge of EPS block respectively for with width of compressible layer extended beyond the width of the culvert (Fig. 7). Therefore, the effect of extending the width of EPS block beyond the width of the culvert has insignificant effect in reducing the vertical overburden pressure on the pipe (Table 1) (Figs. 6 and 7).

Table 1 Material properties used in numerical models

	Materials			
	Sub soil (silty clay)	Fill (dry crust)	EPS geofoam	Concrete Culvert
Material model	Hardening soil	Mohr-Coulomb	Hardening soil	Linear elastic
Drainage type	Drained	Drained	Drained	Non-porous
Unit weight, γ (kN/m ³)	20	20	0.2	24
Secant stiffness, E_{50}^{ref} (MPa)	20	–	4	
Stiffness, E' (MPa)	–	80		9000
Friction angle ϕ' (°)	26	28	30	
Cohesion, c' (kN/m ²)	2	0	35	
Dilatancy angle, ψ (°)	0	0	0	
Poisson's ratio, ν'	0.3	0.3	0.2	0.15
Reference stress, p^{ref} (kPa)	100	–	100	

Culvert with EPS Geofoam

The result from the numerical analysis, (Figs. 5, 6, 7, and 8), show the effect of geofoam block as compressible layer by creating positive arching on top of the culvert, which diverts parts of the vertical soil pressure sideways. The type of fill material is the key factor in creating positive arching. There should be significant stiffness difference between the fill material and the geofoam block to have the desired positive arching on buried culverts. Sensitivity analysis has been carried out by varying the modulus of elasticity of the cohesive fill material for a specific stiffness of EPS Geofoam. The result showed that the fill material should be at least 10 times stiffer than the geofoam block in order to have a desired positive arching which reduces the vertical pressure on buried culverts.

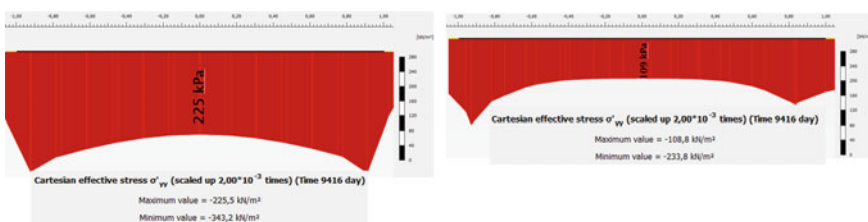


Fig. 5 Comparison of vertical overburden pressure on top of buried culvert. Right: with Geofoam block as a compressible inclusion, Left: without Geofoam block (Plaxis output)

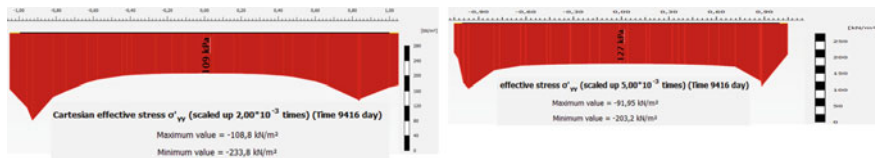


Fig. 6 The vertical overburden pressure on top of the culvert. Left: when the EPS has same width as the width of the culvert. Right: EPS is extended 50 cm beyond the edges of the culvert

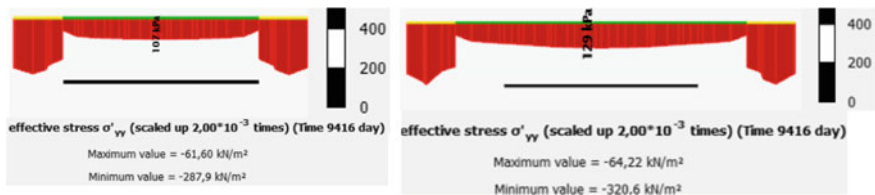


Fig. 7 The vertical overburden pressure across the center of EPS block. Left: For EPS block with the same width as the width of the culvert. Right: The width of EPS extended by 50 cm on both sides (the green line is the width of the EPS)

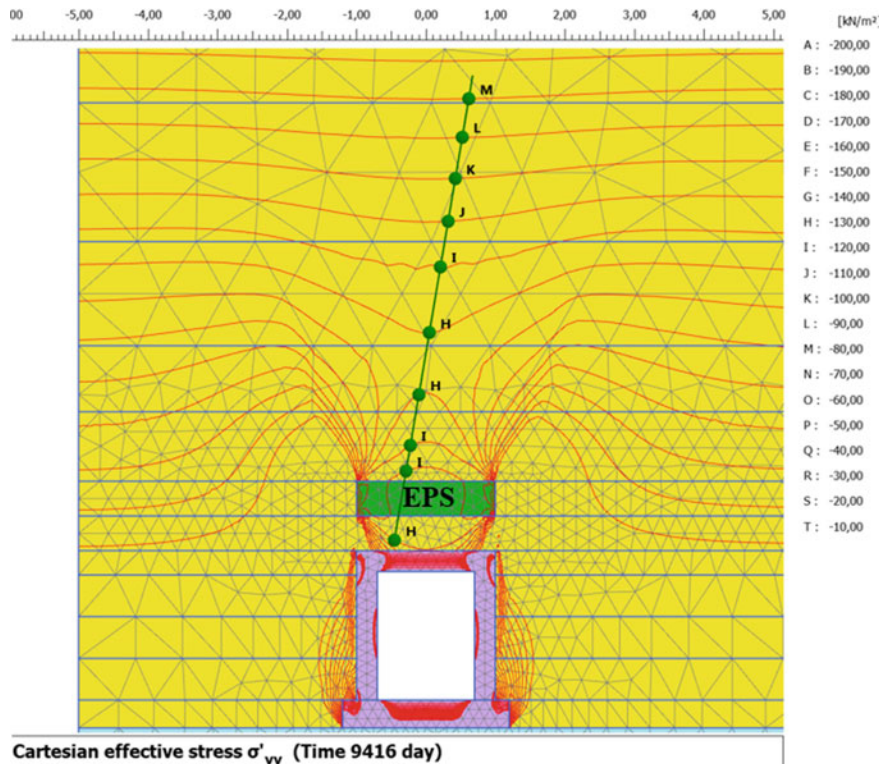


Fig. 8 Vertical overburden pressure distribution over culvert

Culvert without EPS Geofoam

The output result from the analysis, Fig. 9, shows the vertical overburden pressure on the culvert. The pressure contour shows there is pressure concentration on top of the culvert, i.e. negative arching. The pressure on top of the culvert varies from 225 kPa at the mid-span of the culvert to 343 kPa over the walls of the culvert, Fig. 5 (left). The result from the analysis is comparable to the measured pressure, Fig. 4.

2.3 Field Installation—Tømtebekken, 1991

The last field installation built in 1991 is a concrete pipe culvert with inner diameter 1.4 m and outer diameter 1.73 m. The rock-fill embankment above the pipe includes 0.5 m EPS geofoam inclusion situated 0.3 m above the crown of the pipe and a total backfill height of 22 m. The foundation consists of approx. 40 cm well-graded crushed stone, 0–32 mm, and compacted to a minimum of 97% standard proctor. For filling around pipes and EPS block, sand and gravel is used, and compacted to a minimum 97% standard proctor (Fig. 10).

The induced trench installation was instrumented to monitor the long-term performance of the EPS geofoam inclusion and the earth pressure history above the culvert for 24 years. As shown in Fig. 11, the registered vertical earth pressure at the top of the pipe increased in similar pattern to the calculated overburden pressure until 5 m of fill had been placed. Afterwards, only slight increment of the vertical

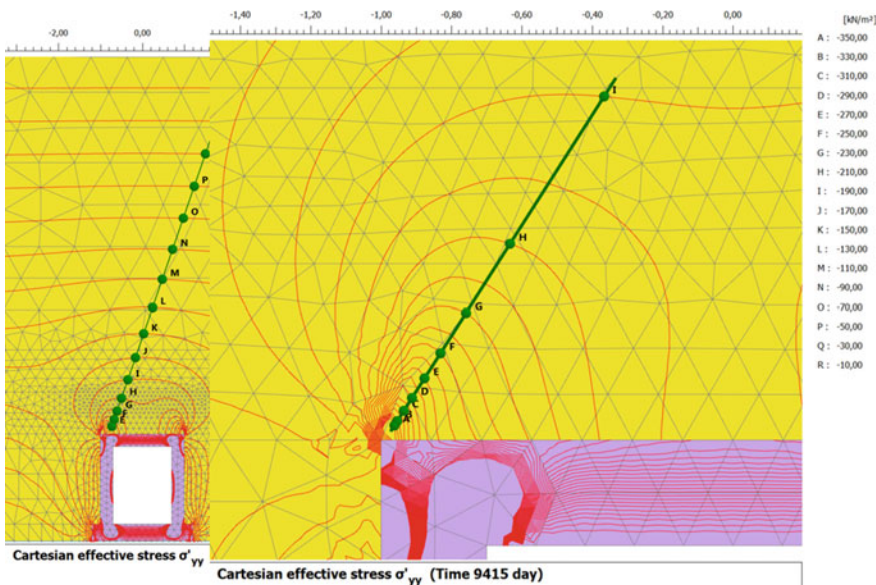


Fig. 9 Contour of vertical overburden pressure over culvert without compressible layer (Plaxis output)

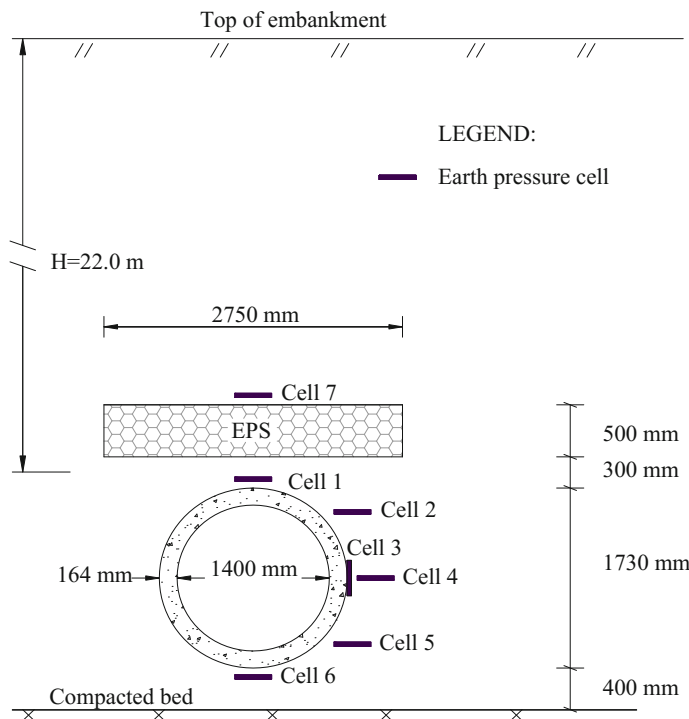


Fig. 10 Locations of pressure cells and EPS geofoam above the pipe

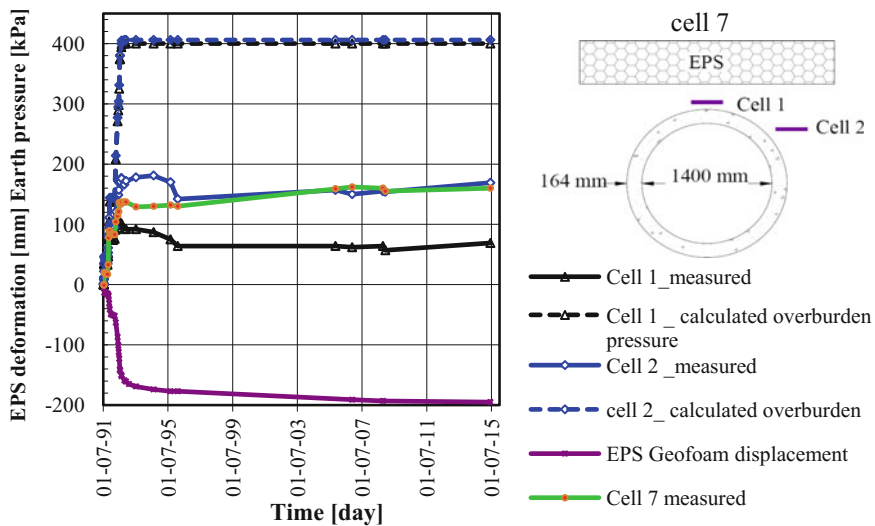


Fig. 11 Vertical overburden pressures and deformation of Geofoam block

earth pressure is registered for further increase of fill height. The earth pressure registered by cell 1 is only 23% of the overburden pressure at the end of construction. The vertical pressure at the crown of the pipe remained fairly constant afterwards. The filling was started in July 1991 and ended in October 1992. The measured vertical deformation of EPS geofoam is shown in Fig. 11. The deformation was about 16 cm at the full fill height of the embankment, October 1992, which is about 32% of the initial thickness of the EPS block.

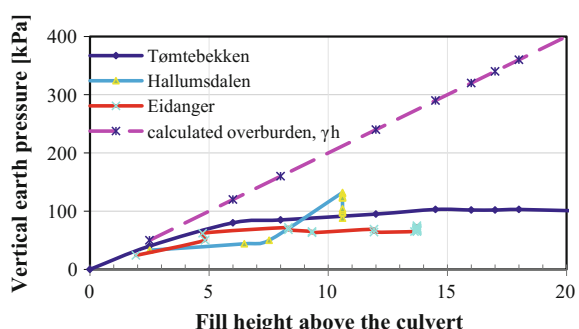
No significant change of deformation was registered after the end of the construction. The result shows the deformation was about 38% according the 2007 and 2015 measurement. Much of the deformation occurred during the construction stage and no settlement has been observed on the existing road above the embankment.

3 Comparison

The long-term measured vertical pressure above the crown of the pipe ranged from 23 to 25% of the overburden pressure for installations with granular backfill material and about 45% for the one with cohesive soil backfill. Results from finite element analysis showed that the performance of induced arching is largely affected by the type of soil used in the embankment construction. The results from finite element modelling are fairly comparable to the measured vertical overburden pressure. The field installations with granular fill reduced the vertical pressure over the culvert more than the one with silty-clay embankment. However, the measured earth pressure for the section of culvert without compressible layer showed 124% of the overburden pressure. Figures 12 and 13 provide quantitative comparison between the calculated overburden and the registered vertical earth pressure values among all field installations discussed above.

The resulting plot clearly shows that the use of induced trench installation successfully reduced the vertical pressure above the buried structure. The final compression of the EPS geofoam at the end of embankment construction ranged from 27 to 32% for concrete pipes with granular fill and 50% for cast-in situ box culvert with cohesive fill.

Fig. 12 Measured vertical earth pressure versus the overburden pressure, γH



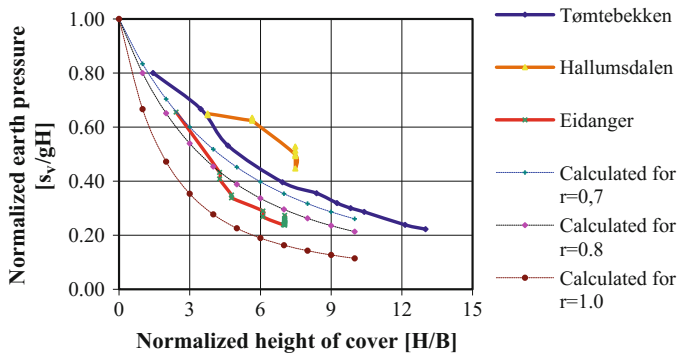


Fig. 13 Comparison of the measured vertical earth pressure with the calculated arching factor

4 Design Method

It may also be interesting to compare the result with the so called *the arching factor*. The vertical earth pressure, σ_v on an imperfect ditch culvert can be found from, Vaslestad [6] as:

$$\sigma_v = N_A \gamma H \text{ (kN/m}^2\text{)} \quad (1)$$

where

N_A = arching factor

γ = unit weight of the soil (kN/m^3)

H = height of cover (m)

and

$$N_A = \frac{1 - e^{-A}}{A} \quad (2)$$

where

$$A = 2S_v \frac{H}{B} \text{ and } B = \text{width of culvert (m)} \quad (3)$$

The friction number S_v was used by Janbu [2] to determine friction on piles.

$$S_v = |r| \tan \rho K_A \quad (4)$$

where $\tan \rho = f \tan \varphi =$ mobilized soil friction,

$$\tan \rho = \frac{\tan \phi}{\gamma_M}, \quad (5)$$

f = degree of mobilization, (ranges from 0 to 1), $\tan \varphi$ = soil friction

K_A = active earth pressure coefficient

$$K_A = \frac{1}{\left[\sqrt{1 + \tan^2 \rho} + \tan \rho \sqrt{1 - |r|} \right]^2} \quad (6)$$

$$r = \frac{(p'_A + c \tan \phi) \tan \delta}{(p'_A + c \tan \phi) \tan \rho} = \frac{\tan \delta}{\tan \rho} \leq 1 \quad (7)$$

where, c = cohesion, p'_A = Active earth pressure, δ = inclination of front wall.

5 Conclusion

The induced trench installations described were successful in reducing the vertical loads on the buried culverts. The pressure on buried structures can be reduced with the appropriate selection of backfill material with higher stiffness like granular material. The average measured earth pressure above the crown of the pipe ranged from 23 to 25% of the overburden pressure for installations with granular backfill material and about 45% for the one with cohesive backfill material. This shows the importance of using high quality well-compacted granular soil at the sides of an imperfect ditch culvert. The vertical earth pressure on the section without EPS geofoam block was measured as 1.24 times the overburden pressure. The long-term full scale tests also showed that compression of the EPS geofoam ranged from 28 to 38% for concrete pipes with granular fill and 54% for cast-in situ box culvert with cohesive fill.

Long term monitoring of the field installations indicate no increased pressure or deformations on the buried culverts compared to the situation right after construction. Much of the deformation in the EPS block occurred during the construction phase and no problem has been observed on the road surfaces due to the long-term settlement of the expanded polystyrene. The measured vertical pressures are comparable with the design method.

Finite element modelling using the finite element program, Plaxis 2D is a useful tool for optimizing and analysing distribution of earth pressure over buried culverts. The effect of extending the width of EPS block beyond the width of the culvert has insignificant effect in reducing the vertical overburden pressure on the pipe, but it can reduce the horizontal pressure at the springline of the culvert.

References

1. <http://www.plaxis.com/> (2017)
2. Janbu N (1976) Static bearing capacity of friction piles. In: 6th European conference SMFE, Wein, proceedings, vol III, pp 479–488
3. McAfee RP, Valsangkar AJ (2008) Field performance, centrifuge test, and numerical modelling of an induced trench installation. *Can Geotech J* 45(1):85–101
4. Tadros MK, Benak JYAM, Abdel-Karin AM, Bexten K (1989) Field testing of a concrete box culvert. *Trans Res Rec, J Transp Res Board*, No 1231, Transportation Research Board of the National Academies Washington D.C., pp 39–54
5. Terzaghi K (1943) Theoretical soil mechanics, Wiley, Hoboken
6. Vaslestad J (1991) Load reduction on buried rigid pipes below high embankments. In: ASCE Specialty Conference, Pipeline Division, Denver, Colorado, pp 47–58
7. Vaslestad J, Johansen TH (2008) Arching on rigid structures below high fills. Long-term behavior of three instrumented full-scale tests. In: Proceedings Nordic geotechnical meeting nr 15, NGM 2008, 3–6 Sept 2008, Sandefjord, Norway
8. Vaslestad J, Yesuf GY, Johansen TH, Wendt M, Damtew T (2009) Instrumented field test and soil structure interaction of concrete pipe with high fill. In: Proceedings of the 17th international conference on soil mechanics and geotechnical engineering: the academia & practice of geotechnical engineering, 5–9 October 2009. Alexandria, Egypt, pp 1802–1805
9. Yang X, Yongxing Z (2005) Load reduction method and experimental study for culverts with thick backfills on roadways in mountainous regions. *China Civil Eng J* 38(7):116–121
10. Zhang W, Liu B, Xie Y (2006) Field test and numerical simulation study on the load reducing effect of EPS on the highly filled culvert. *J Highw Transp Res Dev China* 23(12):54–57

Improving the Behavior of Buried HDPE Pipe by Using EPS Geofoam



Emre Akinay and Havvanur Kılıç

Abstract A buried thermoplastic pipe installed with conventional method deflects vertically downwards under soil load. Because the displacement of the pipe crown is more than that of the sidefill soil, differential settlements in the soil medium above the pipe crown level take place. Differential settlements lead to the development of a mechanism called “positive soil arching” within the soil medium and, consequently, a vertical stress smaller than the geostatic stress acts on the crown of the thermoplastic pipe. The degree of arching depends on the magnitude of the differential settlements. Therefore, the degree of arching can be increased by installing a zone or zones of a compressible material, which will increase the magnitude of the differential settlements, around the thermoplastic pipe when the pipe is being installed. The increase in the degree of arching will provide less vertical stress on the pipe crown and an improved pipe behavior. This paper presents a part of the findings obtained from true-scale laboratory model tests and finite element analysis which were performed to investigate the effects of compressible zone application on buried HDPE pipe behavior. EPS Geofoam with 10 kg/m^3 nominal density was used as the compressible material. Compressible zone with proposed geometry provided a reduction in vertical pipe deflection of up to 89%, in horizontal pipe deflection of up to 96% and in vertical stress on the pipe crown of up to 77%. Finite element analysis showed that the compressible zone provided relatively very small bending moments and almost a uniform bending moment distribution around the pipe. Under 200 kPa surcharge stress, a reduction in the maximum bending moment around the pipe of 78% was provided.

Keywords HDPE pipe · Soil arching · EPS geofoam · Model test PLAXIS

E. Akinay (✉)

Austrotherm Turkey, Istanbul, Turkey
e-mail: emre.akinay@austrotherm.com.tr

H. Kılıç

Yıldız Technical University, Istanbul, Turkey

1 Introduction

After Marston (1922), many studies have been carried out on the induced trench pipe installation method, which provides significant reduction in vertical stresses acting on the buried rigid pipes under high fills [1–11]. In this method, a relatively compressible material zone is installed within the backfill on a positive projecting rigid pipe to induce the trench condition, i.e. positive soil arching. There is no case study in the literature yet in which an HDPE pipe is installed as an induced trench pipe. Kang et al. (2007) proposed the use of a soft zone around PVC pipes to improve the pipe behavior and produced predictor equations for deflections, maximum wall stress and arching factors by using finite element analyses [12]. However, the scope of the study of Kang et al. (2007) is limited to numerical analysis and neither a laboratory nor a field study was carried out [12].

In this study, the effects of a soft zone around an HDPE pipe on the pipe behavior are investigated by true-scale laboratory model tests and finite element analyses. The soft zone geometry is similar to that proposed by Kang et al. [12], but the dimensions are roughly determined.

2 Materials and Methods

2.1 Test Facility

The test facility consists of two main components: these are the test cell and the loading system (Fig. 1). The test cell is a structure composed of four stiff walls, which are 1.5 m long and 1.5 m high, and one steel base. Three of the walls are made of 10 mm-thick steel and the other one is made of 30 mm-thick Plexiglas. The walls are supported by steel-box-profile belts (at top, mid-height and bottom levels) and steel counterforts (four on each wall) to minimize undesirable outward movement due to lateral earth pressures. The loading system consists of two hydraulic pistons with 50 ton loading capacity and one rigid steel plate connected to the pistons. The reaction beam is connected to the walls of the cell by columns, in other words the loading system together with the test cell constitutes a loading frame.

2.2 Test Materials

2.2.1 Test Pipe

The test pipe is a lined corrugated-wall HDPE pipe with nominal diameter of 300 mm ($\varnothing 300$) and nominal stiffness of 8 kPa (SN8, Type 5). Actual inside diameter of the pipe is measured as 294 mm in average. The actual ring stiffness of

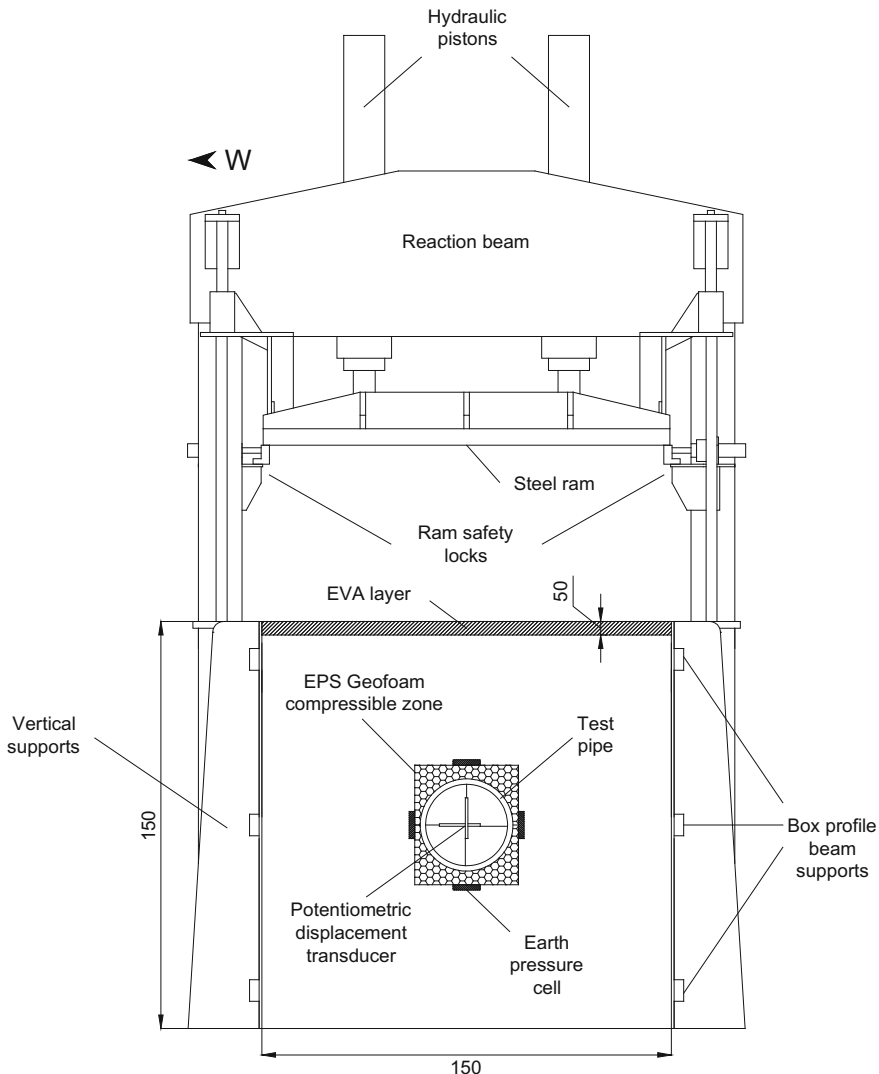


Fig. 1 Test facility (drawing is to scale, units are in cm)

the test pipe is determined as 8.8 kPa by loading test carried out in accordance with TS EN ISO 9969 [13]. Moment of inertia of the pipe wall per unit length is determined as $488.6 \text{ mm}^4/\text{mm}$ and area of the pipe wall per unit length is determined as $7.22 \text{ mm}^2/\text{mm}$. Geometrical properties of the pipe wall is given in Fig. 2.

Three pipe pieces, cut to a length of 490 mm, were supplied. This was required to facilitate placing instrumentation inside the pipe. After placing the instrumentation, the pieces were joined by butt-welding.

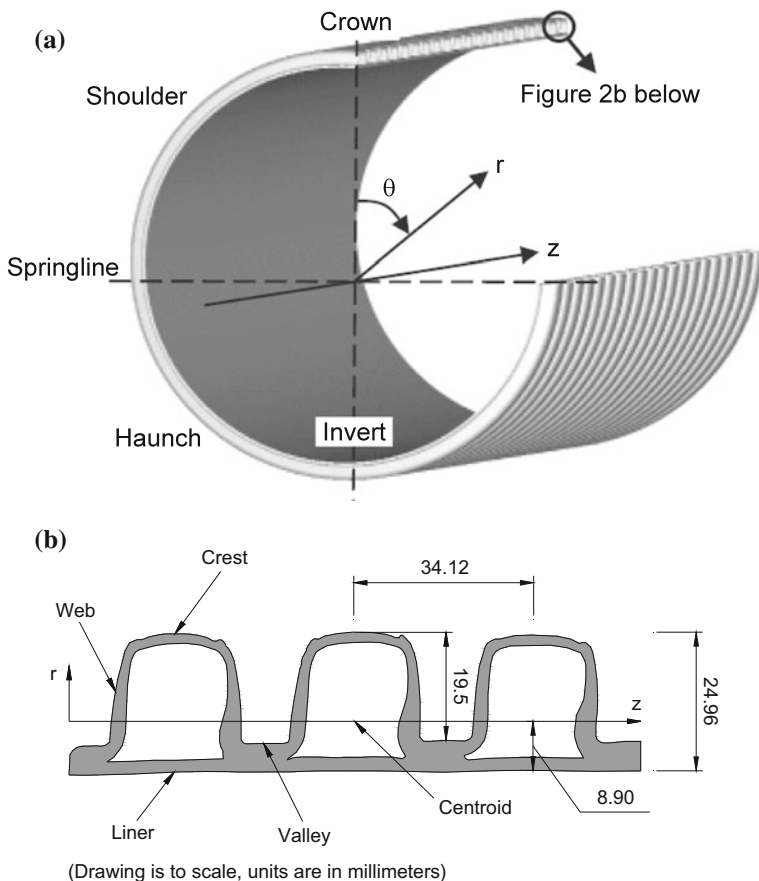


Fig. 2 **a** Section through lined—corrugated pipe [14] **b** geometrical properties of the pipe wall (units are in mm)

2.2.2 Test Soil

The soil used in the tests was angular, medium grained silica sand with a coefficient of uniformity (C_u) of 2.57, a coefficient of curvature (C_c) of 0.92 and an effective size of particle (D_{10}) of 0.35 mm. The specific gravity was 2.65. The soil is classified as poorly graded sand (SP) according to the Unified Soil Classification System. The maximum and minimum dry weights of the sand were found to be 17.3 and 14.4 kN/m³, respectively.

Shear strength angles for two different densities of the test sand were determined by performing consolidated-drained (CD) triaxial compression tests. Triaxial compression tests are performed after completion of the laboratory model tests. In the laboratory model tests the sand was placed in layers with typical thickness of 140–150 mm. For facilitating and speeding up test preparation stage, the sand was

placed in dry condition and as loose as possible. Dry unit weight (γ_{dry}) of the sand placed in a layer was determined by two methods. The first method is the direct and the simplest way of determining the unit weight; to divide the weight of sand by the volume of layer. The second method is an indirect way; to take in situ stiffness measurements by using Humboldt GeoGauge™ and to calculate dry unit weight of sand by using Eq. 1 [15].

$$\gamma_{dry} (\text{kN/m}^3) = 0.441k + 13.38 \quad (1)$$

Given in Eq. 1: k = Stiffness measured by Humboldt GeoGauge™ (MN/m). It should be noted that Eq. 1 can only be used for the sand used in this study and in dry condition. By utilizing the first and the second method, the dry unit weight of the test sand is determined approximately as 15 kN/m^3 . This value corresponds to relative density of 25%.

During installation of the test pipe, one test personnel had got to get inside the test cell and step on the test soil. The soil surface at the pipe invert level, except the soil section where the pipe was laid on, was subjected to body weight of the test personnel. During this operation, care was taken not to step on the soil section where the pipe was laid on. In situ stiffness measurements were taken by using Humboldt GeoGauge™ after installation of the test pipe and by utilizing Eq. 1 dry unit weight of sand at the pipe invert level is determined approximately as 15.5 kN/m^3 . This value corresponds to relative density of 40%.

Consolidated-drained (CD) triaxial compression tests were performed under confining pressures of 50, 100 and 200 kPa with a shear rate of 1% strain per minute. Diameter and height of the triaxial compression test samples are 71 and 154 mm, respectively. Shear strength angles for relative densities of 25 and 40% were found as 30° and 35° , respectively. Possibly due to test conditions a relatively small cohesion (11 kPa) was determined for both soil densities, but was practically assumed as zero. Axial strain versus deviatoric stress and axial strain versus volumetric strain plots are given in Fig. 3. Mohr circles and failure envelopes are given in Fig. 4.

2.2.3 EPS Geofoam

EPS is a lightweight material that can be produced in any desired geometry. One of the most important properties of EPS is that minimum requirements for its engineering properties are specified by the standards. For these reasons, EPS was selected as the compressible material to use in this study.

In this study, EPS Geofoam with nominal density of 10 kg/m^3 (EPS10) is used. Axial strain—axial stress and axial strain—volumetric strain relationships are determined by performing unconfined compression (UC) tests with a shear rate of 1% strain per minute. Diameter and height of the unconfined compression test samples were both 50 mm. The literature was reviewed to determine test procedure, sample dimensions and shear rate [16–18]. Shearing was continued until 30% axial strain was reached. Material properties of the EPS test sample were given in Table 1.

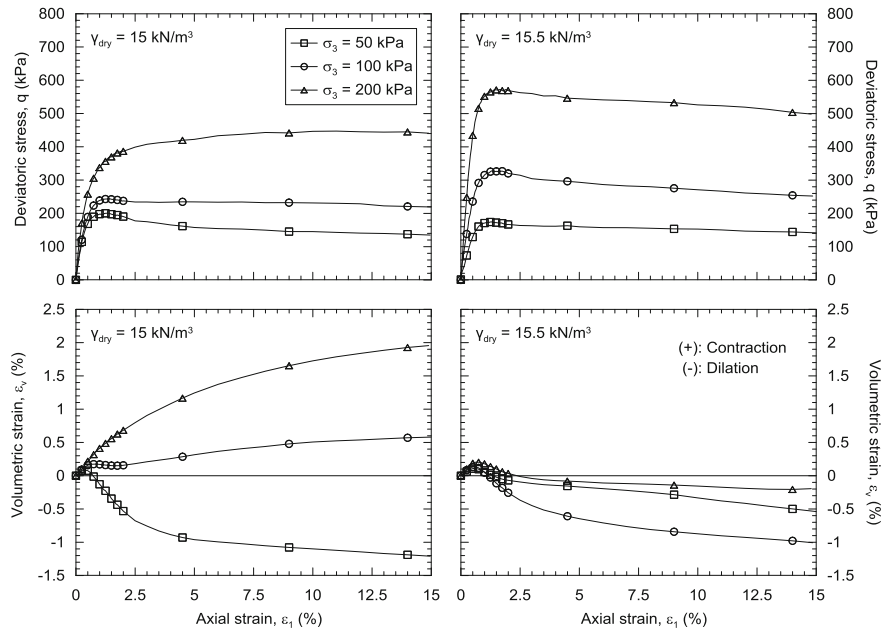


Fig. 3 Axial strain versus deviatoric stress and axial strain versus volumetric strain plots for test soils

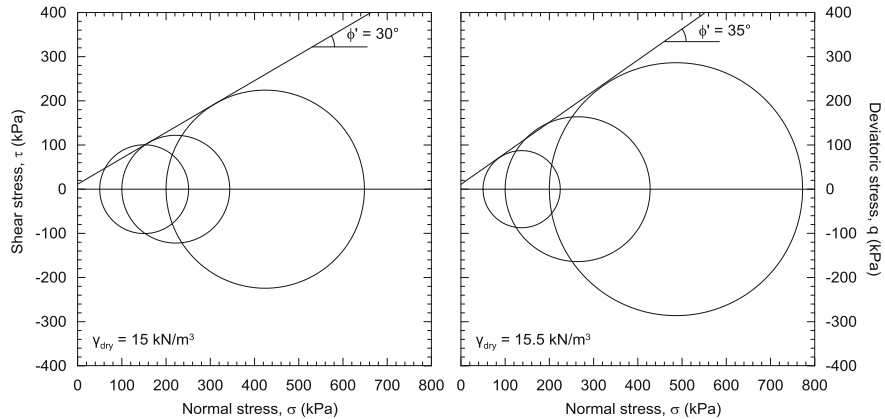


Fig. 4 Mohr circles and failure envelopes for test soils

Table 1 Material properties of the EPS UC test sample

Parameter	Value
H_{EPS} (mm)	48.85
D_{EPS} (mm)	50.00
A_{EPS} (cm^2)	19.64
V_{EPS} (cm^3)	95.92
M_{EPS} (g)	0.98
ρ_{EPS} (kg/m^3)	10.2

H_{EPS} height of the sample

D_{EPS} diameter of the sample

A_{EPS} cross-sectional area of the sample

V_{EPS} volume of the sample

M_{EPS} mass of the sample

ρ_{EPS} density of the sample

Axial strain—axial stress and axial strain—volumetric strain relationships for EPS10 are given in Fig. 5. Material behavior is idealized with three linear segments. The first segment is the slope of the secant line between the origin and 1% axial strain. The second segment is the slope of the secant line between 2 and 6% axial strains. The third segment is the slope of the secant line between 6 and 30% axial strains. The abscissa of intersection point of the first and the second segments was assumed as 1.6% axial strain. Slopes of the linear segments in Fig. 5a (Young's Moduli) are determined as $E_1 = 1440$ kPa, $E_2 = 390$ kPa and $E_3 = 140$ kPa. Using the slopes of the linear segments in Fig. 5b, Poisson Ratios are determined as $v_1 = 0.145$, $v_2 = -0.013$ and $v_3 = 0.049$ [17, 18]. Stark et al. (2004) suggested using of empirical linear Eq. 2 which relates initial tangent modulus of EPS to density [19]:

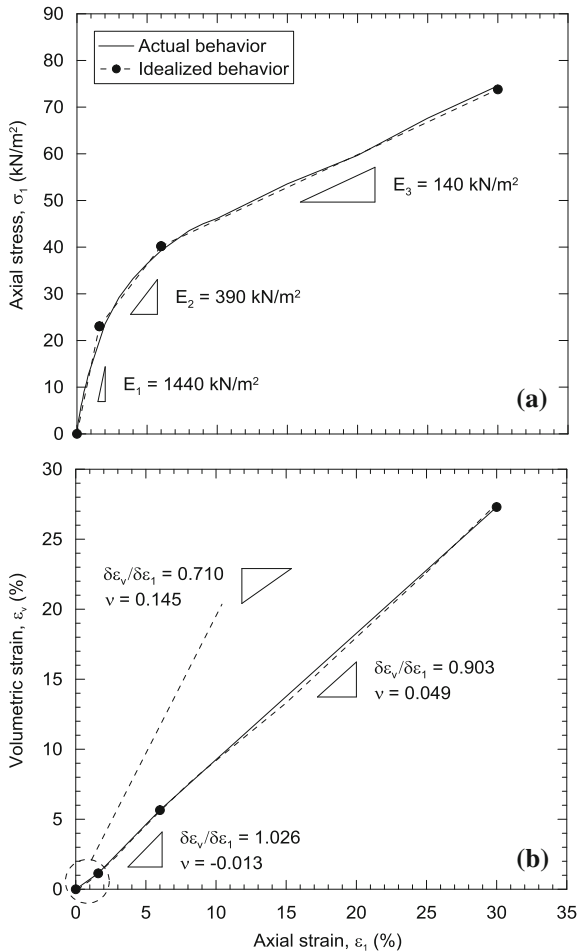
$$E_{ti}(\text{kPa}) = 450\rho_{EPS} - 3000 \quad (2)$$

where E_{ti} is initial tangent modulus of EPS. Using Eq. 2 initial tangent modulus of EPS with density of $10 \text{ kg}/\text{m}^3$ is calculated as $E_{ti} = 1500$ kPa. It's seen that the value of E_t obtained from UC test is almost the same as the value that Eq. 2 yields.

2.3 Instrumentation

Load-cell type earth pressure cells were placed around the cross-section at the pipe mid-length, in contact with the pipe wall, in order to measure vertical soil stress on the pipe crown and the pipe invert, and horizontal soil stress on the pipe springline. Potentiometric displacement sensors were installed inside the pipe, on the cross-section at the pipe mid-length in order to measure vertical and horizontal pipe deflections (Fig. 1).

Fig. 5 Behavior of EPS10 under unconfined compression **a** axial strain—axial stress **b** axial strain—volumetric strain



2.4 Treatment Against Wall Friction

If no treatment is applied to walls, interface strength between the walls and the sand will mobilize as relative displacements on the interface take place. The friction on the walls was minimized by placing two 0.08 mm-thick polyethylene sheets, lubricated with Dow Corning Molykote 44 High-Temperature Bearing Grease (Medium) on the walls. Placing a protection layer on polyethylene sheets for avoiding any possible damage due to particle impingement was also considered to be necessary. Conservatively, placing a non-woven geotextile (with mass per unit area of 150 g/m) layer on which 2 mm-thick HDPE geomembrane plates were attached was adopted for this purpose. This arrangement reduces the boundary friction to less than 5% [20].

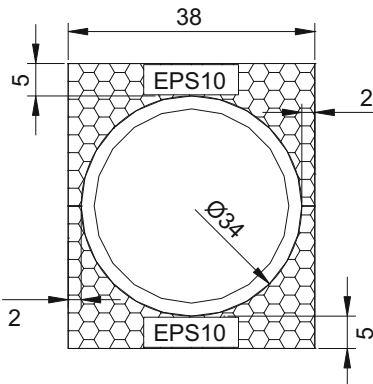


Fig. 6 Geometrical properties of the compressible zone (units are in cm)

2.5 Laboratory Model Tests and Testing Procedure

Results obtained from two laboratory model tests are presented in this paper. The first test is the Reference Test in which no compressible zone is installed around the pipe. In the second test (Test #2), the pipe is located within a compressible zone as proposed by Kang et al. [12]. Geometrical properties of the compressible zone applied in the Test #2 are given in Fig. 6.

Brachman et al. (2001) proposed the use of pressurized air bladder for providing uniform vertical stress distribution on the ground surface [21]. However, in this study vertical load was applied to the ground surface through a rigid plate. Because of flexural rigidity of rigid plate, this way of loading will lead to non-uniform vertical stress distribution on the ground surface. Therefore, a 5 cm thick layer of ethylene vinyl acetate (EVA) was placed on the soil surface for providing a vertical stress distribution as uniform as possible. Ethylene vinyl acetate (EVA) was found to be a proper material because of its high compressibility and linear elastic strain-stress behavior.

Prior to loading stage, readings of earth pressure cells and potentiometric displacement sensors were zeroed. Vertical stress was increased by increments of 25 kPa up to final value of 200 kPa. Each stress increment was maintained for 30 min.

3 Finite Element Analyses

The responses of the pipe and the test soil under conditions in the laboratory model tests were investigated by finite element analyses. For this purpose well-known finite element code PLAXIS 2D was used.

3.1 Model Geometry

Based on the data obtained from the laboratory model tests, the responses of the pipe and the soil were assumed to be symmetrical with respect to the pipe vertical axis. Therefore, using of half-geometry was adopted for finite element analyses. 15-noded triangular elements were used in generating finite element mesh. Preliminary analyses showed that very fine element size provides enough sensitivity for modeling.

As mentioned in subchapter 2.2.2, soil surface at the pipe invert level was subjected to body weight. For this reason, in modeling soil zone below the pipe invert was defined as relatively dense “lower sand” and soil zone above the pipe invert was defined as relatively loose “upper sand” (Fig. 7).

3.2 Model Parameters

3.2.1 Pipe

The pipe was modeled using linear elastic beam elements. The Linear Elastic Model parameters for the pipe wall are given in Table 2.

Fig. 7 Model geometry

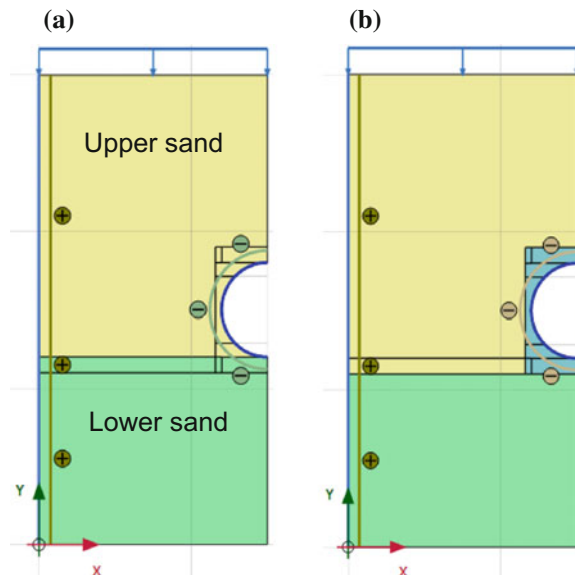


Table 2 Linear elastic model parameters for the pipe wall

Parameter	Value
E (MN/m ²)	390 [22]
v (-)	0.46 [23]
w (kNm/m)	0
I (m ⁴ /m)	4.886×10^{-7}
A (m ² /m)	1.803×10^{-2}
EI (kNm ² /m)	1.906×10^{-1}
EA (kN/m)	7032.41

E Young's modulus

v Poisson's ratio

w weight of the pipe wall per unit length

I moment of inertia of the pipe wall per unit length

A area of the pipe wall per unit length

3.2.2 Soils

The soils were modeled using Hardening Soil Model [24]. Stiffness moduli for upper sand were determined by back-calculating using soil settlement data obtained from Reference Test, while those for lower sand were determined using stress-strain curves obtained from triaxial compression tests. The Hardening Soil Model parameters for the soils are given in Table 3.

3.2.3 EPS

EPS was modeled using Linear Elastic Model. The Linear Elastic Model parameters were determined by back-calculating using settlements of EPS beneath the pipe invert measured in the laboratory model test and the behavior curves obtained from UC test (Fig. 5). The procedure for determining the model parameters for EPS is described as follows:

- Under 25 kPa surcharge stress, the vertical strain in EPS beneath the pipe invert was measured as 5.6%. Using the behavior curve given in Fig. 5a, secant modulus for 5.6% strain was determined as 680 kPa. This value was assigned as Young's Modulus of EPS for 25 kPa loading step (Fig. 8).
- Under higher surcharge stresses (50–200 kPa), the vertical strain in EPS beneath the pipe invert was measured as greater than 6%. Vertical strains greater than 6% lie on the third linear segment of the idealized trilinear curve (Fig. 5a). The slope of the third linear segment (140 kPa) was assigned as Young's Modulus of EPS for 50–200 kPa loading steps (Fig. 8).
- Poisson's Ratios of EPS were determined following the same procedure.

Table 3 Hardening soil model parameters for the soils

Parameter	Value	
	Upper sand	Lower sand
γ_{dry} (kN/m ³)	15	15.5
p^{ref} (kPa)	100	100
E_{50}^{ref} (kPa)	7.5 (Stages 1–2), 10 (Stages 3–9)	60
$E_{\text{oed}}^{\text{ref}}$ (kPa)	7.5 (Stages 1–2), 10 (Stages 3–9)	60
$E_{\text{ur}}^{\text{ref}}$ (kPa)	22.5 (Stages 1–2), 30 (Stages 3–9)	180
m (-)	0.5	0.5
φ (°)	30	35
ψ (°)	0	5
c (kPa)	0.1	0.1

γ_{dry} dry unit weight

p^{ref} reference stress

E_{50}^{ref} reference secant stiffness from drained triaxial test

$E_{\text{oed}}^{\text{ref}}$ reference tangent stiffness for oedometer primary loading

$E_{\text{ur}}^{\text{ref}}$ reference unloading/reloading stiffness

m exponential power for stress-level dependency of stiffness

φ angle of shear strength

ψ angle of dilation

c cohesion

In determining the model parameters for EPS, the assumptions given below were adopted:

- Values for Young's Modulus and Poisson's Ratio determined following the procedure given above are the same at each point in the EPS zone.
- Strains occurred in the EPS zone during placement of test sand were ignored.

The Linear Elastic Model parameters for EPS are given in Table 4.

3.2.4 Walls of the Test Cell

In modeling, the outward movement of the tank walls was assumed to be zero. However, for modeling the behavior of the interface between the tank wall and the sand, beam elements were assigned to the boundaries of the model geometry. The walls were modeled using Linear Elastic Model. The model parameters for the walls are not presented in this paper.

3.2.5 Interfaces

Angles of interface strength adopted for wall—sand interface, HDPE—sand interface, HDPE—EPS interface and EPS—sand interface and corresponding interface strength reduction factors (R_{inter}) are given in Table 5.

Fig. 8 The procedure used in determining the linear elastic model parameters of EPS10

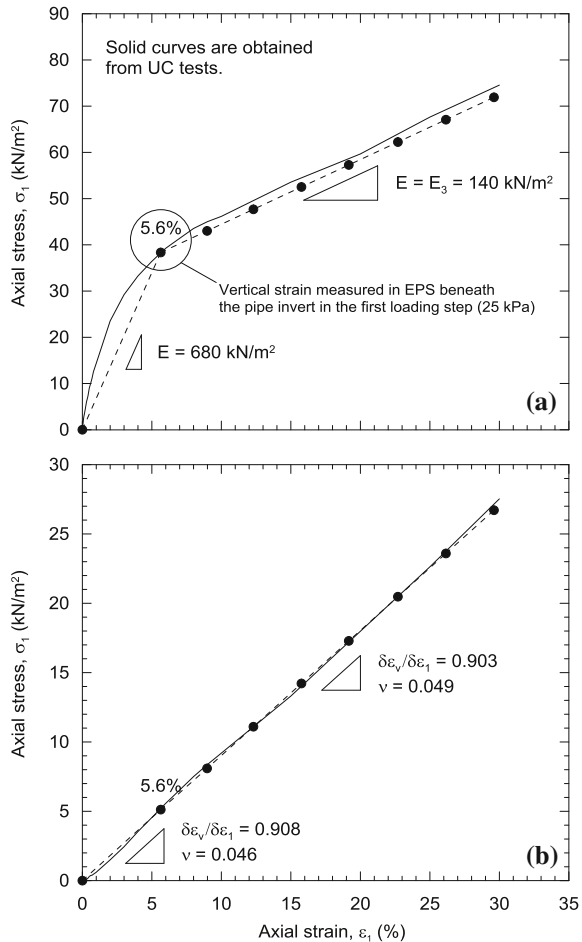


Table 4 The linear elastic model parameters for EPS10

Parameter	Value
E (kPa)	680 (stages 1–3), 140 (stages 2–9)
v (–)	0.046 (stages 1–3), 0.049 (stages 2–9)

E Young's Modulus

v Poisson's Ratio

Interfaces except HDPE—EPS interface were modeled using Hardening Soil Model. Stiffness parameters are as same as those assigned to upper sand (Table 3). Interface strength reduction factors were obtained from the literature review [20, 25, 27].

Mohr-Coulomb (MC) Model was used to model HDPE—EPS interface behavior. Stiffness parameters are as same as those assigned to EPS (Table 4). Angle of shear strength (i.e. angle of interface strength) was assigned as 14° [26] and, therefore, interface strength reduction factor was entered as 1.

Table 5 Angles of interface strength and corresponding interface reduction factors

Parameter	Value			
	Wall—sand	HDPE—sand	HDPE—EPS	EPS—sand
φ_{inter} (°)	5 [20]	20 [25]	14 [26]	>30 [27]
R _{inter} (-)	0.17	0.67	1.00	1.00

φ_{inter} angle of interface strength

R_{inter} interface strength reduction factor

3.3 Modeling the Surcharge Stress

Surcharge stress was modeled by assigning a uniformly distributed line load along the upper boundary of the model geometry (Fig. 7).

3.4 Calculation Stages

Calculation stages are given in Table 6.

4 Results

4.1 Soil Stresses on the Pipe

4.1.1 Vertical Stresses

Vertical stresses at the pipe crown and at the pipe invert measured in the laboratory model tests and obtained from finite element analyses are given in Fig. 9. Under 200 kPa surcharge stress:

Table 6 Calculation stages

Stage	Calculation type	Loading type	Line load (kN/m/m)
Initial stage	Plastic	K ₀ procedure	X
Stage 1	Plastic	Staged construction	0
Stage 2	Plastic	Staged construction	25
Stage 3	Plastic	Staged construction	50
Stage 4	Plastic	Staged construction	75
Stage 5	Plastic	Staged construction	100
Stage 6	Plastic	Staged construction	125
Stage 7	Plastic	Staged construction	150
Stage 8	Plastic	Staged construction	175
Stage 9	Plastic	Staged construction	200

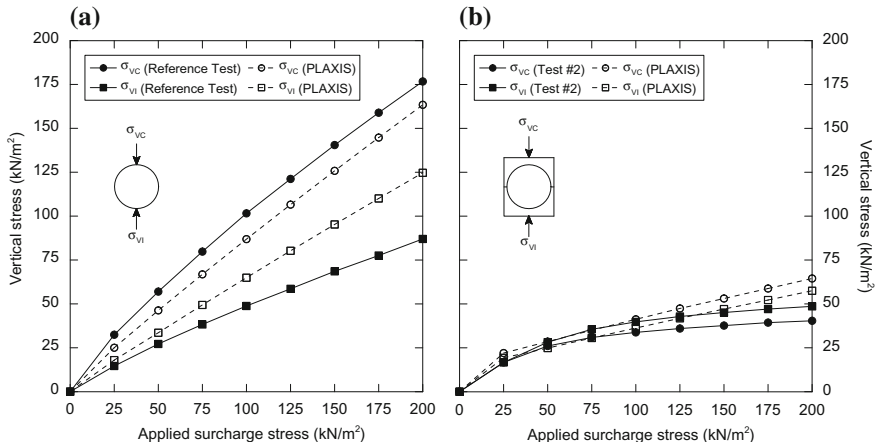


Fig. 9 Vertical stresses at the pipe crown and at the pipe invert

- Vertical stress at the pipe crown is measured as 176.7 kPa in Reference Test and as 40.4 kPa in Test #2. Reduction in vertical stress at the pipe crown is 77.1%.
- Vertical stress at the pipe invert is measured as 87 kPa in Reference Test and as 48.6 kPa in Test #2. Reduction in vertical stress at the pipe invert is 44.1%.

4.1.2 Horizontal Stresses

Horizontal stresses at the pipe springline measured in the laboratory model tests and obtained from finite element analyses are given in Fig. 10. Under 200 kPa surcharge stress horizontal stresses at the pipe springline are measured as 149.8 and 141.5 kPa in Reference Test and as 35.2 and 36.8 kPa in Test #2. Reduction in stress at the pipe springline is 74–76.5%.

4.2 Pipe Deflections

Pipe deflections measured in the laboratory model tests and obtained from finite element analyses are given in Fig. 11. Under 200 kPa surcharge stress:

- Vertical pipe deflection is measured as $-8.86 \text{ mm} (-2.95\%)$ in Reference Test and as $-0.94 \text{ mm} (-0.31\%)$ in Test #2. Reduction in magnitude of vertical pipe deflection is 89.3%.
- Horizontal pipe deflection is measured as $4.93 \text{ mm} (1.64\%)$ in Reference Test and as $-0.22 \text{ mm} (-0.07\%)$ in Test #2. Reduction in magnitude of horizontal pipe deflection is 95.5%.

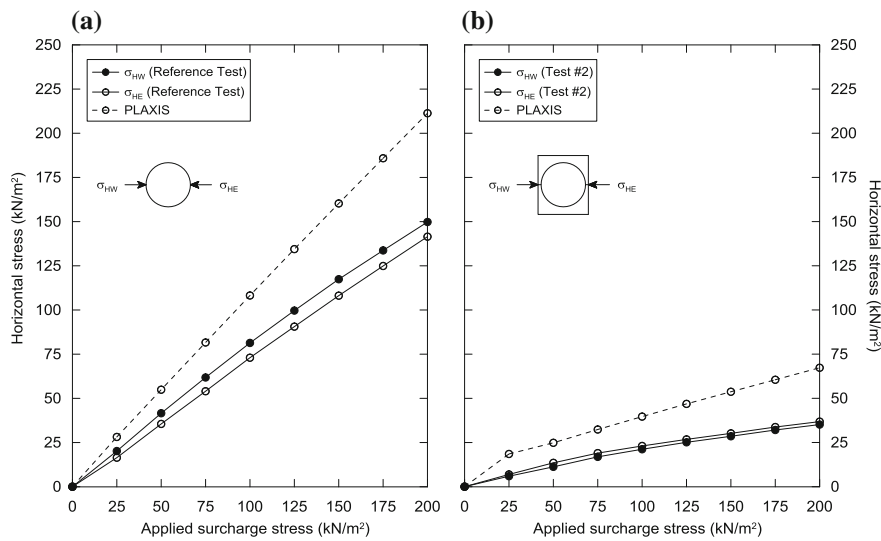


Fig. 10 Horizontal stresses at the pipe springline

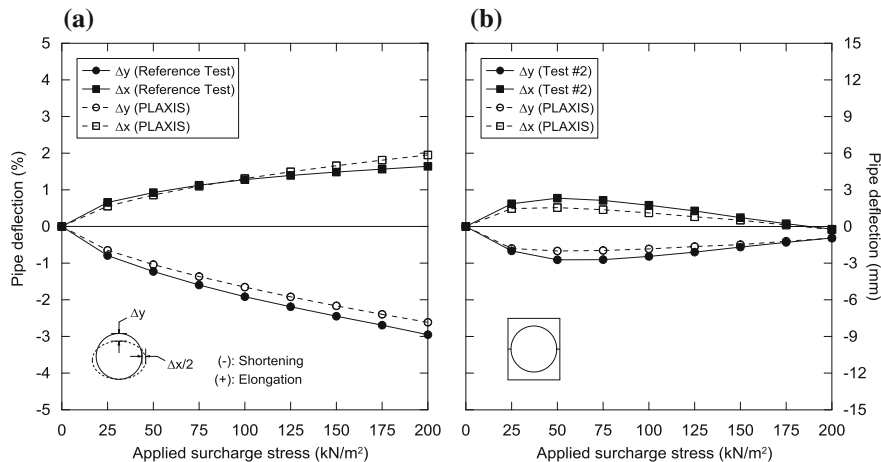
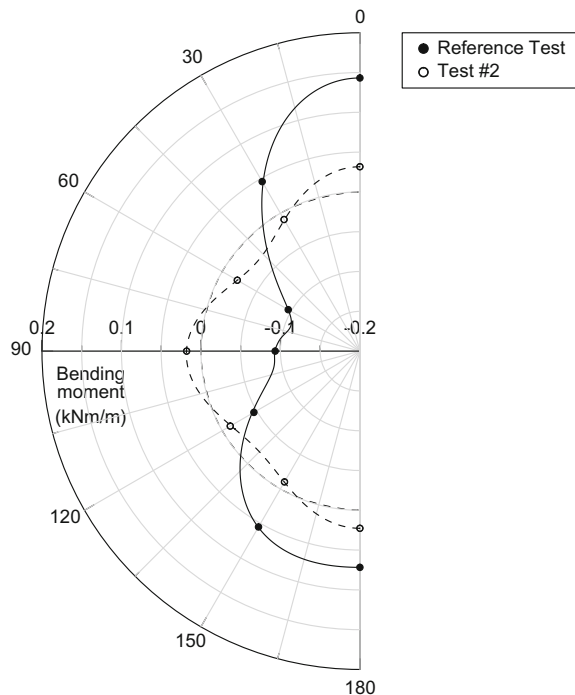


Fig. 11 Pipe deflections

4.3 Bending Moments Around the Pipe

Bending moments around the pipe obtained from finite element analyses are given in Fig. 12. Under 200 kPa surcharge stress:

Fig. 12 Bending moments around the pipe under 200 kPa surcharge stress



- Bending moment at pipe crown is the maximum value around the pipe in both analyses and calculated as 0.143 kNm/m for Reference Test and as 0.032 kNm/m for Test #2. Reduction in magnitude of the maximum bending moment is 77.9%.
- Bending moment at pipe springline is calculated as -0.093 kNm/m for Reference Test and as 0.018 kNm/m for Test #2. Reduction in magnitude of bending moment is 80.7%.
- Bending moment at pipe invert is calculated as 0.072 kNm/m for Reference Test and as 0.023 kNm/m for Test #2. Reduction in magnitude of bending moment is 68.4%.

5 Summary and Conclusions

The effects of compressible zone application on buried HDPE pipe behavior were investigated by true-scale laboratory model tests and finite element analyses. Data obtained from laboratory model tests showed that by applying a compressible zone having similar geometry with that proposed by Kang et al. (2007) the pipe behavior can be improved significantly. Vertical arching factor under 200 kPa surcharge stress was reduced from 0.88 down to 0.20. A reduction of up to 89 and 96% was achieved in magnitude of vertical and horizontal pipe deflections, respectively.

Pipe deflections obtained from finite element analyses showed very good agreement with the measurement data. On the other hand, soil stresses obtained from finite element analyses showed relatively poor agreement with the measurement data. Bending moments calculated in finite analyses showed that compressible zone provided relatively very small bending moments and almost a uniform bending moment distribution around the pipe. Under 200 kPa surcharge stress, a reduction in magnitude of the maximum bending moment around the pipe of 78% was provided.

Acknowledgements This research has been supported by the Scientific and Technical Research Council of Turkey (TUBITAK), Project Number 110M673 and Yıldız Technical University Scientific Research Projects Coordination Department, Project Number: 2014-05-01-DOP01.

References

- Marston A (1922) Second progress report to the joint concrete culvert pipe committee. Iowa Engineering Experimental Station, Ames, Iowa
- Spangler MG (1968) Discussion of the modification of the pressures on rigid culverts with fill procedures. Highw Res Rec 249:41–43
- Rude LC (1979) A study of the imperfect ditch method for rigid culverts. Dissertation, University of Virginia
- Sladen JA, Oswell JM (1988) The induced trench method for buried pipe protection: a critical review and case history. Can Geotech J 25(3):541–549
- McAfee RP, Valsangkar AJ (2004) Geotechnical properties of compressible materials used for induced trench construction. ASTM J Test Eval 32(2):1–10
- McAfee RP, Valsangkar AJ (2008) Field performance, centrifuge testing and numerical modelling of an induced trench installation. Can Geotech J 45(1):85–101
- Parker BA, McAfee RP, Valsangkar AJ (2008) field performance and analysis of a 3-m-diameter induced trench culvert under 19.4-m high soil cover. J Transp Res Board Transp Res Rec 2045:68–76
- Kim H, Choi B, Kim J (2010) Reduction of earth pressure on buried pipes by EPS geofoam inclusions. Geotech Test J 33(4):1–10/GTJ102315
- McGuigan BL, Valsangkar AJ (2010) Earth pressures on twin positive projecting and induced trench box culverts under high embankments. Can Geotech J 47(2):147–163
- Vaslestad J, Sayd MS, Johansen TH, Wiman L (2011) Load reduction and arching on buried rigid culverts using EPS geofoam. Design method and instrumented field tests. Paper presented at the 4th international conference on geofoam blocks in construction applications, Lillestrøm, Norway, 6–8 June 2011
- Sun L, Hopkins TC, Beckham TL (2011) Long-term monitoring of culvert load reduction using an imperfect ditch backfilled with geofoam. Transp Res Rec 2212:56–64
- Kang J, Parker F, Yoo CH (2007) Soil–structure interaction and imperfect trench installations for deeply buried corrugated polyvinyl chloride pipes. Transp Res Rec 2028:192–202
- Turkish Standards Institution (2009) TS EN ISO 9969 Thermoplastics pipes—determination of ring stiffness
- Brachman RWI, Moore ID, Munro SM (2008) Compaction effects on strains within profiled thermoplastic pipes. Geosynth Int 15(2):72–85
- Mert B (2014) Kum Zeminde Rijitliğinin Geogauge ile Belirlenmesi. Dissertation, Yıldız Technical University

16. Wong L, Leo CJ (2006) A simple elastoplastic hardening constitutive model for EPS geofoam. *Geotext Geomembr* 24:299–310
17. Atmatzidis DK, Missirlis EG, Chrysikos DA (2001) An investigation of EPS geofoam behavior in compression. Paper presented at the 3rd international conference on geofoam blocks in construction applications, Salt Lake City, USA, 10–12 Dec 2001
18. Chun BS, Lim H, Sagong M, Kim K (2004) Development of a hyperbolic constitutive model for expanded polystyrene (EPS) geofoam under triaxial compression tests. *Geotext Geomembr* 22:223–237
19. Stark TD, Arellano D, Horvath JS, Leshchinsky D (2004) Geofoam applications in the design and construction of highway embankments. NCHRP web document 65 (project 24-11)
20. Tognon ARM, Rowe RK, Brachman RWI (1999) Evaluation of side wall friction for a buried pipe testing facility. *Geotext Geomembr* 17:193–212
21. Brachman RWI, Moore ID, Rowe RK (2001) The performance of a laboratory facility for evaluating the structural response of small-diameter buried pipes. *Can Geotech J* 38(2): 260–275
22. Deutsches Institut für Normung e.V. (2010) DIN 16961-2 Thermoplastics pipes and fittings with profiled wall and smooth pipe inside—Part 2: technical delivery specifications
23. Dhar AS, Moore ID, McGrath TJ (2004) Two-dimensional analyses of thermoplastic culvert deformations and strains. *ASCE J Geotech Geoenviron Eng* 130(2):199–208
24. Schanz T, Vermeer PA, Bonnier PG (1999) The hardening soil model: formulation and verification. Beyond 2000 in Computational Geotechnics—10 Years of PLAXIS, Balkema, Rotterdam, Netherlands
25. O'Rourke TD, Druschel SJ, Netravali AN (1990) Shear strength characteristics of sand/polymer interfaces. *ASCE J Geotech Eng* 116(3):451–469
26. Sheeley M, Negussey D (2000) An investigation of geofoam interface strength behavior. *ASCE Soft Ground Technol* 112:292–303
27. Xenaki VC, Athanasopoulos GA (2001) Experimental investigation of the interaction mechanism at the eps geofoam-sand interface by direct shear testing. *Geosynth Int* 8(6): 471–499

Part III

Material Properties and Modeling

Creep Behavior of Recycled-Content Expanded Polystyrene Geofoam Under Compressive Loading



Chuanqi Wang, David Arellano and Roger Meier

Abstract This paper presents conventional creep test results for 0, 15 and 30% recycled-content expanded polystyrene (EPS)-block geofoam. The tests were performed on 50-mm (2-in.) cubical specimens with a nominal density of 21.6 kg/m³ under different stress levels for more than 9 months. It is concluded that the creep strain of recycled-content EPS geofoam increases with time and stress level in a manner similar to virgin EPS geofoam. As with virgin EPS geofoam, the elastic-limit stress appears to be a threshold stress level for creep strain development in recycled-content EPS geofoam.

Keywords Creep · Expanded-polystyrene · Geofoam · Recycled-EPS

1 Introduction

Expanded polystyrene (EPS)-block geofoam made of non-recycled, i.e., virgin, expandable polystyrene is being successfully used in many civil engineering applications such as lightweight fill in roadway embankments over soft ground [1, 2] and in landslide stabilization and repair [3–10]. In most geofoam civil engineering applications, the geofoam is subjected to a constant dead load after construction. Creep, which is the slow and continuous deformation of a material under constant stress, may be significant depending on the stress level. Therefore, in geofoam applications that are sensitive to deformation, creep deformation must be considered during design. For example, when EPS-block geofoam is utilized as lightweight fill in roadway embankments over soft soil, a primary consideration is the proper selection and specification of EPS properties so that the geofoam mass can support the overlying pavement system without excessive immediate and

C. Wang
Autozone, Inc, Memphis, USA

D. Arellano (✉) · R. Meier
University of Memphis, Memphis, USA
e-mail: darellan@mempshis.edu

time-dependent (creep) compression. Although research has been performed on the drainage properties of recycled polystyrene [11], the creep behavior of recycled-content EPS has not been studied before. Therefore, recycled-content EPS blocks have not been widely used in civil engineering applications.

This paper presents conventional creep test results. Wang and Arellano [12] present compressive and flexural resistance test results for 0, 15 and 30% recycled-content EPS-block geofoam. Wang et al. [13] and Wang [14] provide an overview of the manufacturing process and methodology used to determine the overall recycled content.

2 Creep Test Design

2.1 *Test Specimens and Stress Levels*

In this research, conventional creep tests were performed on 50-mm (2-in.) cubes with a target density of 21.6 kg/m^3 under various stress levels for a duration of 6700 h (more than nine months). All of the EPS geofoam specimens used in this research were provided by NOVA Chemicals Corporation. The target density of 21.6 kg/m^3 was chosen for this research because it is an ASTM-standard EPS-block density [15] and test data on virgin EPS specimens with this target density are available in the literature [16]. The choice of 50-mm (2-in.) cubical specimens was also made to conform with previous creep research on virgin EPS reported in the literature [16–20]. Although molders manufacture blocks to achieve an overall target density, inherent density gradients occur within the block that yield specimens, which are cut from the block, with various densities that are not equal to the target density of the overall block. The test specimens for each recycled content were obtained from a single block and selected to have densities as close as possible to the 21.6 kg/m^3 target.

The main focus of the creep study was limited to EPS specimens with 30% recycled content because the number of load test frames was limited by space constraints. EPS specimens with 30% recycled content were tested under four different stress levels. EPS specimens with recycled contents of 0 and 15% were tested under only one stress level each to compare test results with results of the 30% recycled content specimens.

The type of virgin polystyrene beads that are mixed with the recycled polystyrene beads can impact the mechanical properties of recycled-content EPS. Therefore, the creep test results presented herein only compares the results obtained on virgin EPS, i.e., 0% recycled-content EPS, made with the same virgin polystyrene beads used to produce the 15 and 30% recycled-content EPS and does not include results of virgin polystyrene reported in the literature to block out the effects of virgin polystyrene bead type on the creep test results.

For virgin geofoam, if the applied stress produces an immediate strain less than 1%, the creep strain will be acceptable (less than 1%) for 50 years or more and if the applied stress produces an immediate strain greater than 1%, creep strain becomes excessive [21, 22]. Therefore, the stress that yields an immediate strain of 1%, which is called the elastic-limit stress, is a design threshold for limiting creep deformation of virgin EPS blocks. In this research, the stress levels used were based on the elastic-limit stresses, shown in Table 1, which were determined from unconfined compressive strength tests performed on companion specimens with the same target density.

For the creep specimens with a recycled content of 30%, four stress levels were applied. The stress levels are 67, 56, 42 and 27 kPa. One stress level exceeded the elastic-limit stress of 63 kPa and three stress levels were less than the elastic-limit stress. For the 0% recycled content specimen, 70 kPa was applied, which exceeded the elastic limit stress of 67 kPa. The stress level applied to the specimen with a recycled content of 15% was 74 kPa, which also exceeded the elastic limit stress of 63 kPa.

Two specimens were tested at each stress level based on the recommendation of ASTM D2990 [23]. Therefore, a total of 12 EPS specimens were tested in this study. The density of each specimen was measured based on the procedure provided in ASTM D1622 [24]. The properties of the specimens and the stress levels used are summarized in Table 1.

2.2 Test System

The creep tests were performed using the load frames shown in Fig. 1, which were designed for this study based on recommendations from ASTM D2990 [23] and on schematics and photos from various literature [20, 25, 26].

Table 1 Specimens and stress levels in creep test

Specimen No.	Measured density (kg/m^3)	Recycled content (%)	Elastic limit stress (kPa)	Applied stress level (kPa)
1	21.50	0	67	70
2	21.75			
3	21.72	15	63	74
4	21.50			
5	21.74	30	63	67
6	21.69			
7	21.62	30	63	56
8	21.96			
9	21.62	30	63	42
10	22.08			
11	21.60	30	63	27
12	22.00			

Fig. 1 Typical creep load test frame system



As shown in Fig. 1, the top plate of the hanger assembly applies the load from dead weights to the specimen, which rests on the load frame. A mechanical dial indicator mounted on the load frame measures the deformation of the specimen.

2.3 Test Procedure

The specimen was initially placed on the load frame as shown in Fig. 1. The hanger assembly was then placed over the specimen carefully to ensure that only the top plate of the assembly touched the specimen and that no portion of the assembly was in contact with any other components of the test system. The mechanical dial indicator was then attached to the load frame and positioned over the center of the hanger assembly top plate. Finally, the dead load weights corresponding to the test stress level were placed on the hanger and the deformation with time due to the combined weight of the load frame and dead load weights was recorded.

The dead load was applied rapidly (within 5 s) but carefully to avoid impact loading to the specimen. The test time started when the dead load weights were placed on the hanger. Deformation readings were recorded at elapsed times of 1, 6, 12 and 30 min; 1, 2, 5, 50, 100, 200, 500, 700, 1000 h and at least one time per month after 1000 h. These time intervals are recommended in ASTM standard D2990 [23].

3 Discussion of Test Results

3.1 Measured Compressive Creep Behavior

The average creep test results for each pair of specimens are shown in Fig. 2. As indicated before, two specimens were tested for each recycled content and stress level as summarized in Table 1. The term “creep strain” used in this research

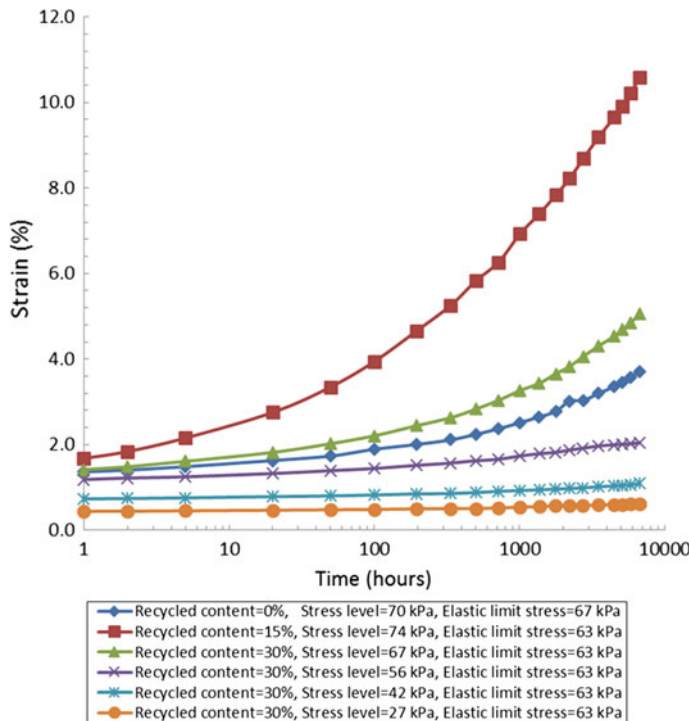


Fig. 2 Average creep response for each pair of specimens

represents the total strain (the immediate elastic strain plus the additional creep strain that accumulates with time) based on ASTM standard D2990 [23]. It does not include the negligible deformation of the specimen due to the weight of the hanger assembly itself, only the dead weights added to the hanger assembly. Preliminary creep test data for duration of 1000 h were provided by Wang and Arellano [12]. The complete 6700 h creep test results are provided herein.

3.2 Analysis of Test Data

Figure 2 shows that creep strain increases with an increase in applied stress level and with time. Dramatic differences in creep strain between the specimens under different applied stress levels can be seen, especially for specimens tested at a stress level greater than the elastic-limit stress (Specimens 1 through 6 in Table 1) compared to the specimens tested at a stress level less than the elastic limit stress (Specimens 7 through 12 in Table 1).

The results shown in Fig. 2 indicate that the creep strain rate is much greater for specimens subjected to stresses greater than the elastic-limit stress compared to

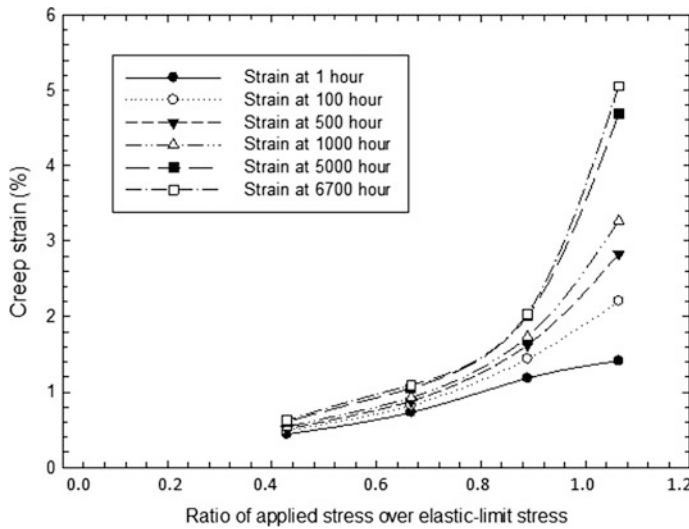


Fig. 3 Isochronous creep strains as a function of the ratio of applied stress to elastic-limit stress

specimens subjected to stresses less than elastic-limit stress. In order to further evaluate this observation, isochronous creep strain versus ratio of applied stress to elastic limit stress curves for the 30% recycled-content EPS specimens are shown in Fig. 3. As indicated in Fig. 3, creep strains increase with an increase in the ratio of the applied stress to the elastic-limit stress, especially if the ratio is greater than 1. Therefore, the elastic-limit stress appears to be a threshold stress level for the development of excessive creep strains in recycled-content EPS geofoam. Horvath [21] and Arellano et al. [22] arrived at a similar conclusion regarding the creep behavior of virgin EPS geofoam.

Figure 4 shows the isochronous stress-strain curves at 1, 100, 500, 1000, 5000 and 6700 h for the 30% recycled content specimens. The isochronous stress-strain curves are useful for estimating the strain from a known stress load in geotechnical applications where sustained loads are involved. From Fig. 4, the time to reach 1% creep strain was determined. Those results are summarized in Table 2.

Table 2 shows that at applied loads less than 67% of the elastic-limit stress, the creep strain will be less than 1% in 5000 h. However, if the applied load is greater than 89% of the elastic-limit stress, the creep strain will be greater than 1% within 1 h. However, it is not known, at this time, what critical ratio of applied stress to elastic-limit stress causes the creep strain to dramatically increase due to lack of information when the applied load is between 67 and 89% of elastic-limit stress.

Another format for plotting creep data is the Sherby-Dorn plot [21]. The vertical axis is creep strain rate on a log scale and the horizontal axis is creep strain on an arithmetic scale. The Sherby-Dorn plots for the specimens with 30% recycled content are shown in Fig. 5.

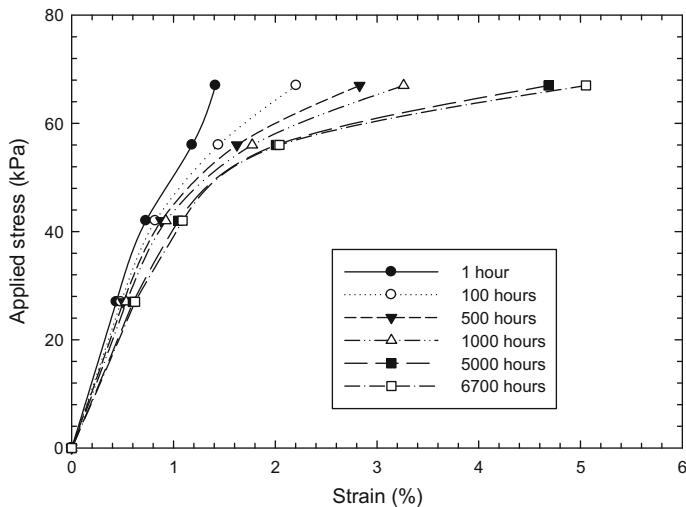


Fig. 4 Isochronous stress-strain curves for 30% recycled-content EPS specimens

Table 2 Time to reach 1% strain at various stress levels for 30% recycled-content EPS specimens

Applied stress (kPa)	Applied stress: elastic-limit stress	Time to yield 1% strain (hours)
27	0.43	>6700
42	0.67	5000
56	0.89	<1
67	1.06	<1

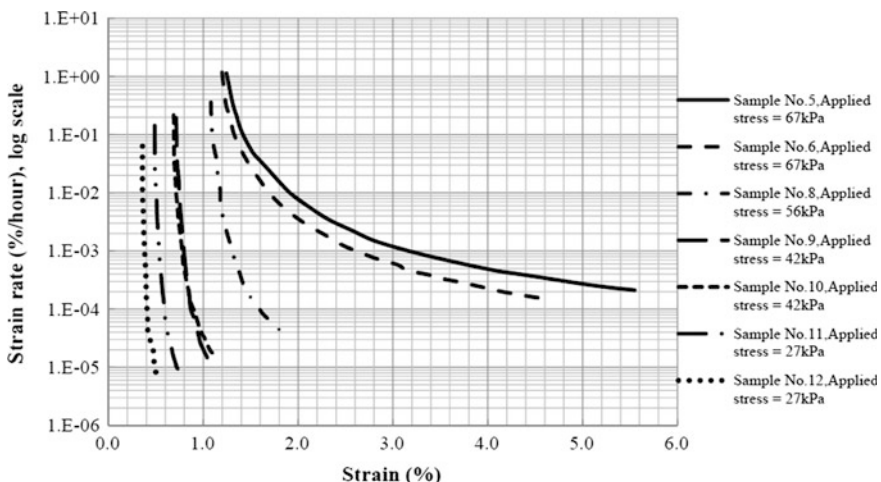


Fig. 5 Sherby-Dorn plot for 30% recycled-content EPS specimens

Figure 5 illustrates that (1) the creep rate decreases with increasing strain, which also means the creep rate decreases over time; (2) the creep rate potentially becomes constant with time, as suggested by Samples 5 and 6; and (3) if that is true, the limiting creep rate under stress levels greater than the elastic-limit stress (i.e., Samples 5 and 6) will be significantly greater than it is under stress levels less than the elastic-limit stress (e.g., Specimen 8).

4 Conclusions

A summary of key conclusions from the creep study and some recommendations for future research are provided below.

- Creep strain of recycled-content EPS geofoam increases with time and stress level in much the same way as it does for virgin EPS geofoam.
- The elastic-limit stress appears to be a threshold stress level for creep strain development in recycled-content EPS geofoam as it is for virgin EPS geofoam.
- The creep rate continues to decrease, and potentially becomes constant, with time.
- When the applied load is less than 67% of the elastic-limit stress, the creep strain will be less than 1% in 5000 h, but if the applied load is greater than 89% of the elastic-limit stress, the creep strain will be greater than 1% within 1 h. It is not known, at this time, what critical ratio of applied stress to elastic-limit stress causes the creep strain to dramatically increase within the first hour because, currently, there is a lack of creep data when the applied load is between 67 and 89% of the elastic-limit stress.
- For future study, additional creep tests are needed at stress levels between 67 and 89% of the elastic-limit stress to better determine the threshold stress level beyond which creep strain becomes unacceptably large.
- For future study, additional creep tests need to be performed on specimens with other recycled contents and densities to study their effects on the creep behavior of recycled-content EPS-block geofoam.

The authors are currently developing an empirical model that can be used to predict creep deformation of 30% recycled-content EPS geofoam based on the creep test results presented herein. It is anticipated that the availability of creep behavior data for recycled-content EPS will expand the use of recycled-content EPS geofoam in civil engineering applications and will contribute to more sustainable infrastructure systems by decreasing the amount of polystyrene that ends up in landfills.

References

1. Stark, TD, Arellano, D, Horvath, JS, Leshchinsky, D (2004) Guideline and recommended standard for geofoam applications in highway embankments. NCHRP Report 529, Transportation Research Board, Washington, D.C., http://trb.org/publications/nchrp/nchrp_rpt_529.pdf. Accessed 20 Dec 2014
2. Stark TD, Arellano D, Horvath JS, Leshchinsky D (2004) Geofoam applications in the design and construction of highway embankments. NCHRP Web Document 65, Transportation Research Board, Washington, D.C., http://trb.org/publications/nchrp/nchrp_w65.pdf. Accessed 20 Dec 2014
3. Negussey D (2002) Slope stabilization with geofoam. FHWA research project no. 2398P62000015, Geofoam Research Center, Syracuse University, Syracuse, NY
4. Arellano D, Tatum JB, Stark TD, Horvath JS, Leshchinsky D (2010) A framework for the design guideline for EPS-block geofoam in slope stabilization and repair. Transp Res Record J Transp Res Board 2170:100–108
5. Arellano D, Stark TD, Horvath JS, Leshchinsky D (2011) Guidelines for geofoam applications in slope stability projects. NCHRP Project 24-11(02) Final Report, Transportation Research Board, Washington, D.C., [http://onlinepubs.trb.org/onlinepubs/nchrp/docs/NCHRPP24-11\(02\)_FR.pdf](http://onlinepubs.trb.org/onlinepubs/nchrp/docs/NCHRPP24-11(02)_FR.pdf). Accessed 20 Dec 2014
6. Arellano D, Stark TD, Horvath JS, Leshchinsky D, Kafash MH, Wang C (2011) Overview of NCHRP design guideline for EPS-block geofoam in slope stabilization. In: Proceedings of the 4th international conference on the use of geofoam blocks in construction applications, EPS 2011, The Norwegian Public Roads Administration, Norway
7. Arellano D, Stark TD, Horvath JS, Leshchinsky D (2013) Guidelines for geofoam applications in slope stability projects, NCHRP Research Results Digest 38, Transportation Research Board, Washington, D.C., <http://www.trb.org/main/blurbs/168692.aspx>. Accessed 20 Dec 2014
8. Akay O, Özer AT, Fox GA, Bartlett SF, Arellano D (2013) Behavior of sandy slopes remediated by EPS-block geofoam under seepage flow. Geotext Geomembr 37:81–98
9. Kafash MH, Arellano D (2013) Seismic stability analysis of slopes stabilized with EPS-block geofoam. In: Proceedings of the 2013 geocongress: stability and performance of slopes and embankments III, pp 1736–1739, ASCE, Reston, VA
10. Özer AT, Akay O, Fox GA, Bartlett SF, Arellano D (2014) A new method for remediation of sandy slopes susceptible to seepage flow using EPS-block geofoam. Geotext Geomembr 42:166–180
11. Arellano D, Zarrabi M, Jafari NH, Bailey LJ (2009) Geosynthetic aggregate drainage systems: preliminary large-scale laboratory test results for expanded recycled polystyrene. In: Proceedings of the geosynthetics 2009 & GRI-22 conference (CD-ROM), IFAI, Roseville, MN
12. Wang C, Arellano D (2014) Are the mechanical properties of recycled-content expanded polystyrene (EPS) comparable to non-recycled EPS geofoam? In: Proceedings of the 2014 geo-congress, geo-characterization and modeling for sustainability, pp 3506–3515, ASCE, Reston, VA
13. Wang C, Arellano D, Ladely L, Koerner DW (2013) Preliminary assessment of the mechanical properties of recycled-content expanded polystyrene (EPS) block geofoam. In: Proceedings of geosynthetics 2013, (CD-ROM), IFAI, Roseville, MN
14. Wang C (2015) Characterizing, testing and modeling the mechanical proper-ties of recycled-content expanded polystyrene-block geofoam. Ph.D. Dissertation, The University of Memphis, Memphis, TN
15. ASTM (American Society for Testing and Materials) D6817 (2011) Standard specification for rigid cellular polystyrene geofoam. West Conshohocken, PA
16. Sheeley M (2000) Slope stabilization utilizing geofoam. M.S. thesis, Syracuse University, Syracuse, NY

17. Sun MCW (1997) Engineering behavior of geofoam (expanded polystyrene) and lateral pressure reduction in substructures. M.S. thesis, Syracuse University, Syracuse, NY
18. Horvath JS (1998) Mathematical modeling of the stress-strain-time behavior of geosynthetics using the Findley equation: general theory and application to EPS-blocks geofoam. Manhattan College Research Report No.CE/GE-98-3, Manhattan College, New York, NY, <http://jsche.com/files/cege-1998-3.pdf>. Accessed 15 Aug 2008
19. Srirajan S, Negussey D, Anastas N (2001) Creep behavior of EPS geofoam. In: Proceedings EPS geofoam 2001 3rd international conference (CD-ROM), University of Utah, Salt Lake City, UT
20. Gnip IJ, Kersulis VI, Vaitkus SI (2005) Long-term prediction of creep strain of expanded polystyrene. *Mech Compos Mater* 41(6):535–540
21. Horvath JS (1995) Geofoam geosynthetic, Scarsdale, NY
22. Arellano D, Aabøe R, Stark TD (2001) Comparison of existing EPS-block geofoam creep models with field measurements. In: Proceedings EPS geofoam 2001 3rd international conference (CD-ROM), University of Utah, Salt Lake City, UT
23. ASTM (American Society for Testing and Materials) D2990 (2009) Standard test method for tensile, compressive, and flexural creep and creep-rupture of plastics. West Conshohocken, PA
24. ASTM (American Society for Testing and Materials) D1622 (2008) Standard test method for compressive properties of rigid cellular plastics. West Conshohocken, PA
25. Yeo S (2007) Evaluation of creep behavior of geosynthetics using accelerated and conventional methods. Ph.D. Dissertation, Drexel University, Philadelphia, PA
26. Yourd RA (1996) Compression creep and long-term dimensional stability in appliance rigid foam. *J Cell Plast* 32(6):601–616

The Influence of Strain Rate on the Stress-Strain Behavior of EPS Geofoam



Djiba Kaké, Engda Kassahun Temesgen and Dawit Negussey

Abstract Modulus, yield and strength properties of EPS geofoam that are reported in standards and specifications vary by density and are typically derived from testing small size samples at 10% per minute strain rate. Such values are augmented by creep test data from published sources in design considerations. Average loading rates during construction and sustained dead loads in post construction induce much slower strain rates. Live loads from truck traffic and extreme events such as earthquakes occur at faster strain rates. The margin of higher strengths that could be justifiably allowed for extreme events of short duration has not been established. This investigation examined the effects of strain rates on moduli and strengths for different densities of EPS geofoam.

Keywords Density · Geofoam · Modulus · Strain · Strain rate · Strength

1 Introduction

EPS geofoam is a super lightweight material that has been used for a wide variety of civil infrastructure projects. The density-strength relation of geofoam is remarkable compared to other geotechnical materials [1]. Geofoam has been used for slope stabilization, retaining structures, embankments and foundations. Because of its very light weight and large block volume, geofoam is easy to transport and install on projects. The use of EPS for thermal insulation of buildings is more widespread. For design proposes, two methods are commonly used relying on stress-strain curves derived from uniaxial compression tests that were performed at a standard strain rate of 10% per minute. One approach consists of taking the value of the strength at 1% strain as total working stress. Whereas a second approach considers 30% of the value of the strength at 10% strain for dead load with an additional 10%

D. Kaké · E. K. Temesgen · D. Negussey (✉)
Syracuse University, Syracuse, NY, USA
e-mail: negussey@syr.edu

for live load. These conservative design approaches were to in part in consideration of the rheological behavior of geofoam. The initial moduli for EPS geofoam have been known to depend on test sample dimensions [2]. This research briefly examines the relative influence of strain rate and density on the stress-strain behavior of EPS geofoam, including cyclic responses from unloading initiated beyond yield states.

2 Investigation Program

The objective of the investigation was to characterize the behavior of EPS geofoam under compressive loads at different nominal densities; 16, 20, 32 and 40 kg/m³. Geofoam compressive properties were measured according to ASTM standards [3]. All test samples were 50 mm cubes. For each density, tests were performed at 0.01, 0.1, 1, 10, and 100% per minute strain rate. Each test sample was loaded to 15% strain, assuming yielding remains below 2%. A 20 kg/m³ sample was loaded at 0.001% strain rate for 4 weeks.

The compression tests were performed using DC motor loading test frames and distributed data acquisition and control (DDAC) systems. DDAC modules receive analog signals to convert to digital. Also when in feedback loop control, receive digital commands to convert to analog messages. The loading frame and data acquisition modules were configured to be in close proximity to minimize noise (Figs. 1 and 2).

All tests except the highest strain rate of 100% per minute were performed using the standard configuration, Fig. 1, and software. For the highest strain rate of 100% per minute, a modified testing arrangement was devised to enable a rapid sampling rate to acquire more data points in the elastic range. The high speed system acquired five times more data than the conventional configuration.

3 Monotonic Test Results

Previous investigations on geofoam have shown initial modulus increases with density [5, 6]. Initial and post yield moduli were obtained from a series tests at different strain rates for each density. Figure 3 shows results for a 40 kg/m³ density samples at five strain rates. Initial moduli, E_i , and post yield moduli, E_p , were determined for each test. The initial moduli were relatively independent of strain rate whereas yield stress values increase with strain rate. Post yield moduli also slightly increase with strain rate. The results for all tests are summarized in non-dimensional form in Fig. 4.

The best fit lines for initial moduli and also post yield moduli with density are shown in Fig. 4. The results suggest the initial moduli increases with density while the post yield moduli tend to increase with strain rate and density. Equations 1 and 2

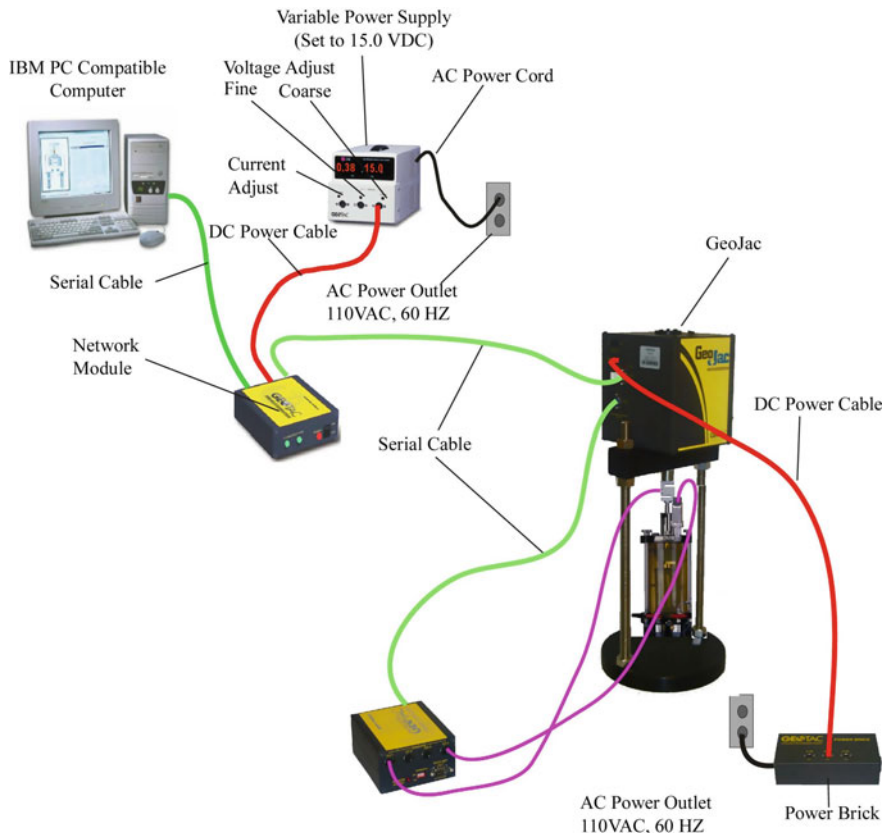


Fig. 1 GeoJac testing system [4]

represent relations of the best fit line for the initial and post yield moduli data respectively.

$$\log_{10} \left(\frac{E_i}{Pa} \right) = 0.03 \left(\frac{\gamma}{\gamma_a} \right) + 1.03 \quad (1)$$

$$\log_{10} \left(\frac{E_p}{Pa} \right) = 0.03 \left(\frac{\gamma}{\gamma_a} \right) - 0.28 \quad (2)$$

Where: E_i is the geofoam initial modulus [kPa], E_p is the geofoam post yield modulus [kPa], P_a is the atmospheric pressure at sea level at 20 °C, γ is the geofoam density [kg/m^3], and γ_a is the air density at sea level at 20 °C [kg/m^3].

The two linear best fit lines in Fig. 4 have the same approximate slope. This suggests the rates at which the initial and post yield moduli increase with density are equal.

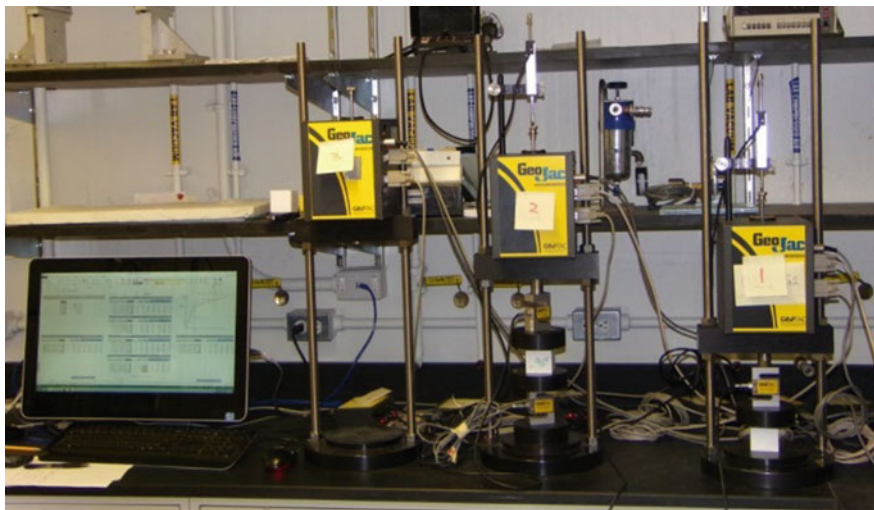


Fig. 2 System installation for multiple tests

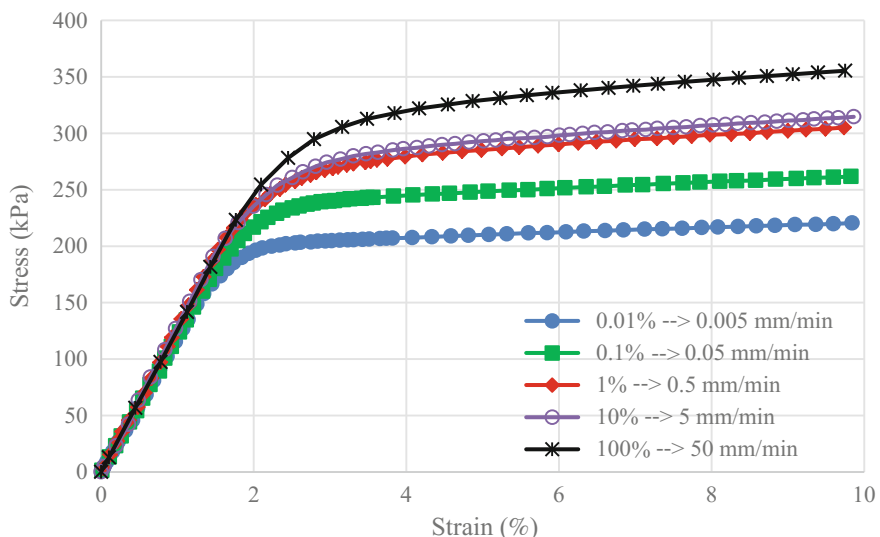


Fig. 3 Stress versus strain plots for a 40 kg/m^3 density 50 mm cube specimen

The transition from elastic to plastic states for EPS geofoam is gradual, as shown in Fig. 5. For each density, the initial modulus line intersects with different post yield lines at quasi yield stress and strain states. These apparent yield stress states increase with strain rate and density as shown in Fig. 6, but on average can be represented by Eq. 3.

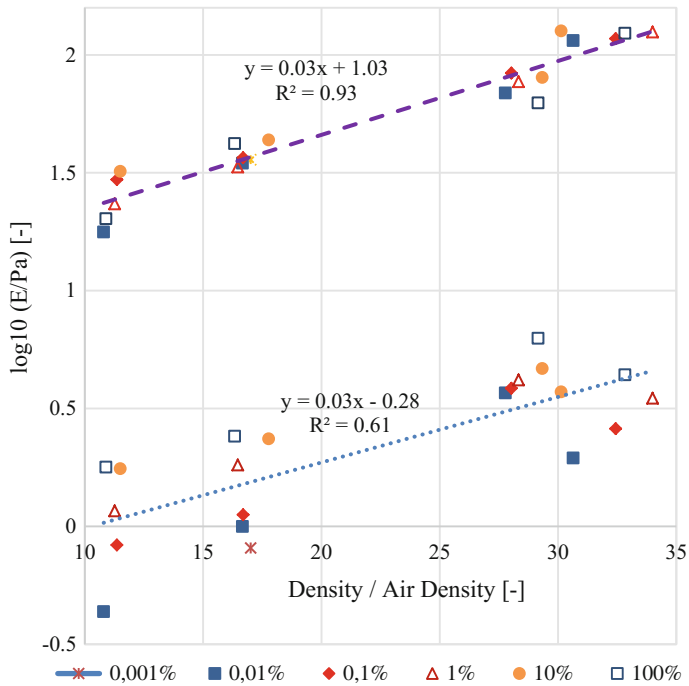
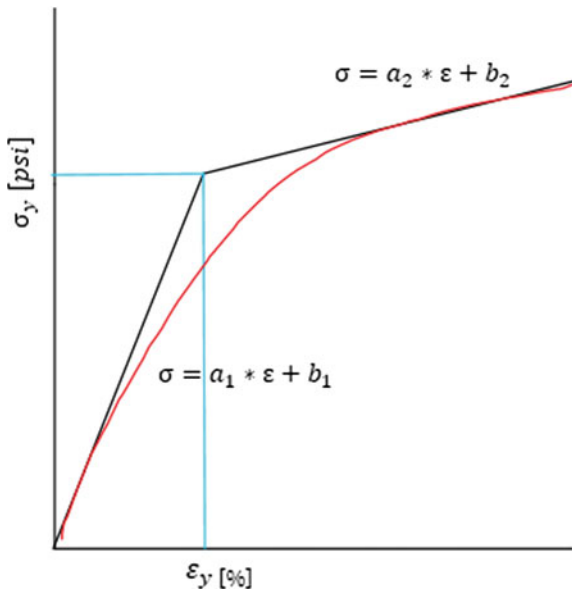


Fig. 4 Normalized initial and post yield moduli versus density

Fig. 5 Definition of the yield stress and strain



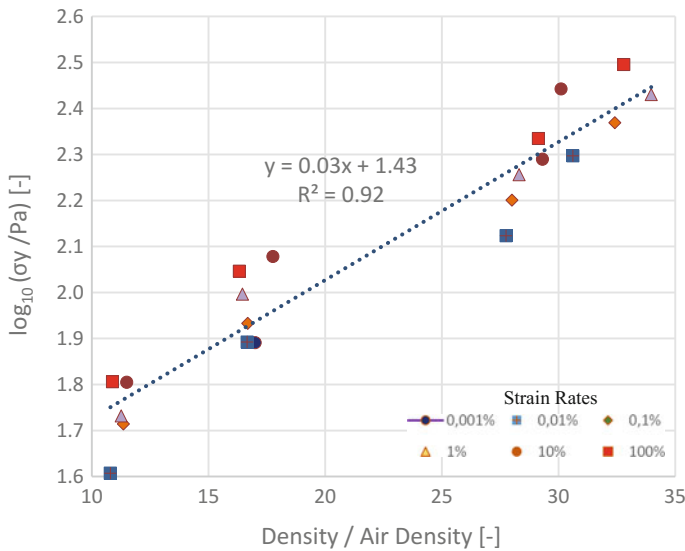


Fig. 6 Normalized yield stress versus density

$$\log_{10}\left(\frac{\sigma_y}{\text{Pa}}\right) = 0.03\left(\frac{\gamma}{\gamma_a}\right) + 1.43 \quad (3)$$

Where: σ_y is the geofoam yield stress.

The apparent yield strain states also tend to increase with strain rate at each density from about 1.7 to 3.5%, Fig. 7. At high strain rate and short duration loading, the strain range over which the elastic modulus applies is greater than at low rates of loading. There would therefore tend to be higher reserve strengths for short duration extreme events such as during seismic loading. The results show that working strengths to 1% strain remain relatively independent of strain rate but increase with density. The apparent yield stress and strengths at 10% strain increase with both strain rate and density.

4 Cyclic Test Results

Results from load cycling from loading to 15% strain for a 40 kg/m^3 density geofoam at different strain rates are shown in Fig. 8. The initial moduli were not sensitive to strain rate changes. Unload-reload cycles from high strain rates developed degraded cyclic loading moduli when compared to the initial moduli. However, at the slowest strain rate, the initial moduli and the reloading moduli were essentially the same. This behavior is also evident in the results for 20 kg/m^3 density samples that were unloaded and reloaded from 10% strain, Fig. 9. When cyclic loading of 20 kg/m^3 nominal density geofoam samples was initiated from 20% strain, Fig. 10,

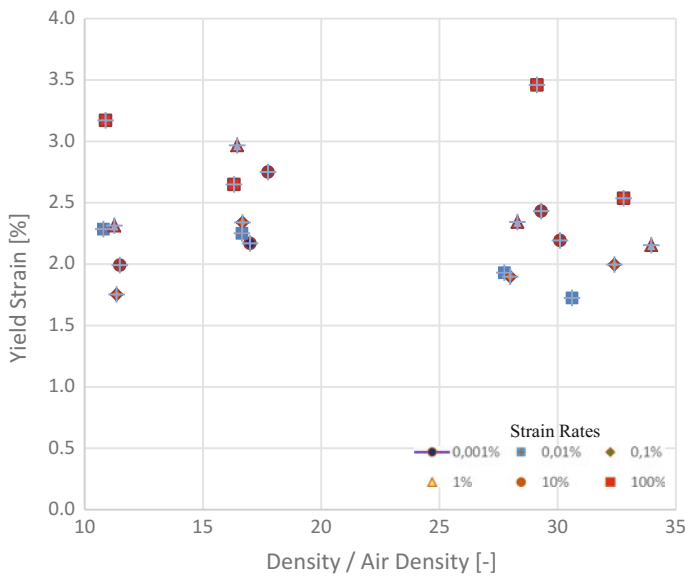


Fig. 7 Yield strain versus normalized density

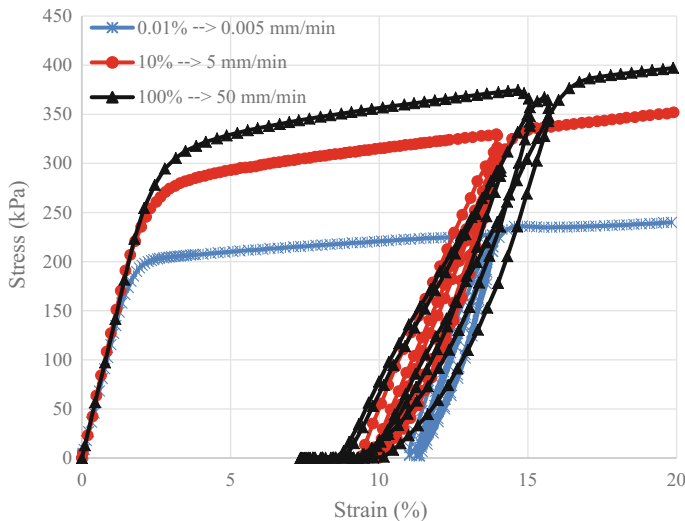


Fig. 8 Cyclic loading at 15% strain of a cubic 40 kg/m³ density 50 mm specimen

the results for the highest strain rate show more severe degradation of the reloading moduli as compared to the initial moduli. The corresponding conditions for the lowest strain rate in Figs. 8, 9 and 10, show a relatively hysteresis loop and approximately the same initial and reload moduli. The more severe modulus

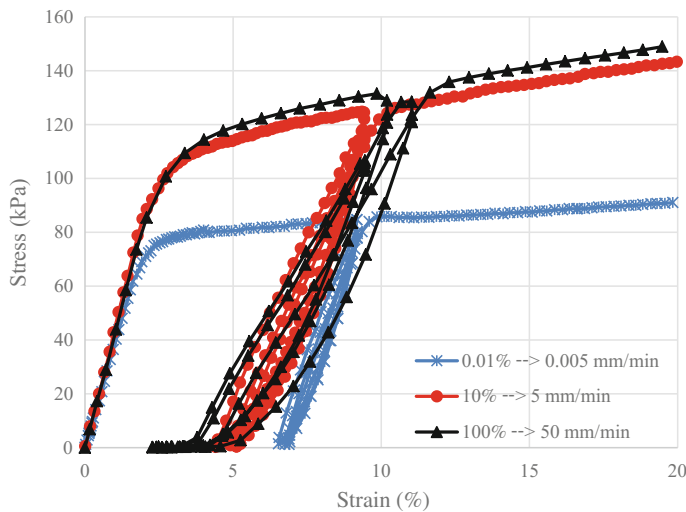


Fig. 9 Cyclic loading at 10% strain of a cubic 20 kg/m^3 density 50 mm specimen

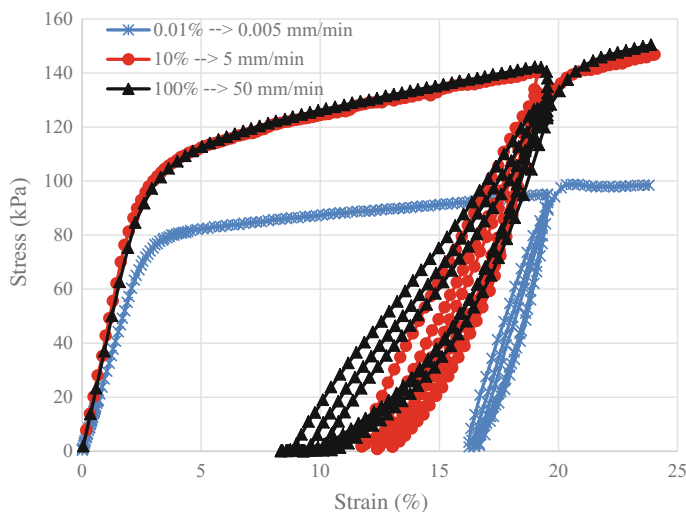


Fig. 10 Cyclic loading at 20% strain of a cubic 20 kg/m^3 density 50 mm specimen

degradation from loading to large strain and cycling at high strain rate suggest the samples may not have completed the rebound phase as re-loading was initiated. The initial segments of the unloading curves provide relatively rate insensitive moduli that are approximately the same as the initial moduli. Degradation of moduli in cyclic re-loading was also observed previously. The results of this investigation suggest degradation of re-loading moduli manifest rate effects.

5 Concluding Remarks

The results of a series of compression tests on 50 mm cube geofoam samples indicate initial moduli and yield stresses increase with density. The initial moduli were relatively independent of strain rate. Yield stresses estimated as the intersection of initial and post yield moduli extensions increased with strain rate. Corresponding yield strain values also increased within a narrow range with strain rate. Yield strain values at the onset of non-linearity can be assumed to remain constant with density. The post yield (plastic) modulus increases with strain rate. As a result, design criteria on the basis of factored strength derived from strength at 10% strain change depending on strain rate. Working stress levels at 30% of strength for dead load and with additional 10% for live load remain well below the strength at 10% strain achieved at the slowest strain rate for the respective densities. Observed modulus degradations on reloading during cyclic tests became more pronounced with increasing strain rate.

Acknowledgements The authors gratefully acknowledge the support of INSA Strasbourg, France, for a summer internship at Syracuse University for the lead author. Steve Trautwein provided a rapid sampling data acquisition software for the high strain rate testing. Thermal Foams of Syracuse provided EPS geofoam samples. R. Chave, John Banas and W. Dossert assisted with the test system set up, equipment modifications and sensor calibrations.

References

1. Negussey D, Jahanandish M (1993) Comparison of some engineering properties of expanded polystyrene with those of soils. *Transp Res Rec J Transp Res Board* 1418:43–50
2. Elragi A, Negussey D, Kyanka G (2000) Sample size effects on the behavior of EPS geofoam. In: Paper presented at the soft ground technology conference, Noordwijkerhout, Netherlands, May 28–June 2, 2000
3. ASTM C165
4. Trautwein catalogs and brochures (2003) Sigma – 1 UU Instruction manual version 1.00. Trautwein soil testing equipment, Houston, Texas
5. Negussey D (2007) Design parameters for EPS geofoam. *Soils Found Jpn Geotech Soc* 47 (1):161–170
6. Duskov M (1997) EPS as a light-weight sub-base material in pavement structures. Delft University of Technology, Delft

Evaluation of Interface Shear Strength Between Interlocked Geofoam Blocks and Precast Concrete



Abdullah Tolga Özer

Abstract The separation layer between the top of an expanded polystyrene (EPS) block (geofoam block) roadway embankment assemblage and the pavement system is usually comprised of a reinforced Portland cement concrete (PCC) slab. The prevailing construction technology is the cast-in-place method. However, there is a growing consensus that the current state of practice may represent a significant cost, especially to project schedules. As an alternative, this study proposes the use of precast concrete panels. In order to guide design engineers, interface friction properties of traditional flat-surfaced geofoam blocks with a minimum density of 18.4 kg/m^3 and precast concrete panels were quantified by using direct shear testing. In addition, four different types of interlock configurations (geofoam blocks with one- and four-square ledges and geofoam blocks with one- and four-triangle ledges) were used to investigate the effects of interlocked geometry and number of ledges in the shear plane between interlocked geofoam block and precast concrete. The interface friction behavior of precast concrete and traditional flat-surfaced geofoam block was found to be purely frictional. The interface friction angle of precast concrete and interlocked geofoam blocks was found to be higher than that of traditional geofoam blocks. Implementing an interlocked configuration, which interrupts the continuous shear plane with ledges, changes the interface friction mechanism of precast concrete and geofoam block from purely frictional to frictional-adhesional. Independent of the geometry of the ledges, adhesion was developed in addition to interface friction. Both adhesion and interface friction angle increased with number of ledges.

Keywords EPS-block geofoam • Interface shear • Precast concrete

A. T. Özer (✉)
Okan University, Istanbul, Turkey
e-mail: tolga.ozer@okan.edu.tr

1 Introduction

Reinforced concrete separation slabs are traditionally constructed between the pavement system and expanded polystyrene (EPS) block geofoam (geofoam block) highway embankments [1]. On the other hand, concrete load distribution slabs can be substituted with granular materials using concrete to gravel gravimetric ratio of 1:3 [1]. However, this increases dead load on the geofoam block assemblage. In addition, a concrete slab also provides a surface to anchor road hardware too [1]. The prevailing technology is cast-in-place for concrete placement. Upon construction of the cast-in-place concrete load distribution slab, a curing period must be waited before the sub-base- and base-material of the pavement section can be constructed over the concrete slab. As an alternative technique, the possibility of using precast concrete as a load distribution slab is investigated in this study.

Design guidelines of geofoam block highway embankments require performing internal stability analysis consisted of hydrostatic sliding, transition due to wind and seismic stability [1]. These analyses are performed to check whether the geofoam embankment assemblage acts as a coherent mass under external loads or not. Therefore, the shear resistance of each interface within the assemblage needs to be quantified.

Shear resistance between traditional geofoam blocks (geofoam-geofoam) [2–6] and between geofoam blocks and bedding sand (geofoam-sand) [3, 4, 7, 8] have been studied by various researchers. On the other hand, there is a significant gap in the literature for interface shear resistances between geofoam and dissimilar materials used in geofoam embankments, especially geosynthetics and cast-in-place concrete [1]. There are limited interface shear strength studies for geofoam and cast-in-place concrete (geofoam-cast-in-place concrete) [2, 9] and geofoam and precast concrete (geofoam-precast concrete) [10].

Geofoam-geofoam interface shear resistance can be improved by using an interlocked geofoam block concept [6, 11]. In this concept, geofoam blocks are prepared using ledges along the top and notches along the bottom. Then, once the blocks are placed on top of each other, an interlocked surface is formed.

In this study, interface shear resistance between interlocked geofoam blocks and precast concrete (interlocked geofoam-precast concrete) has been investigated. In addition, shear strength properties of the interface between traditional flat-surfaced geofoam block and precast concrete (geofoam-precast concrete) was quantified not only to compare improvements provided by interlocking mechanism but also to compare with the existing literature. Direct shear testing was used to quantify the interface shear stress parameters. The results of the study were evaluated in terms of the possibility of using precast concrete as an alternative separation material between the pavement and geofoam blocks.

2 Materials and Methods

Geofoam block classified as EPS19, based on ASTM D6817 [12], was used in the interface shear testing program. Mechanical properties of the EPS19 geofoam blocks, based on the compressive strength testing [13] results from five different specimens, are summarized in Table 1 [6]. In addition, the results are also compared with that of minimum required values of ASTM D6817 [12].

In addition to the interface shear strength of geofoam-precast concrete, the shear strength behavior of four different interlocked geofoam-precast concrete interfaces was investigated (Fig. 1). Geofoam block test specimens were trimmed with a hot wire cutter to the dimensions of 10 cm wide, 15 cm long and 2.5 cm high. Ledges located along the top of the geofoam blocks were 0.5 cm wide, 0.5 cm high and 10 cm long (Fig. 1). Two different ledge geometries (triangle and square) were used to investigate the effect of ledge geometry on the stress-strain behavior. In addition, one and four ledges were tested for each shape to investigate the effect on number of ledges used (Fig. 1). The dimensions of the geofoam specimens were selected in order to represent a 1:20 scale comparison of traditionally produced block sizes.

Interface shear strength properties were measured using ASTM D3080 [14] which was recommended by ASTM D5321 [15]. Even though ASTM D5321 [15] is a standard for quantifying shear strength of soil-geosynthetic and geosynthetic-geosynthetic interfaces, it has been successfully used for quantifying geofoam-geofoam interface shear strength by various researchers [2–6]. Therefore, direct shear testing was also used in this study (Fig. 2). The fully-automated direct shear test frame used in this study includes vertical and horizontal load cells. Application of stresses are controlled by microstepper motors. Horizontal and vertical linear

Table 1 Mechanical properties of EPS19 geofoam blocks [6]

Property	Values	
	Laboratory test values minimum-maximum (average, standard deviation)	ASTM D6817 [12] minimum required values
γ (kg/m ³)	18.08–18.96 (18.54, 0.38)	18.4
σ_1 (kPa)	38.0–45.5 (40.21, 3.54)	40
σ_5 (kPa)	90.2–96.8 (93.9, 2.86)	90
σ_{10} (kPa)	101.2–107.1 (105.0, 2.72)	110
E_i (MPa)	3.5–4.1 (3.73, 0.24)	–

ASTM American society for testing and materials

γ apparent density

σ_1 , σ_5 , σ_{10} compressive resistance at 1, 5 and 10% strain, respectively

E_i initial Young's modulus

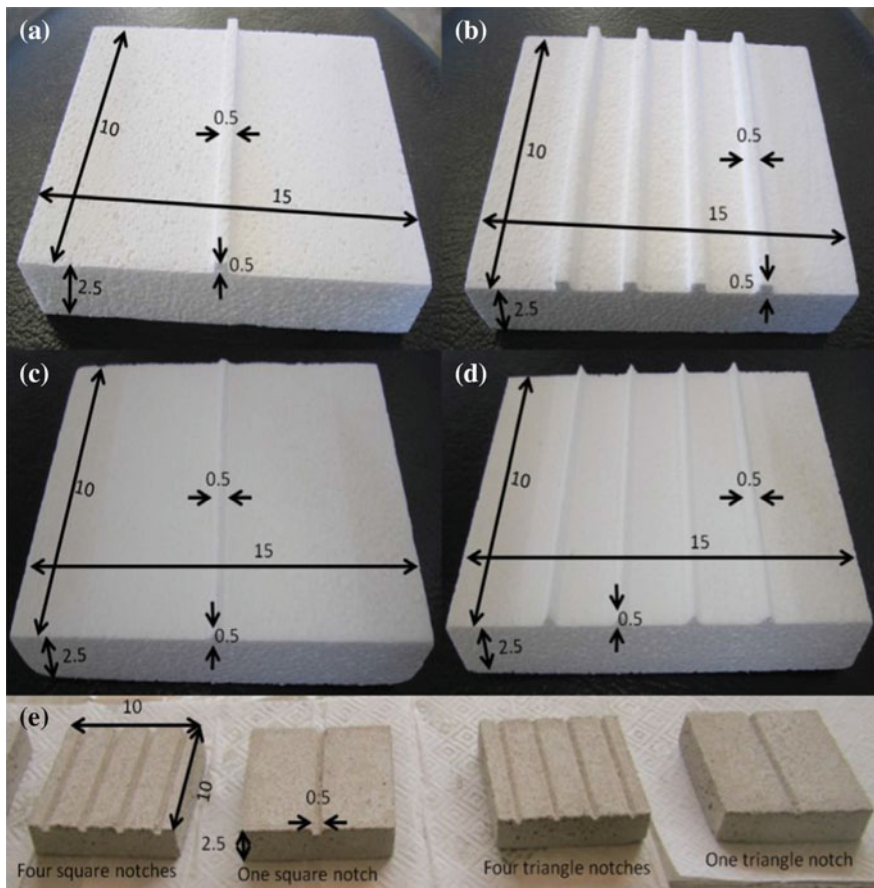


Fig. 1 Interlocked geofoam block specimens with **a** one-square ledge, **b** four-square ledges, **c** one-triangle ledge, **d** four-triangle ledges, **e** precast mortar specimens

variable differential transformers (LVDT) measure horizontal and vertical displacements, respectively. The shear box, houses geofoam specimen, travels toward the horizontal load cell which is fixed to the frame to capture interface resistance during the test. A $10\text{ cm} \times 10\text{ cm}$ loading cap is used to apply vertical stress. Consequently, all interface shear tests were conducted for $10\text{ cm} \times 10\text{ cm}$ interface area (Fig. 2b). As in the previous studies, the horizontal displacement rate was selected as 1 mm/min [3, 4, 6].

Optimum grain size for pumped concrete requires that $40 \pm 8\%$ of the aggregate used in the concrete mix needs to be larger than 8 mm for pumpability requirements [16]. In fact, for conventional concrete, the largest grain size may even reach 63 mm . ASTM D3080 specifies that the width of the interface area (interface specimen size) shall be at least 10 times of the largest particle size used [14]. Therefore, the $10\text{ cm} \times 10\text{ cm}$ interface shear area is not large enough for the use

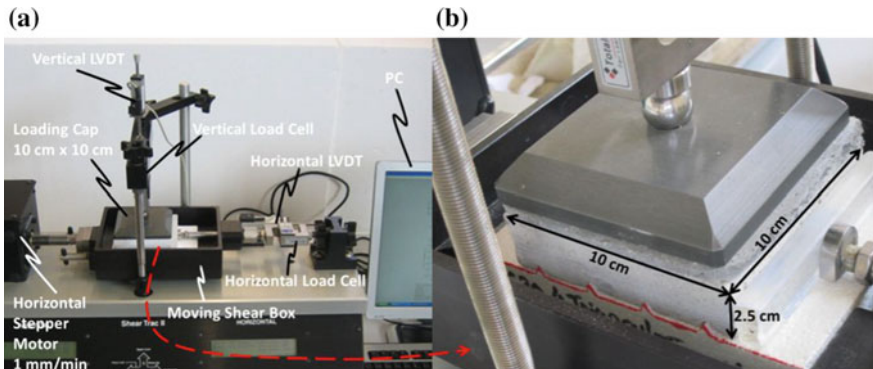


Fig. 2 Interface shear test setup **a** fully-automated direct shear test frame, **b** four triangle interlocked geofoam-precast concrete interface test specimen

of traditional concrete in the tests. Consequently, mortar specimens were prepared to represent concrete in the interface shear tests (Fig. 1e). One part cement (CEM V/A (S-P) 32.5N class composite cement with specific gravity of 2.90), three parts CEN standard sand with specific gravity of 2.62 (largest particle size is 2 mm) and one-half part tap water was used in mortar mix design. The average bending and compressive strength of three mortar specimens were 6 and 31 MPa, respectively, after 28 days of curing.

Precast mortar specimens with notches (Fig. 1e), having the same geometry and number as the ledges of the geofoam blocks along their bottom, provided intimate contact with the interlocked geofoam blocks when they were set on top of each other in the direct shear device (Fig. 2b).

Since the applied normal stress under service loads at any point within the geofoam block assemblage of highway embankments should not exceed the elastic limit stress (defined as the compressive strength of geofoam block at 1% strain [17]), the maximum constant vertical stress was 40 kPa (σ_1 of EPS19, Table 1) during the interface shear tests. Tests were also conducted using 10, 20 and 30 kPa vertical stresses so as to construct failure envelopes.

3 Results and Conclusions

3.1 Traditional Geofoam-Precast Concrete Interface

Geofoam-precast concrete interface shear strength tests were performed not only for evaluating the degrees of improvement by interlocking mechanisms, but also to compare with the existing literature. There are limited studies on the stress-strain characteristics of geofoam-precast concrete interfaces (Table 2).

Table 2 Comparison of EPS19-precast concrete interface shear strength with published values

References	EPS type	Interface type	Interface condition	σ_v (kPa)	Interface friction properties	
					Peak $c_{a,peak}$ (kPa)	Residual $c_{a,residual}$ (kPa)
					$\delta_{a,peak}$ (degrees)	$\delta_{a,residual}$ (degrees)
AbdelSalam and Azzam [10]	EPS19	Geofoam block-smooth precast concrete	Dry	10–30	4.3	—
			Wet		3.7	—
		Geofoam block-rough precast concrete	Dry		0.3	—
	This study		Wet		7.2	—
		Geofoam block-rough precast concrete	Dry	10–40	0	37.5
			Geofoam block-geofoam block		0	38.2
Özer and Akay [6]		Dry			0	35.7

 σ_v vertical stress $c_{a,peak}$ peak interface adhesion $c_{a,residual}$ residual interface adhesion $\delta_{a,peak}$ peak interface friction angle $\delta_{a,residual}$ residual interface friction angle

The stress-strain curves and failure envelopes (both peak and residual) are given in Fig. 3. Interface shear strength parameters for both peak and residual interface shear strengths are also provided in both Fig. 3 and Table 2. Failure envelopes were constructed (Fig. 3b) based on ASTM's definition of the failure as either the peak shear stress or stresses at 10% strain, whichever obtained first [14]. Geofoam-precast concrete interface shear tests were terminated when the residual shear condition was well developed at around 9–10% horizontal strain (Fig. 3a).

Peak shear stresses were reached rapidly for all vertical stresses when horizontal strain was at about 1 and 3% (Fig. 3a). Both the peak and residual shear stresses are well defined, therefore interface shear strength parameters for both peak and residual strengths were reported (Fig. 3b and Table 2). Like traditional geofoam-geofoam interface friction behavior [6], interface friction mechanism for geofoam-precast concrete is purely frictional ($c_a = 0$, $\delta > 0$). However, interface shear strength properties of geofoam-precast concrete are higher than that of geofoam-geofoam interfaces (Table 2). Similar stress-strain curves obtained in duplicate tests using the 30 kPa vertical stress condition showed that the geofoam-precast concrete interface tests are repeatable (Fig. 3a).

The results obtained in this study were also compared with previously published values on geofoam-precast interface testing under similar conditions (rough precast mortar under dry condition) in Table 2. The peak interface friction properties obtained in this study ($c_{a,peak} = 0$, $\delta_{peak} = 42.8^\circ$) were close to that of published values ($c_{a,peak} = 0.3$ kPa, $\delta_{peak} = 44.0^\circ$). For this reason, precast mortar can be considered as a substitute for precast concrete for determining interface friction properties.

3.2 Interlocked Geofoam-Precast Concrete Interfaces

The interface shear stress-strain curves and failure envelope of one-square geofoam-precast concrete is given in Fig. 4. Interface shear strength parameters

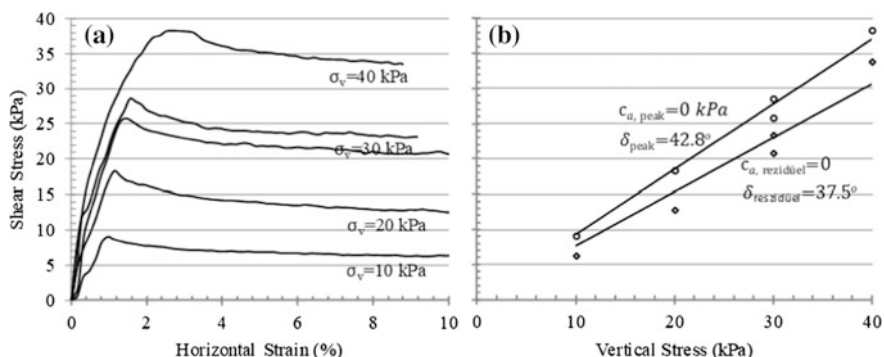


Fig. 3 EPS19-precast concrete interface shear test **a** interface stress-strain behavior, **b** interface failure envelope

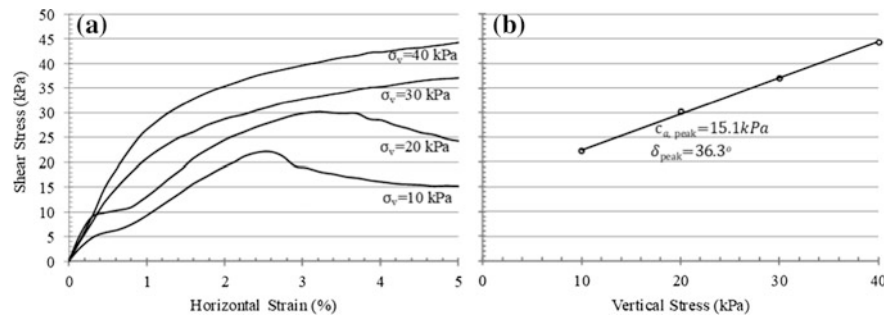


Fig. 4 One-square EPS19-precast concrete interface shear test **a** interface stress-strain behavior, **b** interface failure envelope

are also summarized in both Fig. 4 and Table 3. While the interface shear area of traditional geofoam-precast concrete was interrupted with a 0.5 cm wide, 0.5 cm high and 10 cm long square interlock, the shearing mechanism gained an adhesion of 15.1 kPa. On the other hand, the interface friction angle was less than that of geofoam-precast concrete (Tables 2 and 3). Contrary to geofoam-precast concrete interface shear strength behavior, interrupting the shear plane with a ledge changed the mechanism to frictional-adhesional behavior ($c_a > 0$, $\delta > 0$).

The progress of the interface shear test of one-square geofoam-precast concrete under the 20 kPa constant vertical stress is given in Fig. 5. The square ledge located along the upper surface of the geofoam started to yield at 4% horizontal strain. When the test has reached 5% horizontal strain, the ledge leaned toward the opposite side of the shear direction and started to break (Fig. 5). Consequently, all the interlocked interface shear tests were terminated at 5% horizontal strain.

The peak interface shear stress was obtained prior to reaching 5% horizontal strain under 10 and 20 kPa constant vertical stress, and residual stress was only developed under 10 kPa vertical stress (Fig. 4a). Shear stresses at 5% horizontal strain were taken as peak stresses for the tests conducted under 30 and 40 kPa normal stresses.

Shear stress-strain curves and peak failure envelope of four-square geofoam-precast concrete test are given in Fig. 6. Increasing the number of square ledges from one to four, increased the interface adhesion strength (Fig. 6b). In addition, the peak shear stresses have also been significantly improved under all vertical stresses when compared to that of traditional geofoam-precast concrete (Fig. 3).

Table 3 Summary of interlocked EPS19-concrete interface shear strength tests

Configuration	Peak interface friction properties	
	c _{a,peak} (kPa)	δ _{peak} (degrees)
One-square geofoam-precast concrete	15.1	36.3
One-triangle geofoam-precast concrete	9.9	39.2
Four-square geofoam-precast concrete	24.3	20.3
Four-triangle geofoam-precast concrete	24.1	23.8

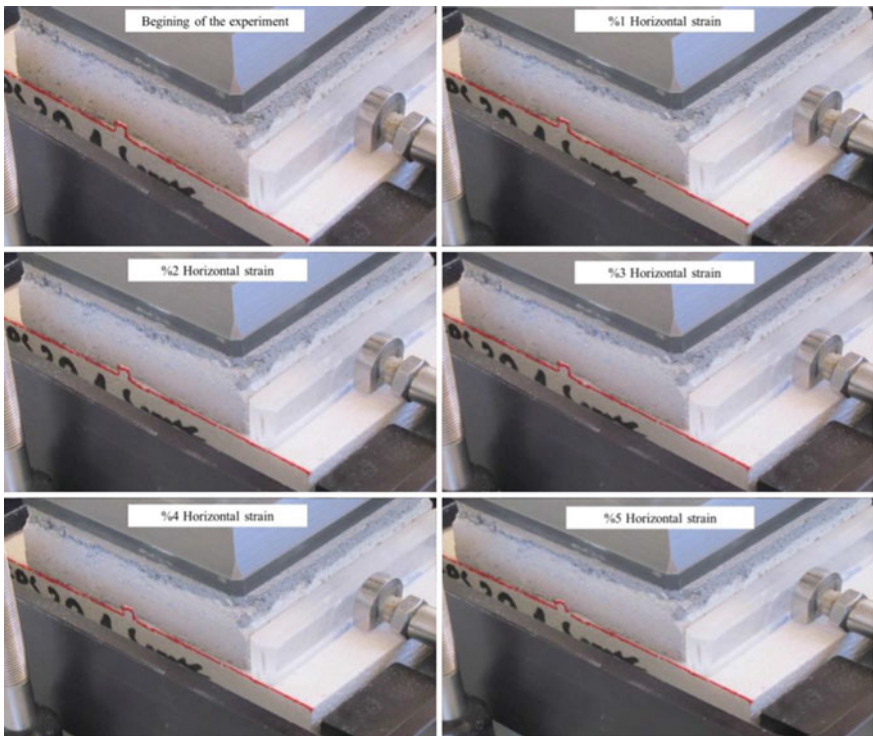


Fig. 5 One-square interlocked geofoam-precast concrete interface shear test progress

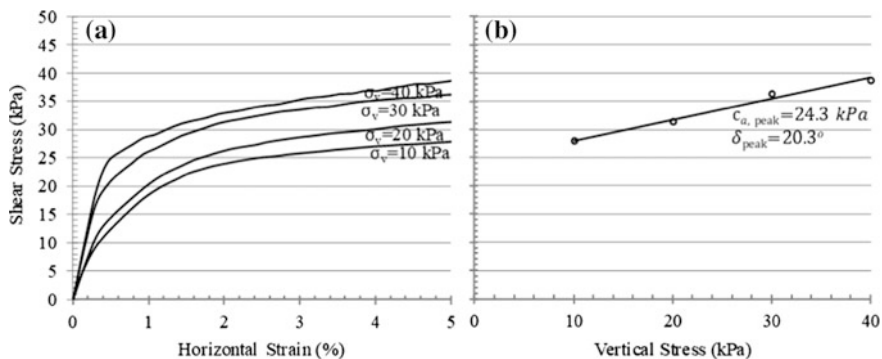


Fig. 6 Four-square EPS19-precast concrete interface shear test **a** interface stress-strain behavior, **b** interface failure envelope

The interface shear stress-strain curves and failure envelopes of one-triangle geofoam- and four-triangle geofoam-precast concrete are given in Figs. 7 and 8, respectively. The interface shear strength parameters are also summarized in Table 3. Similar to that of one-square geofoam- and four-square geofoam-precast concrete interface behavior (Figs. 4 and 6), the interface shear behavior of both one-triangle geofoam- and four-triangle geofoam-precast concrete interfaces are also frictional-adhesional. Interface shear strength tests using 30 kPa vertical stresses were run in duplicate for both one-triangle geofoam- (Fig. 7a) and four-triangle geofoam-precast concrete interfaces (Fig. 8a). Similar stress-strain curves and peak interface shear strength values showed that the interlocked geofoam-precast concrete interface tests are repeatable. Like in the square interface test, as the number of triangle ledges increased, adhesion strength increased (Fig. 8a, b and Table 3).

The failure envelopes from the interface shear tests were plotted to demonstrate the degree of improvement provided by the interlocking mechanism and to compare

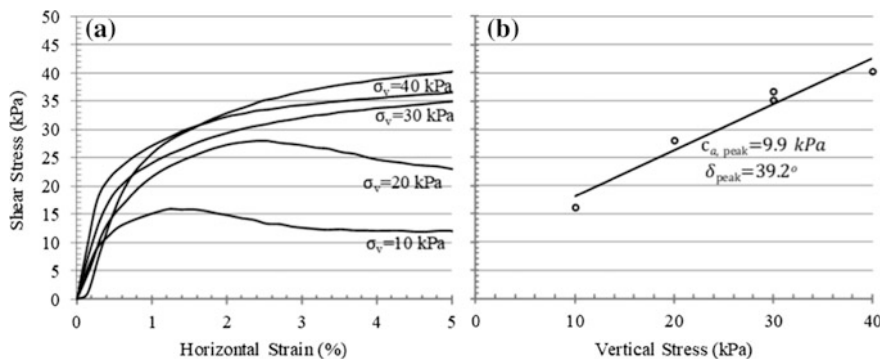


Fig. 7 One-triangle EPS19-precast concrete interface shear test **a** interface stress-strain behavior, **b** interface failure envelope

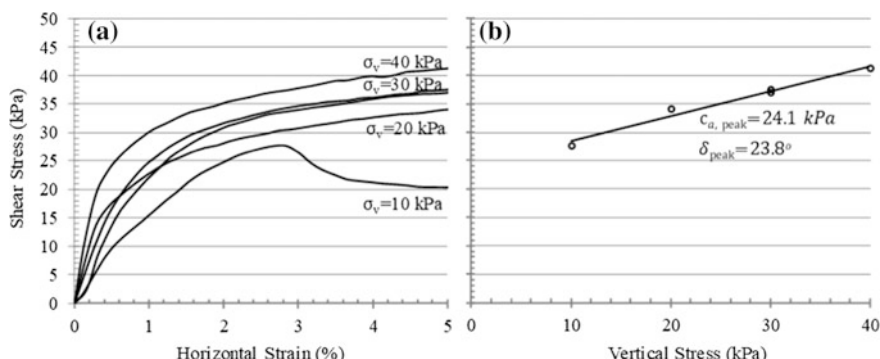


Fig. 8 Four-triangle EPS19-precast concrete interface shear test **a** interface stress-strain behavior, **b** interface failure envelope

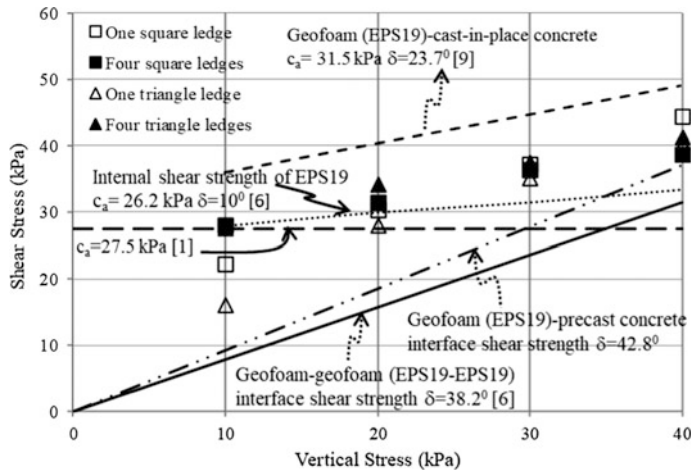


Fig. 9 Comparison of failure envelopes

with the failure envelopes of geofoam-geofoam [6], geofoam-cast-in-place concrete [9], and the internal shear strength of geofoam blocks [1, 6] (Fig. 9). The shear strength of a traditional geofoam-precast concrete interface is higher than that of geofoam-geofoam interface (Fig. 9). Interlocking mechanisms has significantly improved the shear strength of geofoam-precast concrete.

Under 30 and 40 kPa vertical constant stresses, regardless of the interface configuration, the interlocked mechanisms create higher interface strength than the internal shear strength of geofoam block (Fig. 9). Geofoam block-cast-in-place concrete interface has higher shear strength than that of interlocked geofoam-precast concrete.

4 Summary and Conclusions

Interface shear strength properties of interlocked geofoam-precast concrete were evaluated by conducting tests on a total of four interlocked configurations, and were compared with interface shear strength properties of traditional geofoam-precast concrete. Interlocking mechanisms changed the traditional geofoam-precast concrete interface shear behavior from purely frictional to frictional-adhesional. Interrupting the failure plane with ledges significantly improved the interface strength. Not only traditional geofoam-precast concrete but also all the interlocked surfaces has higher interface shear strength than that of internal shear strength of geofoam block under 40 kPa vertical stress. In addition, interface shear strength of geofoam-precast concrete is higher than that of geofoam-geofoam. Therefore, using precast concrete as a separation layer between geofoam blocks and pavement can be a viable alternative technique to cast-in-place concrete. Using precast concrete load

distribution slabs in geofoam highway construction enables the start of road sub-base- and base-materials compaction without waiting for the curing period of traditional cast-in-place concrete, leading to significant reduction in the project completion times.

Due to the scale issues, the laboratory tests were conducted with mortar. Therefore, the strength parameters suggested in this paper need to be verified by using large-scale shear testing prior to using them in the design.

Acknowledgements Interface shear tests were conducted at the Civil Engineering Laboratory of Okan University, Istanbul, Turkey. The author acknowledges the contribution of laboratory technician Halis Şahin and Master student Erdal Usturbelli during the experimental program. In addition, the author extends his gratitude to Dr. Onur Akay for his critiques of the draft version of the study.

References

1. Stark TD, Arellano D, Horvath JS et al (2004) Guideline and recommended standard for geofoam applications in highway embankments. NCHRP Report 529, Transportation Research Board, Washington D.C.
2. Sheeley M, Negussey D (2000) An investigation of Geofoam interface strength behavior. In: Geotechnical special publication No. 112, paper presented at soft ground technology conference, pp 292–303. ASCE, Reston, VA
3. Atmatzidis DK, Missirlis EG, Theodorakopoulos EB (2001) Shear resistance on EPS geofoam block surfaces. In: Paper presented at the EPS Geofoam 2001: 3rd annual conference, Geotechnical Engineering Laboratory, University of Patras, Greece
4. Negussey D, Anasthas N, Srirajan S (2001) Interface friction properties of EPS geofoam. In: Paper presented at the 3rd international conference on geofoam blocks in construction applications, 10–12 Dec 2001, Salt Lake City, USA
5. Barrett JC (2008) Effectiveness of connectors in geofoam block construction. M.Sc. thesis, University of New Brunswick
6. Özer AT, Akay O (2016) Interface shear strength characteristics of interlocked EPS-block geofoam. J Mater Civil Eng 28(4) [https://doi.org/10.1061/\(asce\)mt.1943-5533.0001418](https://doi.org/10.1061/(asce)mt.1943-5533.0001418)
7. Xanaki VC, Athanasopoulos GA (2001) Experimental investigation of the interface mechanism at the EPS geofoam-sand interface by direct shear testing. Geosynth Int 8 (6):471–499
8. Özer AT, Akay O, Ateş Y (2016) Shear strength properties of interlocked EPS-block geofoam-Ottawa sand interface. In: Paper presented at the 4th international conference on new developments in soil mechanics and geotechnical engineering, pp 111–118, Near East University, Nicosia, North Cyprus, 2–4 June 2016
9. Özer AT, Ekincioglu Ö (2018) Evaluation of interface shear strength between interlocked geofoam blocks and cast in place concrete. In: Paper presented at the 5th international conference on the use of EPS geofoam blocks in construction applications, Kyrenia, North Cyprus, 9–11 May 2018
10. AbdelSalam SS, Azzam SA (2006) Reduction of lateral pressures on retaining walls using geofoam inclusion. Geosynth Int 23(6):395–407
11. Özer AT, Akay O, Ateş E (2015) Effect of displacement rate on the interface shear strength properties of interlocked EPS-block geofoam. In: Presented at the IRF Europe & Central Asia Regional Congress, Istanbul, Turkey, 15–18 Sept 2015

12. ASTM (2015) Standard specification for rigid cellular polystyrene geofoam. ASTM D6817, West Conshohocken, PA
13. ASTM (2010) Standard test method for compressive properties of rigid cellular plastics. ASTM D1621, West Conshohocken, PA
14. ASTM (2011) Standard test method for direct shear test of soils under consolidated drained condition. ASTM D3080, West Conshohocken, PA
15. ASTM (2014) Standard test method for determining the shear strength of soil-geosynthetic and geosynthetic-geosynthetic interfaces by direct shear. ASTM D5321, West Conshohocken, PA
16. Türk Standard (2016) Design of concrete mix, in Turkish. TS802, Türk Standartları Enstitüsü, Ankara
17. Horvath JS (2010) Emerging trends in failures involving EPS-block geofoam fills. J Perform Const Fac 24(4) [https://doi.org/10.1061/\(asce\)cf.1943-5509.0000114](https://doi.org/10.1061/(asce)cf.1943-5509.0000114)

California Bearing Ratio (CBR) Behaviors of EPS Geofoam: Experimental and Numerical Studies



Yebelta Zerie Beju and Jnanendra Nath Mandal

Abstract Expanded Polystyrene (EPS) geofoam is ultra-lightweight, closed cell, rigid, plastic foam. It can be used for lightweight fill, compressible inclusion, thermal insulation, drainage and so forth. An experimental study was carried out to investigate the California bearing ratio (CBR) behavior of EPS geofoam. Three different densities of EPS geofoam 12, 15 and 20 kg/m³, and six different piston sizes (0.75D, D, 1.2D, 2D, 2.3D and 2.6D) where D is diameter of standard piston were used for standard CBR sample size. Moreover, in the present study CBR of EPS geofoam is investigated at dry and submerged in water conditions. The effect of piston diameter and density on the CBR values of EPS geofoam were investigated. The study revealed that increase of density of EPS geofoam resulted in an appreciable increase in the CBR value. The CBR test results were found to be 0.87, 1.67, and 1.86% for 12, 15 and 20 kg/m³ densities of EPS geofoam respectively at 2.5 mm penetration with standard piston size. The test result shows that the CBR value increased with an increase in density of EPS geofoam, however, the effects of CBR values were not more pronounced between dry and wet test conditions. The benefit of increasing or decreasing piston diameters beyond 50 mm does not improve the CBR value appreciably. An increase in density is more effective than an increase in piston diameter in improving the CBR value of the EPS geofoam. It is observed that the CBR value of EPS geofoam is very less and equivalent with clay soils. The density of EPS geofoam used for the construction of pavements should be more than 15 kg/m³ concerns related to the quality and the durability of the material. Finite element analysis was also carried out using PLAXIS 2D software to validate with experimental results. A reasonable agreement was observed between the numerical and experimental studies on pressure-displacement response.

Keywords EPS geofoam · Density · Specimen size · CBR · FEM

Y. Z. Beju (✉) · J. N. Mandal
Indian Institute of Technology Bombay, Mumbai, India
e-mail: yzbeju@iitb.ac.in

1 Introduction

Expanded polystyrene (EPS) geofoam has many applications in geotechnical engineering discipline, mostly as lightweight fill material, compressible inclusion, and barrier [1]. EPS geofoam can also be used as a composite material combined with other materials like soil, geotextile, and geogrid [2]. EPS geofoam is ultra-lightweight material that provides easy handling and also environment-friendly and compatible with conventional construction materials. Its properties has been determined by so many researchers in the past: Creep [3]; compressibility [4–6]; modulus of subgrade reaction [7], and resilient modulus [8]. The mechanical behavior of EPS geofoam affected by density and confining stress [9, 10]. Cohesion is a major parameter which contributes the shear strength properties of EPS geofoam and it is a function of density, whereas, the effect of internal friction angle is minor [11, 12]. Water has negligible influence on the strength and stress-strain behavior of EPS geofoam and water absorption of EPS geofoam depends on the applied stress magnitude [13, 14]. The interface strength of EPS geofoam is not affected by density, but, the normal stress has a direct effect on its interface strength especially on interface adhesion [15, 16].

Because of the rapid increment of construction industries in the world accessibility of good construction materials have abridged. Sometimes it might be difficult to find suitable area to build a structure, consequently, pavement structures are needed to be constructed and have been built on soft soil. The construction of pavements on soft ground can be implemented only after extensive ground improvement in view of its less bearing capacity. When a soil infill pavement constructed on soft soil, settlement will develop due to compaction, self-weight of the structure and vehicle loads. Therefore, it is necessary to use either lightweight infill or geosynthetic materials to maintain its stability. Nowadays, using EPS geofoam for pavement structures is common in geotechnical engineering to replace poor soils since the last four decades. To reduce the pavement settlement over soft soils and to increase its stability, the use EPS geofoams are the best solutions. EPS geofoam is categorized by its low density, approximately hundred times lower than typical soils and as a minimum ten to thirty times lighter than other lightweight fill materials like shredded tires and sawdust [17]. The very low density and high strength to density ratio behaviors of EPS geofoam can be used as a backfill material for construction of embankments and pavements over poor soils [13, 18, 19]. Reduction of applied and earth pressure on pavement reduces the structural demand and leads to the overall construction economy. EPS geofoam is a rigid cellular plastic foamed material that has been used in a wide range of geotechnical engineering applications. Due to very low density compared to other conventional fill materials, it can be used as lightweight fill geotechnical structures like higher and steeper embankments and highways. It has high compressibility, good flexural strength and high rupture strength in shear [1].

The properties of EPS geofoam have been investigated experimentally for many years by several researchers who are involved in the design and application of

geofoam product. When EPS geofoam is to be used as a pavement material instead of conventional soils, its California Bearing Ratio (CBR) properties, need to be thoroughly investigated. The aim of the present study is to investigate the CBR behaviors of different low densities of EPS geofoam using the laboratory tests. The effect of EPS geofoam density, piston diameter, and dry and wet conditions on the CBR behaviors of EPS geofoam are reported. Additionally, the experimental results are validated using a finite element program to determine the CBR parameters.

2 Experimental Investigation

The CBR test is penetration test meant for the evaluation of subgrade strength of roads and pavements. The results obtained by these tests are used with the empirical curves to determine the thickness of pavement and its component layers. A series of CBR tests were performed to investigate the CBR behaviors of EPS geofoam. The EPS geofoams of varying densities 12, 15, and 20 kg/m³ with cylindrical in sections were used in the experimental test studies. The EPS geofoam specimens used in this study have been prepared at Packshield Industry in Mumbai, India. The influence of EPS geofoam density and piston diameter at dry and wet conditions on the CBR behaviors EPS geofoam are investigated. Also, the CBR factors were determined to demonstrate the relation between CBR and density of geofoam. Prior to the CBR test, uniaxial unconfined compressive strength tests were performed for all densities of geofoam using 150 mm cubic specimens as per ASTM D1621 [20]. The stress-strain curves shows that the behavior of EPS geofoam under compression loading system depends on its densities; the higher density of EPS geofoam develops high compressive strength. The nature of the stress-strain curves are similar for all densities tested. The stress-strain behaviors of EPS geofoam are found to be non-linear. Meanwhile, it is directly proportional to 1–2% of the strain level, and the slope of this portion defines the initial tangent modulus of the material, and between 2 and 4% of strain level the yield points were developed. The stress-strain curves of EPS geofoam is shown in Fig. 1. The physical and mechanical properties of the EPS geofoam are shown in Table 1.

Fig. 1 Stress-strain curves of EPS for different densities

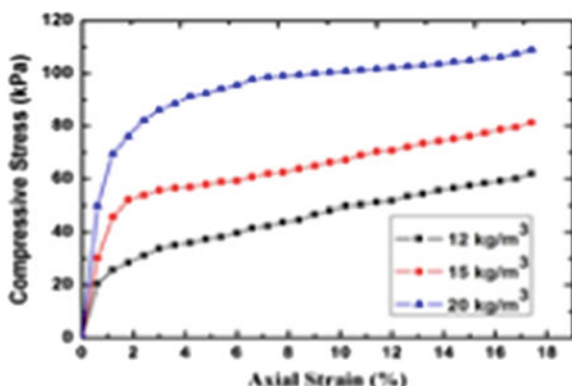


Table 1 Properties of EPS geofoam [12]

Material property	Values		
	EPS12	EPS15	EPS20
ρ_g (Kg/m ³)	11.88	14.81	19.79
w _g (%)	4.41	3.6	2.88
σ_c at 1% (kPa)	16	44	72
σ_c at 5% (kPa)	32	62	97
σ_c at 10% (kPa)	48	71	112
E _i (kPa)	1611	2769	5086
σ_y (kPa)	29	52	96
σ_f (kPa)	88	169	219
c _u (kPa)	28.25	32.75	37.5
ϕ_u (°)	1.25	1.38	2.25

ρ_g density, w_g water absorption, σ_c compressive strength, E_i initial Young's modulus, σ_y yield strength, σ_f flexural strength, c_u cohesion, ϕ_u friction angle

2.1 Test Procedure

The CBR test is penetration test in which a standard piston diameter of 50 mm is used to penetrate the soil at a standard strain rate of 1.27 mm/min as per ASTM D1883 [21]. A series of tests were conducted on EPS geofoam specimens with 12, 15, and 20 kg/m³ densities with dimensions of 150 mm in diameter and standard height (130 mm) were cut from each density EPS geofoam. The cylindrical section EPS geofoam specimen was placed in the CBR mold after the bottom annular space filled by CBR spacer. Figure 2 depicts the schematic view and photograph of sample used for performing the CBR test. The tests were performed in dry conditions (D) and repeated in wet conditions (W) for the same density but new test specimen. For the wet condition test, the EPS geofoam specimen was immersed in water for 24 h before testing and then placed inside the CBR mold. Tests were identified so as to an EPS12 (EPS geofoam specimen with 12 kg/m³ density) tested in dry condition is represented as EPS12 (D) and in wet conditions as EPS12 (W). Moreover, to optimize the suitable piston diameter the CBR of EPS, the CBR tests were performed with various diameters of piston such as: 0.75D, 1.2D, 2D, 2.3D and 2.6D (where D is the standard diameter of piston) for all densities of EPS at dry condition. The piston load was applied with a constant strain rate of 1.27 mm/min. Piston load and vertical penetration were measured by means of 5 ton load cell and linear variable differential transformer (LVDT) respectively. To ensure an accurate reading, the measuring devices were calibrated before use. The CBR tests were conducted as per ASTM D1883 [21] each test was conducted up to a maximum penetration of 12.7 mm. The complete test assembly and placement of EPS geofoam test specimen is displayed in the Fig. 3. The EPS geofoam specimen was placed under the penetration piston and place surcharge load of five ton. The penetration load values (kg) were recorded corresponding to 0.5 mm penetration interval and its

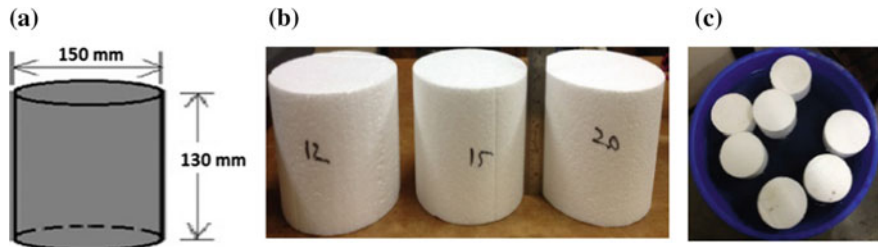


Fig. 2 Test specimen of EPS for CBR tests: **a** schematic view, **b** photographic view at dry state, **c** soaked in water

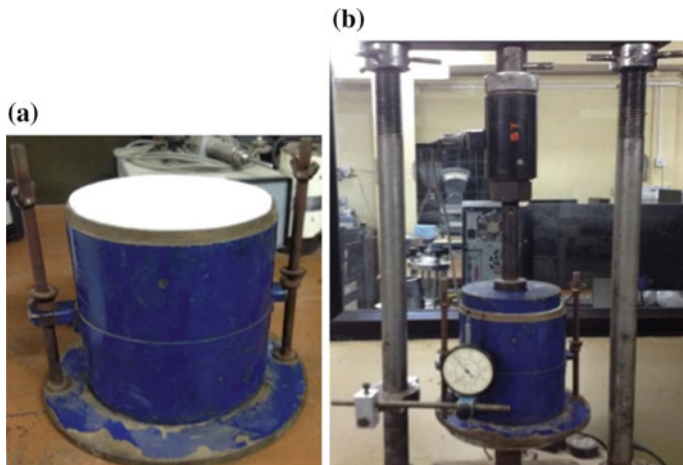


Fig. 3 CBR tests setup, **a** placement of test specimen, **b** penetration of EPS sample in CBR machine

ratio to the bearing value of standard crushed rock expressed in percent is referred to as CBR. Pressure versus displacement response for each test and the percentage of CBR against EPS geofoam density were plotted, and the CBR values for EPS geofoam corresponding to 2.5 and 5 mm penetration were determined for each test.

3 Results and Discussions

The CBR behavior of EPS geofoam was investigated using experimental studies. The nature of stress-displacement curves is found to be almost the same for all densities of EPS geofoam. Density of EPS geofoam and the test conditions (dry and wet conditions) are finds to be affected the pressure-displacement behavior of EPS geofoam. Figure 4 shows the CBR test results for different densities of EPS

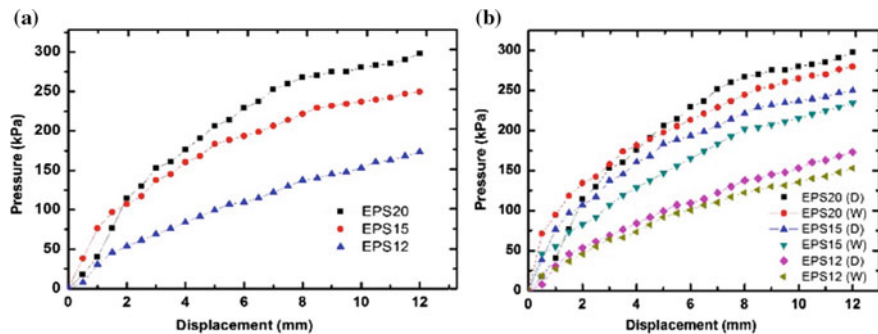


Fig. 4 EPS geofoam CBR tests for different densities: **a** at dry condition only, **b** comparisons at dry and wet conditions

geofoam in dry and wet conditions with standard piston diameter. From these figures, it can be seen that there is a continuous increased in the value of pressure with increased in density of EPS geofoam. The pressure-displacement behavior of EPS geofoam is considerably affected by its density but the effect of water submergence is very less. Higher density EPS geofoam displayed higher CBR value. For a particular density, no significant increase in CBR was observed with soaked in water. Therefore, the CBR behavior of EPS geofoam is affected by density, whereas, the difference between dry and wet test condition was not more noticeable. As EPS geofoam has a closed cell structure, it does not absorb water [22].

The failure of different densities of EPS geofoam specimens after the test and the CBR values for each density of EPS geofoam are illustrated in Fig. 5. As shown in this figure, during the CBR tests punching failure was occurred under the piston at 2.5 mm penetration. It can be seen that the CBR values for all densities tested are not more than 2, even the higher density EPS the CBR is only 1.97. And the lower density EPS12 the CBR is 0.95. FAA pavement design method [23] recommends the subgrade CBR to be more than 3. Because EPS geofoam is highly compressible material it could not carry much load during the test. However, since the last three decades, geofoam was commonly used as sub base or subgrade material in pavement construction. Thus, to achieve the real CBR value of geofoam the obtained CBR test results may be multiplied by some factor for the design of pavements that contain geofoam as the density of geofoam is hundred times lower than soil density. EPS geofoam is categorized by its low density, about 100 times lower than typical soils and at least 10–30 times lighter than other lightweight fill materials [17]. The found correlation between EPS CBR and density of EPS geofoam is very beneficial for estimating the approximate value of the EPS geofoam CBR value. The linear regression analysis is performed for different densities of EPS geofoam and best fitted to a straight line expressed as an equation: $y = mp + c$. Where 'y' is the CBR, 'm' is the gradient of the line, 'p' is the density of EPS geofoam and 'c' is constant.

In addition to the above tests, to optimize the suitable piston diameter for the CBR of EPS geofoam, the CBR tests were performed by varying the diameters of the piston. The piston pressure for different densities of EPS geofoam in dry

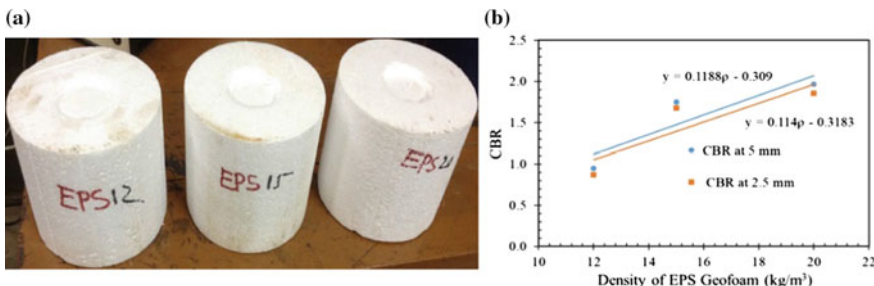


Fig. 5 a The observed punching failure of EPS test specimens, b EPS CBR values

condition are plotted in the form of CBR test against piston displacement as shown in Fig. 6. The nature of the graphs for all densities are found to be almost similar. The test result shows that the CBR value decreased with an increase in diameter of piston for all densities of EPS geofoam. From the experimental investigation, significant parameters that influenced the CBR value of geofoam are found to be the density of geofoam and diameter of the piston, whereas, no significant difference can be underline between dry and wet test cases. However, on a smaller piston diameter (0.75D) marginal increment of CBR value was observed for higher densities, whereas, for the lower density (EPS12) the CBR value was lower than the result obtained by the stranded piston diameter. Generally, the benefit of increasing piston diameter beyond 50 mm does not improve the CBR value and decreasing below 50 mm does not improve appreciably. An increase in density is more effective than an increase in piston diameter in improving the CBR values of the EPS geofoam. It is observed that the CBR value of EPS geofoam is very less and equivalent with clay soils. The density of EPS geofoam used for the construction of pavements should be more than 15 kg/m^3 concerns related to the quality and the durability of the material.

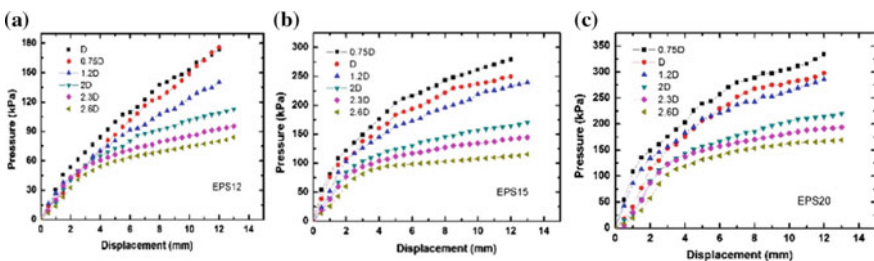


Fig. 6 EPS geofoam CBR tests for different piston diameter: a EPS12, b EPS15, c EPS20

4 Numerical Modeling

Finite element analysis (FEA) was also carried out using PLAXIS 2D software to validate with experimental results. Prior, the FEA of EPS geofoam under unconfined compression loading condition was carried out. To match the actual laboratory measured response of the geofoam under unconfined axial compression, a numerical model was carried out to validate and assure that the modulus of elasticity is matching the lab measured one. After that, another series of FE models using the same program were performed for the CBR test to model the behavior of the various CBRs of different densities of EPS geofoam materials.

4.1 Calibration for the Unconfined Compressive Model

The FEA of EPS geofoam samples under unconfined compression was carried out using an axisymmetric model to simulate the unconfined compression test. The EPS geofoam was modeled using a Mohr-Coulomb nonporous material with 15 node triangular elements. Because the stress-strain behavior of EPS is close to linearly elastic-perfectly plastic material. Similar models for EPS geofoam in PLAXIS have been performed by Ram Rathan Lal et al. [24]. The Poisson's ratio is a useful parameter for the FEA. Chun et al. [4] reported as the Poisson's ratio of EPS geofoam is a function of density and confining stresses. The value of Poisson's ratio of EPS geofoam for this analysis was calculated by using the empirical equation, $v = 0.0056\rho + 0.0024$, where v and ρ are Poisson's ratio and density of EPS geofoam (kg/m^3) respectively [25]. The properties of EPS geofoam used in finite element analyses are given in Table 2. All the displacement of the nodes on the horizontal boundary and the bottom surface were arrested, whereas allowed to undergo vertical displacement. The elastic modulus of the EPS geofoam was determined from uniaxial unconfined compressive strength test (refer to Fig. 1). The cohesion and angle of internal friction of EPS geofoam were determined from unconsolidated undrained (UU) triaxial tests. At the top of the EPS geofoam model

Table 2 Material properties of EPS geofoam used in finite element analysis

Parameters	EPS geofoam designation		
	EPS12	EPS15	EPS20
Material model	Mohr-Coulomb	Mohr-Coulomb	Mohr-Coulomb
Drainage type	Non-porous	Non-porous	Non-porous
Unit weight (kN/m^3)	0.12	0.15	0.2
Young's modulus (MPa)	1611	2769	5086
Poisson's ratio	0.1	0.1	0.12
Cohesion (kPa)	28.75	32.25	37.5
Friction angle ($^\circ$)	1.25	1.38	2.25

a maximum prescribed vertical displacement of 22.5 mm that represents a vertical strain of about 15% for all densities of EPS geofoam.

A typical axisymmetric geometry model of EPS geofoam unconfined compression loading condition is depicted in Fig. 7. As shown in this figure, the numerical results are reasonably agreement with the test results. Pressure versus displacement curves were outside the linear portion at 2.5 and 5 mm penetration depths for all densities of EPS geofoam.

4.2 Numerical Modeling for CBR of EPS

The CBR of EPS geofoam experimental results found by standard piston diameter were validated by using PLAXIS 2D. At the center of the top of the EPS geofoam specimen a surface area of 1935 mm^2 was subjected to 12.7 mm prescribed displacement, which represented a circular rigid plunger 1935 mm^2 being pushed vertically downward up to 12.7 mm penetration for all densities of EPS geofoam. A basic model was set representing a laboratory model test. At the bottom boundary of the model, both horizontal and vertical movements were fixed, whereas, at the side boundaries, only vertical movement was allowed. This denoted the whole model boundary confined in a CBR mold with rigid bottom and side walls.

The CBR behavior of EPS was validated using PLAXIS 2D professional finite element software. The comparison of the experimental and numerical piston pressure with displacement responses for all densities of EPS geofoam, under standard piston and the comparison of CBR values between experimental and numerical results against densities of EPS geofoam is depicted in Fig. 8. The numerical results show a reasonable agreement with the experimental studies on pressure-displacement and CBR values on EPS geofoam.

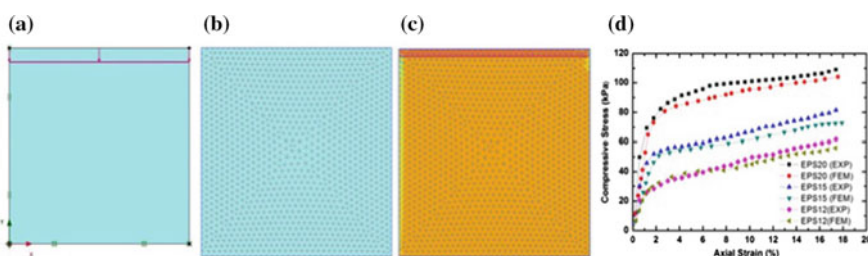


Fig. 7 Comparison of unconfined compression test results for EPS: **a** vertical displacement, **b** mesh distribution, **c** mean effective normal stress, **d** stress-strain of FE with test results

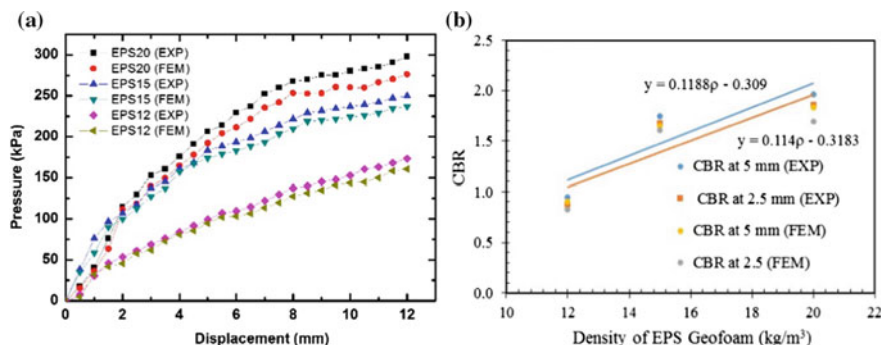


Fig. 8 Comparison of experimental and numerical results for EPS: **a** Pressure-displacement, **b** CBR with density

5 Summary and Conclusions

In the present study, the behavior of EPS geofoam was observed under CBR loading to calculate the CBR parameters and some important relationships. Numerical analysis was also performed by using PLAXIS 2D to simulate the experimental results. The outcome of the this study revealed that the CBR value of EPS geofoam was very low as compared with the conventional fill materials this is because its density is hundred times lower than soil density, in that way, it can be used as a sub base material for railway, highway and other structures that contain EPS geofoam. The conclusions of the study are as follows.

- From the CBR test results, no peak values of piston pressures were observed in all the densities of EPS geofoam. CBR value of EPS geofoam was increased with the increase in the density of geofoam.
- CBR values increases marginally when decrease piston diameter, whereas, decrease in CBR values were observed with increase in the diameter of piston.
- Punching failure was occurred in the CBR tests of EPS geofoam.
- CBR values are achieved maximum for density of EPS geofoam 20 kg/m^3 . And the CBR of EPS geofoam showed a decreasing pattern as the density is decreased.
- No significant difference can be underline between dry and wet tests on CBR of EPS geofoam.
- The obtained relationship between CBR and density of EPS geofoam is very useful for estimating the approximate value of the CBR.
- The experimental results were validated using finite element program. A reasonable agreement was observed between the numerical and experimental studies on pressure-displacement response.

References

1. Horvath JS (1997) The compressible inclusion function of EPS geofoam. *Geotext Geomembr* 15(1–3):77–120
2. Padade AH, Mandal JN (2014) Interface strength behavior of expanded polystyrene (EPS) geofoam. *Int J Geotech Eng* 8(1):66–77
3. Beju YZ, Mandal JN (2016) Compression creep test on expanded polystyrene (EPS) geofoam. *Int J Geotech Eng* 10(4):401–408
4. Chun BS, Lim HS, Sagong M, Kim K (2004) Development of a hyperbolic constitutive model for expanded polystyrene (EPS) geofoam under triaxial compression tests. *Geotext Geomembr* 22(4):223–237
5. Hazarika H (2006) Stress-strain modeling of EPS geofoam for large strain applications. *Geotext Geomembr* 24(2):79–90
6. Leo CJ, Kumruzzaman M, Wong H, Yin JH (2008) Behavior of EPS geofoam in true triaxial compression test. *Geotext Geomembr* 26:175–180
7. Negussey D, Huang X (2006) Modulus of subgrade reaction for EPS geofoam. Paper presented at the Geo Shanghai 2006 international conference, Shanghai, China, Geotechnical Special Publication No. 169, American Society of Civil Engineers, pp 165–172
8. Huang X, Negussey D (2007) Resilient modulus for EPS geofoam. Paper presented at the Geo-Denver 2007 international conference, Denver, Co., Geotechnical Special Publication No. 169, American Society of Civil Engineers
9. Trandafir AC, Erickson BA, Moyles JF, Bartlett SF (2011) Confining stress effects on the stress-strain response of EPS geofoam in cyclic triaxial tests. In: Geo-frontiers 2011 conference, advances in geotechnical engineering, Dallas, Texas, American Society of Civil Engineers, pp 2084–2091
10. Birhan AG, Negussey D (2014) Effect of confinement on creep behavior of EPS geofoam. *Geotech Test J* 37(6):1–8
11. Padade AH, Mandal JN (2012) Behavior of expanded polystyrene (EPS) geofoam under triaxial loading conditions. *Electron J Geotech Eng* 17:2543–2553
12. Beju YZ, Mandal JN (2017) Expanded polystyrene (EPS) geofoam: preliminary characteristic evaluation. Procedia Engineering, Transportation Geotechnics and Geocology (TGG 2017), Saint Petersburg, Russia, 189:239–246
13. Duškov M (1997) Measurements on a flexible pavement structure with an EPS geofoam sub-base. *Geotext Geomembr* 15(1–3):5–27
14. Ossa A, Romo MP (2012) Confining stress influence on EPS water absorption capability. *Geotext Geomembr* 35:132–137
15. Barrett JC, Valsangkar AJ (2009) Effectiveness of connectors in geofoam block construction. *Geotext Geomembr* 27(3):211–216
16. AbdelSalam SS, Azzam SA (2016) Reduction of lateral pressures on retaining walls using geofoam inclusion. *Geosynth Int* 23(6):395–407
17. Stark TD, Arellano D, Horvath JS, Leshchinsky D (2004) Geofoam application in design and construction of highway embankments. Transportation Research Board, NCHRP Web Document, Washington, D.C., 65:792p
18. Fransworth CB, Bartlett SF, Negussey D, Stuedlein AW (2008) Rapid construction and settlement behavior of embankment systems on soft foundation soils. *J Geotech Geoenviron Eng* 134(3):289–301
19. Wang F, Miao L (2009) A proposed lightweight fill for embankments using cement-treated Yangzi River sand and expanded polystyrene (EPS) beads. *Bull Eng Geol Env* 68(4):517–524
20. ASTM (2010) Standard test method for compressive properties of rigid cellular plastics. ASTM D1621, West Conshohocken, PA
21. ASTM (2016) Standard test method for California bearing ratio (CBR) of laboratory-compacted soils. ASTM D1883, West Conshohocken, PA

22. Horvath JS (1994) Expanded polystyrene (EPS) geofoam: an introduction to material behavior. *Geotext Geomembr* 13(4):263–280
23. FAA (1995) Airport pavement design and evaluation. AC 150/5320-6D, FAA, 165p
24. Ram Rathan Lal B, Padade AH, Mandal JN (2014) Numerical simulation of EPS geofoam as compressible inclusions in fly ash backfill retaining walls. *Ground Improvement and Geosynthetics*, American Society of Civil Engineers, GSP 238:526–535
25. Edo (1992) Expanded polystyrene construction method, Riko Toshio Publishers, Tokyo, Japan

Non Destructive Testing for EPS Geofoam Quality Assurance



Engda Kassahun Temesgen, Luke Andrews and Dawit Negussey

Abstract Non Destructive testing (NDT) was used to check the quality of EPS geofoam blocks produced at different manufacturing plants. Strength and deformation parameters for design and construction are dependent on the quality of specified geofoam grades delivered on site. Ultra sound P wave velocities through EPS blocks were measured to obtain estimates of Young's moduli for different densities produced at four molding plants. The moduli values derived from NDT were compared with previously reported results. Differences between P wave velocities and moduli for blocks formed with virgin material and blocks that contain recycled content were examined. The results indicate NDT is a versatile and more practical method for onsite quality assurance monitoring.

1 Introduction

Expanded Polystyrene (EPS) geofoam blocks are used as a lightweight construction material for various types of civil infrastructure projects. The quality of EPS geofoam blocks must be checked on delivery to confirm compliance with the contract specification. Specification standards and quality assurance procedures have evolved in various state and national agencies. ASTM and AASHTO standards are commonly used in the United States in addition to customized standards developed by different Departments of Transportation (DoT). There are also other national and regional standards and practices that have been used since the 1970s.

Commonly used quality assurance guidelines recommend destructive testing to confirm required design properties. The number and locations of test samples is specified as in Fig. 1. A minimum of six 50 mm cubic samples are trimmed from prescribed locations of a full size block. Unconfined compression tests are performed on the selected samples at a standard strain rate of 10% per minute. The strength results obtained at 1, 5, and 10% strains are then compared against

E. K. Temesgen · L. Andrews · D. Negussey (✉)
Syracuse University, Syracuse, NY, USA
e-mail: negussey@syr.edu

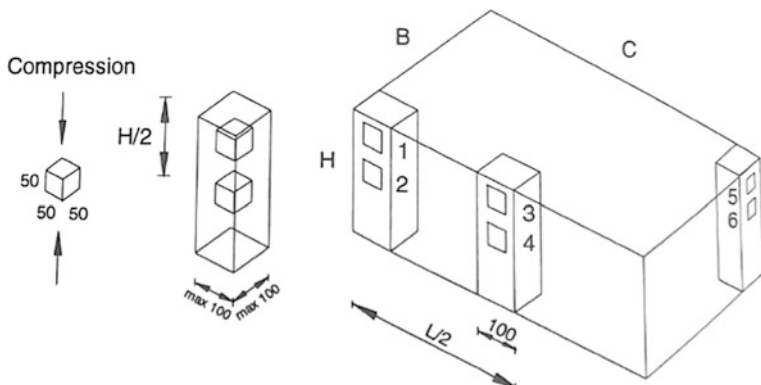


Fig. 1 Test specimen locations for quality assurance testing in current practice [7]

values provided in practice standards. EPS geofoam blocks have more common dimensions of $1.0 \times 1.2 \times 5.0$ m (metric unit based molds), as shown in Fig. 2. EPS geofoam blocks vary in density from 16 to 48 kg/m^3 . Both the strength and unit price of EPS geofoam increase with density. On balance, the most preferred grade for civil infrastructure applications has been the 20 kg/m^3 nominal density EPS geofoam blocks.

The destructive testing recommended in current standards is may be performed in a laboratory for qualification initially but not on site regularly. The destructive test wastes material, takes too long, and would be expensive. The prescribed sample selection method does not represent a statistically acceptable random sampling of the full block. In addition, the six selected samples represent less than 0.01% of the entire block volume. Prior case studies indicate destructive quality assurance tests are used rarely [1].

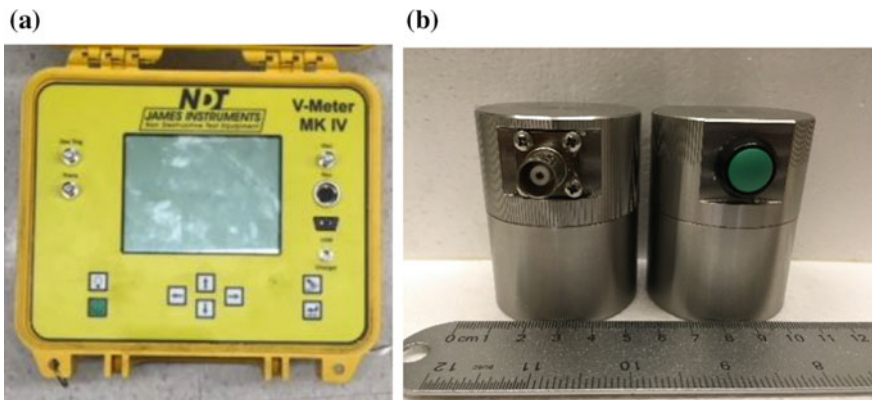


Fig. 2 **a** The NDT equipment **b** trigger and receiver transducers

ASTM C390 and ASTM D7557 recommend testing of one block per 150 blocks delivered on site. Other standards suggest the testing of one EPS geofoam block per truck load. Depending on the block thickness and the truck cargo holding dimensions, a truck load consists of less than 30 blocks. The tests usually consist of weighing and measuring the dimensions of blocks to check the density. Block molders purchase resin beads by weight and supply blocks by volume. They usually quote bids within tight margins. To the extent allowed, supplying low density blocks with some recycled content would improve profits. In addition, to meet a large volume order in limited time, some low and high density blocks may be included in the delivery.

Even when performed, density and dimensional checks neither confirm homogeneity nor detect presence of recycled content. There is need for an effective and practical quality assurance procedure. This investigation of NDT method for EPS geofoam quality assurance is to address such needs.

2 Test Instrument

A Non Destructive Testing (NDT) system consists of ultrasonic signal generation and detection to determine P wave transmission velocities through full size geofoam blocks of different nominal densities. The V Meter Mark IV shown in Fig. 2 has a standard set of triggering and receiving transducers that operate at 54 kHz frequency. The frequency range can be extended to 24 and 150 kHz with optimal sets of transducers. Low level signals can be enhanced with a custom made amplifier. The test results reported in this investigation were obtained with the standard transducers and $\times 4$ and $\times 7$ amplifiers. Higher frequencies (150 kHz) are used for testing small sized (sand and mortar) whereas lower frequencies (24 kHz) are used to test larger aggregates [2].

3 Testing Program

The NDT program was performed at four EPS molding plants located in New York and Pennsylvania. The plants mostly produce virgin EPS blocks and some low density blocks that have up to 10% recycled or re-grind content. The EPS blocks produced at the plants have approximate thicknesses of 0.6 or 1 m, widths of 1.2 m, and length of 5 m.

A total of 42 virgin EPS blocks and 8 blocks containing varying amount of recycled content were tested without amplifying the signal and 5 additional EPS virgin blocks were tested using the amplified signal. An average of 30 readings per block were taken for the 42 EPS blocks that were tested without amplifying the signal. For the 5 EPS blocks tested with the amplified signal, 120 readings

were taken for each three set of tests performed per EPS block (without amplifying, $\times 4$ amplification, and $\times 7$ amplification). The readings were increased from 30 to 120 to acquire more data in the 90% confidence level. Two sets of pulse rates were used; 3 pulses per 6 s for the 42 EPS blocks and 10 pulses per 5 s for the 5 EPS blocks. Changing the pulse rates affected the standard deviation of the P wave data. The higher the pulse rate, the lower the standard deviation. However, the mean (average) of the P wave velocity data collected was unaffected with the change in pulse rates.

The transducers were positioned at opposite sides of pre-selected locations as shown in Fig. 3. Petroleum jelly was used to fill gaps and develop full contact between the transducer and the EPS block surface. EPS blocks of 16, 20, 24, 32, 40, and 48 kg/m^3 nominal densities were tested. P wave signals were not detected across 2.5 and 5 m dimensions of all half and full size EPS blocks. Signals were, however, obtained through the 0.6 to 1 m thickness and 1.2 m width of EPS blocks.

P wave velocity data was collected on locations that were 0.6 and 1.2 m apart on half and full sized blocks, respectively, as shown in Fig. 4. P waves were not obtained through the 1 m thickness and 1.2 m width on 6 of the 42 EPS blocks which were of the lowest nominal density (16 kg/m^3). However, signals were obtained on all locations with the use of a signal amplifier. Signals were not obtained through blocks that had recycled content except one that had a higher density (32 kg/m^3) and 10% regrind content. The tests were done by two persons. However, by using a mounting frame to position transducers at required locations on the EPS geofoam block, the testing program can be conducted by one person.

Fig. 3 P wave detection across the 1.2 m width of an EPS block



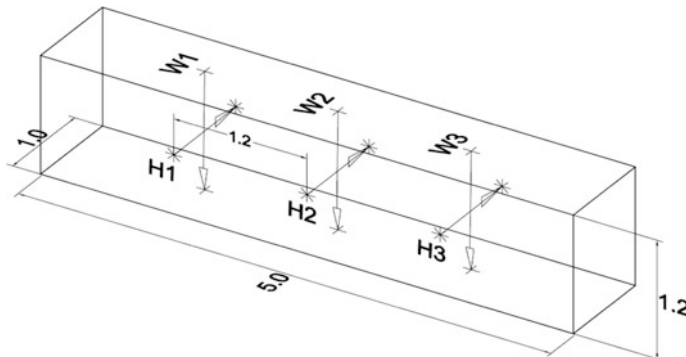


Fig. 4 P wave signal detection locations on full sized blocks (6 locations per block)

4 Results

EPS blocks were weighed and the dimensions were measured to confirm the nominal density designation and the results are shown in Fig. 5. All EPS blocks that transmitted signals at all four plants met the required 90% of the nominal density usually set as criteria in construction projects. About 95% of the block densities were below the respective nominal grade designation. Only 5% of the blocks exceeded the respective nominal density. If the acceptance of full blocks were to be based on conformance to nominal density, about 95% of the EPS blocks would have been rejected. The production line density at the EPS molding plants appear to be targeted to meet the 90% criteria and not the nominal density. Locations on where signal was not obtained indicate zones of non-uniformity, low density, or presence of regrind within the EPS geofoam block.

Best fit lines for average P wave velocities and densities observed at each molding plant are presented in Fig. 6. The P wave velocity increases with density for Plants 1 and 3 are more consistent than for Plants 2 and 4. Selecting recommended bead types for the desired density, the shelf life of resin beads as well as the plant equipment and operations likely contribute to variability in measured P wave velocities [3].

Young's moduli of geofoam blocks can be estimated using the relation between P wave transmissions velocity and the block density as in Eq. 1.

$$E = V^2 * \rho \quad (1)$$

E Young's modulus of the block

V average P wave velocity through the block

ρ mass density of the block

The Young's moduli values determined from the NDT readings increase with density, Fig. 7. The trend lines for NDT observation at each molding plant indicate

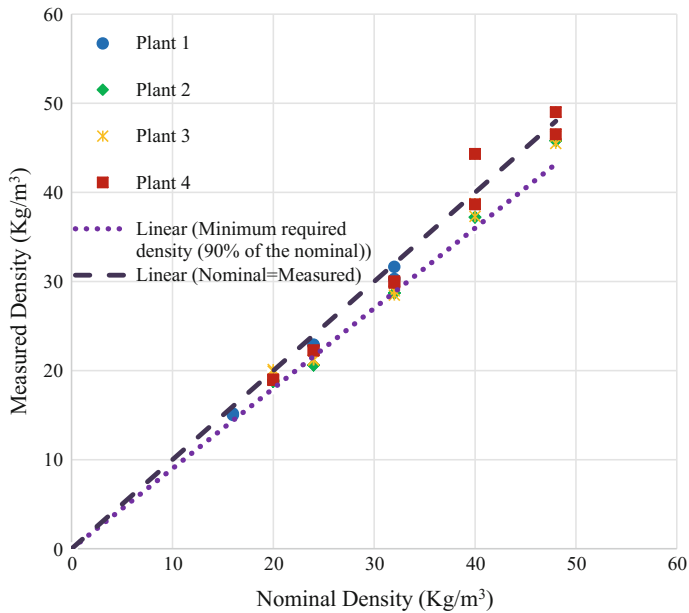


Fig. 5 Actual densities of geofoam blocks produced at four molding plants

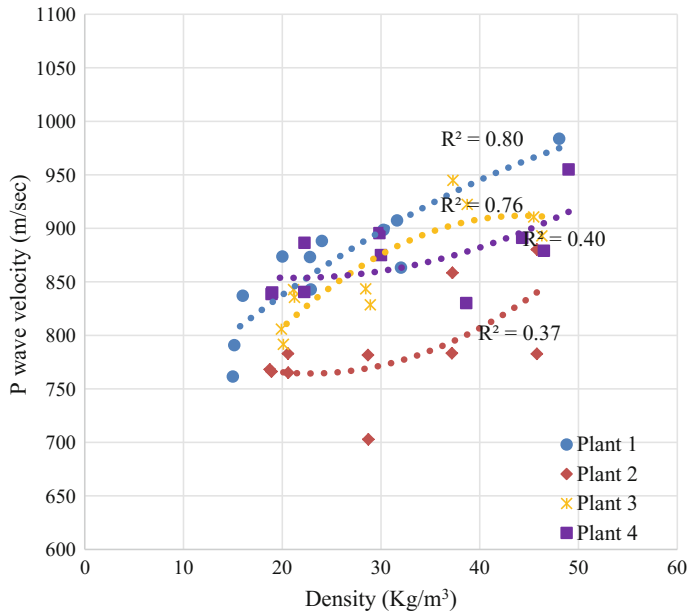


Fig. 6 P wave velocities and measured densities at four molding plants

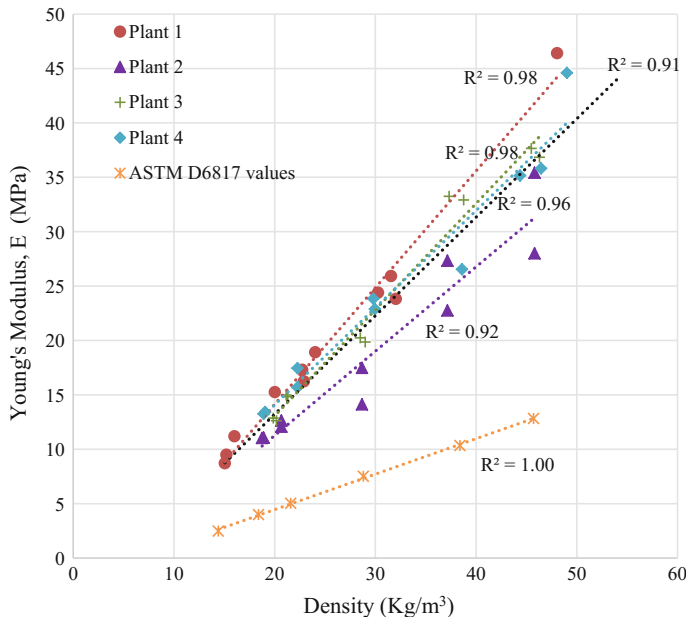


Fig. 7 Young's moduli values from NDT testing at four molding plants

reasonably good correlation between modulus and density. In contrast with the Young's modulus values inferred from uniaxial compression test on small samples, such as from ASTM D6817 values at 1% strain, the NDT moduli at all densities are much higher.

The Young's moduli values obtained from the NDT agree reasonably well with values previously reported from large scale tests [4], bending tests [5], and by back calculation from field observations [6] as shown in Fig. 8. The trend line from the NDT data form the upper bound of the trend lines for all observations. The trend line for the moduli derived from testing small samples in accordance with ASTM standards is on average about 3 times lower than the moduli from the four methods.

NDT data collected at Plant 1 on virgin EPS blocks and EPS blocks that contain recycled content indicate P wave velocities and Young's moduli decreased when the test blocks contained regrind, Fig. 9. The signals through EPS blocks with recycled material could only be detected after amplification. Weak signals through EPS blocks can be used to identify suspect blocks that may contain regrind or recycled content. A maximum of about 5% increase in average velocities were obtained for the lowest density virgin EPS block (16 kg/m^3) with amplified signal as shown in Fig. 9. Amplified P wave velocities through blocks that contain regrind were much more variable than velocities through virgin blocks.

Based on 90% confidence level fit of the velocity data from all plants, the corresponding Young's moduli for NDT results are shown in Fig. 10. Equation 2 is a non-dimensional relationship between moduli and density for NDT results.

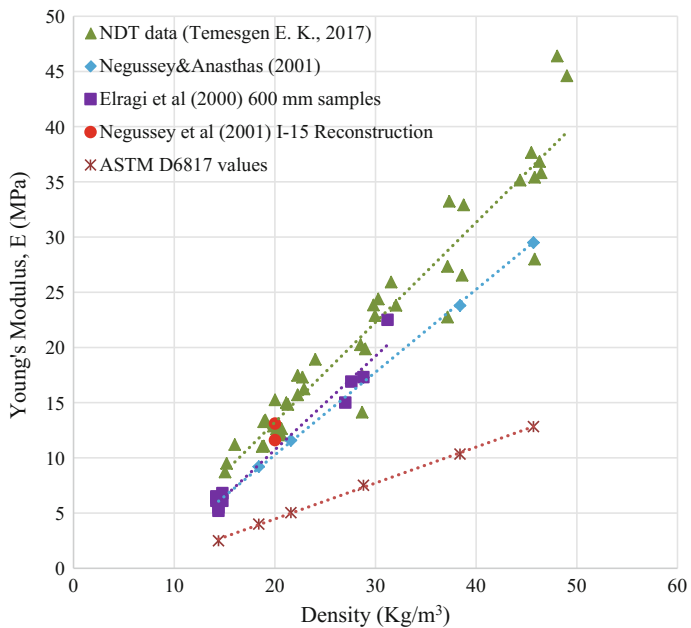


Fig. 8 Comparison of Young's moduli values from NDT with previous results

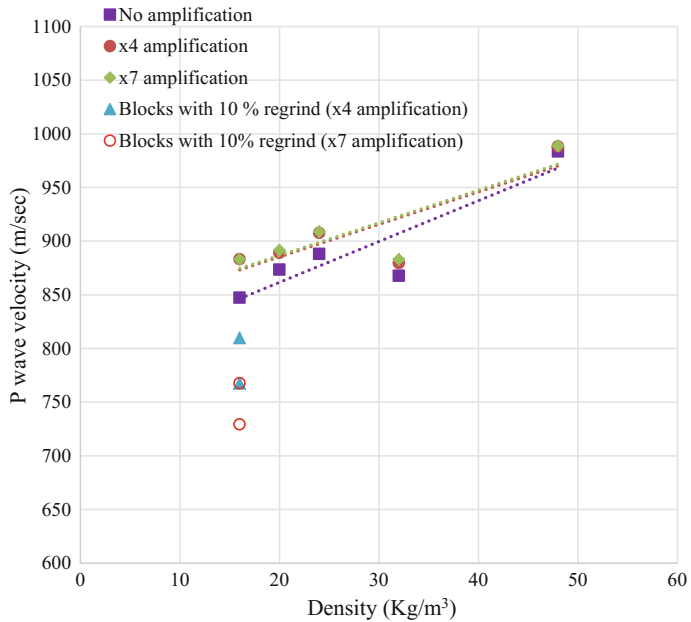


Fig. 9 P wave velocities from amplified and non-amplified signals at Plant 1

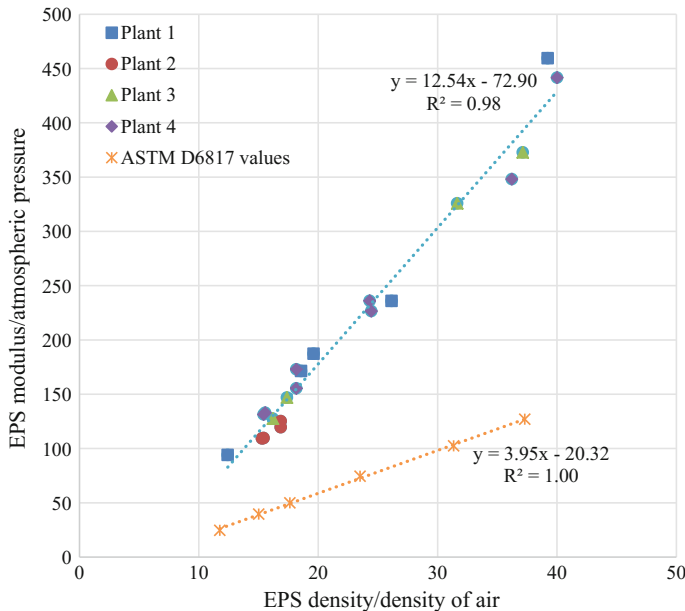


Fig. 10 Normalized Young's moduli from NDT with normalized density

Comparatively the ASTM D6817 moduli equivalent at 1% strain, Eq. 3, are much lower than the values resulting from Eq. 2. Typical moduli values for organic silts and very soft to soft clays plot at or below 50 on the normalized scale of Fig. 10. This suggests the moduli for the lower density EPS blocks, including the most commonly used density type (EPS19 in D6817 or nominal 20 kg/m³ density) would have equivalent moduli to organic silts and very soft clays. The moduli values from NDT are more realistic and in better agreement with moduli inferred from field observations. Thus destructive testing for quality assurance has further disadvantage of providing unrealistic results.

$$E_{eps}/P_{atm} = (12.5 * \rho_{eps}/\rho_{air}) - 72.9 \quad (2)$$

$$E_{eps}/P_{atm} = (4.0 * \rho_{eps}/\rho_{air}) - 20.3. \quad (3)$$

E_{eps}/P_{atm} Young's modulus of the block normalized by atmospheric pressure
 ρ_{eps}/ρ_{air} Density of the block normalized by density of air at sea level

5 Conclusions

- Young's moduli of full size EPS blocks determined from NDT increase with density.
- Nominal density and modulus criteria for full size EPS blocks can be specified and confirmed by NDT on site without material waste.
- The NDT program resulted in Young's moduli values for different densities that were higher than those obtained from small specimen testing.
- Young's moduli obtained from NDT are in a consistent and complementary range when compared with compressible soils.
- Young's moduli values for EPS geofoam blocks from NDT are in good agreement with previous results for large sample tests and inferred values from field observations.
- NDT may be helpful to identify EPS blocks that have recycled content.
- The non-dimensional relationship provided in Eq. 2 can be used to estimate realistic Young's moduli values for full size EPS blocks.
- NDT for EPS geofoam is a practical on-site quality assurance method. More blocks can be tested with NDT for efficient and tight quality assurance.

Acknowledgements Thermal Foams Syracuse and Buffalo, Shelter Enterprises, Albany and Insulation Corporation of America, Allentown, PA enabled non-destructive testing of EPS geofoam blocks at their plants. The authors gratefully acknowledge their assistance and collaboration.

References

1. Negussey D, Birhan A, Liu C, Andrews L (2014) Investigation of the Carrs Creek geofoam project: final report. University Transportation Research Center—Region 2, New York
2. James Instruments Inc. (2013) V—meter MK IV manual. James Instruments, Chicago, Illinois
3. Temesgen EK (2017) Non destructive testing For EPS geofoam quality assurance. Master's Thesis, Syracuse University
4. Elragi A, Negussey D, Kyanka G (2000) Sample size effects on the behavior of EPS geofoam. In: Paper presented at the Soft ground technology conference, Noordwijkerhout, Netherlands, 28 May–2 June 2000
5. Negussey D, Anastas N (2001) Young's modulus of EPS geofoam by simple bending test. In: 3rd international conference on geofoam blocks in construction applications, Salt Lake City, USA, 10–12 Dec 2001
6. Negussey D, Stuedlein A, Bartlett S, Fransworth C (2001) Performance of A geofoam embankment at 100 South, I—15 reconstruction project, Salt Lake City, Utah. In: 3rd international conference on geofoam blocks in construction applications, Salt Lake City, USA, 10–12 Dec 2001
7. Frydenlund TE, Cheney RS, Cobbe MI, Maagdenberg AC, Valkeisenmaki WPE, Yamamura K (1997) Lightweight filling materials. PIARC World Road Association, Paroi Nord

Evaluation of Interface Shear Strength Between Interlocked Geofoam Blocks and Cast-in-Place Concrete



Abdullah Tolga Özer and Özgür Ekincioğlu

Abstract Expanded polystyrene (EPS) block (geofoam block) roadway embankment typically involves the construction of cast-in-place reinforced Portland cement concrete (PCC) slab as a traffic load distribution layer since it reduces live load stresses and also provides lateral confinement of the overlying unbound pavement layers. Therefore, in addition to the geofoam block to geofoam block and geofoam block to bedding sand, interface properties of geofoam block to cast-in-place concrete slab should also be investigated for the stability calculations regarding transitional sliding failure mode. In order to enhance the traditional geofoam block to cast-in-place concrete interface shear strength, previously introduced interlocked geofoam block concept has been utilized. Flat-surfaced traditional geofoam blocks were trimmed by a hot-wire to form interlocked geofoam blocks with ledges along their contact surface with the cast-in-place concrete. EPS19 with a minimum density of 18.4 kg/m³ was used in the experimental program. Four different types of interlock configurations (blocks with one- and four-square ledges and blocks with one- and four-triangle ledges) were used to investigate the effect of interlocked geometry and number of ledges in the shear plane. In addition, interface friction properties of traditional geofoam block and cast-in-place concrete surface was also quantified to highlight the improvement provided by the interlocking mechanism. The adhesion bond between traditional geofoam blocks and cast-in-place concrete was close to that of internal shear strength of geofoam blocks. Regardless of the shape, the interface adhesion bond was slightly improved by the number of ledges when compared to that of traditional geofoam and cast-in-place concrete.

Keywords EPS-block geofoam • Interface shear • Cast-in-place concrete

A. T. Özer (✉)
Okan University, Istanbul, Turkey
e-mail: tolga.ozer@okan.edu.tr

Ö. Ekincioğlu
Istanbul Technical University, Istanbul, Turkey

1 Introduction

Expanded polystyrene (EPS) block geofoam (geofoam block) has been used in many different geotechnical engineering applications such as constructing highway and railway embankments on soft soil sites, compressible inclusion behind the retaining structures, seismic buffers, backfill above the buried pipes and culverts etc. After following the first geofoam embankment application in Norway [1], constructing highway embankments over soft soil sites to mitigate settlement is now a mature technology which has been successfully adapted in many different countries.

The guideline for geofoam applications in the design and construction of highway embankments requires performing both internal and external stability analysis [2]. Internal stability analysis includes transition due to water (hydrostatic sliding), transition due to wind and seismic stability [2]. All of these ultimate limit state (ULS) analyses are performed to determine whether the geofoam embankment will act as a single mass under external loads. Therefore, the available shear resistance of the interfaces within the geofoam block assemblage needs to be considered as design parameters under horizontal loading. Geofoam-geofoam [3–7], geofoam-sand [4, 5, 8, 9] and geofoam-concrete [3, 10] interface shear strength properties have been investigated by various researchers. In order to enhance the traditional geofoam-geofoam interface resistance, interlocked geofoam block concept was introduced [7, 11]. Interlocked geofoam blocks have ledge(s) along the top and notch(s) along the bottom so that when two geofoam blocks were placed on top of each other they were configured to provide interlocked interface [7, 11]. This interlocking mechanism has improved the interface shear strength properties when compared to that of traditional geofoam-geofoam interface [7].

In this study, interface shear strength properties of interlocked geofoam block and cast-in-place concrete (geofoam-cast-in-place concrete) have been investigated. Direct shear testing was used to quantify the effect of four different interlocked configurations on the interface shear stress-strain characteristics. In addition, interface shear strength properties of traditional geofoam-cast-in-place concrete have been quantified to demonstrate the improvements provided by the interlocked geofoam blocks.

2 Materials and Methods

EPS19 (with a minimum density of 18.4 kg/m³ [12]) was used in the experimental program. Compressive strength properties of geofoam blocks on five different specimens was determined based on ASTM D1621 [13] and results were summarized in Table 1. In addition to the interface friction properties of traditional geofoam block-cast-in-place concrete surface, the interface properties of two different interlocked shapes (square and triangle) with two different numbers of ledges

Table 1 Mechanical properties of EPS19 geofoam blocks [7]

Property	Values	
	Laboratory test values minimum–maximum (average, standard deviation)	ASTM D6817 [12] minimum required values
γ (kg/m ³)	18.08–18.96 (18.54, 0.38)	18.4
σ_1 (kPa)	38.0–45.5 (40.21, 3.54)	40
σ_5 (kPa)	90.2–96.8 (93.9, 2.86)	90
σ_{10} (kPa)	101.2–107.1 (105.0, 2.72)	110
E_i (MPa)	3.5–4.1 (3.73, 0.24)	–

ASTM American Society for Testing and Materials

γ apparent density

σ_1 , σ_5 , σ_{10} compressive strength at 1, 5 and 10% strain, respectively

E_i initial Young's modules

(one and four ledges) were also quantified to investigate the effect of interlocking mechanism on the stress-strain behavior of geofoam-concrete (Fig. 1). Test specimens were trimmed with a hot wire cutter to the dimensions of 2.5 cm high, 10 cm wide and 15 cm long (Fig. 1). Each ledge which interrupted traditional geofoam-cast-in-place concrete surface was 0.5 cm wide 0.5 cm high and 10 cm long (Fig. 1). The dimensions of the specimens were selected to represent a 1:20 scale of traditionally molded block size of 50 cm high, 200 cm wide and 300 cm long.

There is no standard testing procedure to quantify interface shear strength properties of geofoam-cast-in-place concrete. However, ASTM D5321 [14] was adapted by various studies to quantify both geofoam-geofoam [3–7] and geofoam-concrete [3, 10] interface stress-strain behavior. Interface shear strength properties are determined by direct shear testing technique [15] based on ASTM D5321 [14]. Therefore, fully automated direct shear testing device was used in this study (Fig. 2). This test system has both vertical and horizontal load cells to measure the constant vertical stress and the interface shear resistance, respectively. Systems microstepper motors control both vertical and horizontal loads (Fig. 2).

There are both horizontal and vertical differential transformer (LVDT) to measure both vertical and horizontal displacements. Test system also includes a shear box, where geofoam specimens were housed, moved horizontally towards the horizontal load cell which is fixed to the frame to capture interface forces. Vertical stresses applied by a 10 cm × 10 cm loading cap to the specimens (Fig. 2a), therefore 10 cm × 10 cm interface shear areas were created (Fig. 2b). Following the previous studies [4, 6, 7, 11] horizontal shear displacement rate was selected as 1 mm/min.

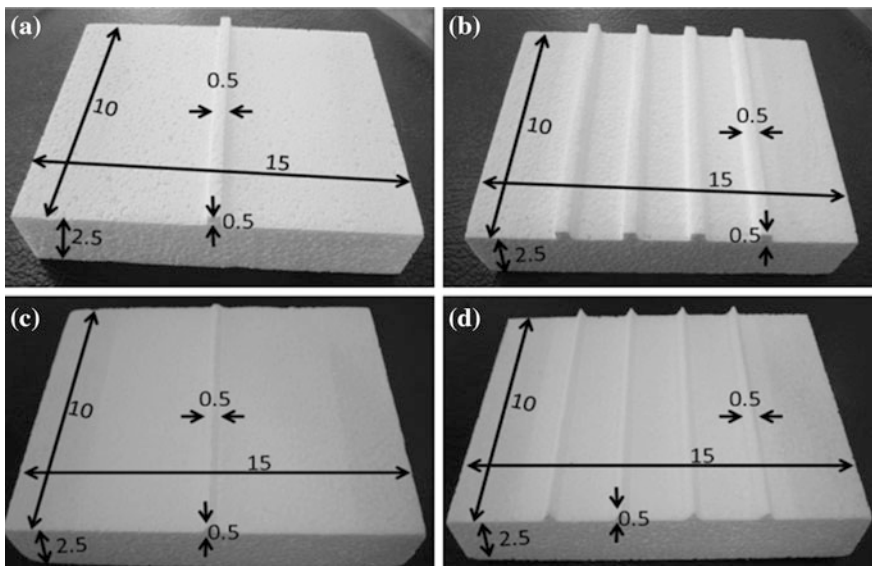


Fig. 1 Interlocked geofoam specimens with **a** one square ledge, **b** four square ledges, **c** one triangle ledge, **d** four triangle ledges

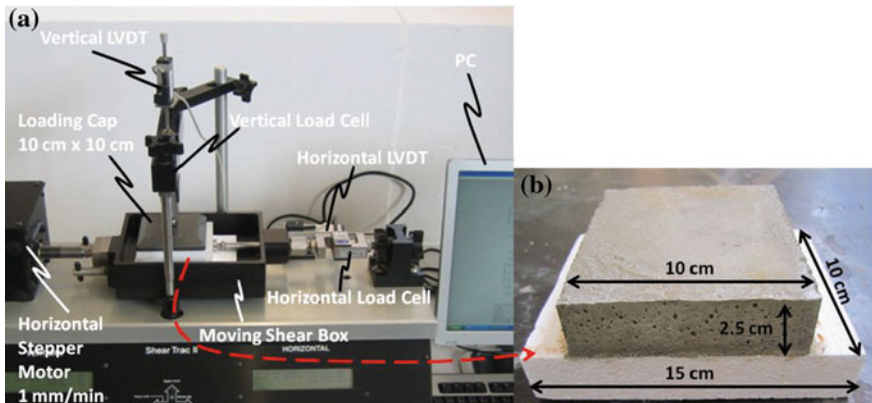


Fig. 2 Test setup **a** interface shear test equipment, **b** traditional geofoam-cast-in-place concrete interface test specimen

Largest grain size in pumped concrete is 31.5 mm, and based on optimum grain size analysis of pumpability of concrete, approximately $40 \pm 8\%$ of the aggregate needs to be larger than 8 mm [16]. For conventional concrete, largest grain size may even reach to 63 mm. The minimum interface specimen size (width of interface surface area) shall not be less than 10 times of the maximum particle diameter used in direct shear tests [15]. Therefore, $10 \text{ cm} \times 10 \text{ cm}$ interface

surface area is not large enough to use traditional concrete in the interface tests. Consequently, to represent the concrete for interface tests, mortar was used. A 10 cm × 10 cm split cast has been manufactured to pour the mortar on top of both traditional geofoam and interlocked geofoams (Fig. 3) surfaces. Upon curing the mortar under water for 28 days, top surface of the mortar was capped to provide uniform vertical stress application during the interface shear tests (Fig. 3f). Mortar mixtures were consisted of one part cement, three parts pre-packed CEN Standard sand and one half part water (water/cement ratio 0.50). CEM V/A (S-P) 32.5N class composite cement with 2.90 g/cm³ and a CEN Standard sand with 2.62 g/cm³ specific gravities were used in all mortar productions. Maximum particle size for CEN standard sand was 2 mm. In order to make sure to prepare homogeneous mortar production in all of six different mortar batches, the consistencies of fresh mortars were determined by using flow table [17] and the air contents were calculated [18] in each batch. In addition, unit weight of fresh mortars was also

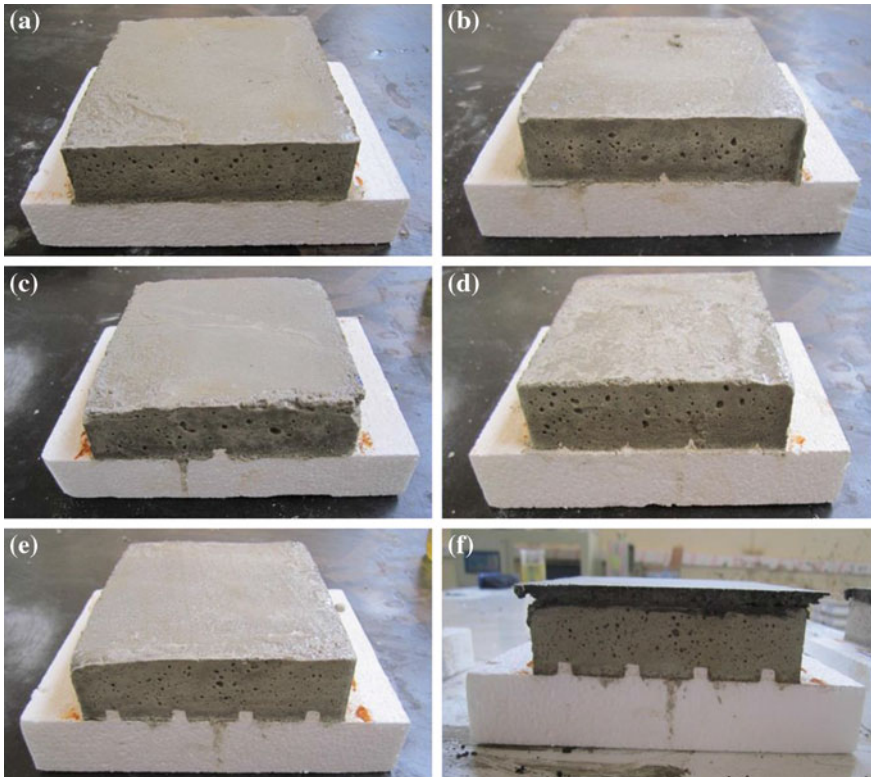


Fig. 3 Interface shear test specimens **a** traditional geofoam-cast-in-place concrete, **b** one-triangle geofoam-cast-in-place concrete, **c** one-square geofoam-cast-in-place concrete, **d** four-triangle geofoam-cast-in-place concrete, **e** four-square geofoam-cast-in-place concrete, **f** capping over the cast-in-place-concrete

measured during productions of each batch. The flow values of mortars were varied between 14 and 15.2 cm, air content varied between 3.06 and 4.2% and the unit weight varies in between 2.16 and 2.19 g/cm³ which indicated similar mortars were prepared for each batch. Three-point bending tests were conducted [19] on the specimens cured 7 and 28 days. After the bending tests, compressive strength tests were also carried out over each halves of the bending test specimens. Average bending strength of the mortars was 6.0 MPa and the average compressive strength of the mortars was 31.0 MPa for 28 days cured specimens, respectively.

3 Results and Conclusions

3.1 Traditional Geofoam-Cast-in-Place Concrete Interface

Traditional geofoam-cast-in-place concrete test was performed to evaluate the effect of proposed interlocking mechanism. In addition, results were also compared with the published values (Table 2). Even though there are various studies about geofoam-geofoam [3–7] and geofoam-sand [4, 5, 8, 9] interfaces, studies are limited in geofoam-cast-in-place concrete (Table 2). The interface shear stress-strain curves and failure envelope is given in Fig. 4. Interface friction angle (δ) and interface adhesion (c_a) is also provided in both Fig. 4 and Table 2.

Following ASTM's suggestion [15] all of the interface shear tests have been terminated at 10% horizontal strain. Therefore, peak interface shear stresses reported in the interface failure envelopes were the peak interface stresses during the shear phase or interface shear stress at 10% strain whichever was obtained first [15].

Current design practice for geofoam highway embankments limits the applied normal stresses at anywhere in the block layout no more than the elastic limit stress of geofoam blocks (corresponds to compressive strength at 1% strain) under the service loads [20]. Therefore, the maximum vertical stress used in the interface shear strength tests was 40 kPa which corresponds the compressive resistance of

Table 2 Comparison of EPS19-cast-in-place interface shear strength with published values

Reference	EPS type	Test method and sample size (mm × mm)	σ_v (kPa)	Interface friction properties	
				c_a (kPa)	δ (°)
Sheeley and Negussey [3]	EPS19	Direct shear 100 × 100	32	76.0	–
This study			10–40	31.5	23.7

σ_v vertical stress

c_a interface adhesion

δ interface friction angle

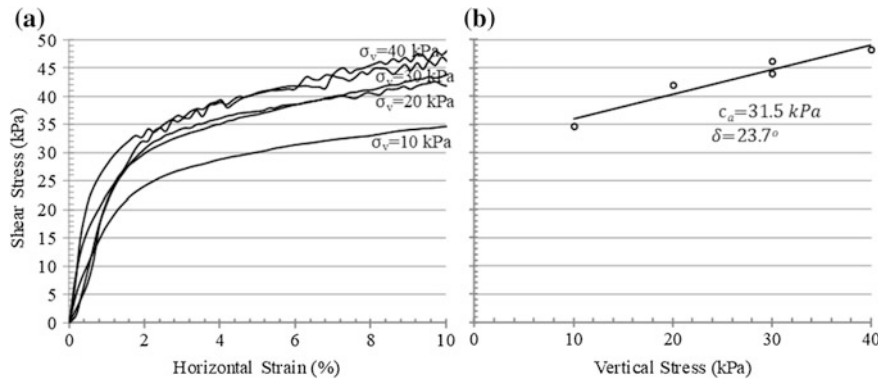


Fig. 4 EPS19-cast-in-place concrete interface shear test **a** interface stress-strain behavior, **b** interface failure envelope

EPS19 under 1% strain (Table 1). In addition, to construct the interface failure envelopes, interface shear strength tests were also conducted under 10, 20 and 30 kPa vertical stresses.

The traditional geofoam-cast-in-place concrete interface has strong adhesion strength (Fig. 4). This adhesion strength is higher than that of internal shear strength of geofoam block (27.5 kPa for EPS19) recommended by design guideline [2]. In addition to the high adhesion, geofoam-cast-in-place concrete has also exhibited interface friction angle (Fig. 4b). Therefore, interface friction behavior of geofoam-cast-in-place concrete is frictional-adhesional ($c_a > 0$ and $\delta > 0$). Under all of the vertical stresses no clear peak strength has been obtained (Fig. 4a); therefore shear stresses under 10% horizontal strain was used as peak shear stresses per ASTM [15].

A failure envelope (i.e. interface shear strength parameters) was not provided in the previous study by Sheeley and Negussey [3] (Table 2). Consequently, it is not possible to make direct comparison with their results. However, peak shear stress under 32 kPa of vertical stress was reported as 76 kPa (Table 2). Interface tests were run in duplicate under 30 kPa of vertical stress and the peak interface shear stress were obtained as 43.9 and 46.1 kPa. These duplicate experiments showed that interface stress-strain behavior of geofoam-cast-in-place concrete is repeatable. Interface shear strength of geofoam-cast-in-place-concrete is the function of vertical stress. Peak interface shear stress increased with increasing vertical stress (Fig. 4).

3.2 Interlocked Geofoam-Cast-in-Place Concrete Interfaces

The interface shear stress-strain curves and failure envelopes of one-triangle geofoam-, one-square geofoam-, four-triangle geofoam- and four-square geofoam-cast-in-place concrete are given in Figs. 5, 6, 7 and 8, respectively. Interface friction angle (δ) and interface adhesion (c_a) are also summarized in Table 3.

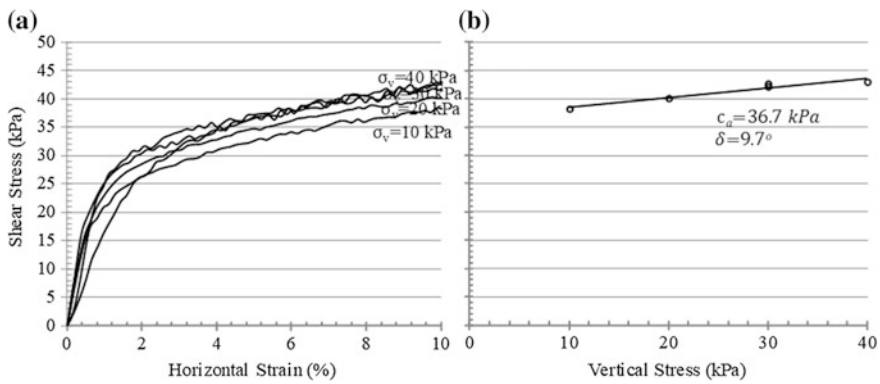


Fig. 5 One-triangle EPS19-cast-in-place concrete interface shear test **a** interface stress-strain behavior, **b** interface failure envelope

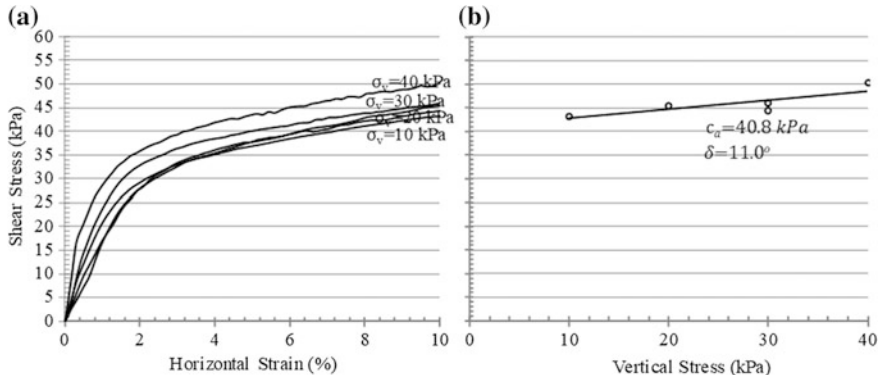
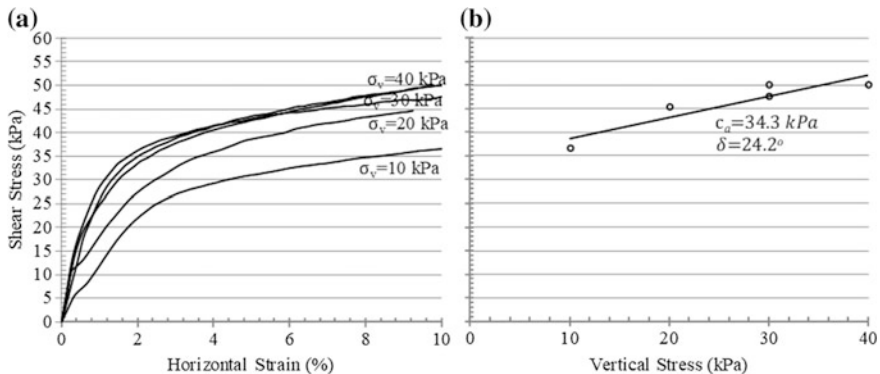


Fig. 6 One-square EPS19-cast-in-place concrete interface shear test **a** interface stress-strain behavior, **b** interface failure envelope



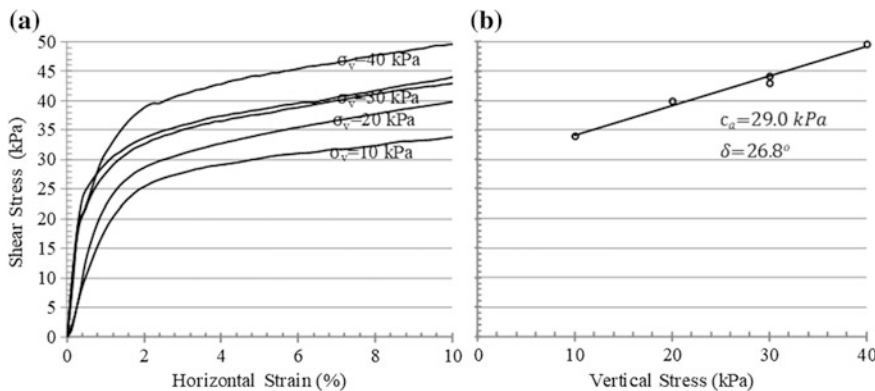


Fig. 8 Four-square EPS19-cast-in-place concrete interface shear test **a** interface stress-strain behavior, **b** interface failure envelope

Table 3 Summary of interlocked EPS19-cast-in-place interface shear strength tests

Configuration	Interface friction properties	
	c_a (kPa)	δ ($^\circ$)
One-triangle geofoam-cast-in-place concrete	36.7	9.7
One-square geofoam-cast-in-place concrete	40.8	11.0
Four-triangle geofoam-cast-in-place concrete	34.3	24.2
Four-square geofoam-cast-in-place concrete	29.0	26.8

Regardless of the interlock configuration, interface friction behavior of interlocked geofoam-cast-in-place concrete is also frictional-adhesional ($c_a > 0$ and $\delta > 0$). Like traditional geofoam-cast-in-place concrete interface (Fig. 4a), regardless of configuration, under all of the vertical stresses no clear peak strength has been obtained (Figs. 5a and 8a); therefore shear stresses under 10% horizontal strain was used as peak shear stresses per ASTM [15].

Interrupting the shear plane with 0.5 cm wide, 0.5 cm high and 10 cm long ledges (which corresponds to 10 cm wide and 10 cm high ledge cross-section in prototype scale based on 1:20 scale used in specimens) the interface adhesion was slightly improved compared to that of traditional configuration except for four-square configuration. Duplicate tests conducted under 30 kPa vertical stress showed the repeatability of the test results for all the configurations tested (Figs. 5a and 8a).

Failure envelopes of all the configurations tested are compared in Fig. 9. In addition, geofoam-geofoam (EPS19-EPS19) interface shear strength envelope [7] and internal shear strength failure envelopes of EPS19 [2, 7] were also shown in Fig. 9 for comparison purposes. Regardless of the configuration, geofoam-cast-in-place concrete interface shear strength is higher than both internal

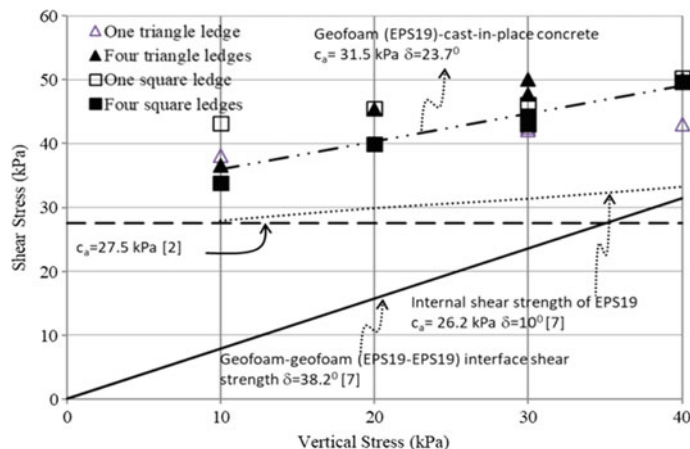


Fig. 9 Comparison of interface failure envelopes

shear strength of geofoam block and geofoam-geofoam interface shear strength (Fig. 9). While the geofoam-geofoam interface shear strength is purely frictional ($c_a = 0$ and $\delta > 0$), geofoam-cast-in-place concrete exhibited frictional-adhesional interface shear behavior regardless of the configurations (Fig. 9). Regardless of the shape or number of ledges, interface shear strength properties (Table 3) and failure envelopes (Fig. 9) of interlocked configuration are close to that of traditional geofoam-cast-in-place concrete interface properties. Even though interrupting the failure plane with ledge or ledges slightly improved interface adhesion strength of traditional configuration (except for four square configuration, Table 3), under the service loading (elastic limit stress of 40 kPa for EPS19) shear stresses were closed to that of traditional configuration except for one triangle configuration (Fig. 9).

4 Summary and Conclusions

Interface shear strength properties of interlocked geofoam-cast-in-place concrete were studied. A total of four interface shear strength tests were conducted using interlocked blocks and one test conducted using traditional block. Traditional geofoam block-cast-in-place concrete has an adhesion bond which is higher than internal shear strength of geofoam block. In addition, it also exhibited interface friction angle. Therefore, geofoam-cast-in-place concrete interface shear behavior is frictional-adhesional. Previous studies showed that the interlocking concept has improved the geofoam-geofoam interface shear strength significantly [7]. Contrary, interrupting the interface shear plane with ledge or ledges slightly improved this adhesion bond in three configurations out of four interlock configurations.

Due to the limitations of the direct shear device used in the experimental program in laboratory, all interface shear tests were conducted with mortar instead of concrete. All the test results were recommended in this study needs to be verified by conducting large-scale testing with prototype size blocks and cast-in-place concrete prior using in the design. In addition, effect of geofoam hardness on the interface properties needs to be investigated.

Acknowledgements The authors acknowledge the contribution of Okan University Department of Civil Engineering laboratory technician Halis Şahin and Master student Erdal Usturbelli during the experimental program. In addition, authors like to extend their gratitude to Dr. Onur Akay for his constructive critiques for early version of the manuscript.

References

1. Aabøe R (2011) 40 years of experience with the use of EPS geofoam blocks in road construction. Paper presented at the 4th international conference on geofoam blocks in construction applications, Lillestrøm, Norway, 6–8 June 2011
2. Stark TD, Arellano D, Horvath JS et al (2004) Guideline and recommended standard for geofoam applications in highway embankments. NCHRP Report 529, Transportation Research Board, Washington, D.C
3. Sheeley M, Negussey D (2000) An investigation of geofoam interface strength behavior. Geotechnical special publication No. 112, Paper presented at soft ground technology conference, ASCE, Reston, VA, pp 292–303
4. Atmatzidis DK, Missirlis EG, Theodorakopoulos EB (2001) Shear resistance on EPS geofoam block surfaces. Paper presented at the EPS geofoam 2001: 3rd annual conference, geotechnical engineering laboratory, University of Patras, Greece
5. Negussey D, Anasthas N, Srirajan S (2001) Interface friction properties of EPS geofoam. Paper presented at the 3rd international conference on geofoam blocks in construction applications, Salt Lake City, USA, 10–12 Dec 2001
6. Barrett JC (2008) Effectiveness of connectors in geofoam block construction. M.Sc. thesis, University of New Brunswick
7. Özer AT, Akay O (2016) Interface shear strength characteristics of interlocked EPS-block geofoam. J Mater Civil Eng 28(4). [https://doi.org/10.1061/\(asce\)mt.1943-5533.0001418](https://doi.org/10.1061/(asce)mt.1943-5533.0001418)
8. Xanaki VC, Athanasopoulos GA (2001) Experimental investigation of the interface mechanism at the EPS geofoam-sand interface by direct shear testing. Geosynth Int 8 (6):471–499
9. Özer AT, Akay O, Ateş Y (2016) Shear strength properties of interlocked EPS-block geofoam-Ottawa sand interface. Paper presented at the 4th international conference on new developments in soil mechanics and geotechnical engineering, Near East University, Nicosia, North Cyprus, 2–4 June 2016, pp 111–118
10. AbdelSalam SS, Azzam A (2016) Reduction of lateral pressures on retaining walls using geofoam inclusion. Geosynth Int 23(6):395–407
11. Özer AT, Akay O, Ateş E (2015) Effect of displacement rate on the interface shear strength properties of interlocked EPS-block geofoam. Presented at the IRF Europe & Central Asia Regional Congress, Istanbul, Turkey, 15–18 Sept 2015
12. ASTM (2015) Standard specification for rigid cellular polystyrene geofoam. ASTM D6817, West Conshohocken, PA
13. ASTM (2010) Standard test method for compressive properties of rigid cellular plastics. ASTM D1621, West Conshohocken, PA

14. ASTM (2014) Standard test method for determining the shear strength of soil-geosynthetic and geosynthetic-geosynthetic interfaces by direct shear. ASTM D5321, West Conshohocken, PA
15. ASTM (2011) Standard test method for direct shear test of soils under consolidated drained condition. ASTM D3080, West Conshohocken, PA
16. Türk Standard (2016) Design of concrete mix, In Turkish. TS802, Türk Standartları Enstитüsü, Ankara
17. EN (2000) Methods of test for mortar for masonry—Part 3: determination of consistence of fresh mortar (by flow table). EN 1015-3
18. ASTM (2015) Standard test method for air content of hydraulic cement mortar. ASTMC185, West Conshohocken, PA
19. EN (2016) Methods of testing cement determination of strength. EN 196-1
20. Horvath JS (2010) Emerging trends in failures involving EPS-block geofoam fills. J Perform Const Facil 24(4). [https://doi.org/10.1061/\(asce\)cf.1943-5509.0000114](https://doi.org/10.1061/(asce)cf.1943-5509.0000114)

Stress-Strain Behavior of EPS Geofoam with Multiple Grades by Using FlexiForce Sensors



Chen Liu and Dawit Negussey

Abstract Design and construction of geotechnical projects with EPS geofoam can involve consideration of interactions between structures, surrounding soils and geofoam blocks. Within large volume installations of geofoam blocks there can be unintended variability in block densities. Such conditions can lead to non-uniformities in stress distribution and development of uneven deformations. This study examines the effects of mixed use of geofoam density grades on stress-strain behavior in laboratory test settings. Interface loads at both geofoam to rigid plate and geofoam to geofoam mating surfaces were observed with FlexiForce sensors. Both uniform low and high density configurations were tested. Effects of mixing densities were also examined for both one and two layer block configurations.

Keywords Geofoam · Mix densities · FlexiForce sensors · Stress distribution

1 Background

EPS geofoam blocks have been used as light weight material in a variety of geotechnical applications around the world for over 40 years. The large number of successful applications of geofoam and very few reported failures were mainly designed by rule of thumb and shared experiences. Sensing of interface contact pressures in geofoam block installations in the field and in large size laboratory samples and models would be useful for calibrating computer models and to improve design practice. Needs for load distribution slabs or requirements for adequate fill over geofoam to reduce stress increments can be assessed more reliably with interface pressure distribution investigations. Specifications usually call for protecting geofoam surfaces from exposure to heavy construction traffic, but associated stress levels are not known. Combining of different densities in EPS

C. Liu · D. Negussey (✉)
Syracuse University, Syracuse, NY, USA
e-mail: negussey@syr.edu

installation was identified to be potential cause for differential settlement [1, 2]. To guide future improvements in design and rapid construction with geofoam, use of new sensor systems in both lab tests and field observations are essential. Anasthas [3] performed laboratory tests on a 600 mm cube instrumented EPS block with embedded stress cells to investigate load distribution patterns within an EPS block. ARAMIS, a 3D optical non-contact displacement tracking system was used to analyze the local stress-strain distribution within one geofoam block [1]. Negussey [4] investigated interface pressures at a rigid plate and geofoam interface using tactile pressure sensors. Stress distributions at foam to foam interfaces and the effects of mixed densities were not well understood. This study extends the use of FlexiForce sensors to test the interface stress as well as the plate-foam and foam-foam boundary stress distribution. Different density groups were arranged to further examine the effects of multiple grades on EPS geofoam behaviors.

2 FlexiForce Sensors

The FlexiForce sensors [5] use a resistive-based technology. The force applied to a sensing area of the FlexiForce sensors changes the resistance of the sensing element. FlexiForce sensors (Fig. 1) are thin and can measure forces between two mating surfaces. The sensors are constructed of two layers of polyester film substrate. A conductive paint (silver) is applied to a circular area and connecting leads on each layer. The conductive paint circle active sensing area is covered by a slightly larger diameter pressure sensitive ink. The ink areas are mated to form a FlexiForce sensor and each sensor is treated as a contact point. To ensure consistent

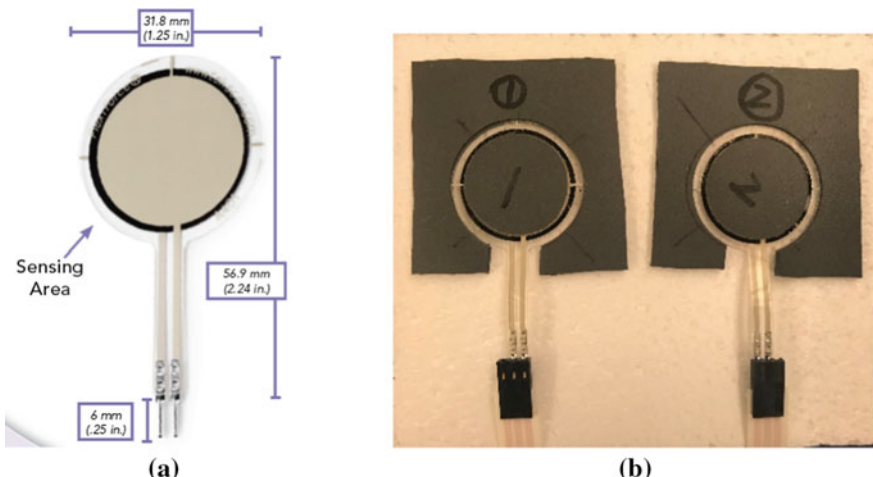


Fig. 1 FlexiForce sensor A401 [5]

force readings, applied loads must be distributed evenly across the sensing area. After testing different “puck” materials, a thin geomembrane square sheet of the same size as the test sample end area was trimmed. A center circle of the same size as the active area and an opening for the leads were cut out. The geomembrane square, FlexiForce sensor and the puck cover were assembled to be placed between contact test surfaces as shown in Fig. 1b.

3 Test Process

The test setup with a load cell, top platen, FlexiForce sensing assembly over a test sample are shown in Fig. 2. The load cell is suspended from the crossbar of the loading frame detects the applied vertical forces. Corresponding deformations are registered by the displacement transducer (LVDT). The data acquisition system is centrally located to which all the transducers, power supplies, and A/D-D/A converters are linked. Values of load and displacement are recorded with time stamp.

The first single layer test configurations are shown in Table 1. Three tests with one layer of EPS geofoam were arranged with different density combinations. FlexiForce A401 sensor assembly was placed at the center of each test block top surface and the rigid end plate (Fig. 3). The second two layer test configurations are shown in Table 2. Six tests were arranged in sets of four blocks with different density combinations. FlexiForce A401 sensors were placed at each interface of upper and lower EPS blocks (Fig. 4).

Fig. 2 Loading setup

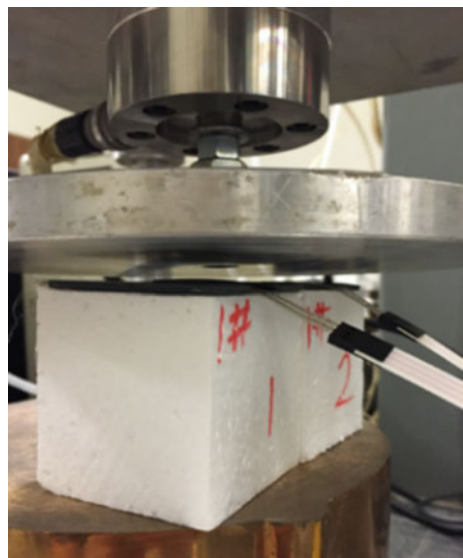
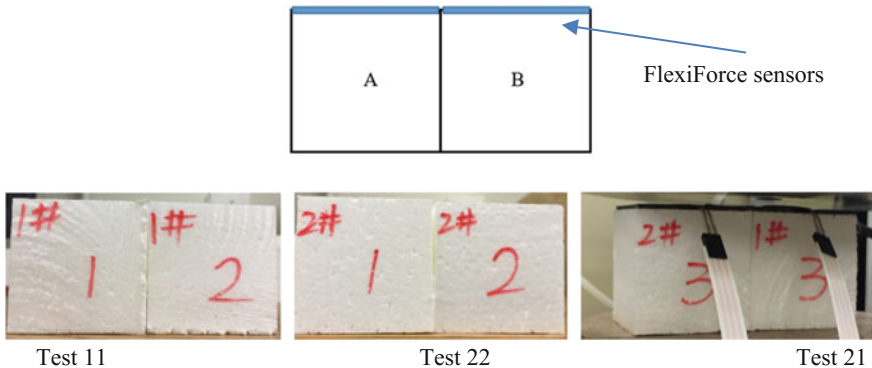
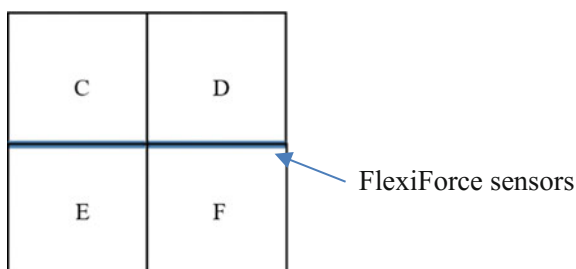


Table 1 Test setup 1

Test number	Density combination (unit: pcf)	
	A	B
11	1	1
22	2	2
21	2	1

1pcf = 16 kg/m³2pcf = 32 kg/m³**Fig. 3** Test setup—first test series (one layer)**Table 2** Test setup 2

Test number	Density combination (unit: pcf)			
	C	D	E	F
1111	1	1	1	1
2222	2	2	2	2
2221	2	2	2	1
1211	1	2	1	1
1112	1	1	1	2
1221	1	2	2	1

**Fig. 4** Test setup—second test series (two layers)

4 One Layer Test Results

Figures 5, 6 and 7 present the force/stress-strain results for one layer tests of different density combinations with FlexiForce sensors at rigid plate and geofoam interfaces. The load cell derived forces/pressure curves indicate applied overall loads on top of both EPS blocks. The FlexiForce curves show the forces/pressure states on the left and right interface boundaries separately.

As shown in Fig. 5, FlexiForce sensors registered equal forces on adjacent blocks of the same density. The higher density pair of blocks carried higher loads than the lower density pair. FlexiForce sensors registered higher forces on a higher density block when two blocks of different densities were loaded together.

As shown in Fig. 6, average contact pressures inferred from the load cell were equal to each of the average pressures derived from the FlexiForce sensors on adjacent blocks of the same density. When the adjacent blocks were of different densities, the higher density block was under larger pressure than the average

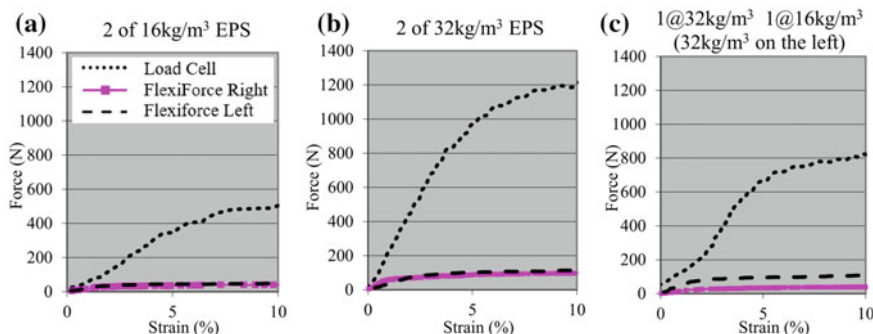


Fig. 5 Force-strain curves for load cell and FlexiForce sensors

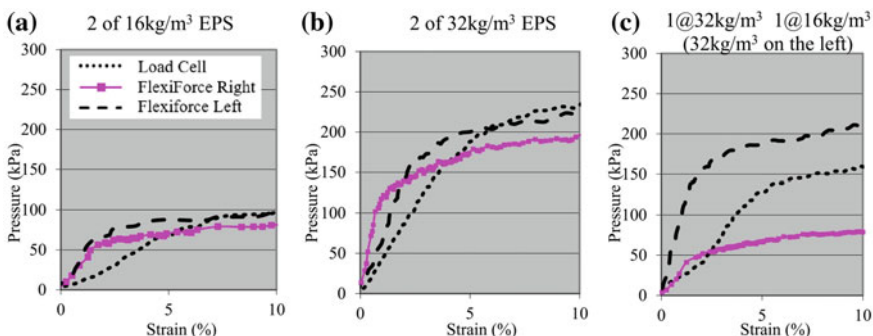


Fig. 6 Pressure-strain curves

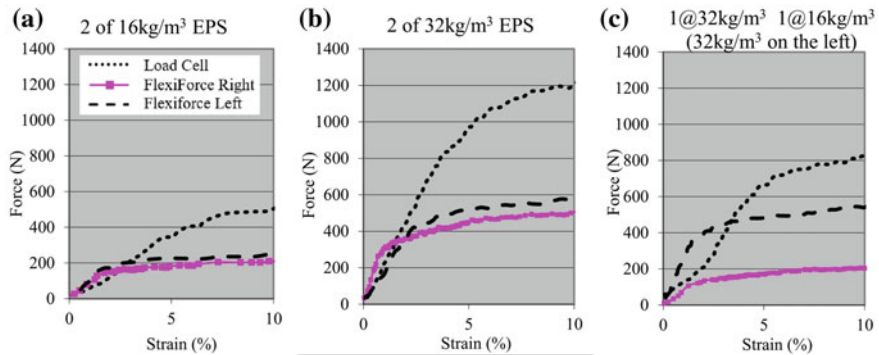


Fig. 7 Force-strain curves based on pressure-strain curves

pressure derived from the load cell. The lower density block was under lower pressure than the average pressure derived from the load cell.

Average forces over each sample, Fig. 7, derived from the respective FlexiForce sensors were equal when the adjacent blocks were of the same density. The higher density pair of blocks supported higher loads than the lower density pair of blocks. In each case, the sum of the average forces from FlexiForce sensors was equal to the respective average forces derived from the load cell output. However, when the test blocks were of different densities, the average forces on the higher density block was higher than the average forces derived from the load cell and also the lower density test block. The sum of average forces on each block derived from the respective FlexiForce sensors was about equal to the average forces registered by the load cell.

Figure 8 shows Young's Modulus values from the one layer tests together with equivalent modulus values as strength at 1% strain provided in ASTM D6817 [6]. The mixed densities test indicates lower Young's Modulus compared to the Young's Modulus value reported in D6817 for EPS of the same average density. The mixed density condition tends degrade the dual capacity of the EPS blocks. For tests performed at the same strain rate of 10% per minute, the combination of high and low density samples in a single layer developed comparable strengths at 10% strain to values in D6817. One layer configurations mimic lab test conditions whereas field conditions typically consist of multiple layers.

5 Two Layer Test Results

Figures 9, 10 and 11 present the force/stress-strain results for two layer tests of different density combinations derived from FlexiForce sensor observations at geofoam and geofoam interfaces. The load cell derived forces/strength curves indicate applied overall loads on top of both EPS blocks. The FlexiForce curves show the forces/strength states on the left and right interface boundaries separately.

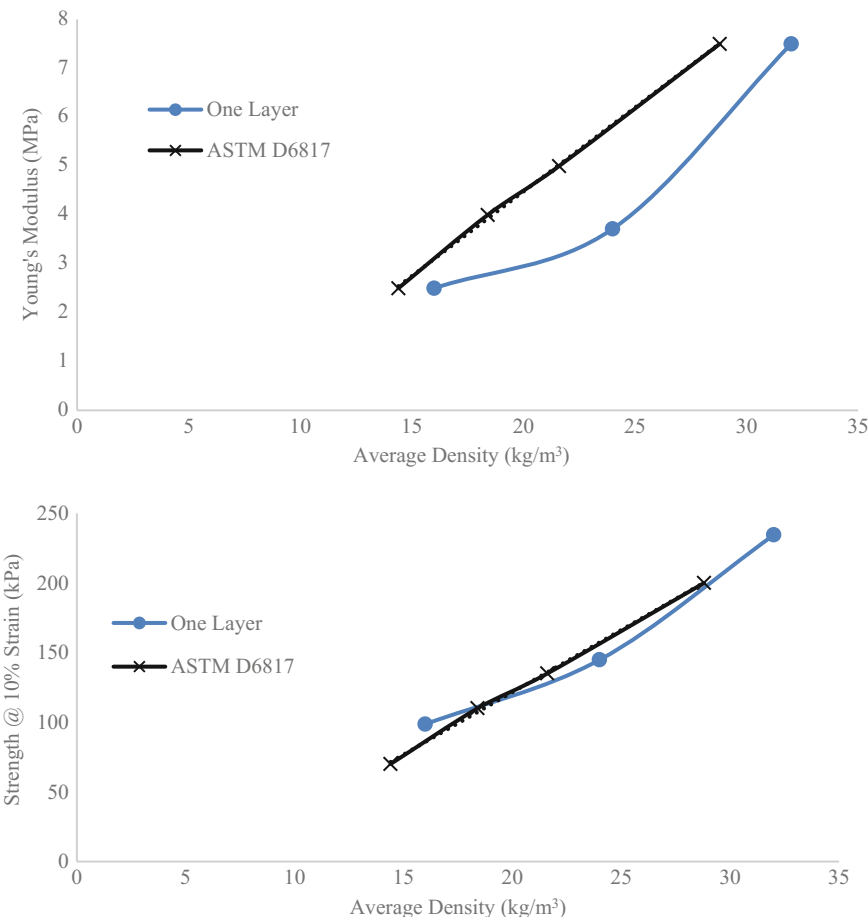


Fig. 8 Comparison of Young's modulus values and strength at 10% strain of single layer tests with ASTM standard single density tests

As shown in Fig. 9, FlexiForce sensors registered equal forces between adjacent stack of blocks of the same density. The higher density configuration of four blocks carried higher loads than the lower density arrangement. The strength of a four block dense configuration significantly reduced when one of four dense blocks was replaced by a low density block. Whereas when a higher density block replaced one of four low density blocks, the change in overall strength was minor. When each column of two blocks contained a high and a low density block, the force between each upper and lower blocks was the same.

Results shown in Fig. 10a and b indicate uniform density blocks carried the same pressure at 10% strain for foam/foam boundaries of the same density as the overall average pressure derived from the load cell output. Figure 10c indicates that when EPS blocks were installed with different densities, the higher density blocks

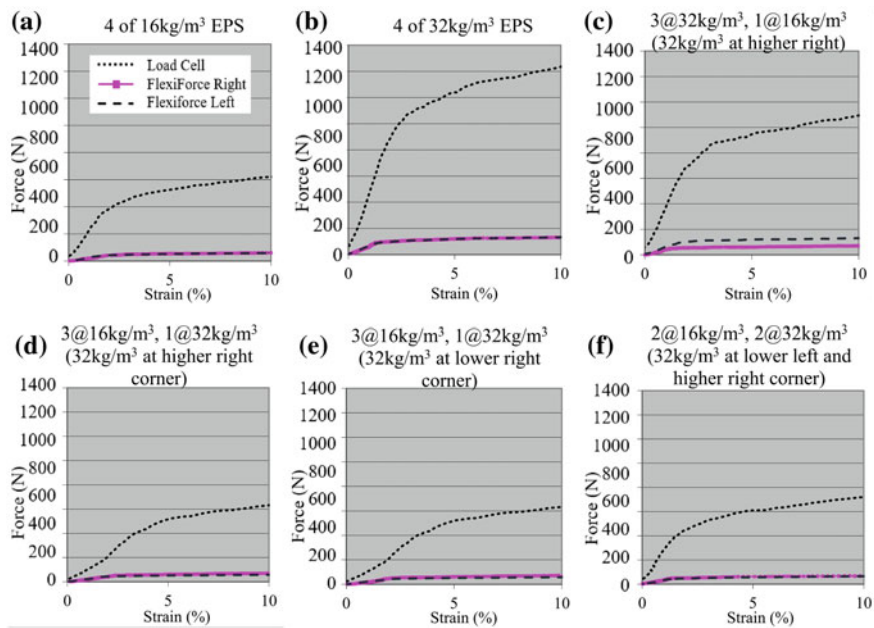


Fig. 9 Force-strain curves from load cell and FlexiForce sensors

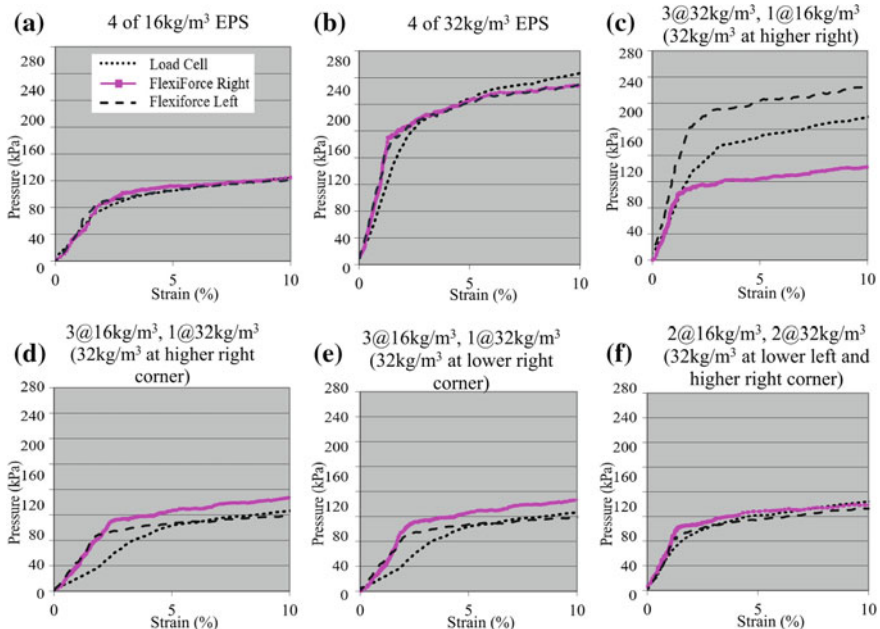


Fig. 10 Pressure-strain curves

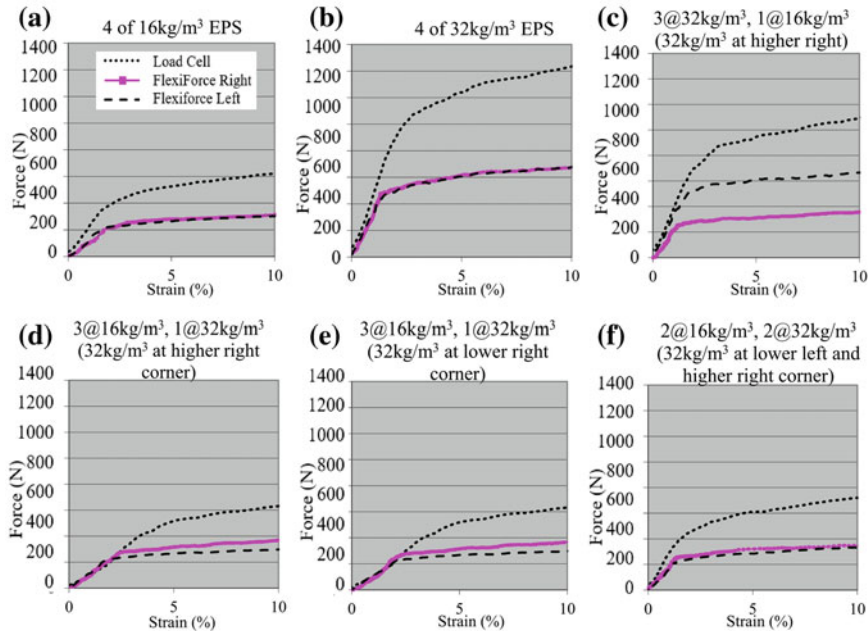


Fig. 11 Force-strain curves based on pressure-strain curves

carried more pressure at 10% strain than for the low density combinations tests. The applied pressure (180 kPa at 10% strain) was lower than the pressure carried by high density blocks (234 kPa at 10% strain) but higher than the pressure carried by high and low density combined blocks (110 kPa at 10% strain). The applied overall pressure was the average of the pressure carried by high and low density EPS blocks. Figures 10d, e present the stress-strain curves for three low density blocks and one high density block combination tests. The applied pressure (110 kPa at 10% strain) was lower than the pressure carried by high density blocks (124 kPa at 10% strain) and slightly higher than the pressure carried by high and low density combined blocks (103 kPa at 10% strain). The differences of about 3% was less than the pressure difference for the three high density blocks mixed with one low density block compared to three low density blocks mixed with one high density block. Figure 10f shows the stress-strain curves for mixed low and high density blocks on both left and right sides. The pressure at the interface boundaries were the same for both sides and were the same as the applied pressure.

The higher uniform density (32 kg/m^3) blocks carried more overall load than lower uniform density (16 kg/m^3) blocks. Figure 11 indicates a low density block within a high density cluster made the load distribution non-uniform. The higher density blocks carried more load (538 N at 10% strain) compared to the load (356 N at 10% strain) carried by low density EPS blocks. The one low density block inclusion degraded the overall strength of the specified all high density

blocks. Figure 11f shows the Force-strain curves for mixed low and high density blocks on both left and right sides. Since this test contained two high density blocks and two low density blocks, the overall strength was in between the strength of the all high density blocks and the strength of the all low density blocks.

Figure 12 shows comparison of the Young's Modulus values from the combined densities tests and ASTM D6817 [6]. The mixed densities tests resulted in lower Young's Moduli and strength at 10% strain compared to the results from the tests with the same density samples. Mix density conditions degrade the overall performance of the EPS blocks.

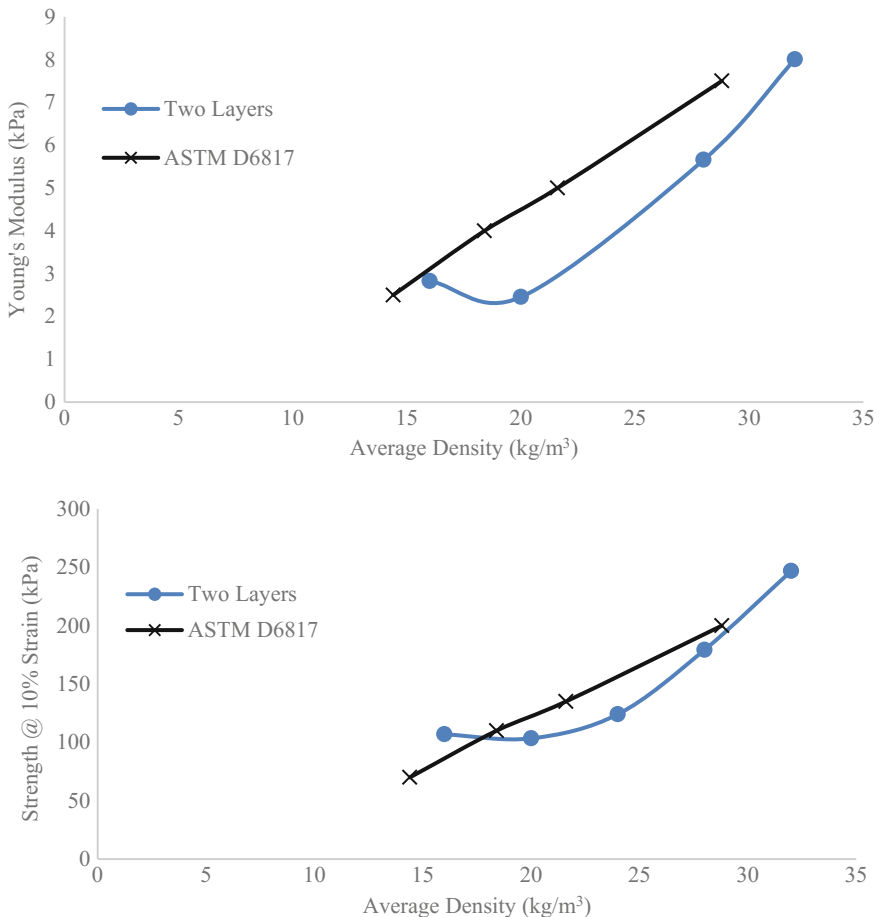


Fig. 12 Comparison Young's modulus values and strength at 10% strain of two layers tests with ASTM standard single density tests

6 Conclusions

Based on the test results, the following conclusions can be made:

- In a one layer test on two uniform density blocks, both blocks carry the same pressure as the applied average pressure. The higher uniform density (32 kg/m^3) blocks carry more overall load than the lower uniform density (16 kg/m^3) blocks.
- In a one layer test on two blocks with different densities, non-uniform boundary pressures develop. The higher density block carried the higher load compared to the load carried by the lower density block.
- In a two-layer test on four uniform density blocks, all four blocks carried the same pressure as the applied average pressure. The higher uniform density (32 kg/m^3) blocks carry more of the overall load than the lower uniform density (16 kg/m^3) blocks.
- When one of four specified low density (16 kg/m^3) blocks is replaced by a high density (32 kg/m^3) block, the overall strength degraded. The higher density block interface carried more load than the lower density block interface.
- When one of four specified high density (32 kg/m^3) blocks is replaced by a low density (16 kg/m^3) block, the overall strength degraded severely. The higher density block interface carried more load than the lower density block interface.
- In general, for mixed density tests, the higher density block carried higher load compared to loads carried by the lower density block at both plate-foam interface and foam-foam interface.

Acknowledgements The authors gratefully acknowledge the assistance of Tekscan whose FlexiForce sensors enabled observation of interface loads. R. Chave, J. Banas and W. Dossett helped with setting up test equipment and data acquisition systems.

References

1. Liu C (2015) Stress-strain behavior by image analysis, mix density and pre-strain effects of EPS geofoam, Master's Thesis, Syracuse University, Syracuse, NY
2. Singh S (2016) Pressure reduction on wide culverts with EPS geofoam backfill, Master's Thesis, Syracuse University, Syracuse, NY
3. Anasthas N (2001) Young's modulus by bending tests and other engineering properties of EPS geofoam, Master's Thesis, Syracuse University, Syracuse, NY
4. Negussey D (2007) Design parameters for EPS geofoam. Soils Found Jpn Geotech Soc 47 (1):161–170
5. Tekscan Inc (2010) FlexiForce® sensors user manual
6. ASTM D 6817

Behavior of Expanded Poly Styrene (EPS) with Experimental and Numerical Methods



S. N. Moghaddas Tafreshi and S. M. Amin Ghotbi Siabil

Abstract Using EPS in highways projects as subgrade material requires a substantial understanding of its behavior when subjected to static and cyclic loadings. Several research examples are available up to now regarding this issue, however, the concepts for the latter seems to have been paid less attention due to its complexity and time consuming nature. In an attempt to overcome the shortcomings, several test have been performed to determine the effect of static and cyclic loading on the performance of EPS geofoam. A simple numerical method is also proposed to simulate EPS behavior under cyclic loading. Further research is needed to derive more accurate results.

Keywords EPS behavior · Experiments · Simple numerical method

1 Introduction

EPS blocks are widely used as highway subgrades since the 1970s. The extreme low weight of this material provides numerous benefits to the project. They help to encounter common struggles (e.g. settlements and failures of embankments) faced in projects. In addition, construction with EPS is far more rapid compared to other materials used as highways subgrades. EPS geofoam is also a robust method to reduce backfill pressure on abutments or retaining walls.

However, evidence show that the practical experience of incorporating EPS in conjunction with soil materials can introduce major threats to the safety working life of the structure, if not properly designed. A major part of the proper design is related to the necessity of broad knowledge about the stress-strain and mechanical behavior of EPS material, which is not completely understood yet.

In this study, a number of EPS samples with various densities were examined in a uniaxial loading apparatus. Each density was tested under static and cyclic loads

S. N. Moghaddas Tafreshi (✉) · S. M. Amin Ghotbi Siabil
K.N. Toosi University of Technology, Tehran, Iran
e-mail: nas_moghaddas@kntu.ac.ir

to gain their stress-strain and hysteresis curves. A simple numerical method based on previous studies was also proposed to create a foundation for further investigations.

2 Materials and Test Results

In this section, results of the static and cyclic tests on EPS specimens are presented and different aspects of the diagrams will be discussed. The dimensions are 20×20 cm in plan, 10 cm in height for static and 20 cm height for cyclic tests. The specimens were cut and prepared from the main larger blocks by hot wire. The reason for selecting a lower height for static test is to prevent the test sample from failure modes that are not expected to happen in the full scale usage of EPS blocks (e.g. local failures or buckling). Static and cyclic results are presented in the following sections.

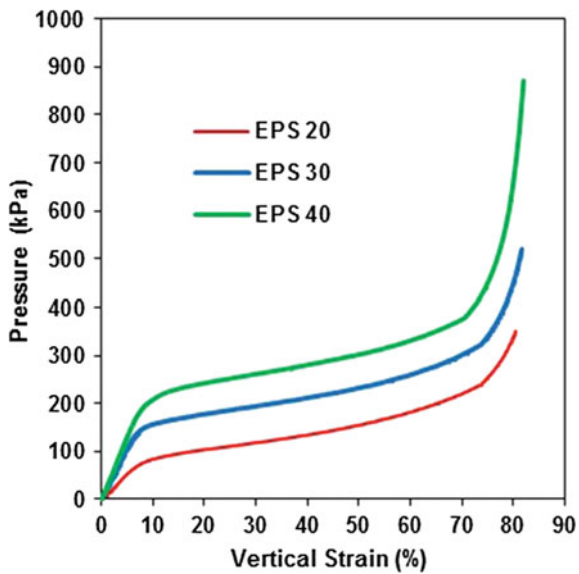
2.1 Static Tests

Figure 1 displays the stress strain curve of EPS with 20, 30 and 40 kg/m^3 densities. These tests were performed at the stress rate of 1 kPa/sec. The overall trend of curve for all of the densities is analogous and consists of three major parts: starting with a linear part, continued by a yielding section and finishing with a hardening part. The compressive strength at 1% strain are 8.06, 21.61 and 28.61 kPa for EPS 20, EPS 30 and EPS 40, respectively. The compressive strength at 10% strain are 83.67, 156.40 and 244.14 kPa for EPS 20, EPS 30 and EPS 40, respectively. The trend of the stress-strain curve is comparable to the results presented by Horvath [1] and Bartlett et al. [2]. However, the threshold stress of each section on the diagram for each of the densities is lower than the value reported by the latter mentioned research. The reason can be attributed to the characteristics or quality of raw material which constitute the basis for EPS production. This difference implies the importance for quality control and sample tests before starting construction phase in practical applications.

2.2 Cyclic Tests

Cyclic tests were performed with two or three different cyclic stresses for each density. Loads were applied in the shape of sine wave starting from zero, reaching the peak level and reducing to zero in 10 s (frequency of 0.1 Hz). The cyclic stresses were selected in a manner to be consistent with the pressure values that might be applied to each density during future full scale tests. All tests were performed with a total number of 100 cycles for different cyclic stresses.

Fig. 1 Stress-strain curve of EPS 20, EPS 30 and EPS 40



The result of the cyclic tests on EPS 20 are shown in Fig. 2 for cyclic stresses of 50, 100 and 150 kPa. For 50 kPa, the hysteresis curve is stable and does not move forward along the horizontal axis (i.e., accumulated cyclic strain is small). The maximum vertical stain is slightly larger than 2% and the minimum strain is below 1%. A substantial part of the vertical strain occurs after the first cycle of load is applied.

Fig. 2 Cyclic test results for EPS 20

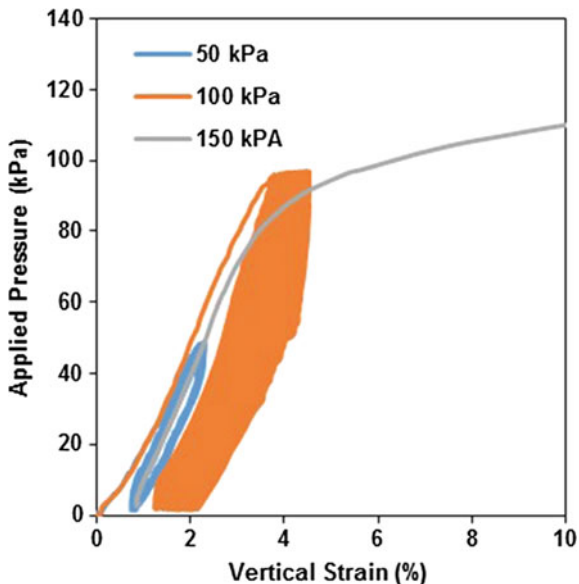
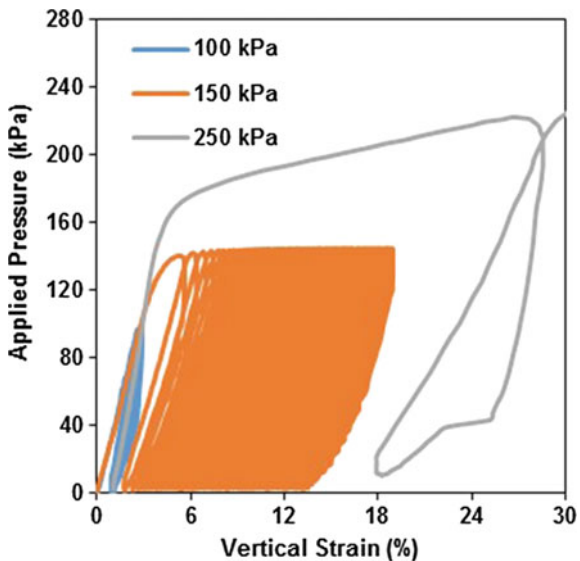


Fig. 3 Cyclic test results for EPS 30



When the applied cyclic stress is increased to 100 kPa, the vertical strain at the first cycle exceeds 3.5%, which shows an approximately twofold increase compared to the value corresponding for the 50 kPa case. Vertical strain also tends to increase with the repetition of applied pressure and does not show the stable pattern as observed in the 50 kPa stress (i.e., accumulated cyclic strain is considerable). It is also clear that the major part of vertical strain has been taken place with the application of first cycle. Thus, the ratio of permanent deformation to resilient deformation becomes larger with increase in the amount of cyclic stress.

For cyclic stress of 150 kPa, an extremely unstable strain response is perceptible. The material cannot sustain stresses at such level and it strains very rapidly before reaching 110 kPa. Thus, the amplitude of cyclic stress plays an important role in stability or instability of the response under cyclic loads and it must be evaluated precisely.

Figure 3 displays the results of cyclic tests for EPS 30. Three amplitudes of cyclic stress were selected as 100, 150 and 200 kPa. EPS 30 exhibits a stable response under cyclic stress with 100 kPa magnitude and an increasing response for 150 kPa amplitude. For 250 kPa, it shows a very unstable increase in vertical strain and can sustain only on the first cycle of stress application.

3 Simple Numerical Method

Numerical simulation of cyclic response of material can be a complex issue. As it was observed in the experiments, EPS undergoes permanent deformation under high cyclic pressure and corresponds to kinematic hardening during repetition of

loading. To mimic this kinematic behavior, the method introduced by Anastasopoulos et al. [3] was used. A Von-Mises yield criterion with nonlinear kinematic hardening and associated plastic flow rule would be proper to calculate the accumulated plastic strain during cyclic loading. The basic equations of the constitutive law include: the development of stress (Eq. 1), yield surface (Eq. 2), plastic flow rate (Eq. 3), isotropic hardening component (Eq. 4), kinematic hardening component (Eq. 5), undrained shear strength (Eq. 6), shear strain amplitude (Eq. 7), parameter for controlling initiation of nonlinear behavior (Eq. 8) and Young's modulus at very small strains (Eq. 9). In the defined equation, λ and α are the calibration parameters and were determined by trial and error method.

$$\sigma = \sigma_0 + \alpha \quad (1)$$

$$F = f(\sigma - \alpha) - \sigma_0 \quad (2)$$

$$\dot{\epsilon}^{pl} = \dot{\bar{\epsilon}}^{pl} \frac{\partial F}{\partial \sigma} \quad (3)$$

$$\sigma_o = \sigma_0 + Q_\infty \left(1 - e^{-b\bar{\epsilon}^{pl}} \right) \quad (4)$$

$$\dot{\alpha} = C \frac{1}{\sigma_o} (\sigma - \alpha) \dot{\bar{\epsilon}}^{pl} - \gamma \alpha \dot{\bar{\epsilon}}^{pl} \quad (5)$$

$$\sigma_y = \sqrt{3} S_u \quad (6)$$

$$\gamma = \frac{C}{\sqrt{3} S_u - \sigma_0} \quad (7)$$

$$\sigma_0 = \lambda \sigma_y \quad (8)$$

$$C = a \sigma_y \quad (9)$$

By using the stress-strain curve data obtained from static tests (see Fig. 1) and by means of a user subroutine, the stress (or strength) corresponding to each strain was assigned to the material during each step of loading. Using this method, a cylinder of EPS specimen tested by Trandafir and Erickson [4] was modeled and simulated in Abaqus under 15 cycles of loading and the results show a good agreement (in terms of accumulated plastic strain) for the first 15 cycles of loading. However, a visual comparison of the loops area indicate that the damping might not be modeled correctly by this method. Although the pavement loading is dynamic in nature, the dynamic characteristics of the pavement might have been considered as less influential and hence, the amount of damping would not have a considerable effect on the results. However, the results are expected to improve for dynamic loading and larger numbers of loading repetitions by introducing a viscous part into the material model. The viscous network can enhance energy absorption of the material and increase the area of hysteresis loops (Fig. 4).

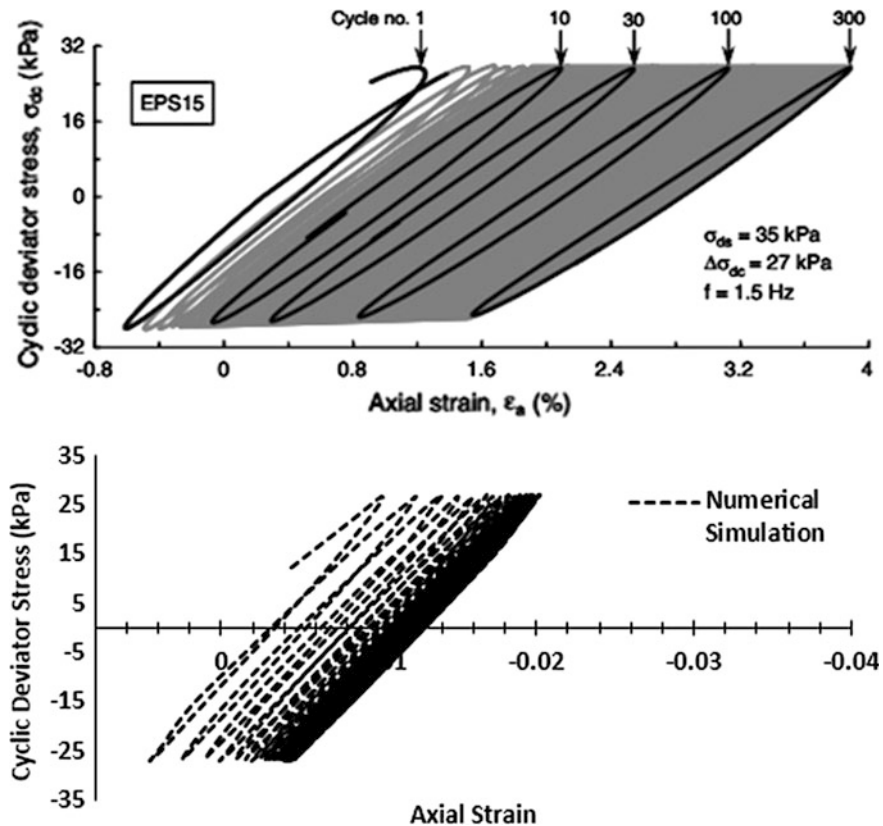


Fig. 4 Cyclic test results for EPS (top: Trandafir and Erickson [4])

4 Conclusion

Uniaxial static and cyclic tests on EPS specimens determine that each density shows a unique behavioral diagram, when subjected to loadings of various intensities. It is essential to obtain a threshold stress amplitude at which EPS with a specific density stays in a stable situation and strains extremely beyond that. To simulate cyclic behavior of the material, a simple subroutine in conjunction with Mises criterion can be utilized and a viscous network can be added to it to improve its performance.

References

1. Horvath JS (1994) Expanded polystyrene (EPS) geofoam: an introduction to material behavior. *Geotext Geomembr* 13(4):263–280
2. Bartlett SF, Lingwall BN, Vaslestad J (2015) Methods of protecting buried pipelines and culverts in transportation infrastructure using EPS geofoam. *Geotext Geomembr* 43(5): 450–461
3. Anastasopoulos I, Gelagoti F, Kourkoulis R, Gazetas G (2011) Simplified constitutive model for simulation of cyclic response of shallow foundations: validation against laboratory tests. *J Geotech Geoenvironmental Eng (ASCE)* 137(12)
4. Trandafir AC, Erickson BA (2012) Stiffness degradation and yielding of EPS geofoam under cyclic loading. *J Mater Civil Eng (ASCE)* 24(1)

Effects of Installation of Different Density Geofoam and Continuous Vertical Gaps



Chen Liu and Dawit Negussey

Abstract The mechanical properties of EPS geofoam vary with density. Usually, only one density or grade of EPS geofoam is specified per project. To maximize performance while reducing costs, higher density or grade EPS geofoam blocks have been specified for the top layers of fills in a few cases. The consistent best practices in EPS geofoam block installation have been: (a) not to install blocks of different densities in the same layer; (b) not to place blocks of lower density above higher density blocks; and (c) to stagger joints between blocks in successive layers so as to prevent continuity of inter-block vertical gaps. In practice, either by inadvertent misplacement or due to lax quality assurance and installation control, one or more of these three conditions can be violated. This investigation examined the effects of mixed densities and continuous vertical gaps between block layers. Groups of EPS block samples of the same density and also of mixed densities were tested with either staggered or continuous joints. The laboratory tests were simulated in computer models. The deformed shapes and dimensions indicated by the computer simulations were compared with the observed shapes and dimensions of the laboratory tests.

Keywords Geofoam · Density · Gaps · Image analysis · FLAC

1 Introduction

Expanded Polystyrene (EPS) Geofoam refers to block or planar rigid cellular foam polymeric material used in geotechnical engineering applications [1]. Since the earliest use in Norway in 1972 [2–4], EPS geofoam blocks have been widely used in geotechnical engineering as lightweight fill. EPS blocks are cuboid with typical width of 1.2 and 5 m length but thickness dimensions of 0.6–1.2 m depending on the size of the molding equipment at the plant. The densities of EPS geofoam in

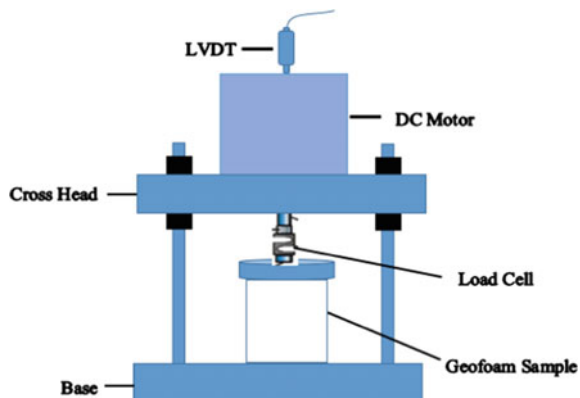
C. Liu · D. Negussey (✉)
Syracuse University, New York, NY, USA
e-mail: negussey@syr.edu

common use range between 16 and 32 kg/m³, but the 20 kg/m³ has been the most preferred in civil engineering applications. In the process of installing EPS geofoam blocks, assuring acquisition of the specified density and avoiding continuous vertical gaps across layers are suggested. The unit price of EPS blocks increase with density. For large volume use of EPS, significant savings can be achieved by specifying low-density blocks. For some projects, multiple-density grades of EPS geofoam were specified to reduce costs. In such cases, either inadvertently or carelessly EPS blocks of different density grades can be misplaced during installation. In addition, block molders purchase resin beads by weight and sell blocks by volume. There is therefore inherent incentive to deliver low density blocks to maximize profits. When a large volume of EPS blocks has to be supplied with short load time, a mixed batch of different densities may be delivered to meet time deadlines. In the absence of a robust quality assurance program, EPS blocks of wide density variability have been accepted and installed. The effects of using mixed density blocks and installation with continuous vertical gaps were investigated in lab tests and computer simulation. The investigation was motivated by failure of an accelerated construction of a wide culvert for which EPS geofoam blocks were used as light weight backfill [5–8].

2 Lab Tests

A loading frame system (Fig. 1) was used for unconfined compression tests on EPS blocks in accordance with ASTM D1621. An external load cell detected the applied vertical force. The vertical displacement was registered by a displacement transducer (LVDT). The data collection system was a centrally located data logger and a controller, to which all the transducers, power supplies, and A/D-D/A converters were linked. For each test, values of force and displacement were recorded with time.

Fig. 1 Loading system



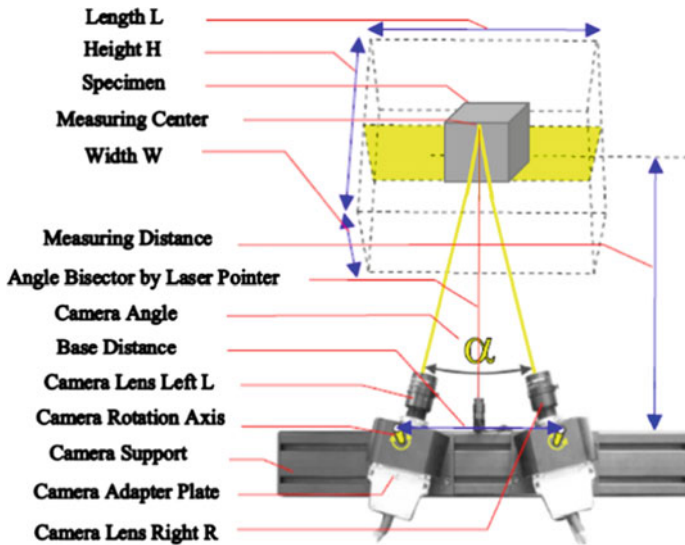


Fig. 2 ARAMIS optical sensing system

Together with the uniaxial loading system, two high resolution CCD cameras, (Fig. 2), captured sequential images for follow up image analysis using proprietary software, ARAMIS [9]. Surface structures of the test material were observed using advanced techniques of tracking and distributing pixel coordinates. Deformation and strain states were determined over the full field of view. In addition, the contact pressure distribution at the bottom metal-geofoam interface for left/right blocks were captured separately by tactile sensors [10].

2.1 One Layer Tests with Optical Sensing

The EPS block sample sizes and density configurations are shown in Fig. 3a. Five density arrangements were tested. Figure 4 presents the stress strain curves from unconfined compression tests for the different density arrangements. Young's moduli and strength @ 10% strain are compared with values for corresponding average densities reported in ASTM D6817. The uniform 32 kg/m³ (2pcf) blocks showed the highest Young's Modulus (7.5 MPa) and highest strength @ 10% strain (222 kPa), followed by the combination blocks with highest to lowest average densities. The uniform 16 kg/m³ (1pcf) blocks had the lowest Young's Modulus (2.52 MPa) and lowest strength @ 10% strain (87 kPa). The overall strength of EPS blocks with multiple-density configurations reduced compared to the strength of uniform high-density blocks. More higher-density EPS blocks present relatively higher strength while more lower-density EPS blocks have relatively lower strength. Young's Moduli and strength at 10% strain from the combined density

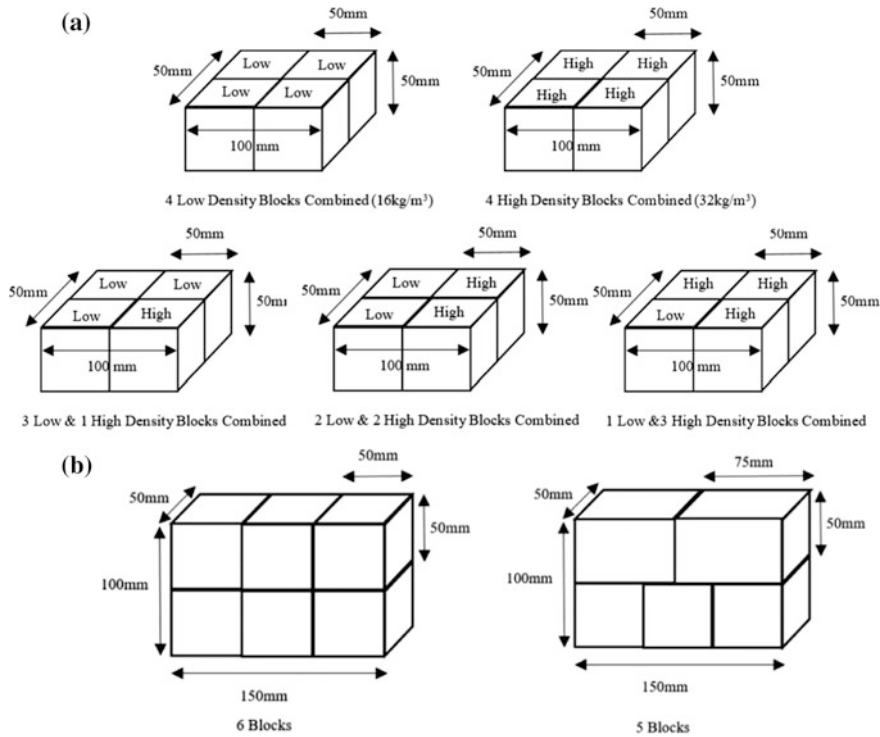


Fig. 3 Prepared samples **a** One layer configuration with 4 samples (Low: 16 kg/m^3 ; High: 32 kg/m^3) **b** Two layer configuration with 5 and 6 samples

tests are smaller than results from the ASTM standard. The densities and properties from D6817 represent the lower bound of acceptable values. Comparison with nominal values for D6817 would show greater difference than represented in Fig. 4b, c.

The images in Figs. 5, 6, and 7 indicate the strain distribution was uniform at the beginning of the loading process. The strain distribution over the face of the test samples started to become non-uniform on loading. Time laps images and video recordings suggest the progressive strain development for the cellular structure of EPS is in crushing normal to the direction of loading rather than inclined shear bands as occur for soils and other rigid materials that fail in shear. As for the uniform density blocks (Fig. 5, 16 kg/m^3 ; and Fig. 6, 32 kg/m^3), the strain distribution for two different density blocks, 16 kg/m^3 on the left and 32 kg/m^3 on the right, also show transition from uniform to non-uniform strain distribution with loading, Fig. 7a, b. The tactile pressure sensors (I-Scan) at the boundary indicated that the higher density EPS supported more load compared with the adjacent lower density block.

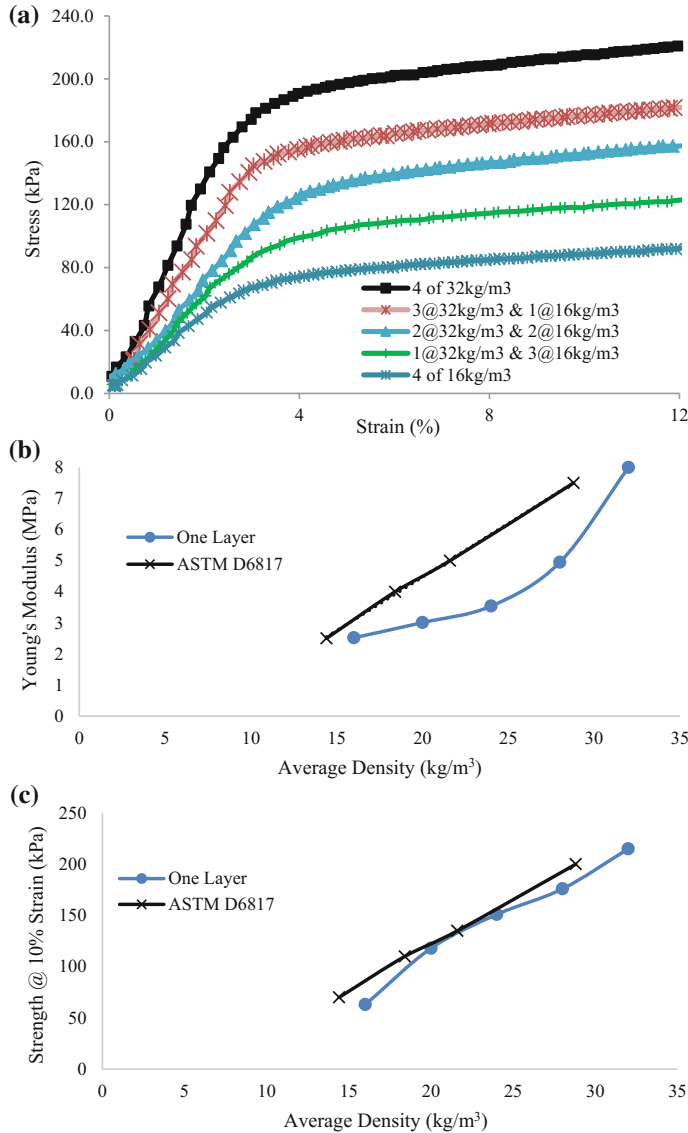


Fig. 4 Young's moduli and strength @ 10% strain VS density results

2.2 Two Layers Tests

Tests on two layers capture upper and lower block interactions at foam to foam interfaces as occur in the field. Progressive differential movements at foam/foam horizontal interfaces were captured by a tripod mounted camera. Subsequently,

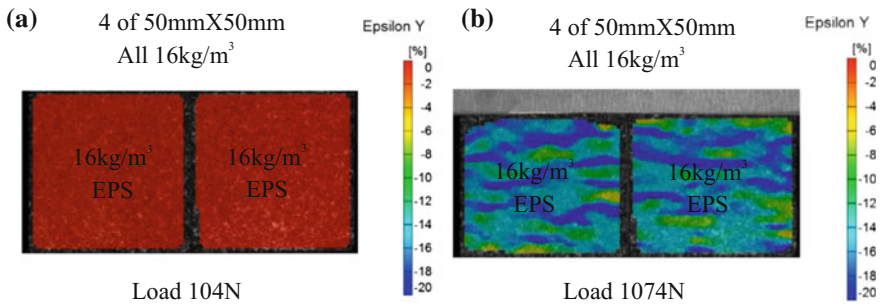


Fig. 5 Images captured at the beginning and end of the loading process for the 100 mm by 50 mm by 100 mm samples with same low density **a** Beginning, **b** End

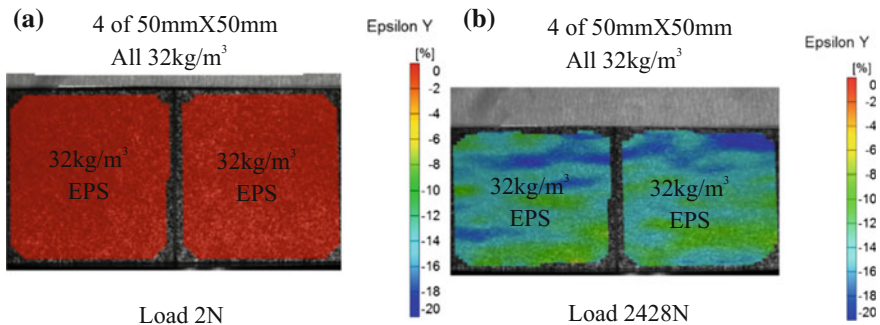


Fig. 6 Images captured at the beginning and end of the loading process for the 100 mm by 50 mm by 100 mm samples with same high density **a** Beginning, **b** End

positions of EPS blocks at particular loading stages were observed and compared with positions of EPS blocks before loading.

Five or six EPS blocks as shown in Fig. 3b in 2 layers with either uniform or mixed densities were tested. The six 50 mm cube blocks were stacked in 2 layers with continuous vertical joints. The five EPS blocks were also stacked in 2 layers but without continuous vertical joints.

The images from the camera shown in Fig. 8 indicate that all samples deformed equally when the densities were the same and the interface between the upper and lower blocks remained horizontal. The deformation of the sample blocks with the same density was uniform before and after loading for cases with or without continuous vertical joints.

Figure 9 presents before and after images of sample blocks with mixed density grades. The mixed density sample sets deformed unevenly. Lower density blocks deformed more than higher density blocks. The initially horizontal interface became uneven after loading. However, the unevenness of the interface between the upper and the lower blocks was less for the tests with five blocks without continuous joints. The six blocks with continuous vertical joints deformed abruptly and unevenly.

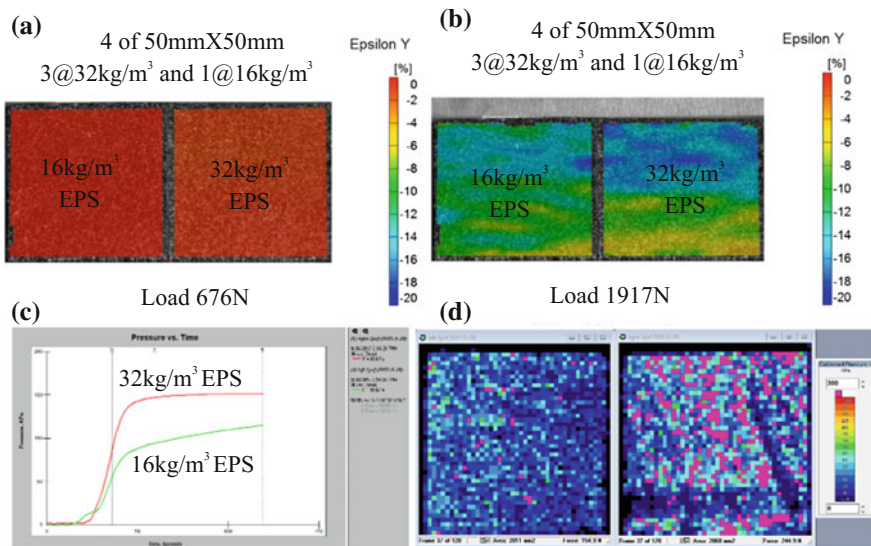


Fig. 7 Images captured at the beginning and end of the loading process for the 100 mm by 50 mm by 100 mm samples with combined 16 & 32 kg/m³ densities **a** Beginning, **b** End; **c** Combined density with I-Scan sensors, **d** Stress distribution (left 55 kPa, right 85 kPa)



Fig. 8 **a** Uniform density stacked in 2 layers with continuous vertical joints, **b** uniform density stacked in 2 layers without continuous vertical joints; before (left) and after (right) loading

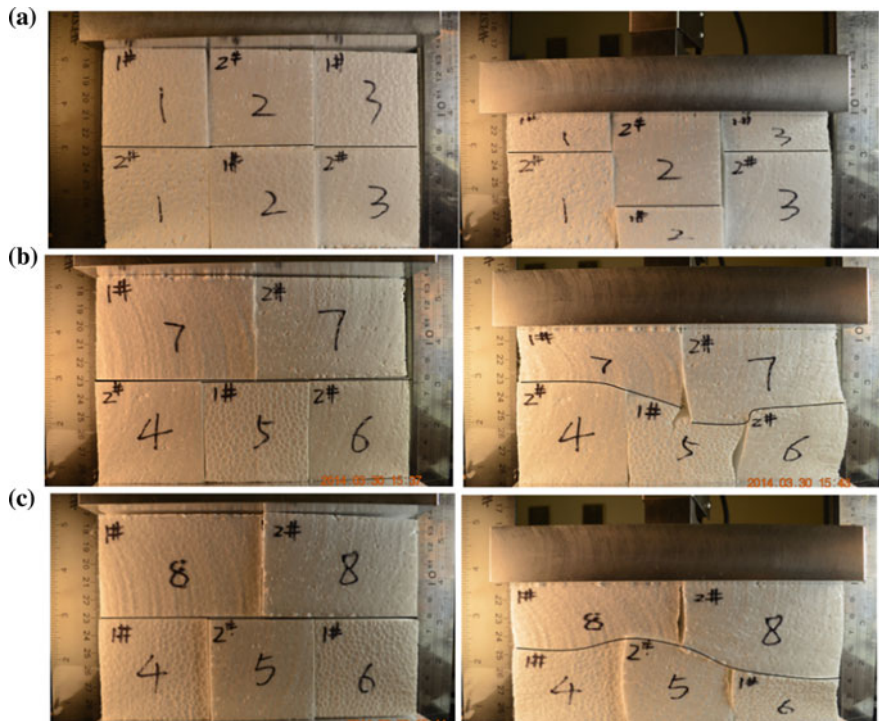


Fig. 9 **a** Mixed densities stacked in 2 layers with continuous vertical joints, **b** mixed densities stacked in 2 layers without continuous vertical joints, **c** mixed densities stacked in 2 layers without continuous vertical joints; before (left) and after (right) loading

The results in Fig. 10 illustrate that EPS blocks with mixed densities have smaller initial moduli than the uniform samples of the same average density. Mixing densities in the field can result in pockets of stress and deformation anomalies. EPS blocks with continuous vertical joints developed relatively lower Young's moduli and strengths at 10% strain compared to the cases without continuous vertical joints. Other than reducing differential settlements, installing EPS blocks with staggered joints also improve the integral strength of the EPS block system.

3 FLAC Modeling

The two layers lab tests were modeled in FLAC [11] to further examine stress and deformation distributions. The lab tests represent unconfined compression between rigid end plates that impose uniform displacement of the top platen interface. Therefore, to simulate the rigid end boundary, a constant velocity is applied at the

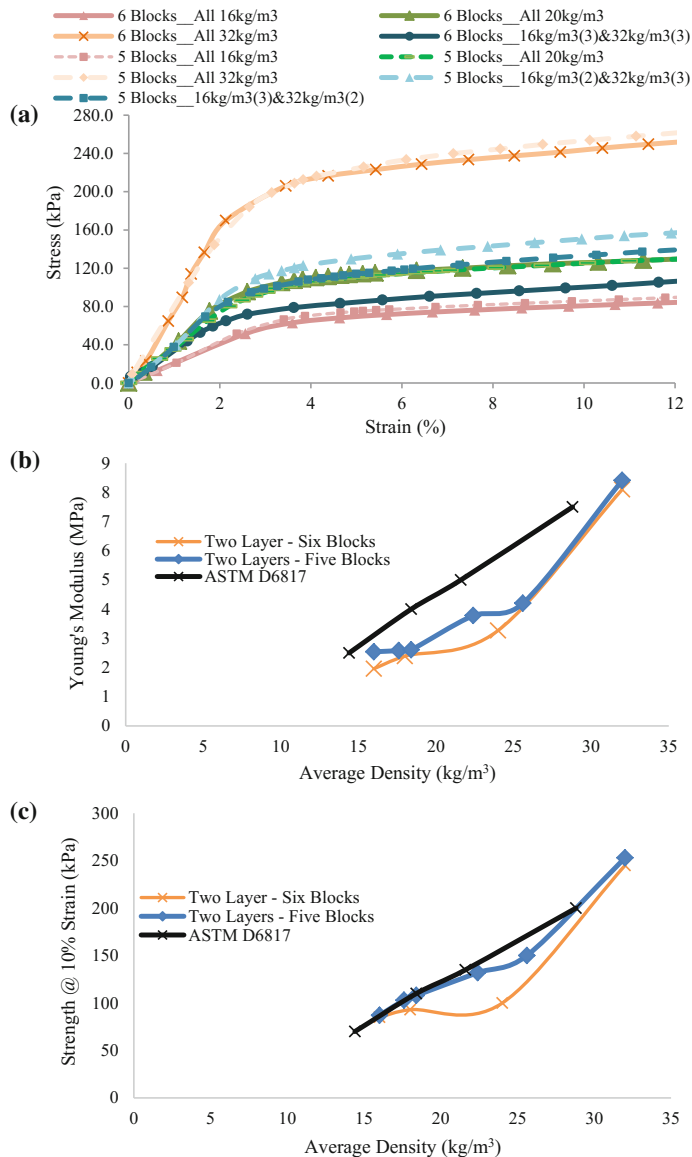


Fig. 10 Young's moduli and strength @ 10% strain results based on different density for various combination

top of the sample and the bottom of the model is fixed. The modeling results for uniform density and multiple density grades are displayed in Figs. 11 and 12 and show the same displacement pattern as the lab test results. Uniform density blocks show relatively uniform deformation after loading for cases with or without continuous joints (Fig. 11). For EPS blocks with multiple density grades (Fig. 12),

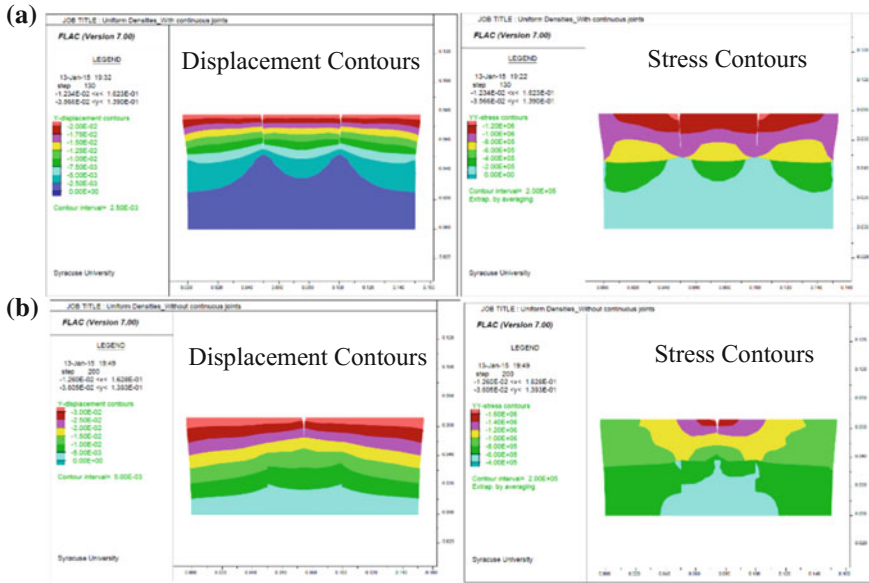


Fig. 11 Modeling result of uniform density blocks for rigid boundary condition **a** with continuous joints, **b** without continuous joints

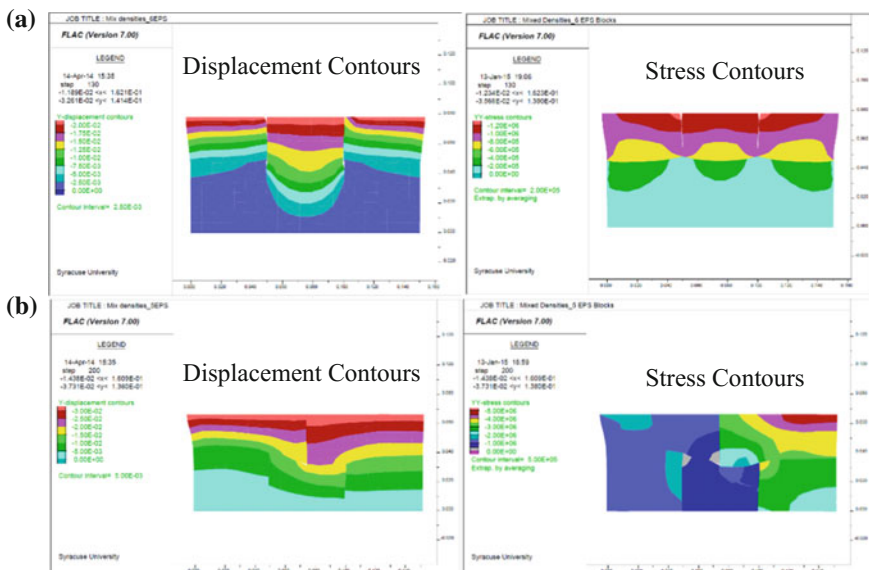


Fig. 12 Modeling result of mixed density blocks for rigid boundary condition **a** with continuous joints, **b** without continuous joints

differential movements developed for cases with/without continuous joints. Low density blocks developed maximum deformation and distortion at the transition sections. High differential internal pressures that exceeded the average pressure applied at the top boundary developed in dense blocks adjacent to low density blocks. The non-uniformity in density contributed to the development of internal pressures that exceeded allowable levels. The edges of adjacent blocks of different densities deformed unevenly. Installing EPS blocks with mixed densities and with continuous vertical joints resulted in non-uniform stresses, uneven deformations, and internal block damage. The FLAC models simulated the lab test observation reasonably well.

4 Conclusions

Based on the lab test results and FLAC simulations, the following conclusions can be made:

- (1) For tests performed at the same strain rate of 10% per minute, moduli and strength at 10% strain were lower or inferior for mixed density blocks within the same layer than for uniform density blocks.
- (2) As uniform and mixed density blocks were loaded together in uniaxial compression, the un-deformed initial states and deformed final states indicate the deformations were uniaxial and the sample widths remained relatively unchanged.
- (3) Tracking the compression loading states of 16 and 32 kg/m³ EPS combined densities with the I-Scan system at the same deformation (strain) levels, the lower density blocks supported lower loads.
- (4) For uniform densities in 2 layer tests with and without vertical joints, all blocks deformed evenly. The horizontal plane between the upper and lower blocks remained horizontal.
- (5) For mixed densities in 2 layer tests with and without vertical joints, lower density blocks deformed more than the higher density blocks. The initially horizontal plane between upper and lower blocks became uneven.
- (6) The case of intercepted vertical joints (5 blocks) was better (higher moduli and strength at 10% strain) than (6 blocks) with continuous vertical joints.
- (7) The FLAC models simulated the observed interface deformation patterns for uniform and mixed densities with and without continuous vertical joints.

Acknowledgements The authors gratefully acknowledge the assistance of Tekscan staff and Tim Schmidt of ARAMIS. R. Chave, J. Banas and W. Dossert of Syracuse University helped with setting up test equipment and data acquisition systems.

References

1. ASTM D 6817; ASTM D 1621
2. Coleman TA (1974) Polystyrene foam is competitive lightweight fill. Civ Eng 44(2):68–69
3. Frydenlund TE, Aabøe R (1996) Expanded polystyrene—the light solution. In: Proceedings of the international symposium on EPS construction method, Tokyo, Japan, pp 31–46
4. Refsdal G (1972) Short technology note. Norwegian Tech J Bd 119, No. 37
5. Negussey D (2014) Investigation of the Carrs Creek geofoam project, University transportation center—region 2, Research and innovative technology administration. Department of Transportation, USA
6. Elragi A, Negussey D, Kyanka G (2000) Sample size effects on the behavior of EPS geofoam. In: Proceedings of the soft ground technology conference, ASCE geotechnical special publication 112, Noordwijkerhout, The Netherlands
7. Liu C (2015) Stress-strain behavior by image analysis, mix density and pre-strain effects of EPS geofoam, Master's Thesis, Syracuse University, Syracuse, NY
8. Singh S (2016) Pressure reduction on wide culverts with EPS geofoam Backfill, Master's Thesis, Syracuse University, Syracuse, NY
9. Trilion (2007) ARAMIS v 6.1 user manual
10. Tekscan Inc (2017) I-SCAN™ & high-speed i-scan user manual, Tactile force & pressure measurement system version 7.6x
11. Itasca Inc (2011) FLAC (Fast Lagrangian Analysis of Continua) version 7.0 user's guide

Effect of Using EPS Geofoam on Deformation Behavior of Square Footings on Clay Subjected to Static and Dynamic Loads: Experimental Study



M. El. Gendy, I. El. Araby, W. El. Kamash, E. Sallam and A. El. Labban

Abstract The recent and continuous industrial development at Port-Said necessitates many factories and gas plants to be constructed on its thick graduated clay soil. Accordingly, suitable foundation systems are to be developed to resist the expected dynamic effects and vibrations of the heavy machinery and rotating masses utilized for such activities. Expanded Polystyrene (EPS) Geofoam was introduced as an efficient dynamic damper and lightweight solution for many geotechnical problems. In this research, the effect of the static loads in machinery shutdown state and the dynamic loads in working state on the settlement behavior of a square footing resting on Port-Said clay is studied experimentally, both in the presence and absence of EPS. The results showed that the use of EPS can considerably reduce the maximum settlement under machine foundation.

Keywords Machine foundation · EPS · Expanded-Polystyrene geofoam
Dynamic analysis

1 Introduction

Machine foundations require special consideration due to the combination of dynamic and static loads. The suitable foundation is selected, depending on the machine type. Foundations that support the machines are subjected to vibrations caused by machine unbalanced forces. The amplitude of vibration and the natural

M. El. Gendy · I. El. Araby · E. Sallam · A. El. Labban (✉)
Faculty of Engineering, Port Said University, Port Fouad, Egypt
e-mail: ahmedelabban@hotmail.com

W. El. Kamash
Faculty of Engineering, Suez Canal University, Ismailia, Egypt

frequency of a machine foundation soil system are the most important parameters in designing a machine foundation.

Prakash and Puri [1] classified types of machines that generate different periodic forces depending on the operating speed of such machine to three categories: (a) Reciprocating machines, (b) Impact machines, and (c) Rotary machines. The magnitude and characteristics of the operating loads depend on the type, size, speed, and machine layout. Fattah et al. [2] investigated the effect of the foundation geometry, the amplitude and frequency of the dynamic load, and the damping ratio on the structural behaviour of a machine foundation on piles in homogeneous sandy soil. Vlad [3] presented some practical cases of machine foundation vibrations; which were technically evaluated throughout a program of vibration measurements. Then, he illustrated some corrective solutions leading to eliminate those dangerous vibrations. EPS foam was one of those vibration absorbers.

Alzawi [4] presented comprehensive experimental and numerical investigations on the use of in-filled geofoam trench barriers to scatter machine foundations vibration, taking into account all the parameters that adequately describe the vibration screening process. Experimental results confirmed that in-filled geofoam trench barriers can effectively reduce the transmitted vibrations. They also developed an artificial neural network (ANN) model; which is capable to predict the in-filled geofoam wave barrier protective effectiveness in different soil profiles with different geometric dimensions.

Elragi [5] presented a comprehensive review on EPS geofoam and discussed many practical examples of its engineering application. Arellano [6] presents a deformation-based load bearing analysis procedure that utilizes the elastic limit stress to design EPS for roadway embankments. Bartlett [7] used EPS to support highway bridge structures without deep foundations which can accelerate construction on soft compressible soil.

Abdelrahman and Elragi [8] showed, both experimentally and numerically, that the natural weak clay soil underneath the footing might be replaced efficiently by EPS blocks in order to reduce the footing settlement under static loading.

On the other side; EPS subjected to dynamic loading, Athanasopoulos [9] presents an experimental investigation of the dynamic properties of expanded polystyrene (EPS) geofoam materials. Two tests were conducted on EPS block; Torsional resonant column tests and cyclic uniaxial tests. It was found that EPS behaves linearly for strain values of up to 0.1% and nonlinearity for strains greater than 1%. In the same study, EPS density affected the dynamic moduli values while no noticeable effect on damping ratio values was establish. Also, Athanasopoulos [10] executed the experimental investigation of (a) the mechanical behaviour of EPS under both static and dynamic loads and (b) the mechanical behaviour of EPS Geofoam-sand mixture.

The aim of the present investigation is to study the deformation behaviour of a square footing specimen resting on Port-Said clay (in the presence of EPS geofoam as a settlement reducer), when subjected to both monotonic and dynamic loading.

2 Experimental Modeling

The experimental studies in this research were performed in the geotechnical laboratory of the faculty of the engineering at Port-said University.

2.1 Investigated Soil

Soft clay is used for the current experimental investigation. The clay is obtained from pile excavation-photo (1)- at depth 40 m from the new ZOHR gas treatment plant located at the west of Port-said city, as shown in Fig. 1 (Photo 1).

Several laboratory tests were executed to determine the properties of the tested soil.

The average properties of clay used in tests are as follows:

Water content (W_c)	68%
Bulk Unit Weight (γ_b)	16.0 kN/m ³
Shrinkage Limit (S.L)	13.5%
Liquid Limit (L.L)	70.0%
Plastic Limit (P.L)	38.0%
Plasticity Index (P.I)	32.0%

Two specimens were tested under Oedmeter apparatus to measure a soil's consolidation properties. Oedometer tests were performed by applying different loads to a soil sample and measuring the deformation response. The maximum

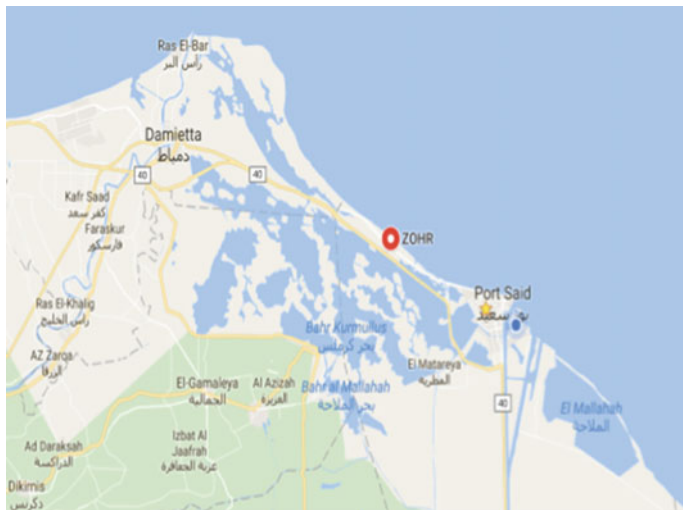


Fig. 1 Location of soil sample extraction

Photo 1 Soil sample extraction at ZOHR plant

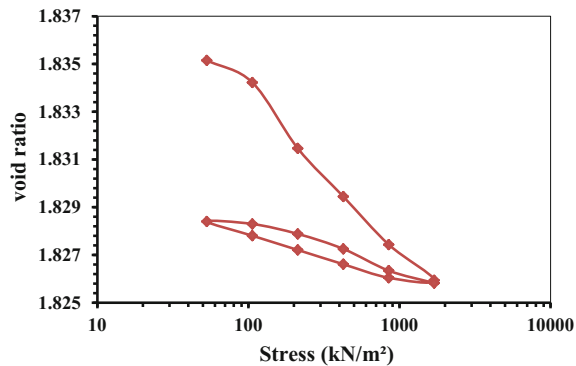


applied stress was 1100 kN/m^2 for all tests. Figure 2 shows the void ratio values with the different stresses which were applied gradually on Oedemeter test.

The compressibility of the clay layers was evaluated in laboratory to calculate the consolidation properties which are as follows:

Average voids ratio (e_o)	1.83
Coefficient of volume compressibility	$2 \text{ cm}^2/\text{kN}$
Coefficient of consolidation (C_v)	$0.179 \text{ m}^2/\text{year}$
Coefficient of permeability (k_z)	$1\text{E}-9 \text{ cm/sec}$
Drained Modulus of Elasticity (E_d)	2130 kN/m^3
Over-consolidation Ratio (OCR)	1.8
Compression Index (C_c)	0.413
Recompression Index (C_r)	0.11

Fig. 2 Variation of void ratio with log stress



2.2 Used Geofoam

In the current study, EPS is serving as settlement reducer and vibration damper with the same area of footing 15×15 cm, thickness 5 cm and density 0.3 kN/m^3 .

2.3 Boundary Tank

Photo 2 shows the reinforcement concrete tank having dimensions of 1.40×1.40 m with 1 m in depth with soil filled till 0.8 m of its height. The wall thickness of the tank is 7 cm to be rigid enough to prevent any lateral side movement during testing under dynamic loads. The inside walls of the tank were covered by linoleum to prevent the absorption of water from the soil and maintain the moisture content as much as possible. The dimensions were sufficient to minimize any effect of dynamic load reflection from tank walls or bottom.

2.4 Foundation and Loading

The footing models were made of $15 \times 15 \times 3$ cm thick steel plates. As shown in Photo 3, the loading frame consists of two parts:

- The first part: is fixed to the four side walls of the square tank and it consists of $7 \times 7 \times 0.2$ cm welded box sections.
- The second part: is movable arm of 90 cm length and $6 \times 6 \times 0.2$ cm box cross-section, mounted at the centerline of the tank.

Photo 2 Boundary tank



Photo 3 Experimental model setup



Two steel plates, one above the other, were welded to the movable vertical arm in order to transmit the applied loads to the center of footing. The first is a 50×30 cm and 0.8 cm thick rectangular plate fixed directly under the motor to generate the dynamic loading, while the second is a 20×20 cm and 0.8 cm thick square plate; which is fixed on 4-legs apart from the motor to apply the static loading. A steel box of 50 cm height is put above the top plate to apply the static loading during simultaneously with the vibrating dynamic load.

The soft clay was consolidated by applying a uniform vertical pressure on the steel plate to bring the soil bearing capacities to 20, 40 and 60 kN/m².

During the vertical consolidation, the settlement of the steel plate was measured by two dial gauges fixed on the top surface of the footing specimen. The dial gauge had a maximum travel of 25 mm and an accuracy of 0.01 mm and it would be reset after each 25 mm.

2.4.1 Static Loading

The weight of the movable part which acts as the static load during all the tests is 0.34 kN. A load of 0.11, 0.56 and 1.01 kN were chosen to act on the first plate to give a pre-stress clay of bearing capacity equal to 20, 40 and 60 kN/m², respectively.

2.4.2 Dynamic Loading

Two motors with different velocities; 1000 and 450 rpm were used to generate the dynamic loading. From elementary dynamics and referring to Florjanic and Frei [8]

a mass m_e connected to a motor shaft with an arm of y rotating at a circular frequency of ω produces a force at any instant in time of F_m .

$$F_m = U \cdot \omega^2 \quad (1)$$

where:

U is the unbalance force = $m_e \cdot y$

ω is the circular operating frequency of the motor, ($\omega = 2\pi f$)

f is the operating frequency.

In this study, the rotating mass was changed with the different motors velocity to get the same dynamic force. Thus, the only variable is the circular operating frequency of the motor. The rotating mass is equal to 0.65 and 3.2 N for the motor frequency 1000 and 450 rpm; respectively, effect on the same distance in the two cases which equal 7 cm from the center of motor shaft. According to Eq. (1), the generated dynamic forces are 0.05 kN.

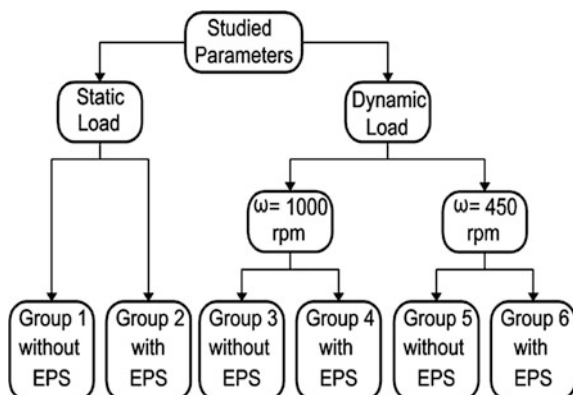
3 Studied Parameters

In this study, Eighteen case studies have been tested in the laboratory to investigate the settlement response of footing resting on Port-said medium soft clay. The main features of the study for experimental model are shown in Fig. 3 and divided to main six groups.

Each group has three case studies according to the subjected stress 20, 40 and 60 kN/m², forming eighteen cases.

In case of static loads, load of 0.11, 0.56 and 1.01 kN was chosen to give a pre-stress clay of bearing capacity equal to 20, 40 and 60 kN/m², respectively. Under dynamic loads, and after minus the value of dynamic force, load of 0.06, 0.51 and 0.96 kN was chosen to get the above stresses.

Fig. 3 Classification of parametric study



4 Testing Procedure

The following work sequence is applied to configure the testing model.

- The clay used in this study is saturated medium soft clay obtained from the result of excavation during pile works at Zohr project; the new gas plant at west of Port-said city.
- The clay is stored at the soil laboratory in wooden box covered from all the sides by linoleum and also during the test to keep their water content unchanged.
- The tank is filled with clay in layers to reach the total required height of 80 cm. After each group, the half of clay layers is changed and rechecked water content (W_c) to ensure that changes in W_c didn't exceed $\pm 5\%$.
- After reaching the top of clay level (80 cm), the final soil surface is carefully leveled.
- The footing is carefully placed on the tank centerline, two dial gauge are fixed on the top of footing, then the vertical load is applied.
- In case of using EPS; (Group 2, 4 and 6), EPS is placed at the same level of clay under the footing with the same dimension 15×15 cm.
- The loading is applied by increments for each group resulting contact pressure ranging from 20 to 60 kN/m². Each load step on the footing is kept for around two days in all the cases.

Photos 4 and 5 shows the experimental model during and after subjected to loading.

Photo 4 Experimental model during loading



Photo 5 Soil settlement after loading



5 Test Results

5.1 Behavior of Clay Under Static Load (Groups 1, 2)

Static loads included two models, denoted as group 1 without using EPS and group 2 with utilizing EPS. As described in Table 1, the partial settlement was measured under applied pressure 0.2 and 40 kN/m² after 2 days for each, while that final settlement was measured after six days (8640 min) under applied pressure 60 kN/m². The measured settlements for the three cases for group 1 ranged between 4 and 29 mm, while for the same pressures but with utilizing EPS (group 2) ranged between 0.6 and 8.6 mm. It is clear that the existence of EPS has a noticeable effect in reducing the measured settlements for different applied pressures.

In this case, reductions in the total settlements was about 70% and giving the highest reduction in the total settlements of all the studied groups.

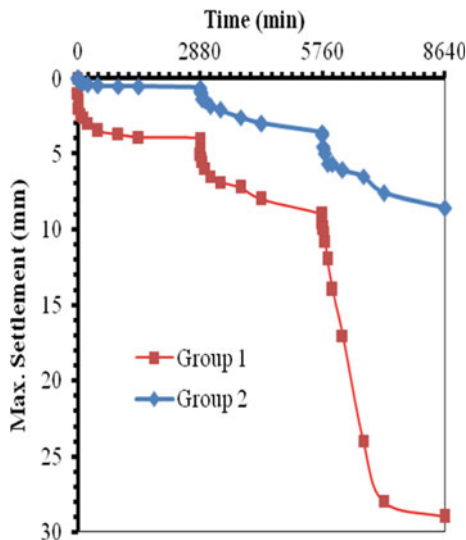
Figure 4 shows time-settlement curve for the cases of static loads for six days loading period.

5.2 Behavior of Clay Under Dynamic Load with $\omega = 1000$ Rpm (Groups 3, 4)

Dynamic loads with angular frequency (ω) = 1000 rpm included two models, denoted as group 3 without using EPS and group 4 with utilizing EPS. The recorded maximum settlements for group 3 are shown in Table 2 ranged between

Table 1 Maximum deformation subjected to static load

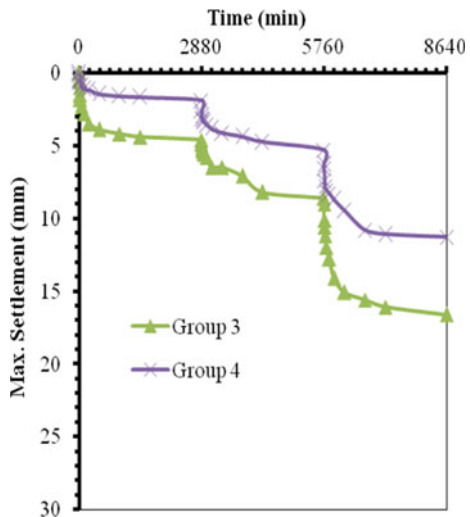
Applied pressure (kN/m ²)	Max. deformation (mm)		Decrease percentage (%)
	Group 1	Group 2	
20	4	0.6	85.0
40	9	3.6	60.0
60	29	8.6	70.3

**Fig. 4** Time-settlement curve for the cases of static loads**Table 2** Maximum deformation subjected to dynamic loads with $\omega = 1000$ rpm

Applied pressure (kN/m ²)	Max. deformation (mm)		Decrease percentage (%)
	Group 3	Group 4	
20	4.6	1.9	58.7
40	8.6	5.3	38.4
60	16.6	11.3	31.9

4.6 and 16.6 mm, giving reductions in the settlements values ranging between 58.7 and 31.9% in case of using EPS. Figure 5 also shows a settlement rate with time for groups 3, 4.

Fig. 5 Time-settlement curve for the cases of dynamic loads with $\omega = 1000$ rpm



5.3 Behavior of Clay Under Dynamic Load with $\omega = 450$ Rpm (Groups 5,6)

Dynamic loads with $\omega = 450$ rpm included two models, denoted as group 5 without using EPS and group 6 with utilizing EPS. The Time-settlement curve for groups 5 and 6 is shown in Fig. 6. The figure shows a relatively decreasing in settlement value when using EPS under all the applied stress stages except for the last loading step. The recorded maximum settlements for groups 5 and 6 are shown in Table 3 ranged between 6 and 14.5 mm, giving low reductions in the settlements values 16.7 and 4% in case of using EPS at stresses values 20 and 40 kN/m², respectively, giving the lowest reduction in the total settlements of all the studied groups.

At applied pressure 60 kN/m², EPS didn't decrease the settlement value, but increase by 21.4%. In this case, it can say that large amplitude oscillations was produced due to the resonant frequencies. This phenomenon occurred when the frequency of the motor matches the system's natural frequency. At resonant frequencies, small periodic driving forces have the ability to produce large amplitude oscillations, due to the storage of vibrational energy. Thus, we can conclude that increasing the value of the deformation in this case, despite of utilizing EPS, is due to the resonance.

Figures 7, 8 and 9 shows a settlement rate with the time at applied stresses 20, 40 and 60 kN/m² after 2, 4 and 6 days, respectively. Furthermore, Fig. 10 shows accumulation Time-Settlement curve of all groups under all different applied stresses

Figures 11, 12 and 13 shows the variation of the measured settlement at the end of each loading step with the applied pressure for all the cases. Test results showed a steep increase in settlements with increasing applied pressure. It is clear that the decreasing rate of settlements in the applied pressure over 40 kN/m² at the most cases.

Fig. 6 Time-settlement curve for the cases of dynamic loads with $\omega = 50$ rpm

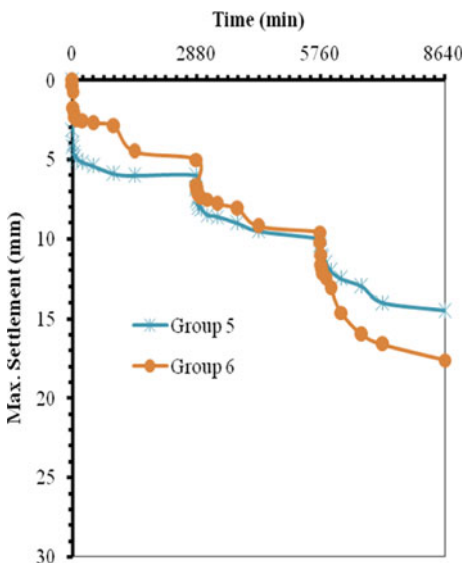
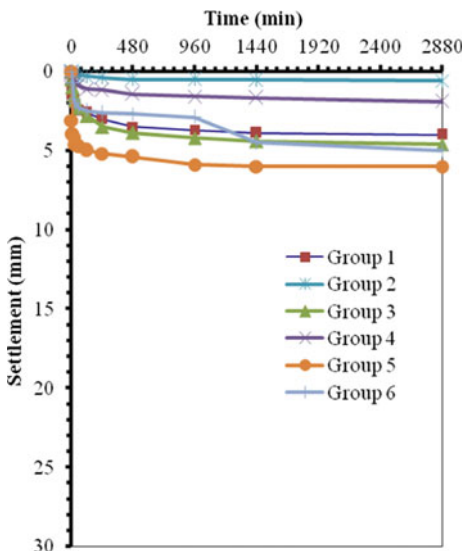


Table 3 Maximum deformation subjected to dynamic loads with $\omega = 450$ rpm

Applied pressure (kN/m ²)	Max. deformation (mm)		Decrease percentage (%)
	Group 5	Group 6	
20	6	5	16.7
40	10	9.6	4.0
60	14.5	17.6	-21.4

Fig. 7 Time-Settlement curve of all groups under stress 20 kN/m²



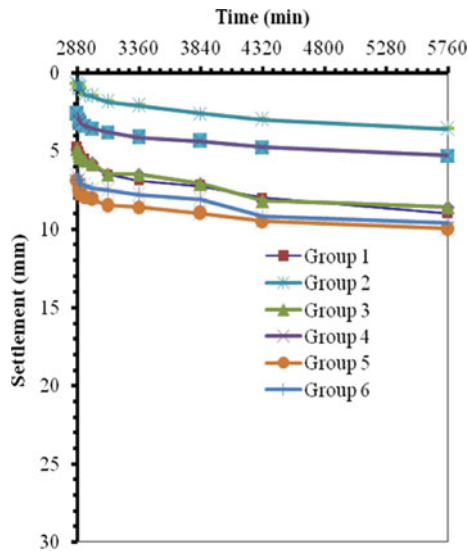


Fig. 8 Time-Settlement Curve of all groups under stress 40 kN/m^2

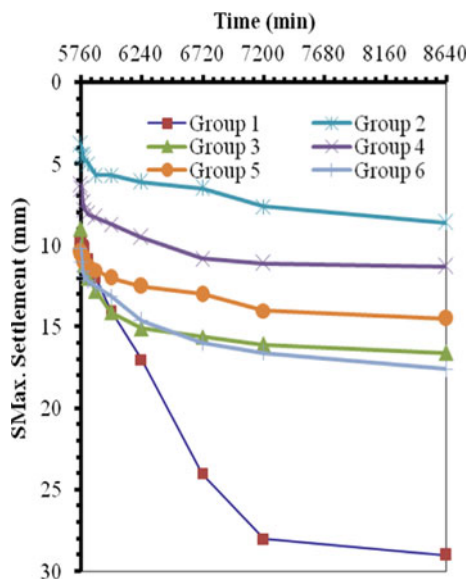


Fig. 9 Time-Settlement Curve of all groups under stress 60 kN/m^2

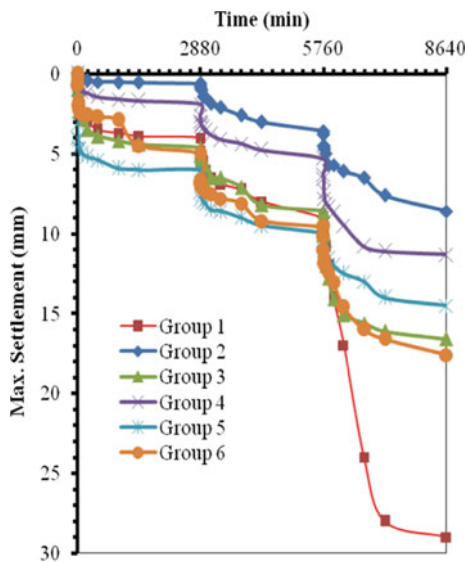


Fig. 10 Time-settlement curve of all groups

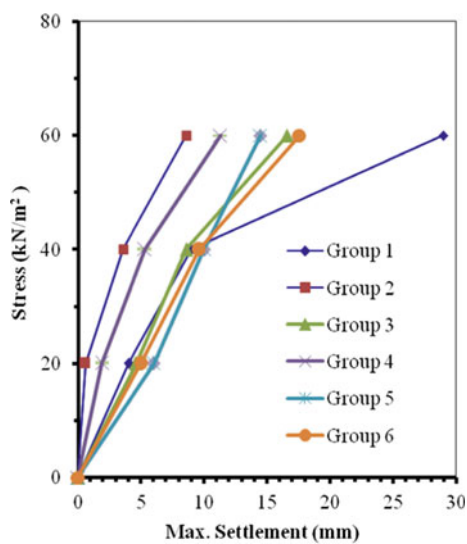


Fig. 11 Applied stress—Max. settlement curve all groups under all applied stresses

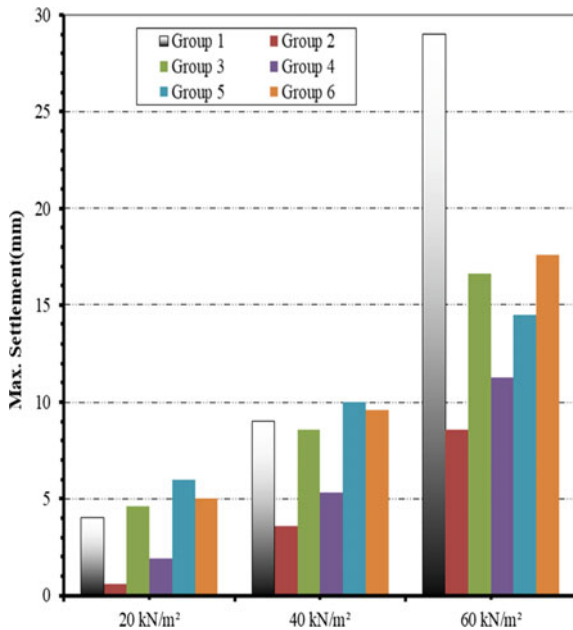


Fig. 12 Max. settlement for all groups under different applied pressure

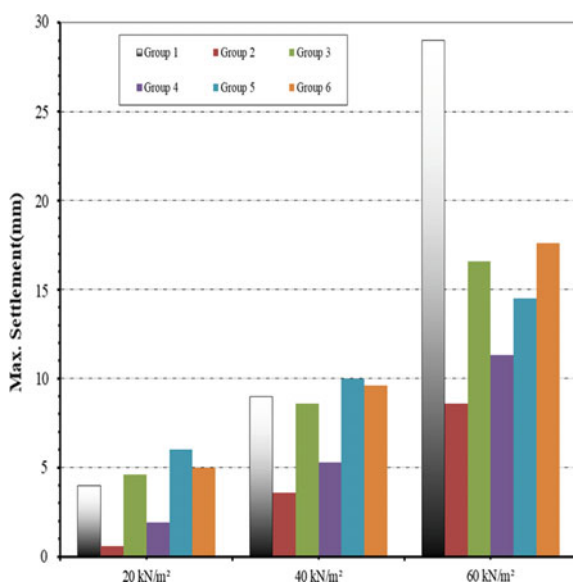


Fig. 13 Max. settlement curve at all stresses

6 Conclusions

This paper presents an experimental study for deformation properties for footing resting on saturated medium soft clay and subjected to both static and dynamic loading. The aim of the study is to highlight the effect of utilizing Expanded Polystyrene Geofoam as settlement reducer. The experimental work was divided into six groups with total eighteen different case studies depending on the applied pressure at each group.

Based on the results of this study, the following may be concluded:

1. Static loads cases gave the highest settlement reductions when using EPS. In this case, about 70% reductions in the total settlements were recorded.
2. The circular operating frequency of the dynamic loads affects the settlement value, whereas the lower value of circular operating frequency gave higher settlement especially at earlier loading stages.
3. Under dynamic loading, the utilization of EPS as a replacement layer for medium soft clay would be considerably beneficial, especially at higher circular operating frequency. The resulting reductions in the total settlement will allow for higher design loads.

References

1. Prakash S, Puri VK (2006) Foundation for vibrating machine, Special Issue, April–May 2006. J Struct Eng SERC, Madras. INDIA
2. Fattah MY, Hamood M, Al-Naqdi IAA (2015) Finite element analysis of a piled machine foundation. Struct Build. Article Struct Build
3. Alzawi AMA (2011) Vibration isolation using in-filled geofoam trench barriers. Electronic Thesis and Dissertation Repository. Paper 265
4. Elragi AF (2006) Selected engineering properties and applications of eps geofoam. Dissertation, Softoria
5. Arellano D, Stark TD (2011) Load bearing analysis of EPS-block geofoamembankments. In: Proceedings of 8th international conference on the bearing capacity of roads, railways and airfields, Champaign, IL, pp 981–990
6. Bartlett S, Arellano D, Vaslestad J Bridge foundations supported by EPS geofoam embankments on soft soil
7. Abdelrahman GE, Elragi AF (2006) Behaviour improvement of footing on soft clay utilizing geofoam. In: The 10th arab structural engineering conference, Kuwait
8. Florjanic S, Frei A (1995) Dynamic loading on pumps. In: Proceedings of the tenth international pump
9. Athanasopoulos GA, Pelekis PC, Xenaki VC (1999) Dynamic properties of EPS geofoam: an experimental investigation. Geosythe Int 6(3):171–194
10. Athanasopoulos, GA, Xenaki VC (2011) Experimental investigation of themechanical behavior of EPS geofoam under static and dynamic/cyclic loading. In: 4th international conferences on geofoam blocks in construction application (EPS 2011 Norway)

Mechanical Properties of EPS Geofoam Under Various Loading Conditions



Vinil Kumar Gade and Satyanarayana Murty Dasaka

Abstract This study presents experimental studies on EPS geofoam using cyclic uniaxial compression (CUC), accelerated creep and pseudo-long-term tests. For all experiments 100 mm cube geofoam samples of 15 kg/m³ density (EPS15) are used. Servo-hydraulic actuator and temperature regulated water chamber (TRWC) are used. CUC tests are performed at two loading frequencies 0.5 and 3 Hz, *R* values of 0.4, 0.6, 0.8, 1 and 1.2 and 5000 loading cycles. Term ‘*R*’ defined as ratio of combined axial static and cyclic stress component to the yield strength of geofoam. To understand creep behavior of geofoam Time temperature stress superposition (TTSS) accelerated creep testing method is adopted. Master creep curve is developed for a designed strength of 20% compressive strength (σ_c) and reference temperature of 29 °C. From CUC tests it is observed that effect of number of cycles is insignificant on secant modulus (E_{dyn}) compared to *R* and loading frequencies. Also, Poisson’s ratio (ν) is observed to vary from positive to negative, and it majorly depends on *R* values and number of cycles. From TTSS method 2.12% compressive creep (CC) strain is observed at 100 years for EPS15 geofoam. Pseudo-long-term tests are performed at various CC intervals and it is noted that Young’s modulus (*E*) decreases with increase in CC. *E*, compressive strength and yield strength of CC sustained samples are decreased from that of initial or non-CC sustained samples. Moreover, Young’s modulus of geofoam reduces with time.

Keywords Young’s modulus · Poisson’s ratio · Compressive creep CUC · TTSS

V. K. Gade · S. M. Dasaka (✉)
Indian Institute of Technology Bombay, Mumbai, India
e-mail: dasaka@civil.iitb.ac.in

V. K. Gade
e-mail: gadevinilkumar23@gmail.com

1 Introduction

In view of improving the serviceability and economize the cost of different civil engineering structures and also to reduce the usage of natural resources various types of geosynthetic materials, such as geogrids, geotextiles, geomembranes, geofoam, etc. are extensively used to serve specific applications. Among the above, geofoam is only a three dimensional material, with considerable thickness compared to its length and width, which is introduced by Horvath [1] to geosynthetic group. Geofoam comprised of closed cells (also known as beads) which are enlarged by using a blowing agent (gas) to a required density and makes cellular structure. EPS geofoam had been widely used in various civil engineering applications like thermal insulation, lightweight fill, compressible inclusion and small amplitude wave damping [1–8]. Geofoam density is nearly 100 times lower than the soil, but its Young's modulus is only 10 times lower than soil. With low density and higher stiffness, it can be effectively used in many applications, such as light weight backfill, embankment over soft soils to reduce overburden pressure, etc. Recently, geofoam has been used for reducing the earth pressure on retaining wall [4, 6, 9], buried pipes [10] and to reduce swelling pressure in expansive soils [5]. Short and long-term properties of geofoam and its behavior must be thoroughly studied to augment its use in various infrastructure projects, to effectively reduce cost and time of construction. In the present study, short and long-term geofoam behavior under different loading conditions has been performed. The experimental program adopted and the relevant results are discussed briefly in this paper.

2 Experimental Program

Series of laboratory tests viz., static and cyclic uniaxial compression (CUC) tests, accelerated creep and Pseudo-long-term tests were conducted on EPS geofoam samples in the study to evaluate their short- and long-term mechanical properties. EPS geofoam samples were procured from Thermoshell Industries, Mumbai, India. Cube specimens with 100 mm each side in size of 15 kg/m³ (EPS15) density EPS geofoam samples was used. Servo-hydraulic actuator was used in the study to apply various loads on the geofoam samples according to type of test. A temperature regulated water chamber (TRWC) setup [11] was used in accelerated creep tests on geofoam samples. Schematic view of uniaxial compression and stress controlled CUC experimental set-up is shown in Fig. 1. Pictorial view of TRWC along with accelerated creep testing set-up is shown in Fig. 2. Two linear variable displacement transducers (LVDTs) were used to measure lateral deformation of geofoam samples at their mid-height during both uniaxial compression and CUC tests. At the end of LVDT's small fixture of 10 mm × 10 mm × 2 mm is attached to reduce stress concentration of geofoam sample surface as shown in Fig. 1. Static uniaxial compression and cyclic uniaxial compression (CUC) tests are conducted to understand geofoam behavior subjected to static and cyclic loading. Uniaxial tests

Fig. 1 Pictorial view of Static and CUC tests configuration

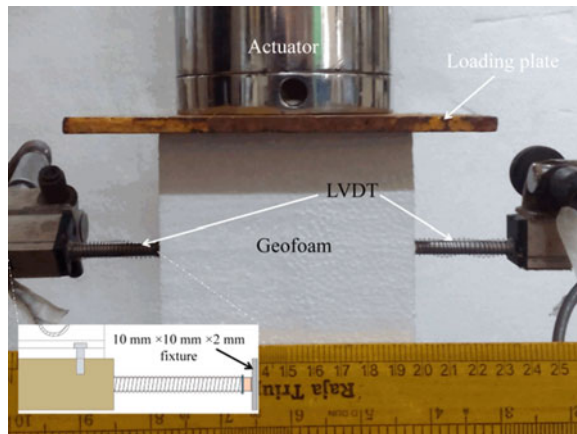
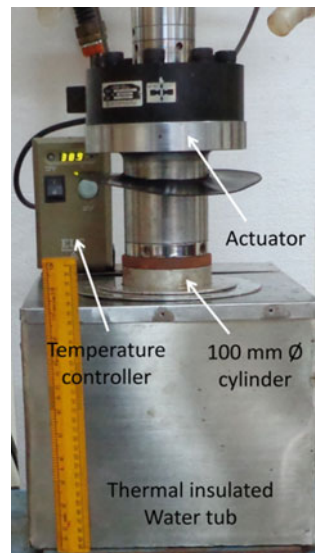
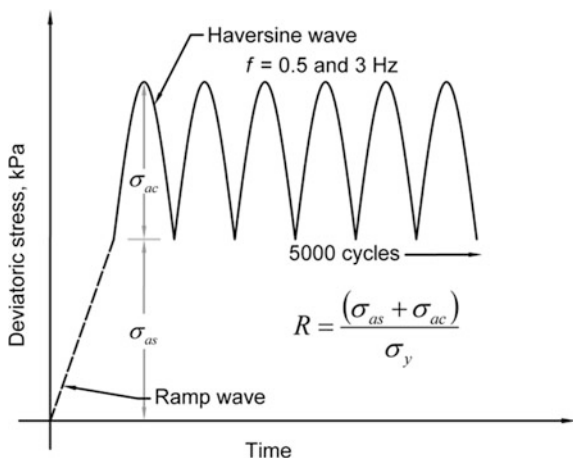


Fig. 2 Pictorial view of TRWC



are performed in accordance with Stark et al. [12] and ASTM D1621 [13] and used recommended a strain rate of 10%/minute in the present study. Stress controlled CUC tests were performed at two different loading frequencies (f) viz., 0.5 and 3 Hz, for 5000 number of loading cycles, and using different yield strength factor (R), in the range of 0.4–1.2 (at 0.2 intervals), where factor ' R ' is defined as ratio of combined static and cyclic deviatoric stress component to the yield strength of geofoam. To maintain the vertical stress always in compression mode, ratio of deviatoric cyclic stress (σ_{ac}) and static stress (σ_{as}) was maintained as 0.85 for all CUC tests in the present study [14]. Schematic representation of CUC testing procedure and definition of R value were shown in Fig. 3. All measurements from

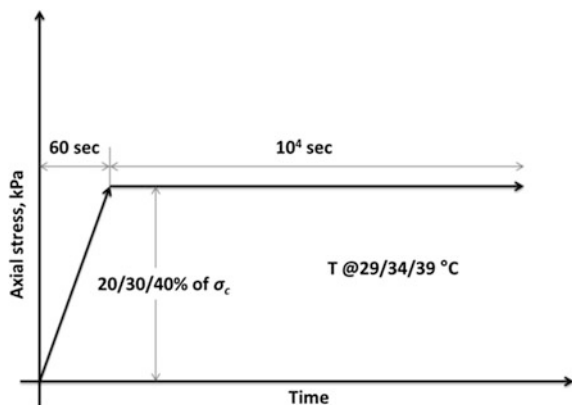
Fig. 3 Schematic representation of CUC test procedure



the tests except CUC tests were recorded at 10 Hz (0.1 s) intervals and 100 data points were logged for each cycle in CUC tests.

To determine long-term behavior of geofoam one of the widely used accelerated creep testing method is time temperature stress superposition (TTSS) and also pseudo-long-term tests were conducted on geofoam samples in the present study. TTSS method testing procedure adopted in the study was similar to the studies of Yeo [15] and Yeo and Hsuan [16]. The TTSS accelerated creep testing method generates creep behavior for a longer duration of any material by conducting a series of short duration tests on a desired material. Two parameters in TTSS method viz., reference temperature and stress need be selected prior to testing. Reference temperature and stresses are represents the temperature at which material is exposed in application and the design strength of material. Next step after choosing the reference temperature and stress values of geofoam, is to select elevated temperature and stress intervals. In the past, 20–50% of σ_c as reference stress values adopted in TTSS method to evaluate creep behavior of geofoam [16–19]. Based on the available literature, design strength of geofoam was considered in the present study as 20% σ_c . A reference temperature of 29 °C was considered in the present study, as average laboratory temperature in any season varies in the range of 28 ± 2 °C. As stated above that elevated temperature and stress levels are required to perform TTSS tests, it is necessary to choose regular intervals of compressive stress amplitude and temperature [16, 19]. In line with above 10 kPa and 5 °C were selected as incremental stress and temperature in the present study respectively. Stress amplitudes and temperature intervals selected in the study were 20, 30 and 40% σ_c , and 29, 34 and 39 °C, respectively. Prior to applying sustained compressive load, geofoam samples were placed in the TRWC for 3 h at desired temperature. Afterwards, sustained compressive load corresponding to required stress value (20 or 30 or 40% of σ_c) was applied on the geofoam samples and maintained it for 10,000 s. Throughout the testing of samples, temperature and stress amplitude were maintained constant. Schematic representation of TTSS test procedure is shown in Fig. 4.

Fig. 4 Axial stress-strain behavior of EPS15 geofoam



3 Results and Discussion

Static uniaxial compression tests were performed on five identical samples of EPS15 geofoam, typical stress strain response of EPS15 geofoam was shown in Fig. 5. Mechanical properties of geofoam evaluated from compression tests were graphically described in Fig. 5. Young's modulus (E) reported from the compression test was calculated from the initial tangent of the stress-strain curve. Compressive strength (σ_c) of geofoam was defined as axial (or deviatoric) stress corresponding to 10% axial strain. Yield strength (σ_y) of geofoam corresponds to intersection point of initial and back tangents obtained from the stress-strain curve. Average values from uniaxial compression tests on five identical EPS15 geofoam samples are reported here viz., Young's modulus (E) is 3.03 MPa, compressive strength (σ_c) is 66.5 kPa and yield strength (σ_y) is 55 kPa.

For comparison stress-strain behavior of EPS15 geofoam obtained from the present study is complied with Duskov [20], Ossa and Romo [21] and Awol [17], as shown in Fig. 5. Trend of EPS15 stress-strain behavior observed from the present study is matches well with that of other researchers. But there are significant differences in properties of geofoam, and the differences may be due to different strain rates, non-uniformity and spatial variation within the samples, if any.

For each combination of loading frequency and R values in CUC tests three identical samples of EPS15 geofoam were performed and their average properties values were reported. Secant modulus (E_{dyn}) and damping ratio properties of EPS geofoam from CUC tests were evaluated based on the method suggested by Athanasopoulos et al. [22] and ASTM D3999-91 [23]. Effect of number of cycles, R values and loading frequency on secant modulus (E_{dyn}) and cyclic axial strain of EPS15 geofoam were shown in Figs. 6 and 7 respectively. It was observed that, irrespective of loading frequency and number of loading cycles, secant modulus (E_{dyn}) and cyclic axial strain of geofoam were decreasing and increasing respectively with increase in R values. Also, it was observed that for R values less than or equal to 0.6 cyclic axial strain is constant irrespective of number of loading cycles. For

Fig. 5 Axial stress-strain behavior of EPS15 geofoam

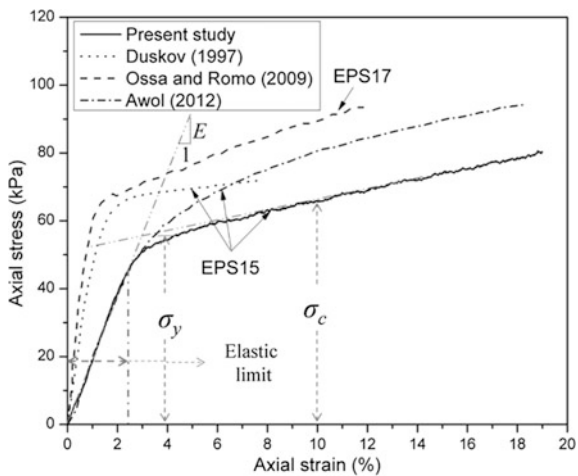
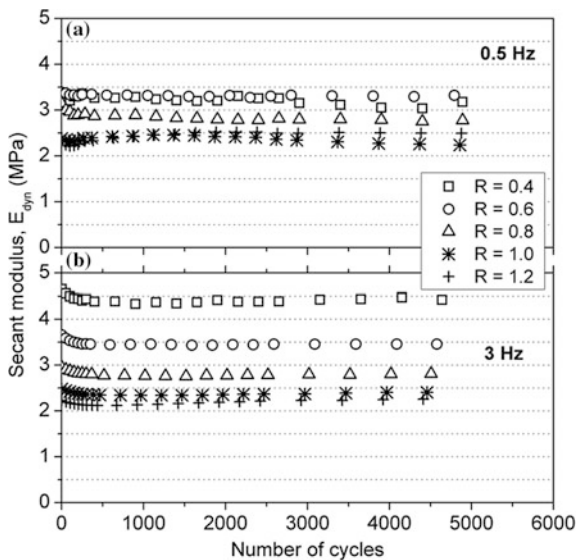


Fig. 6 Effect of number of cycles, R value and loading frequency **a** 0.5 Hz and **b** 3 Hz on secant modulus of EPS15 geofoam



R values more than 0.6, cyclic axial strain of geofoam continuously increases with increasing number of loading cycles. Effect of cyclic axial strain on secant modulus and damping ratio of EPS15 geofoam were shown in Fig. 8. It was observed that, secant modulus and damping ratio were decreasing and increasing with increase in cyclic axial strain respectively.

From both static uniaxial compression and CUC tests lateral deformation of geofoam samples measured along with axial deformation and evaluated Poisson's ratio for all samples. Effect of axial and cyclic axial strain on Poisson's ratio of EPS15 geofoam is shown in Fig. 9. It was observed irrespective of loading type

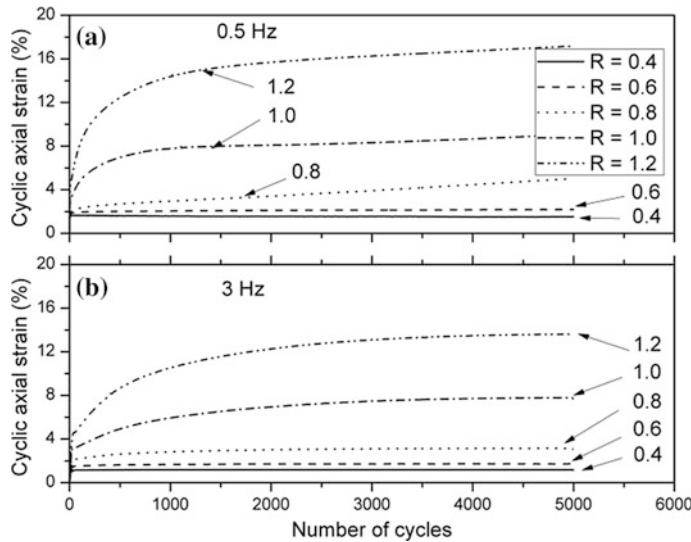


Fig. 7 Effect of number of cycles on cyclic axial strain of EPS15 geofoam **a** 0.5 Hz and **b** 3 Hz

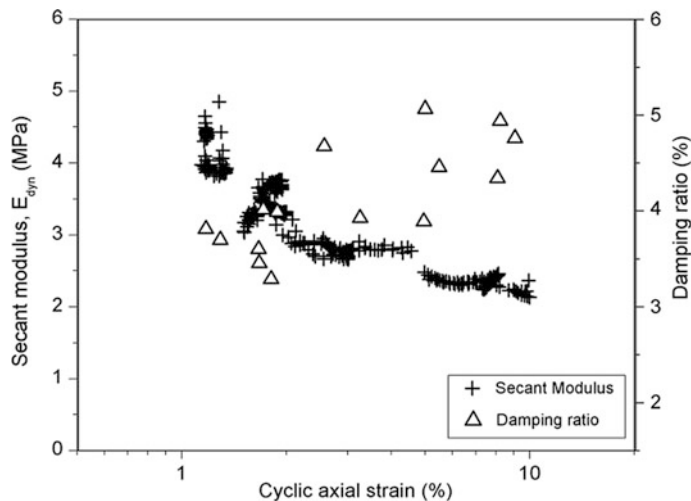


Fig. 8 Effect of cyclic axial strain on secant modulus and damping ratio

Poisson's ratio of geofoam decreasing with increase in axial or cyclic axial strain. Wide range of Poisson's ratio values from positive to negative were observed with respect to axial and cyclic strain values. Whereas in literature majority of the researchers were adopted Poisson's ratio values based on density dependent equation developed by Horvath [24]. Poisson's ratio from static tests was reached

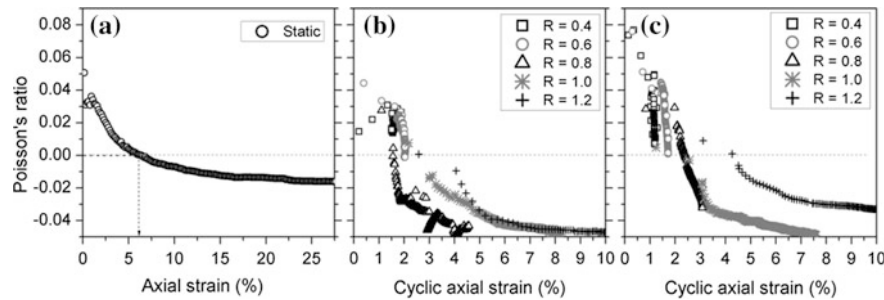


Fig. 9 Poisson's ratio of EPS15 from **a** static and CUC tests **b** 0.5 Hz and **c** 3 Hz

zero value at 6% axial strain as shown in Fig. 9a. Positive Poisson's ratio values of geofoam were observed for low R (≤ 0.6) values from CUC tests as shown in Fig. 9b, c. Maximum, average and minimum Poisson's ratio values of EPS15 from both static and CUC tests are 0.077, −0.031 and −0.057 respectively for a 0–10% of axial and cyclic strain range. As average and minimum values of EPS15 geofoam were continuously decreasing with increase in axial strain, so above mentioned average and minimum values are valid only for 0–10% axial strain range, if any change in the axial strain range their average and minimum Poisson's ratio values were also change accordingly.

All materials used in civil engineering structures and their properties must be known to ensure serviceability of the structures over the design period (~100 years). Long-term behavior of material is mainly depends on the percentage of creep developed with time. By using TTSS method long-term behavior of EPS15 geofoam compressive creep (CC) strains with time can be obtained. Compressive stresses of EPS15 geofoam corresponding to 20% of σ_c is 13.8 kPa and the respective axial strain from stress-strain curve (from Fig. 5) is 0.98% and it is less than 1% axial strain, and adopted stress level is in accordance with guidelines given by Horvath [25]. Geofoam sample were tested at different combinations of temperature and stress intervals, as stated in the previous section. Initial creep axial strain-time response of geofoam samples subjected to different combination of stress and temperatures according to TTSS method were shown in Fig. 10a. For developing the master creep curve for long duration (~100 years) from initial/short duration creep curves, method described by Yeo [15] was adopted in the present study. Developed master compressive creep curve for EPS15 geofoam is shown in Fig. 10b. It was observed that obtained master curve is more than 100 years duration and 2.12% creep strain is noted at 100 years duration. Compressive creep strain of EPS15 geofoam is compared with creep curves of EPS20 geofoam reported by Yeo [15] and field observations from Bartlett et al. [26] as shown in Fig. 10b. As per Authors knowledge, none of the earlier studies were reported EPS15 geofoam creep behavior due to which in the present study results were compared with available creep behavior of EPS20 geofoam. Trend of creep strain with time from present study is matches with Yeo [15] but higher creep strain

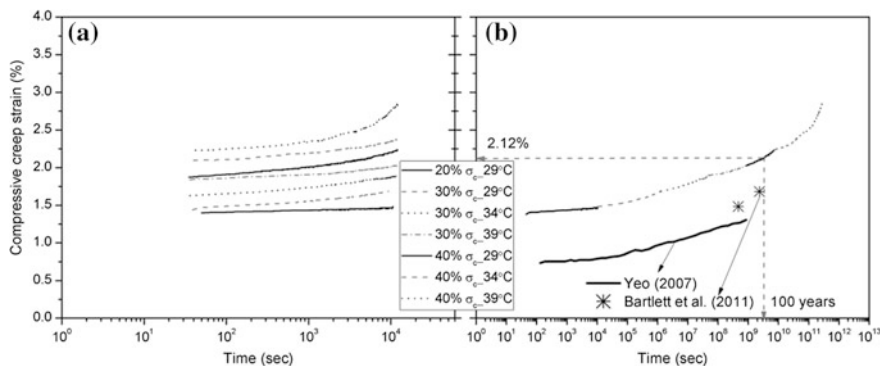


Fig. 10 TTSS results of EPS15 geofoam **a** test data **b** master curve

values were observed in the present study. Observed differences between the present study and previous studies compressive creep strains are may be due to difference in the density of geofoam, adopted method of temperature controlling equipment and manufacturing process.

To predict the long-term behavior of structures involving geofoam their properties E , σ_c and σ_y are also need to be evaluated along with creep strain under long-term sustained loading conditions. In the past none of researchers reported long-term studies on geofoam. In the present study, pseudo-long-term tests were performed at different values of compressive creep (CC) strain on geofoam at room temperature ($29 \pm 1^\circ\text{C}$). This test procedure is divided into four parts, viz. (i) desired CC is applied on geofoam samples within 60 s using servo-hydraulic actuator; (ii) applied CC is maintained for 3 h, in line with accelerated TTSS method; (iii) removal of loading from geofoam sample; and (iv) CC sustained geofoam samples are subjected to 10%/minute strain rate uniaxial compression tests. Schematic view of pseudo-long-term tests on geofoam samples adopted in the study was shown in Fig. 11a.

Pseudo-long-term tests were performed at different compressive creep (CC) strain values, viz., 1.5, 2, 2.5, 3 and 4% and these values were within the range of compressive creep strains obtained from TTSS method. From compressive creep strain sustained static tests on three identical geofoam samples at each compressive creep strain, E , σ_c and σ_y were evaluated, similar to the procedure shown in Fig. 5. Axial stress-strain behavior of compressive creep sustained and non-sustained EPS15 geofoam samples were shown in Fig. 11. It is observed that resistance offered by compressive creep sustained geofoam samples in static compression loading tests was much lesser compared to non-compressive creep sustained samples. From the above observation it can understand that geofoam material is also degrading with time similar to other construction materials which were adopted in structures. The Young's modulus (E) obtained from pseudo-long-term tests of CC sustained geofoam samples were plotted in Fig. 12. Young's modulus of EPS15 geofoam decreases with increase in compressive creep strain. E , σ_c and σ_y values for 3% CC sustained geofoam specimens are 2338, 61.4

Fig. 11 Stress-strain behavior of initial and 3% CC sustained samples of EPS15, EPS20 and EPS25

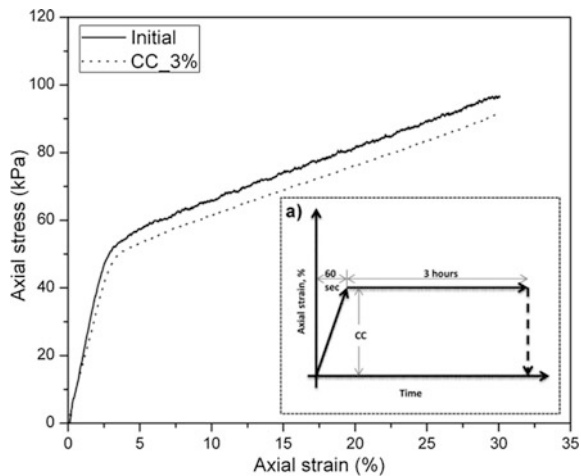
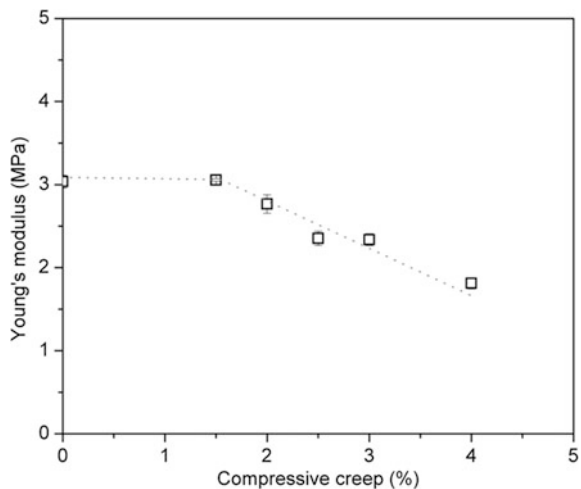


Fig. 12 Effect of compressive creep on Young's modulus of EPS15 geofoam



and 51.5 kPa respectively which were lower than the initial or non-sustained geofoam samples values are 3036, 66.6 and 55 kPa. Based on the above observation it can be conclude that geofoam material properties also degrades similar other construction materials.

4 Summary and Conclusions

From the series of static, CUC, creep and pseudo-long-term tests on EPS15 geofoam specimens, the following conclusions are drawn:

- Bi-linear axial stress-strain response of geofoam is observed from static tests.
- Secant modulus (E_{dyn}) of geofoam decreases with increase in cyclic axial strain, irrespective of density of geofoam.
- Damping ratio increases with increase in cyclic axial strain.
- Poisson's ratio of geofoam varies from positive to negative values, depending on loading type and number of cycles.
- Poisson's ratio reaches zero value at low cyclic axial strain (<2%) and higher R values from CUC tests, compared to that of static tests (6.5%).
- For R values near to or above unity, cyclic axial strain increases abruptly with number of cycles compared that at lower R values.
- Predicted compressive creep strain at the end of 100 years for EPS15 geofoam is 2.12%.
- From Pseudo-long-term tests, it was observed that Young's modulus, compressive strength, and yield strength of geofoam samples decrease compared to their initial values.

References

1. Horvath JS (1994) Expanded polystyrene (EPS) geofoam: an introduction to material behavior. Geotext Geomembr 23:00001. [https://doi.org/10.1016/0266-1144\(94\)90048-5](https://doi.org/10.1016/0266-1144(94)90048-5)
2. Partos AM, Kazaniwsky PM (1987) Geoboard reduces lateral earth pressures. Paper presented at the Geosynthetics'87. Industrial Fabrics Association International. New Orleans, LA, USA, pp 628–639
3. Rajagopal K, Pitchumani NK, Purnanandam K (2000) Earth pressure reduction behind rigid box culverts: a case study. Paper presented at the Indian Geotechnical Conference 2000, The millennium conference, 38(3):317–333
4. Zarnani S, Bathurst RJ (2008) Numerical modelling of EPS seismic buffer shaking table tests. Geotext Geomembr 26(5):00001. <https://doi.org/10.1016/j.geotexmem.2008.02.004>
5. Ikizler SB, Aytekin M, Vekli M (2009) Reductions in swelling pressure of expansive soil stabilized using EPS geofoam and sand. Geosynthetics Int 16(3):00001. <https://doi.org/10.1680/gein.2009.16.3.216>
6. Dave TN, Dasaka SM (2012) Transition of earth pressure on rigid retaining walls subjected to surcharge loading. Int J Geotech Eng 6(4):00001. <https://doi.org/10.3328/IJGE.2012.06.04.427-435>
7. AbdelSalam SS, Azzam SA (2016) Reduction of lateral pressures on retaining walls using geofoam inclusion. Geosynthetics Int. <https://doi.org/10.1680/jgein.16.00005>
8. Withoefdt AF, Kim H (2016) Numerical investigation of earth pressure reduction on buried pipes using EPS geofoam compressible inclusions. Geosynthetics Int 26(4):00001. <https://doi.org/10.1680/jgein.15.00054>
9. Purnanandam K, Rajagopal K (2008) Lateral earth pressure reduction due to controlled yielding technique. Indian Geotechnical J 38(3):317–333
10. Kim H, Choi B, Kim J (2010) Reduction of earth pressure on buried pipes by EPS geofoam inclusions. Geotech Test J 33(4):0001. <https://doi.org/10.1520/GTJ102315>
11. Srinivas FC (2014) Laboratory performance evaluation of bituminous mixes containing recycled asphalt pavement. Master's thesis IITBomab India

12. Stark TD, Arellano D, Horvath JS, Leshchinsky D (2004) Geofoam applications in the design and construction of highway embankments. NCHRPWeb Document 65, Transport Research Board, Washington, D.C.
13. ASTM (2010) Standard Test Method for compressive properties of rigid cellular plastics. ASTM D1621-10, West Conshohocken, PA
14. Trandafir AC, Erickson A, Moyles JF, Bartlett SF (2011) Confining stress effects on the stress-strain response of EPS geofoam in cyclic triaxial tests. Paper presented at the Geo-Frontiers, 2084–2091 p. [https://doi.org/10.1061/41165\(397\)213](https://doi.org/10.1061/41165(397)213)
15. Yeo SS (2007) Evaluation of creep behavior of geosynthetics using accelerated and conventional method. Ph.D. Thesis, Drexel University, PA
16. Yeo SS, Hsuan YG (2009) Effects of temperature and stress on the short- and long-term compressive behaviour of expanded polystyrene. *Geosynthetics Int* 16(5):374–383. <https://doi.org/10.1680/gein.2009.16.5.374>
17. Awol TA (2012) A parametric study of creep on EPS geofoam embankments. Norwegian university of science and technology, Master thesis
18. Birhan AG, Negussey D (2014) Effect of confinement on creep behaviour of EPS geofoam. *Geotech Test J* 37(6):1–8. <https://doi.org/10.1520/GTJ20140010>
19. Gnip IY, Vaitkus S, Kersulis V, Vejjelei S (2008) Long-term prediction of compressive creep development in expanded polystyrene. *Polym Test* 27:378–391. <https://doi.org/10.1016/j.polymertesting.2008.01.005>
20. Duskov M (1997) Material research on EPS20 and EPS15 under representative conditions in pavement structures. *Geotext Geomembr* 15:147–181
21. Ossa A, Romo MP (2009) Micro- and macro-mechanical study of compressive behavior of expanded polystyrene (EPS) geofoam. *Geosynthetics Int* 16(5):327–338. <https://doi.org/10.1680/gein.2009.16.5.327>
22. Athanasopoulos GA, Pelekis PC, Xenaki VC (1999) Dynamic properties of EPS geofoam: An experimental Investigation. *Geosynthetics Int* 6(3):171–194. <https://doi.org/10.1680/gein.6.0149>
23. ASTM (2003) Standard test methods for the determination of the modulus and damping properties of soils using the cyclic triaxial apparatus. ASTM D3999-91 West Conshohocken, PA
24. Horvath JS (1995) Geofoam geosynthetics. Horvath Engineering, Scarsdale, NY
25. Horvath JS (2010) Lateral pressure reduction on earth-retaining structures using geofoams: correcting some misunderstandings. Paper presented at the ASCE, Geo-Institute ER2010: Earth retention conference 3, Washington, USA, [https://doi.org/10.1061/41128\(384\)86](https://doi.org/10.1061/41128(384)86)
26. Bartlett S, Negussey D, Fransworth C, Stuedlein A (2011) Construction and long-term performance of transportation infrastructure constructed using EPS geofoam on soft soil sites in Salt lake valley, Utah. Presented at the 4th International conference on geofoam-EPS2011, Lillestrom, Norway, 10p

Part IV

New Concepts and Special Topics

Bridge Foundations Supported by EPS Geofoam Embankments on Soft Soil



Jan Vaslestad, Steven Floyd Bartlett, R. Aabøe, H. Burkart, T. Ahmed and David Arellano

Abstract EPS geofoam can be used to support highway bridge structures without the aid of deep foundations. The development of this technology is important to accelerate construction on soft compressible soil. EPS geofoam allows for the rapid construction of bridge foundations on such soils without the time and cost involved in installing traditional foundations. Because EPS geofoam is an extremely light weight fill, it can be used to avoid settlement impacts at bridge approaches. In Norway, bridges have been directly supported by EPS geofoam. Norwegian Public Roads Administration has pioneered this application for a few bridges underlain by soft, clayey deposit where the bridge structure rests solely on EPS geofoam blocks. Investigating bridge foundations supported by EPS geofoam embankments is a joint effort starting summer 2013 between the University of Utah, University of Memphis and Norwegian Public Roads Administration. This paper includes some tasks and conceptual designs that address development of performance goals, design criteria, material testing, prototype analyses, numerical modeling and constructability of this innovative bridge support system.

Keywords Geofoam · Bridges · Foundations · Soft clay

J. Vaslestad (✉) · H. Burkart · T. Ahmed
Norwegian Public Roads Administration Eastern Region, Oslo, Norway
e-mail: jan.vaslestad@vegvesen.no

S. F. Bartlett
University of Utah Civil Engineering, Salt Lake City, USA

R. Aabøe
Norwegian Public Roads Administration Road Directorate, Oslo, Norway

D. Arellano
Department of Civil Engineering, University of Memphis, Memphis, USA

1 Introduction

In 1972, the Norwegian Public Roads Administration (NPRA) adopted the use of Expanded Polystyrene (EPS) geofoam as a super light-weight fill material in road embankments. The first project involved the successful reconstruction of a road embankment adjacent to a bridge founded on piles to firm ground. Prior to reconstruction, the pre-existing embankments, resting on a 3 m thick layer of peat above 10 m of soft marine clay, experienced a settlement rate of more than 200 mm per year. However, by replacing 1 m of ordinary embankment material with two layers of EPS blocks, each 0.5 m thick, the settlement was successfully halted. The EPS blocks deployed had a density of 20 kg/m^3 , which is nearly 100 times lighter than the replaced materials [1].

Subsequently, EPS geofoam technology has been successfully used elsewhere in Europe, Japan and the United States as a super light-weight material which in highway bridges supported on deep foundations.

The extremely lightweight nature of EPS allows for rapid embankment construction atop soft ground conditions without causing damaging settlement to the deep foundations, bridge structure and approach pavements. The EPS embankment technology is well-developed for such applications, but except for a few cases in Norway, it has not been used elsewhere for the direct support of bridge structures (i.e., placing the bridge foundation support directly on the EPS without the installation of deep foundations e.g., piles, shafts, caissons or piers). However, in Norway, bridges have been directly supported by EPS geofoam without deep foundations. The NPRA has pioneered this application for a few bridges underlain by soft, clayey deposits where the bridge structure rest solely on EPS blocks. These sites are: (1) the Lokkeberg Bridge (2) the Gimsøyvegen bridge (3) the Hjelmungen bridge (4) three pedestrian bridges in the City of Fredrikstad, which consisted of EPS block supports clad with protective panels. The NPRA reports that an EPS bridge support system has provided considerable cost and time savings when compared with traditional bridge support systems [1].

The overall goal of the research summarized herein is to develop a guideline for design of EPS bridge support systems that will include the requisite engineering evaluation(s) and recommended design methodologies to support the design and construction of EPS bridge support systems. The objectives of the proposed research are: (1) evaluate an EPS support system for single span structures and pedestrian overpasses supported on EPS using the knowledge and data gained from the Norwegian case studies, (2) evaluate the expected performance of this system(s) under static and dynamic loading using material testing and numerical modeling of prototypes and full-scale systems previously used and installed in Norway, and (3) develop recommendations for future research/testing/development required for implementation of this technology. This paper summarizes the tasks to be performed to accomplish these research objectives and will address development of performance goals, design criteria, material testing, prototype analyses, numerical modeling and constructability of this innovative bridge support system.

2 Performance Goals

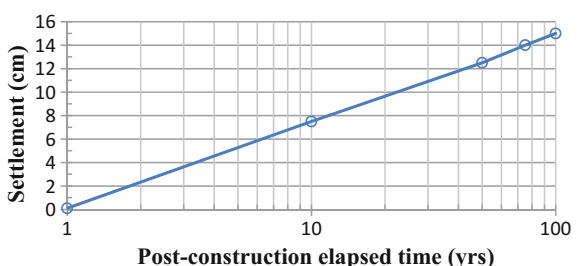
The types of structures considered for the EPS bridge support system will consist of permanent or temporary construction consisting of 1–2-lane highway overpass structures and pedestrian bridges. In general, it is anticipated that the candidate bridges will be generally single-span structures with span lengths of 35 m or less. Steel construction is believed to be preferable over concrete and wood, but these latter materials will also be considered, if feasible.

Candidate sites for the EPS bridge support system will consist of soft or problematic soil sites (e.g., compressible and sensitive soils). However, we recommend that the candidate bridge sites not be located on modern flood plains, or at major river crossings having significant flooding potential.

For soft and compressible soil sites, limiting the amount of construction and post-construction settlement of the bridge support system is an important consideration and the total settlement of the EPS bridge support and foundation system should be determined on a project-by-project basis using project-specific loading and soil data. The settlement of the bridge system can occur from three primary mechanisms: (1) elastic compression of the EPS blocks from the applied structural and pavement loads which is recommended to remain in the allowable elastic range under the combination of dead, live and traffic loads and that the construction-related vertical strain of the blocks be limited to 1 percent during the construction of the bridge and pavement system., (2) creep strain of the blocks resulting from long-term dead loads which is recommended to be limited to about 2% vertical in 50 years, and (3) consolidation settlement of foundation soils.

In addition, the underlying foundation soils will undergo consolidation settlement resulting from the applied dead loads of the bridge structure, approach slab and roadway pavement materials. The subsequent consolidation settlement is generally associated with the long-term creep (i.e., secondary consolidation settlement) of the foundation soils. Farnsworth et al. [2] have noted based on field measurements that bridge system approach systems will generally have acceptable performance, if the post-construction creep settlement of the foundation soils is limited to about 7.5 cm in a 10-year period post-construction period. Figure 1 shows this proposed, post-construction settlement performance goal projected to 50, 75 and 100 years by assuming a semi-log linear relationship for the creep settlement of the foundation soils.

Fig. 1 Proposed post-construction foundation settlement performance goal versus post-construction elapsed time



In addition to the traffic loading, the EPS bridge support system must be designed to withstand loadings from seismic events in earthquake prone regions of the world. Regarding seismic events, it is proposed that the bridge support system for permanent bridges be designed to withstand earthquake ground motion associated with a 1000-year return period event (i.e., 7.5% chance of exceedance in 75 years), which is commonly used design basis event in the U.S. for highway bridge design.

3 Design Criteria

In developing the EPS bridge support system, design guidance and material standards developed in Europe and the U.S. will be reviewed and incorporated. These will consist of EN14933 found in the “EPS White Book” [3], “Use of Expanded Polystyrene in Road Embankments” [4], “Guideline and Recommended Standard for Geofoam Applications in Highway Embankment” (NCHRP 529, [5]) and its companion document “Geofoam Applications in the Design and Construction of Highway Embankment” (NCHRP Web Document 65, [6]).

For permanent bridge structures located in the United States, the American Association of State Highway and Transportation Officials has developed design criteria for highway bridges based on load and resistance factored design (LRFD) [7]. The design of pedestrian bridges is completed according to LRFD Guide Specifications for Design of Pedestrian Bridges [8]. Seismic design of permanent bridge structures is completed using the AASHTO Guide Specifications for LRFD Seismic Bridge Design (2014). In addition AASHTO HL93 truck load which consists of a “design truck plus design lane load” or “design tandem plus design lane load,” whichever is the worst case can be used for traffic loading.

For seismic design, Bartlett and Neupane [9] recommend that the applied dead, live and earthquake loads in the EPS blocks be limited to a combined stress level that does not exceed the compressive resistance associated with 2% axial strain, as measured in a monotonic uniaxial lab test for the selected density of EPS. This recommendation is similar to that found in the EPS White Book [3] for the factored allowable stress for short-term loading conditions which is taken to be 80% of the compressive resistance at 10% axial strain. Bartlett and Neupane [9] recommend the use of the compressive resistance measured at 2% axial strain, which is approximately equivalent to 85% of the compressive resistance at 10% strain. However, these latter authors also recommended that the applied dead load not exceed the compressive resistance measured at 1% axial strain in order to avoid the potential for unacceptable post-construction creep deformation.

4 Materials Testing

Laboratory testing will used to define the stress-strain, creep (time-dependent or stress-strain-time behavior) and dynamic (cyclic) properties of EPS. Some of the testing has already been completed by various researchers (Stark et al. [6]; Kafash [10]), but additional material testing may be required to address some of the behaviors introduced in development of the conceptual design. For example, analysis and design methods for EPS geofoam as lightweight fill are based on explicit deformations of the geofoam mass [5, 6]. Therefore, the most important properties of block-molded EPS to test are those related to the overall mechanical (stress-strain-time) behavior of an entire EPS block in compression as this is what will be loaded in the final bridge structure. However, testing of full-size blocks is not feasible on a routine basis and, in practice, testing is performed on 50 mm cube-shaped specimens prepared from samples cut from blocks. Additionally, there are inherent property variations within the block that result from the molding process [6, 10]. Therefore, larger specimen sizes than the traditional 50 mm cube-sized specimen currently used in practice will be evaluated under static unconfined uniaxial compression loads to obtain the effect of specimen size on the stress-strain behavior of EPS blocks.

Both the stress-strain and stress-strain-time behavior of EPS is related to the density of an EPS block [6]. Traditional EPS densities that are currently readily available in the market and utilized for lightweight fill applications in stand-alone embankments over soft ground and for slope stabilization range from 18.4 to 45.7 kg/m³ based on the ASTM D6817 property requirements. Creep test data is available for these density ranges and are summarized by Stark et al. [6] and Arellano et al. [11]. However, ASTM has incorporated higher density EPS blocks with densities of 38.4 and 45.7 kg/m³ for which creep and cyclic test data is not readily available. Therefore, shear strength tests, creep and cyclic tests will be performed on specimens with 38.4 and 45.7 kg/m³. In addition, cyclic, creep and flexural tests will be performed for samples which have higher densities than 45.7 kg/m³. Reduced-scale test embankments may also be used to explore the stress distribution created in the EPS by various long-term and live loading conditions.

Bartlett and Neupane [9] completed a series of stress-controlled cyclic uniaxial tests on EPS specimens of various densities to assist in defining the earthquake and post-earthquake deformation and creep potential of bridge support systems. Based on these tests, EPS specimens showed a larger amount of permanent plastic strain at higher levels of applied cyclic deviatoric stress, as expected. This was also true for tests where the deviatoric stress was kept constant, but the number of cycles were increased. Therefore, the amount of permanent cyclic strain increased with increasing amount of applied cyclic deviatoric stress and with increasing number of applied stress cycles. These results were expected and consistent with the known cyclic behavior of EPS undergoing cyclic permanent deformation.

Bartlett and Neupane [9] also measured the amount of post-cyclic creep for these specimens and used these results to estimate the total permanent vertical strain in a

proto-type EPS bridge support embankment for a 50-year post construction period. The estimated deformation included the combination of cyclic plastic deformation (i.e., earthquake deformation) and post-cyclic (i.e., post-earthquake) creep deformation. Based on the test results, they estimated that the total permanent strain will not exceed 0.7% for cases where the seismic design criteria found in Sect. 3 of this paper are followed, and that the post-earthquake vertical stress from gravity loading does not exceed the compressive resistance found at 1% strain for the selected density of EPS. In fact, the cycling of the specimens and the associated cyclic axial strain appears to have slightly “conditioned” (i.e., stiffened) the specimens so that the post-cyclic creep strain rate was somewhat diminished when compared with the pre-cyclic creep strain rate.

5 Prototype Analyses

The selection of EPS embankment geometries, block layout pattern and material quality to be used vary according to the bridge clearance, the subsoil condition and other project design specific criteria. From practical experiences gathered through monitoring programmes on EPS embankments as well as full scale laboratory tests, EPS blocks with 2H:1V slopes and vertical EPS fills have given satisfactory results and the same slope geometry will be used for further analysis. In addition, the study will use sub soil conditions which have compressible non-sensitive soil profiles, crust over compressible sensitive profile and granular over compressible soil profile.

Depending on the extent of the load that is coming from the bridge deck, several combination of EPS density can be used in the design. However, this study will consider three different EPS density and configurations: uniform density, increasing density near top of EPS system and intermediate load distribution slabs. EPS blocks will be placed in such a way that spaces between two EPS blocks in the same row will not exceed 3 cm and a vertical staggering of blocks by avoiding a continuous vertical gap.

6 Numerical Modeling

Numerical models which are able to capture the EPS behaviour during loading and unloading can fill the gap of data limitation and gives us a better insight over the stress-strain-time relationship. Different models exist for soils and rocks from sophisticated to simpler ones. Nevertheless, in built models specifically prepared to analyse the EPS behaviour is not available commercially. However, using similarities in stress-strain relationships between soil and EPS geofoam, therefore, one can calibrate EPS parameters using models usually used for soils/rocks.

Simple hand calculations together with simplified techniques based on elastic theories and PLAXIS & FLAC, the performance of the EPS support system will be evaluated and potentially implemented in future design of such systems.

7 Bridges Supported on Geofoam Embankments, Cases from Norway

7.1 Løkkeberg Bridge

7.1.1 Introduction

Løkkeberg bridge is a 36.8 m long, single span and acrow steel bridge across the E6 (on Rv. 121 road) to facilitate the traffic flowing temporarily in that area. The bridge was built and opened in 1989 and it had been expected to function between 3 and 5 years. However, it lasted until 2005/6 (for a total of 16 years) before it has been removed. Due to the soft clay deposit, which ranges from 6 to 16 m in thickness below the abutment, and low bearing capacity, it was decided to use EPS embankment as an abutment to carry the weight of the bridge as an alternative to end bearing piles. It is the first bridge to be constructed on EPS embankments.

7.1.2 Dimension and Material Quality

Løkkeberg bridge is constructed as a single lane bridge which ranges 36.8 m in length and is built 5.5 m above the ground level. The bridge weighs 68 t and it rested on a 7.4 m × 7.5 m footing slab which had a thickness of up to 1 m below the girder and 0.5 m elsewhere. In order to support the traffic and dead load coming from the bridge deck, a 5 m and 4.5 m high EPS fill embankment had been used on either ends of the bridge. Three types of EPS had been used for this project, EPS240 (40 kg/m^3) on the first top layer immediately below the bridge deck, EPS180 (30 kg/m^3) until halfway through the embankment and the rest was filled with EPS100 (20 kg/m^3). A 10 cm concrete slab was laid down on the middle layer of EPS embankment (Fig. 2).

7.1.3 Stress Distribution

As one part of the monitoring program, stress distribution in the EPS embankment was measured using 10 hydraulic earth pressure cells (7 in the EPS and 3 in the sand layer beneath the EPS) 10 years after the construction ended. A consistent data was able to be obtained one year after installation of the cells. Figure 3 illustrates the measured data on EPS blocks after 10 years of operation.

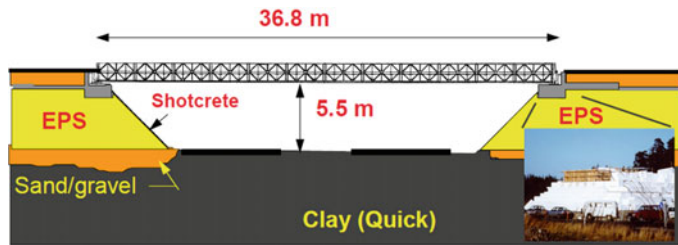


Fig. 2 Temporary single-lane steel truss bridge structure supported on EPS block at Løkkeberg, Norway. (Note the absence of deep foundation system at this location.) (after Aabøe and Frydenlund [1])

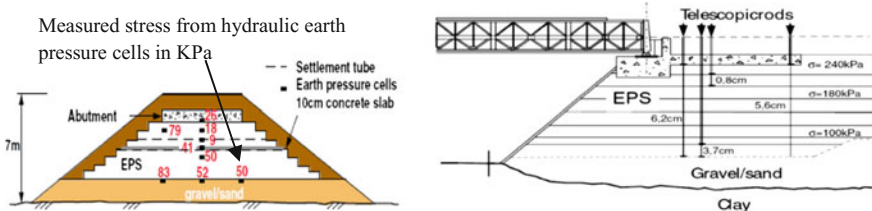


Fig. 3 Observed stress distribution and deformation at Løkkeberg bridge after 10 years in operation

7.1.4 Measured Deformation

Total deformation measured 12 years after operation is nearly 6 cm which accounts about 1.3% of the EPS thickness. Average creep measured for 10 years on the bottom layer of EPS accounts for 6.5% of the thickness. On performance point of view, a satisfactory result was obtained.

7.2 Hjelmungen Bridge

7.2.1 Introduction

This is an overpass bridge over the E6 road in which the bridge is founded directly on EPS embankment. It is located in a close proximity to Løkkeberg bridge. Hjelmungen bridge is 54 m long and has three spans over which it connects a local road over an E6 motorway in Østfold county.

The bridge is built in 1992 and it was originally founded on concrete piles together with a 5 m high approach embankment which was filled partially with light weight leca-blocks ($\gamma = 8 \text{ kg/m}^3$) and commonly used fill material ($\gamma = 20 \text{ kg/m}^3$).

The foundation soil is mainly composed of clay which is highly sensitive and weak with thickness ranging from 11 to 14 m. High settlement, nearly 600 mm, was registered in the approach embankment which lead to an immediate reparation of the bridge foundation. The high settlement is known to be caused by the heavy weight of the fill material and an overestimation of pre-consolidation stress for the underlying clay. The reparation started in 1995 and is finished in 1996. The abutment and the approach embankment fill was dug out and replaced by EPS geofoam blocks. The original concrete pile where the bridge was supported on, got trimmed off and made to be rested directly on EPS filled embankment.

7.2.2 Dimension and Material Quality

The bridge was 54 m long with three spans (16 m at either end of the bridge and 22 m in between). The EPS filled embankment was composed of three different EPS blocks: EPS235 on the first top three layers, further below was EPS180 and EPS100 for the rest of the filling. A 10 m long and 20 cm thick friction plate, which is made of a reinforced concrete, was installed in the abutment to resist horizontal load and a concrete plate with thickness 10 cm was used in the approach EPS embankment (Fig. 4).

7.2.3 Stress Distribution

Monitoring program was carried out to check the development of settlement after reconstruction of the abutment. Pressure cells and settlement tubes were installed for this purpose as shown in Fig. 5.

Measured stresses, shown in Fig. 5, shows that higher stresses are measured on the middle than to the either sides of the embankment. However, the excess pressure measured in the middle of the embankment taught to have come from while jacking up the bridge deck during reconstruction.

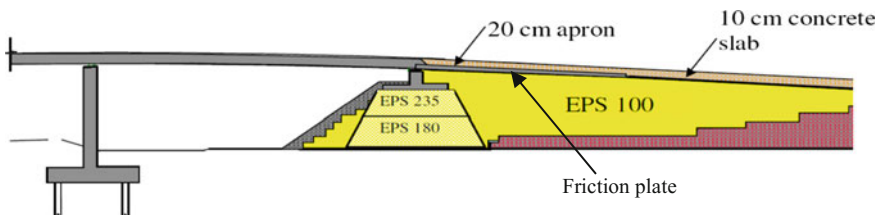


Fig. 4 Principal sketch for re-foundation of Hjelmungen bridge

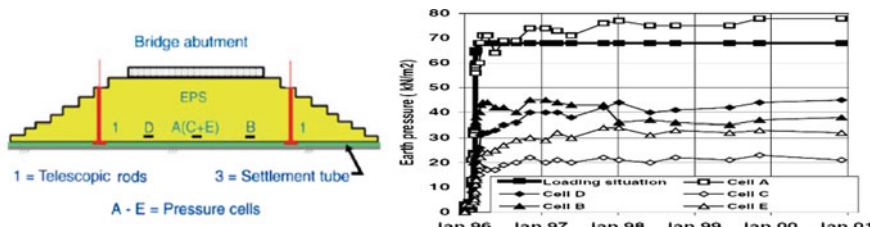


Fig. 5 Location of pressure cells, measured total deformation and settlement tubes and observed stress distribution below EPS layer at Hjelmungen bridge

7.2.4 Measured Deformation

Development of deformation was monitored using measurement gauges installed under the lower EPS layer, in the leveling sand. A total deformation of 3.5 cm registered which constitutes about 0.7% the filling height.

7.3 Gimsøyveien Bridge

7.3.1 Introduction

This is a temporarily bridge which was constructed across a highway during the expansion of E6 road from two to four lane in Østfold county. EPS blocks which were used in the Løkkeberg bridge is re-used for this construction as well. A highly sensitive, soft clay is discovered during ground investigation. Settlement and local stability were expected to be a major problem. Therefore, EPS fill embankment was selected to carry the load from the bridge.

7.3.2 Dimension and Material Quality

The bridge was founded on top of 4.5 and 5 m EPS filled embankments at either side of the road. From 8 to 9 EPS layers were used where the top three layers were EPS300. The EPS blocks were staggered to form a front slope and vertical to the sides. The blocks were laid down on top of a levelled gravel material and protected with sprayed concrete and geotextiles.

7.3.3 Measured Deformation

During the bridges lifetime a total settlement of 5 cm (<1%) is registered, which was less than the calculated value beforehand (Fig. 6).



Fig. 6 Gimsoyveien bridge during construction

7.4 *Leie, Skovbøle and Høiendal Bridges*

7.4.1 Introduction

In the mid-1990s four pedestrian and cycle bridges are constructed in Fredrikstad, Norway in connection with the expansion of Rv. 109 road from two lane into four. Out of the four bridges three of them are founded directly on EPS blocks.

The bridges are constructed across the main road, Rv.109, which follows the bottom of the valley. The area is characterised by thick sediments of clay which ranges up to 50 m in depth. A part of the clay deposit is known to be very sensitive (quick clay) and susceptible for large settlements. Depending on the ground investigation results, it was decided to use EPS blocks to undergo the likely problem of bearing capacity and settlement if the foundation were to be shallow concrete foundation.

7.4.2 Dimension and Material Quality

EPS embankment is used as a direct foundation to the bridge deck and the total height of the EPS blocks in the embankment is 3 m from which 1 m of the EPS filling is under excavation, minimizing settlement on the subsoil. EPS150 is used in this case and the design compression load coming from the deck of the bridge is 36 kPa. The abutment is finished with a 10:1 slopped wall, made of plastered granite stone, on either side of EPS blocks and extends 1.5 m vertically over the top EPS layers, see Fig. 7.

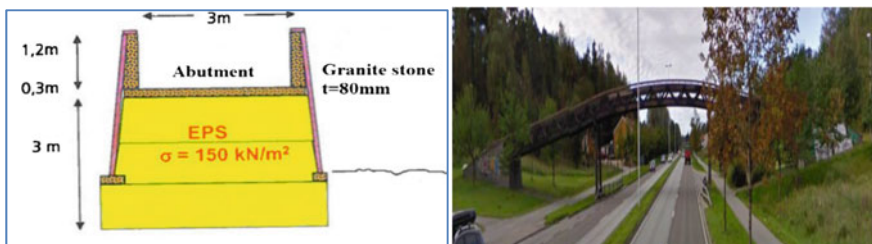


Fig. 7 Principal abutment dimension for Leie, Skovbølle and Høiendal bridges (left). Leie bridge (right)

7.4.3 Measured Deformation

Monitoring programmed with regard to settlement and stress measurements are not performed in these bridges, however, successive site visits indicate that the bridges are on satisfactory performance condition.

8 Development of a Seismic Restraint System for Free-Standing EPS Support Embankments

Additional strategies may be included in the design and construction to improve the seismic resistance, redundancy and robustness of the EPS bridge support system when subjected to large earthquakes. These may include material, physical and mechanical devices or countermeasures deployed within, or external to, the geofoam support system. For example, Bartlett and Lawton [8] and Amini [12] explored the deployment of several mechanisms for reducing the potential for interlayer or basal sliding of the EPS blocks under seismic loading: (1) shear keys constructed of high density geofoam blocks placed in strategic locations within the embankment, (2) adhesion (adhesive) placed between the geofoam blocks and (3) embedment of the support system. In addition, Amini [12] recommended that consideration be given to increasing the density (i.e., modulus) of geofoam blocks in zones susceptible to overstressing near the basal edges of the embankment.

An example of a mechanical restraint system was proposed by Bartlett and Neupane [9] which featured a cable restraint system. The overall objective of the cabling system is to reduce the amount of interlayer sliding, sway and rocking so that the bridge support system is not compromised due to excessive translation or internal overstressing of the EPS blocks. The primary mechanism used to achieve this was to include high-strength steel cabling as a mechanical restraint system that connects the bridge foundation (i.e., footings) with a basal foundation slab, grade beam or anchorage system placed below the EPS blocks (Fig. 8). Bartlett and Neupane [9] recommended that this foundation connection be made using a diagonal or crisscross cabling pattern. Such cabling provides a load path for uplift

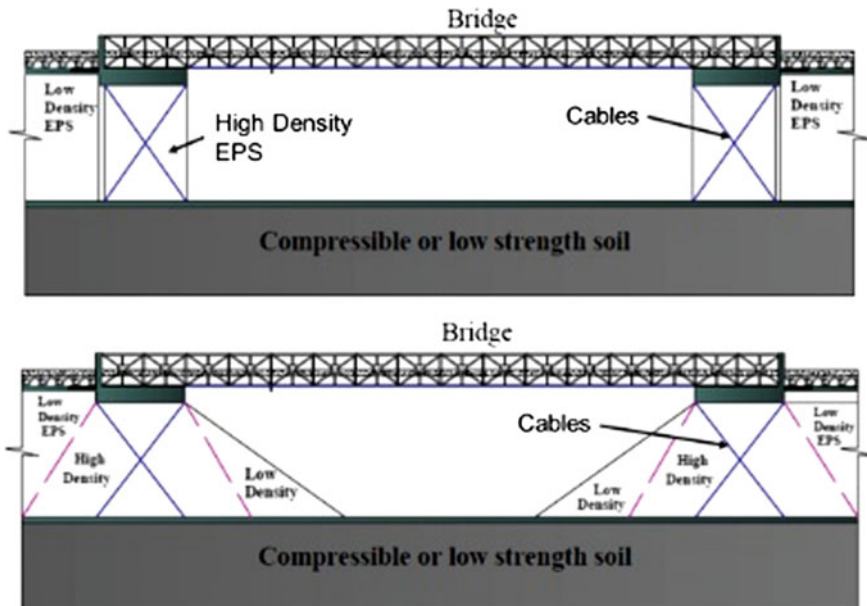


Fig. 8 Conceptual cable restraint system for EPS bridge support system

tensile and shear forces to be transferred from the bridge system to the embedded basal slab or other means of anchorage. The cabling also functions as lateral restraint system that can be used to limit the amount of interlayer sliding.

9 Conclusions

Light-weight temporary and permanent bridges supported directly on EPS geofoam have shown success according to engineering evaluation and field observations. Further studies regarding a conceptual and standard design of such bridge foundation are highly recommendable with the view of adopting similar experiences to a different candidate sites, in addition to reducing construction time and cost on soft ground sites.

References

1. Aabøe R, Frydenlund TE (2011) 40 years of experience with the use of eps geofoam blocks in road construction, EPS 2011. Lillestrom, Norway
2. Farnsworth CF, Bartlett SF, Negussey D, Stuedlein A (2008) Construction and post-construction settlement performance of innovative embankment systems. I-15

- Reconstruction Project, Salt Lake City, Utah. J Geotech Geoenvironmental Eng ASCE 134:289–301
- 3. EUMEPS (2011) EPS white book. EUMEPS background information on standardization of EPS, Version 31/03/11
 - 4. NPRA (1992) Use of expanded polystyrene in road embankments. Norwegian Public Roads Administration, Directorate of Public Roads, Norwegian Roads Research Laboratory (NRRL), Oslo, Norway, August 1992 in English
 - 5. Stark TD, Arellano D, Horvath JS, Leshchinsky D (2004) NCHRP report 529: guideline and recommended standard for geofoam applications in highway embankments. Transportation Research Board, Washington, D.C., 71 pp. Available at http://trb.org/publications/nchrp/nchrp_rpt_529.pdf
 - 6. Stark TD, Arellano D, Horvath JS, Leshchinsky D (2004) NCHRP web document 65 (Project 24-11): geofoam applications in the design and construction of highway embankments. Transportation Research Board, Washington, D.C., 792 pp. Available at http://trb.org/publications/nchrp/nchrp_w65.pdf
 - 7. AASHTO LRFD Bridge design specifications, customary U.S. units, 6th edn, with 2013 Interim Revisions
 - 8. Bartlett SF, Lawton EC (2008) Evaluating the seismic stability and performance of freestanding geofoam embankment. In: Proceedings 6th national seismic conf. on bridges and highways, Federal highways administration (FHWA) and multidisciplinary center for earthquake engineering research (MCEER) Charleston, SC, 17
 - 9. Bartlett SF Neupane R (2017) Seismic evaluation of expanded polystyrene (EPS) geofoam bridge support system for overpass structure. Mountain plains consortium (MPC) Technical Report No. MPC-422, 133 p
 - 10. Kafash MH (2013) Seismic stability analysis of landslides stabilized with expanded polystyrene (EPS)-block geofoam. Ph.D. Dissertation, The University of Memphis
 - 11. Arellano D, Stark TD, Horvath JS, Leshchinsky D (2011) Guidelines for geofoam applications in slope stability projects. NCHRP Project 24-11(02) Final Report, Transportation Research Board, Washington, D.C., 602 pp. Available at [http://onlinepubs.trb.org/onlinepubs/nchrp/docs/NCHRP24-11\(02\)_FR.pdf](http://onlinepubs.trb.org/onlinepubs/nchrp/docs/NCHRP24-11(02)_FR.pdf)
 - 12. Amini ZA (2014) Dynamic characteristics and seismic stability of expanded polystyrene geofoam embankments. Ph.D. thesis, The University of Utah, Utah, USA
 - 13. AASHTO LRFD Guide Specifications for Design of Pedestrian Bridges, 2nd edn. 2009

Guidance on Use of Geofoam Lightweight Fill and Complementary Technologies Using *GeoTechTools*



Ryan R. Berg, Vernon R. Schaefer and Silas C. Nichols

Abstract Geofoam provides sustainable solutions for embankment and pavement construction, provided it is appropriately designed and detailed, specified, and installed. Prior to selecting geofoam, an engineer will evaluate the potential use of alternate lightweight fill materials and of other ground modification technologies on their project. Thus, the engineer must access and assess information on a variety of materials and ground modification techniques. Today, this information can be readily accessed on one website—www.GeoTechTools.org. *GeoTechTools* is a knowledge system that provides a synthesis of critically important information about geofoam, as well as other ground modification techniques, and makes the information readily accessible. The two primary components of this comprehensive toolbox are a Catalog of Technologies and a Technology Selection Assistance System. For each technology, eight distinct tools can be accessed through the Catalog of Technologies. Technology selection assistance is provided by use of an interactive selection system. This system aids the user in identifying a short-list of potential technologies for a particular project. *GeoTechTools* was developed to assist engineers make more informed decisions on issues to reduce risk and minimize construction surprises. The value of this system is that it collects, synthesizes, integrates, and organizes a vast amount of critically important information about geotechnical solutions on a readily accessible website. This paper discusses the system and its application on the use of geofoam for transportation projects.

Keywords Ground modification · Lightweight fill · Geofoam · Technology selection

R. R. Berg (✉)
Ryan R. Berg & Associates, Inc., Woodbury, MN, USA
e-mail: ryanberg@att.net

V. R. Schaefer
Iowa State University, Ames, IA, USA

S. C. Nichols
Federal Highway Administration, Washington, DC, USA

1 Introduction

Geofoam lightweight fill is one of many potential ground modification options for construction over challenging soils. Before an engineer uses geofoam, one must first determine if its use is even applicable to their specific project, and what alternative (ground modification) geotechnologies are also applicable. Once a short-list of applicable geotechnologies has been developed, the engineer must evaluate each potential solution versus the project-specific conditions.

The purpose of this paper is to demonstrate how the web-based *GeoTechTools* system is used to develop a short-list of geotechnologies applicable to a given project. Additionally, step-by-step guidance on how to take this short-list and determine the preferred solution for a particular project is detailed.

2 Potential Solutions

The process to identify potential poor ground conditions, the need for ground modification, and the selection of an appropriate geotechnology to use on a specific project conditions follows a logical sequence. The steps involved are summarized in Table 1 and are discussed in more detail within.

In Step 1, the engineer will identify poor ground conditions which could require ground modification. Poor ground conditions are those that will not provide adequate support for a structure. These are typically characterized by soft or loose foundation soils, which, under load, would cause immediate or long-term deformation, or cause construction or post-construction instability.

Table 1 Ground modification technology selection steps [5]

Step	Description
Step 1	Identify potential poor ground conditions and need for ground modification
Step 2	Identify or establish performance requirements
Step 3	Identify and assess general site conditions
Step 4	Assessment of subsurface conditions
Step 5	Develop a short-list of geotechnologies applicable to site conditions
Step 6	Consider project constraints
Step 7	Consider project risks
Step 8	Prepare a preliminary design
Step 9	Identify alternative solutions (bridge, re-route, deep foundations, etc.)
Step 10	Evaluate project requirements, constraints, and risks against factors affecting geotechnology selection
Step 11	Compare short-list of geotechnology alternatives with geotechnology selection factors
Step 12	Select a preferred geotechnology

In Step 2, general performance requirements for the project are established. Such requirements may include deformation limits (horizontal and vertical), minimum factors of safety for stability, improved nominal resistance, drainage, and the available time for construction.

In Step 3, the general site conditions that may affect selection of an appropriate geotechnology are identified and assessed. These conditions include physical space, constructability, and environmental constraints. Space constraints typically refer to accessibility for construction equipment to operate safely and for storage of equipment and materials onsite. Work in an urban environment might be congested to the point that construction operations and scheduling are affected. Some ground modification technologies have large equipment footprints and headroom requirements that must be considered for their use. Environmental constraints may include the disposal of spoil materials (hazardous or nonhazardous); disposal of water from dewatering operations; and the effects of construction vibrations, noise, and/or dust.

Step 4 is the assessment of subsurface conditions. This step may be broken into two substeps. One is at this stage of identifying potential solutions, where the initial investigation provides basic subsurface information; and the second later in the design process where specific subsurface properties are required to complete the design of the selected ground modification solution. The level of detail regarding the assessment of subsurface conditions will vary significantly across the wide range of projects. Regardless of the project type, the soils which will affect the performance requirements must be identified and the necessary engineering properties defined to perform preliminary designs for the project. At a minimum the type, depth, and extent of soils must be considered, as well as the location of the groundwater table. Furthermore, it is valuable to have at least a preliminary assessment of the shear strength and compressibility of the identified poor soils.

Step 5 is where a short-list of geotechnologies applicable to general project conditions is developed. The Technology Selection feature of the *GeoTechTools* system, available at www.geotechtools.org, can be used to complete this step. This comprehensive system is a great aid to both project personnel who are well-experienced with ground modification technologies and those with little experience. The use of *GeoTechTools* to develop a short-list of applicable technologies is discussed and demonstrated in the following section.

3 GeoTechTools

3.1 *GeoTechTools* Background

GeoTechTools is a web-based geotechnologies guidance and selection system. *GeoTechTools* is accessible through the website at <http://www.geotechtools.org>. There is no cost to use this system. First time users must register and set up a log-in and password for future access. *GeoTechTools* was developed under the auspices of

the second Strategic Highway Research Program (SHRP2), which was created by the U.S. Congress in 2006 to address challenges of moving people and goods efficiently and safely on the nation's highways. The SHRP2 R02 project was aimed at identifying geotechnical solutions for four elements: (1) construction of new embankments over unstable soils, (2) widening and expansion of existing embankments, (3) construction of new and widening of existing pavements, and (4) stabilization of the working platform. The project was conducted under the SHRP2 Renewal Focus Area, in which the goal was to develop a consistent, systematic approach to the conduct of highway renewal that is (1) rapid, (2) causes minimal disruption, and (3) produces long-lived facilities. Although developed for the transportation industry, the *GeoTechTools* system can be equally as valuable to other civil construction industries, and should have broad appeal to the overall geotechnical community both nationally and internationally [1].

The project included identification of existing and emerging geotechnical materials and systems for ground modification. A catalog of materials and systems for rapid renewal projects was developed and the current state of the practice of design, QC/QA, costs, and specifications for each technology was assessed. The resulting information was cataloged in a database and made accessible through a web-based system. The Catalog of Technologies provides detailed information on more than 50 geotechnologies. The value of the system is that it collects, synthesizes, integrates, and organizes a vast amount of critically important information about geotechnical solutions in a system that makes the information readily accessible to the user.

3.2 Initial Screening of Geotechnologies

The Technology Selection section of *GeoTechTools* was developed to aid in identifying a short-list of applicable geotechnologies for a user defined set of project conditions [2, 3]. The Technology Selection section provides both a listing of the technologies sorted by classification and a dynamic, Interactive Selection Tool.

To develop a short-list, the user inputs some essential information about the project. First, the type of structure or application element is identified. As illustrated in Fig. 1, the user can select from one of the four elements listed above. Also note in Fig. 1 the right-hand list of 50 plus geotechnologies contained on this system.

Once an application is selected, the list of applicable technologies shortens, and the next input question on the subsurface conditions appears. For the embankment construction over unstable soils application selected (Fig. 1), the right-hand list of applicable technologies shortens to 27. The user can then select soil type and water conditions from the list provided. For example, if the wet and weak, fined-grained soils condition is selected, the right-hand list of applicable technologies then shortens to 17 (Fig. 2).

The list of applicable technologies is further shortened by inputting the depth of unstable soils. For example, if a depth of greater than 50 feet (15 m) is selected, the

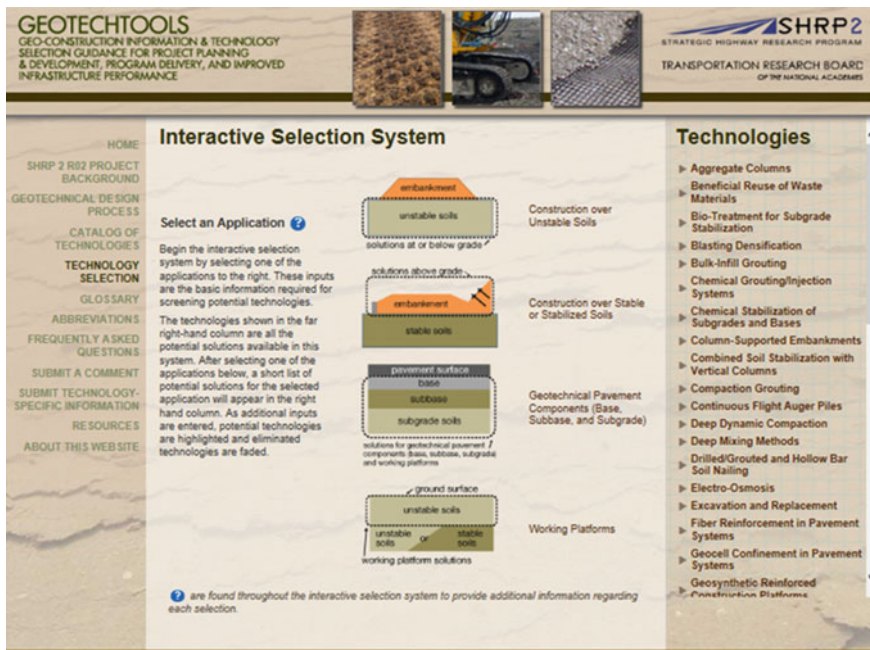


Fig. 1 Screenshot of interactive selection webpage with 4 application areas [6]

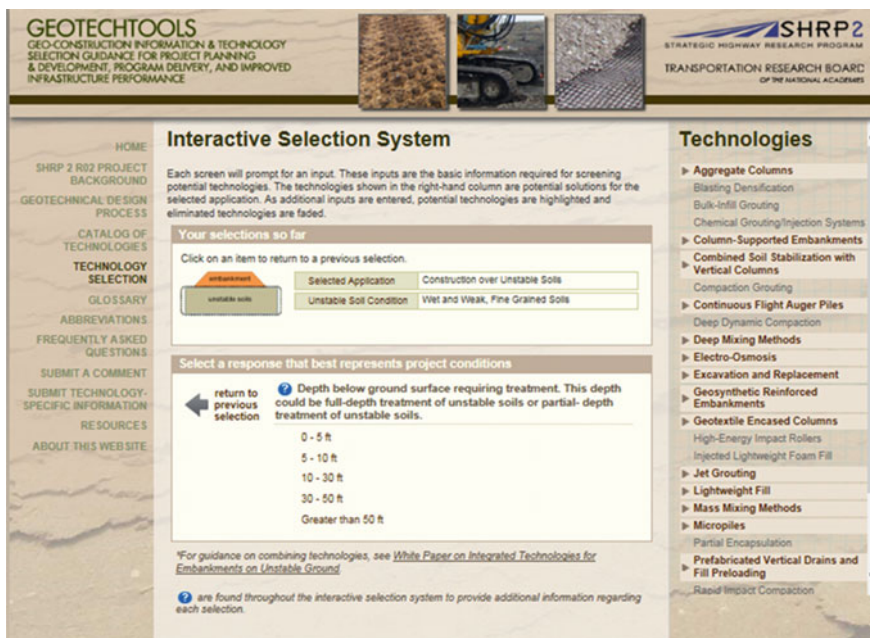


Fig. 2 Second screening question for embankments [6]

list is shortened to 12. The user has the option to stop at this point with a summary of their selection or to enter more information under the project-specific selection questions to further refine and reduce the number of applicable technologies. One or more of these can be addressed, in any order, to see the effect on reducing the number of applicable geotechnologies listed.

With a short-list developed, the engineer then moves on to a project-specific selection process, using Steps 6 through 12 of Table 1. Generally, a short-list length of 3–5 geotechnologies, for moving forward with, is targeted.

4 Project-Specific Evaluation and Geotechnology Selection

The initial screening with *GeoTechTools* produces a short-list of geotechnologies that can be used. The selection of a preferred solution now proceeds with project-specific factors, many of which are not geotechnical in nature, but can affect the selection. This process continues with Step 6 of Table 1 Ground modification technology selection steps.

4.1 Selection Steps 6 Through 12

Step 6 is the consideration of project constraints. Specifically, those constraints that might affect selection of a preferred geotechnology need to be identified and listed. These include both general and geotechnical constraints.

General constraints include all those items not connected with the geotechnical aspects of the project. Included are items such as the project schedule and time; budget and cost; project conditions such as right-of-way limits, geometry, scale, utilities and sequence; traffic flow/interruption; weather; environmental; availability of agency personnel, agency organization and structure, project management philosophy; and contracting processes. The contracting process, i.e., project delivery method, and the role it might have on use of these techniques for the specific project should also be assessed. Identification of as many of these constraints affecting the project as possible will allow better selection of an appropriate and preferred geotechnology.

The geotechnical constraints to be considered are those specific to geotechnical aspects of the project and to short-listed ground modification geotechnologies. Such constraints include subsurface conditions, including archaeological remains, contaminated groundwater, obstructions, and buried utilities; proprietary products/processes; knowledge and experience with specific technologies; allowable movements—both vertical and horizontal; stability requirements; noise and vibrations due to construction equipment; time for improvement to be effective; spoils

development and disposal; environmental impacts of the technology; availability of qualified contractors, personnel, materials and specialty equipment, including availability and shipping costs of materials (e.g., lightweight fills); and constructability of the selected technology. Identification of the poor soil types, their depths and extent, along with their engineering properties, is perhaps the most important consideration here in terms of selecting a preferred geotechnology.

Step 7 is the identification, listing and consideration of general project and geotechnical risks. Project risks can occur from not meeting schedule and/or budget targets, from not identifying geotechnical issues correctly, and from not providing an appropriate or adequate fix to the poor ground situation. Schedule and budget risks can occur due to contractual issues between the general contractor and a specialty contractor, a late notice to proceed, weather affecting production, site access issues, material supply problems, equipment availability issues, and so on. These risks need to be continuously identified and addressed as the project proceeds.

Identification of geotechnical risks generally follows from consideration of the possible occurrence of such issues as slope instability, settlement, liquefaction, contamination, problem soils, etc. These should be identified as part of the subsurface investigation and carried forward as potential risks that can affect the project schedule and performance. The attempted use of a ground modification method that is inappropriate for the actual site soil conditions, which were unidentified in a limited subsurface investigation program, is also a risk that should be identified.

In step 8, preliminary designs for each of the short-listed technologies should be developed. The preliminary designs should define sizes, strengths, and spacing of materials; or at least bound such if some design information is not yet well enough defined. Upon completion of preliminary designs for the candidate technologies, preliminary cost and construction time estimates should be developed.

Tools for use in completing preliminary (and final) designs and for cost estimating are available on the *GeoTechTools* website. Eight assessment and engineering tools for each of the 50⁺ geotechnologies can be accessed through the Catalog of Technologies.

In Step 9, potential alternative, non-ground modification solutions should be identified and listed. There are always alternate solutions available, and these should be evaluated along with the short-listed geotechnologies. Alternative solutions include the use of a bridge system, the use of deep foundations to support the structure, or perhaps rerouting the alignment to avoid the poor ground conditions.

Step 10 is the evaluation of project requirements, constraints, and risks against the factors affecting selection of a solution, for this particular project. For this step, additional geotechnology selection factors are considered. These factors are in addition to the primary factors of application, purpose of ground modification, soils type(s), depth of soils to be improved, etc. considered in the Step 5 development of a short-list of applicable technologies. Additional selection factors may vary by application and project, but may include the following factors: constructability (i.e., availability of material, equipment, staging, access, groundwater, and etc.); speed of construction; construction disruption (amount to traveling public and/or adjacent

structures); longevity of constructed works (service life and maintenance requirements); ROW requirements or restrictions; aesthetics; environmental aspects and concerns; local familiarity with geotechnology; degree of establishment of the geotechnology; design procedure (availability, complexity, codified, etc.); contracting means and practices; cost (initial and life cycle); additional project constraints; and project risks. In this step constraints and risks are explicitly evaluated for their potential effect on the project.

This listing is not project specific and is presented as a tool to help evaluate the short-listed geotechnologies developed in Step 5. For a given project, additional selection factors may be applicable. Many of items may be of little to no importance on a particular project.

The evaluation should be performed by the party that is responsible selection of the geotechnology to be used. Depending on the contracting method used for the project, this evaluation may be performed by the owner, the consulting engineer representing the owner, or the contractor.

Each geotechnology selection factor is evaluated based on its relevancy and importance to the project requirements and site constraints and they are assigned a rating number between zero (0) and three (3). This is termed the weight factor (WF) for a given geotechnology selection factor. Three is assigned to the most relevant or important factors, one is assigned to the least relevant ones and zero (or NA-not applicable) is assigned to non-relevant items. The evaluation results should be tabulated as shown in Table 2. For example, speed of construction, amount of disturbance, longevity of constructed works, and cost are often important selection factors and would, therefore, carry a weight factor of 3.

Table 2 Geotechnology selection factors [5]

Geotechnology selection factor	Weight factor (WF)
Speed of construction	0–3
Minimize construction disturbance	0–3
Longevity of constructed works	0–3
Cost of construction	0–3
Constructability	0–3
ROW requirements or restrictions	0–3
Aesthetics	0–3
Environmental	0–3
Degree of establishment	0–3
Familiarity with geotechnology	0–3
Design procedure	0–3
Contracting	0–3
Life-cycle cost	0–3
Additional project constraint	0–3
Additional project constraint	0–3
Project risk	0–3
Project risk	0–3
Project risk	0–3

In Step 11, the short-listed geotechnologies are assigned a selection factor value. The applicability of all the short-listed alternatives (from Step 5) should be evaluated against Geotechnology Selection Factors that are defined here using a rating between one (1) and four (4). This is a relative rating (RR) of how well the short-listed technologies meet the specific geotechnology selection factor for this project. For each factor, four is assigned to the most suitable factor for the geotechnology being evaluated and one is assigned to the least suitable factor for the geotechnology being evaluated. These ratings are selected based on engineering experience with the short-listed geotechnologies in meeting the selection factors.

Step 12 is the selection of a preferred geotechnology to use on this specific project. This is the final step where alternatives are compared to each other in a geotechnology selection matrix format and the one that has the highest score is selected for the project. The scoring of each alternative is obtained for each geotechnology selection factor by multiplying WF from Table 2 with the 1–4 relative rating for each to obtain the weighted rating (WR) for each geotechnology selection factor. The WR for all the selection factors are then added together to obtain the Total Score for each short-listed technology. The geotechnology which has the highest score should be developed as the base design. Other high scoring geotechnologies may also be included in the Contract Documents as acceptable alternates. An example project selection matrix for one of the short-listed geotechnologies is shown in Table 3. A similar table, or spreadsheet, would be developed for each short-listed geotechnology.

4.2 Additional Considerations

4.2.1 Additional Options with Select Geotechnology

At this stage, the preferred ground modification technology may include additional options. For example the preferred geotechnology could be the use of lightweight fill; but the specific type of lightweight fill is not fully defined. A short-list of potential lightweight fill materials, with geofoam as an option, can be developed, and a similar selection process (see Steps 8, 10, 11, and 12) can be used to find the preferred material for this specific project.

4.2.2 Detailed Subsurface Investigation, Design, and Cost Estimate

Once a geotechnology is selected additional information may be necessary to develop the final design and project cost estimate. Ground modification technologies often require specialized geomaterial parameters for design and construction that are not obtained during preliminary or initial site investigations. Supplemental detailed subsurface investigations are sometimes necessary to obtain the additional

Table 3 Example project selection matrix for one of the short-listed geotechnologies [5]

Geotechnology selection factor	Weight factor (WF)	Geotechnology A relative rating	Geotechnology A weighted rating
Speed of construction	2	3	6
Minimize construction disturbance	2	1	2
Longevity of constructed works	3	4	12
Cost of construction	2	3	6
Constructability	3	1	3
ROW requirements or restrictions	NA	0	0
Aesthetics	NA	0	0
Environmental	1	0	0
Degree of establishment	3	3	9
Familiarity with geotechnology	2	2	4
Design procedure	2	3	6
Contracting	1	4	4
Life-cycle cost	1	3	3
Constraint—construction season	3	2	6
Risk—delay due to settlement time	3	4	12
Risk—quality assurance	2	1	2
Total score			75

information. Details of needed geomaterial parameters are provided in the respective technology summaries of *GeoTechTools*.

A detailed design and cost estimate can then be prepared, with the additional subsurface information in hand. This can be used to confirm preliminary design and cost estimate used in the selection process, and to compare to alternatives.

4.2.3 Other Solutions

This selection process has focused on finding the preferred ground modification geotechnology, for a specific project. In Step 9 of this process, alternative, non-ground modification solutions were identified and listed. These alternative solutions should be compared to the preferred ground modification solution. A similar selection process (see Steps 8, 10, 11, and 12) can be used to evaluate the preferred ground modification solution to the viable, alternative, non-ground modification solutions.

4.2.4 Combination of Geotechnologies

Combinations of geotechnologies can also be considered in the geotechnology selection process. For example, lightweight fill has been used in combination with prefabricated vertical drains and preloading, deep soil mixing, and column supported embankment technologies [4]. Typical complementary technologies and typical combinations are listed on the Technology Fact tool on the *GeoTechTools* system.

5 Lightweight Fill Geotechnology

When one arrives at a list of preferred technologies, the Technology Information pages for each technology can be examined. For example, clicking on the Lightweight Fill link will bring up the screenshot shown in Fig. 3. In addition to geofoam; wood fiber, shredded tires, fly ash, cellular concrete, and lightweight aggregate materials are addressed under this geotechnology. Ratings are provided for each technology on the degree of technology establishment and a technology's potential application to SHRP2 objectives.

Technology Information

Lightweight Fill

A lower unit weight of fill is used for roadway embankment construction and for other applications in combination with other technologies to reduce the magnitude of applied load and seismic horizontal forces so that the total embankment settlement can be reduced and stability can be increased. Advantages include accelerated construction, reduced structural requirements for resisting lateral loads, reduced settlement and stability problems, and suitability for wide variety of projects. This technique is applicable to embankments on soft soils and embankment widening.

Lightweight fill technology refers to six different categories of lightweight fill materials:

- Aggregate (includes pumice, scoria, Expanded Shale, Clay & Slate (ESCS), and slag)
- Cellular concrete (something referred to as foamed concrete)
- Fly ash
- Geofoam
- Shredded tire (sometimes referred to as Tire Derived Aggregate (TDA))
- Wood fiber

Technology Fact Sheet
 Photos
Case Histories

- Boston Central Artery/Tunnel, Boston, Massachusetts
- I-15 Reconstruction, Salt Lake City, Utah

 Design Guidance
 Quality Control/Quality Assurance
 Cost Information
 Specifications
 Bibliography
 Check All Clear



Image credits

Technologies

- ▶ Aggregate Columns
- ▶ Beneficial Reuse of Waste Materials
- ▶ Bio-Treatment for Subgrade Stabilization
- ▶ Blasting Densification
- ▶ Bulk-Infill Grouting
- ▶ Chemical Grouting/Injection Systems
- ▶ Chemical Stabilization of Subgrades and Bases
- ▶ Column-Supported Embankments
- ▶ Combined Soil Stabilization with Vertical Columns
- ▶ Compaction Grouting
- ▶ Continuous Flight Auger Piles
- ▶ Deep Dynamic Compaction
- ▶ Deep Mixing Methods
- ▶ Drilled/GROUTed and Hollow Bar Soil Nailing
- ▶ Electro-Osmosis
- ▶ Excavation and Replacement
- ▶ Fiber Reinforcement in Pavement Systems
- ▶ Geocell Confinement in Pavement Systems
- ▶ Geosynthetic Reinforced Construction Platforms

Fig. 3 Major components of EPS block slope systems [6]

As shown in Fig. 3 a number of information documents about a given technology are accessible from the system. These documents are hot-linked and can be opened from this page or the box shown can be clicked and the selected documents can be printed or saved to a file for further use. These documents are tools for the engineer to use in assessing applicability, developing preliminary designs and cost estimates, developing final designs, writing specifications, and in construction quality assurance for geofoam, and other, lightweight fill applications.

6 Summary

The *GeoTechTools* website is a knowledge base compilation with more than 50 geotechnologies. It includes a geotechnology selection guidance system for embankment and pavement projects to assist users in identifying and screening a variety of geotechnologies for an application. This guidance system assists users in making informed decisions for the selection and implementation of a suitable geotechnology for site specific conditions. Detailed information contained on *GeoTechTools* provides user tools for optimization of design, cost estimating, specifying, constructing, and assuring quality to meet specific project requirements, of the geotechnology selected for a specific project.

Acknowledgements The authors gratefully acknowledge the efforts of research and development team of the SHRP2 R02 project. See www.GeoTechTools.org for a complete listing of this team. This study was funded by the Strategic Highway Research Program 2 of The National Academies. The opinions, findings and conclusions presented here are those of the authors and do not necessarily reflect those of the research sponsor.

The geotechnology selection process presented within, is derived from the U.S. Department of Transportation, Federal Highway Administration's Ground Modification reference manual set [5].

References

1. Schaefer VR, Mitchell JM, Berg RR, Filz GM, Douglas SC (2012) Ground improvement in the 21st century: a comprehensive web-based information system. In: Rollins K, Zekkos D (eds) Geotechnical engineering state of the art and practice, keynote lectures from geocongress 2012, Geotechnical Special Publication No. 226, Geo-Institute of ASCE, Reston, VA, pp 292–293
2. Douglas SC, Schaefer VR, Berg RR (2012) Selection assistance for the evaluation of geoconstruction technologies for transportation applications. J Geotech Geol Eng 30 (5):1231–1247
3. Douglas SC, Schaefer VR, Berg RR (2014) Development of the Geoconstruction information and technology selection guidance system. SHRP2 Report S2-R-2-2, Transportation Research Board, Washington, D.C.

4. Barnsgrover AL, Berg RR, Mitchell JK, Collin JG (2013) White paper on integrated technologies for embankments on unstable ground, Virginia Tech Center for Geotechnical Practice and Research, Report CGPR #74, Blacksburg, VA, 85 p
5. Schaefer VR, Berg RR, Collin JG, Christopher BR, DiMaggio JA, Filz GM, Bruce DA, Ayala D (2016) Ground modification methods. U.S. DOT, Federal Highway Administration, Washington, D.C., FHWA NHI-16-027 (vol I) 386 p and FHWA NHI-16-028 (vol II) 542 p
6. Iowa State University (2010–2017) <http://www.geotechtools.org>. Accessed 16 Oct 2017

N222 Roundabout upon EPS Embankment with Integrated Corrugated Steel Tunnel Structure Without Pile Foundation



Milan Duškov and Jeroen Tameling

Abstract In April 2015 on a location with settlement sensible subsoil surrounded by greenhouses and water channels a large roundabout has been realized using 25,000 m³ EPS geofoam blocks. The roundabout is a part of the regional road N222 which connects Flora Holland (a huge marketplace for floriculture) with the nearest highways. The region is characterized by the largest greenhouse concentration in Europe. Due to its important economic function more than 11,000 vehicles pass the new roundabout over the lightweight embankments daily. During construction, unimpeded traffic passage had to be guaranteed. Below the roundabout a tunnel for the passage of bicycles was designed. Adjacent power line pylons made it impossible to place pile foundations as conventionally used in Dutch areas with peat subsoil. Consequently a structure using concrete tunnels was not an option. Therefore a 3.7 m high egg-form corrugated steel tunnel structure without pile foundations was integrated through the EPS embankment. The applied tunnel system with 7-mm-thick corrugated steel plates supports lightweight foamed concrete built in around. The tunnel structure is settlement free without pile foundations. Additional advantages include its lower building costs compared with conventionally designed tunnels made of concrete. Finally, the construction time was reduced thanks to this innovative design method. The paper deals with the design aspects related to the N222 roundabout structure with the lightweight embankments in general, and with the implemented tunnel solution in particular.

Keywords Project case • Lightweight embankment • Innovative tunnel design
Integrated tunnel construction • Corrugated steel tunnel structure
No pile foundation

M. Duškov (✉)
InfraDelft, Delft, The Netherlands
e-mail: milan.duskov@infradelft.nl

J. Tameling
Waalpartners, Naaldwijk, The Netherlands

1 Introduction

As part of improving the accessibility of greenhouse horticulture, and to stimulate restructuring of the Wateringveldse Polder region, a new connection road has been realized by the municipality of Westland near The Hague. Within that framework, a double-lane roundabout was realized at the junction of the Wateringveldse Polder accessing the regional road N222 (so-called Auction Route). In order to connect the roundabout, a height difference of about 5.5 m had to be realized. The new roundabout was finished in mid-April 2015.

This project had a variety of complex (boundary) conditions. During construction, traffic on the regional road N222 had to have virtually unimpeded passage due to the economic function of the nearby auction. To minimize the settlements despite very weak subsoil layers, a total of approximately 25,000 m³ of EPS was used under the roundabout and in the adjacent road embankments. The project location is characterized by flat polder land and shallow groundwater and it is enclosed between adjacent greenhouse horticulture and the regional access road. Further, west of the new roundabout, the N222 crosses over a 10 m wide canal (called Lange Watering). A new bridge was constructed next to the existing one (Fig. 1).

A new recreational bicycle connection was also part of the project. Because an additional connection over the water was not desirable, tunnel construction beneath



Fig. 1 The realized double-lane roundabout between the Wateringveldse polder and the regional road N222 (=the auction route)

the roundabout and existing provincial road had to be realized. However, a concrete tunnel with pile foundations would cause too much nuisance to the project, due to the longer construction time. High-voltage masts were also in the way, inhibiting construction of conventional pile foundations, so a lightweight variant was considered in order to meet project restraints and to minimize settlements. An original solution was designed and realized through the EPS embankment. The bicycle tunnel includes 7 mm thick corrugated steel sheets with a foamed concrete enclosure integrated into the EPS embankment. Such a prefabricated tunnel system is cheaper and constructable in a shorter period of time than a tunnel made of concrete because no pile foundation is needed.

The municipality of Westland was the owner of this multidisciplinary project, which was coordinated from planning and contracting up to the design by Waalpartners Civil Engineering. The specialists of InfraDelft (responsible for the lightweight road embankments, pavement structures and the tunnel design) and Bergschenhoek Civil Engineering (responsible for the tunnel construction with the corrugated steel sheets) took care of engineering. This paper describes the boundary conditions, selection method for settlement reduction during the design process and the unique integrated bicycle tunnel construction.

2 Complex Boundary Conditions and Trade-Offs

Characteristic of the project is the diversity of design challenges. As the Cone Penetration Test results explicitly pointed out the roundabout location had an evident problem related to thick compressible peat layers. Implementation of traditional preloads within the available construction time was not possible due to the presence of adjacent greenhouses and the regional access road. A bridge height of about 5.5 m had to be realized. Also, the regional road N222 to the west of the new roundabout is crossed underneath by a 10 m wide water canal (*Lange Watering*). Furthermore, the high voltage masts and the local ‘peat quay’ (*veenkade*), within the boundaries of the project, were factors that had to be considered. Finally, traffic on the N222 to nearby Flora Holland auction could not be hindered during construction (Fig. 2).

During the design process, an evaluation was made between possible consolidation mitigation approaches such as implementation of (a) conventional preload, (b) vacuum method, (c) ‘lightweight’ granular materials, (d) piled supported embankments and (e) EPS embankments. Based on the extent to which the evaluated options have influence and/or limitations, the choice was reduced to a further elaboration of three variants. These elaboration methods have been assessed on the following factors: occurring settlements, consolidation period, influence/damage on the ‘peat quay’ (*veenkade*), environmental impact, implementation restrictions and costs. The evaluation finally pointed out that the use of the EPS blocks was the overall, including economically, the best solution for this project. The solution does not provide the lowest construction costs but scores very well on other factors,

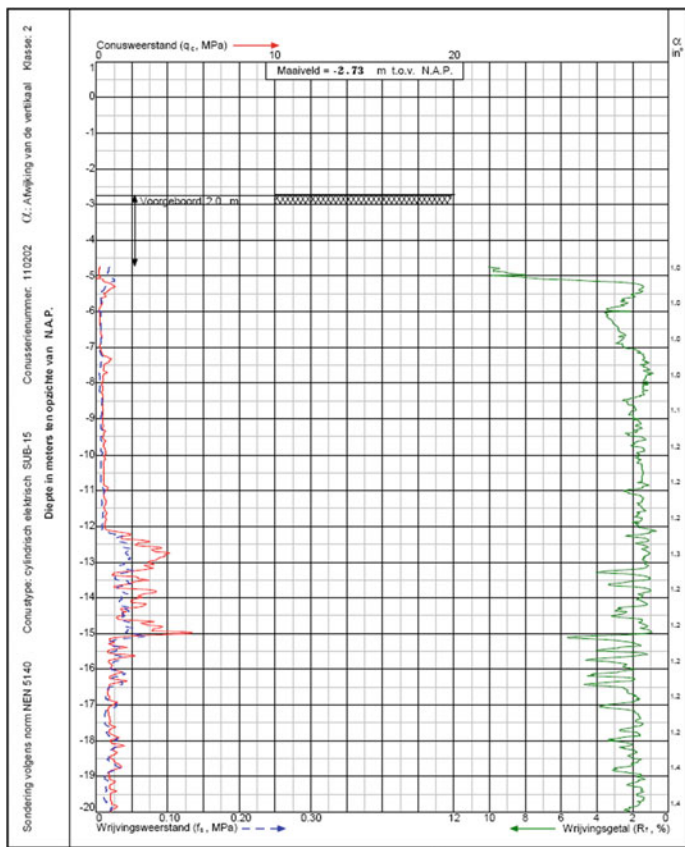


Fig. 2 Characteristic cone penetration test (CPT) results for the project location

including maintenance costs. Given the economic importance of minimizing traffic interruption delays, the municipality of Westland chose the variant which included implementation of EPS geofoam blocks.

During the project process, the municipality of Westland added the recreational bicycle link to the scope. This decision created a design challenge regarding not only technical and financial aspects, but also the realization of such a connection. An additional bridge connection over the canal was not desirable, so a connection through the future roundabout and existing provincial road embankment became the economically most interesting solution. Still, a concrete tunnel was practically not constructable. Therefore, lightweight variants were investigated which could prevent settlement differences between the existing and new road parts and could be quickly constructed.

3 Lightweight EPS Embankments

The height difference between the lower part of the ground level and the highest point in the center of the roundabout is more than 5 m. The local soil is notorious for its settlement sensitivity due to the thick peat and clay layers. The exceptionally high percentage of freight traffic on this Auction Route made the design of such a high roundabout embankment at this location with such unfavourable soil conditions even more challenging. Indeed, the amount of freight traffic had consequences for the asphalt pavement thickness, which was unfavourable to the weight of the pavement structure. Thanks to the ultra lightweight EPS blocks used (approximately 25,000 m³), the vertical load on the subsoil was reduced to a great extent. This also minimized the settlement-related consequences for neighboring objects. Optimum dimensions of the realized EPS embankment were determined iteratively from finite elements analysis using Plaxis models. By using these sophisticated models the expected stress values within the relevant roundabout and road embankment profiles were also controlled. Additionally, those calculations enabled the use of a less expensive type EPS in the embankment parts where lower stress values are expected (Figs. 3, 4 and 5).

4 Unique Design for Lightweight Cycling Tunnel Construction

In order to design a settlement-free tunnel integrated in the EPS embankment of the roundabout, the arching principle was used. The tunnel system used 7-mm-thick corrugated steel plates supporting lightweight foamed concrete. The modular system of corrugated steel sheet elements without a pile foundation fulfilled the specific project requirements of free space for cyclists and pedestrians and suitability for the expected traffic load over the tunnel. In terms of both building costs

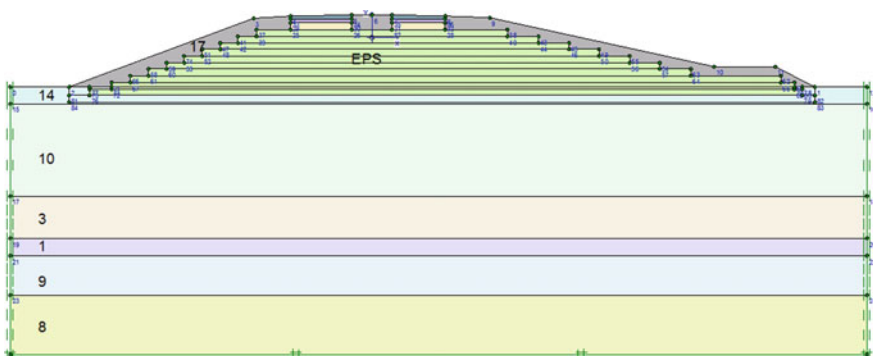


Fig. 3 Plaxis model of a representative profile of the regional road N222

Fig. 4 Lightweight EPS-geofoam embankment (in the north) of the access road and the roundabout of the N222



Fig. 5 Lightweight EPS-geofoam embankment (eastward) of the roundabout of the N222



and construction time reduction, the system offered advantages. The high-voltage masts also made it impossible to use a conventional pile foundation necessary for a concrete tunnel alternative.

The oval tunnel system is based on the load distribution by normal force along the “pressure points” in the steel shell construction. According to the Klöppel & Glock method, interaction between the thin corrugated steel wall of the tunnel and the support pressure—generated by the surrounding mass—was considered. As an alternative to the standard design with compacted sand around the culvert, adequate side support is ensured by a lightweight foamed concrete enclosure combined with stronger EPS blocks. There were no technical restrictions regarding either the profile or the traffic load over the considered tunnel system. In the strength calculation, the tunnel was tested in three aspects.



Fig. 6 Construction of the corrugated steel sheets tunnel under the N222

- Both the arch of the profile and the joint plate connections had to be sufficiently strong.
- The weight of the cover on the tunnel construction had to be sufficient to provide adequate back pressure when maximum traffic loading passes over.
- The foamed concrete enclosure had to be sufficiently strong (Fig. 6).

Considering this project, the lightweight character of the tunnel construction including the foamed concrete enclosure was essential. Obviously, conventional sand fills would lead to unacceptable settlements. A newly developed design methodology offered a cause oriented solution. A reference project did not exist because such a design solution had never been realized before (Figs. 7, 8 and 9).

The entire tunnel design has been calculated using Plaxis models for various representative profiles. Plaxis models were used to analyze and optimize the behaviour of the N222 bicycle tunnel section. In this way, the effects of applying a variety of foamed concrete and EPS types were calculated to figure out adequate tunnel designs (Fig. 10).

Fig. 7 Assembling the corrugated steel sheets





Fig. 8 The corrugated steel sheets covered by the membrane before pouring the foamed concrete enclosure of the cycling tunnel

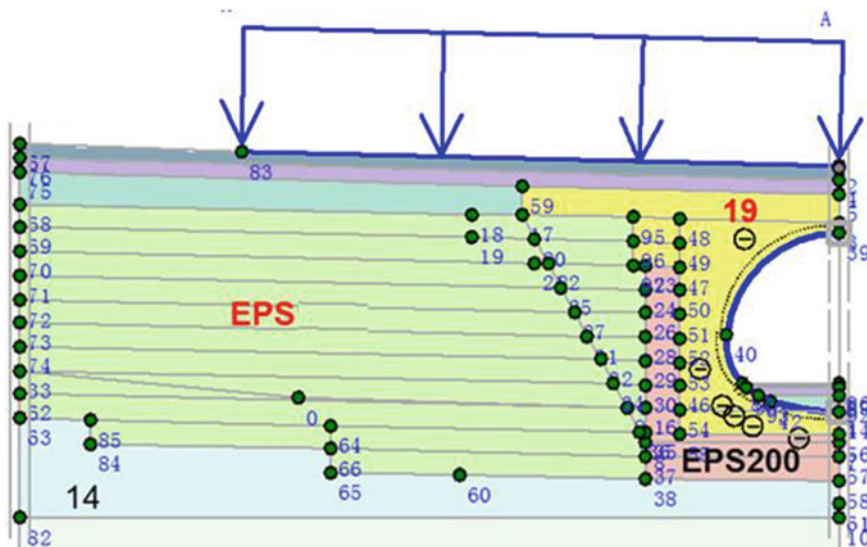


Fig. 9 Plaxis model upper part with the EPS fill under the auction route (N222) and a foamed concrete enclosure around the cycling tunnel



Fig. 10 The auction route (N222) with the cycling tunnel in service

5 Conclusion

The realized road constructions for the Auction Route (N222), with the cycling tunnel below, complies with the project requirements including the required design life. This tunnel design method for modular steel elements integrated in the EPS fill is an ingenious but multi-beneficial solution. The tunnel system with 7-mm-thick corrugated steel sheets and a foamed concrete enclosure was more cost effective than a tunnel made of concrete because no pile foundation was required.

Design and Evaluation of Seismic Stability of Free-Standing EPS Embankment for Transportation Systems



Steven Floyd Bartlett and Zahra Amini

Abstract This paper summarizes a simplified method for evaluating the interlayer sliding potential of free-standing, rectangular, prismatic-shaped EPS geofoam block embankments subjected to strong ground motion associated with major earthquakes. The steps of the method are: (1) estimate the fundamental period of the embankment, (2) determine the design horizontal acceleration for the design earthquake, (3) determine the horizontal inertial force acting at each interface (4) estimate the sliding resistance and factor of safety against sliding at each interfaces and (5) evaluate the need for countermeasures, if necessary. The methods and evaluations summarized herein suggest that interlayer sliding may initiate if free-standing embankments are exposed to pulses of horizontal acceleration exceeding about 0.5–0.6 g. They further suggest that sliding is generally initiated at the lowermost interlayer and propagates upwards through the embankment to its crest. In severe cases, shear keys, adhesive bonding or other restraint mechanical mechanisms may be appropriate to locally disrupt potential sliding planes as a preventative countermeasure against interlayer sliding or excessive block movement near the outer edges of the embankment. Also, results of numerical modeling suggest that the basal edges of the EPS embankment may begin to experience overstressing due to horizontal sway of the embankment when the design horizontal acceleration values are large. For such cases, consideration should be given to using higher modulus EPS blocks at the outer edges of the basal layer to reduce the potential for overstressing.

Keywords Geofoam · Seismic · Earthquakes · Sliding · Design

S. F. Bartlett (✉) · Z. Amini
University of Utah, Salt Lake City, Utah, USA
e-mail: bartlett@civil.utah.edu

1 Introduction and Prior Full-Scale Testing

Free-standing, rectangular prismatic-shaped EPS embankments have been widely used in the United States for transportation facilities including some found in geographical areas with relatively high seismicity (Fig. 1). These embankments must be designed and constructed to resist earthquake shaking. Because the potential for interlayer sliding of the EPS geofoam embankment due to seismic horizontal loads is one of the mechanisms that can affect the internal stability of the geosystem, it is important to fully understand if and at what level of acceleration does sliding initiate during earthquake.

Limited research has been done on seismic stability analysis of free-standing EPS geofoam embankment. In one configuration, Kuroda et al. [1] discuss the testing and numerical modeling of shake table tests on 1/4-scale EPS blocks stacked in a vertical rectangular prismatic configuration that was approximately 1 m high by 1.5 m wide by 1 m deep with a vertical applied stress of 2250 kg/m^2 . These tests showed minor sliding (2 mm) at the base of the EPS test fill for a case without metal fasteners (gripper plates) and where the basal coefficient of friction was estimated to be 0.4 and the test fill subjected to 40 cycles of 400 gal horizontal acceleration applied at the resonant frequency of the fill.

Hotta et al. [2] and Tsukamoto [3] describes full-scale tests on free-standing vertical geofoam embankments conducted in Japan by the EPS Development Organization (EDO). Fills with heights of 3.3, 6.4 and 8.5 m were constructed on a 5 m by 5 m^2 shake table having base/height (B/H) aspect ratios of 1.52, 0.78 and 0.59 m, respectively. Because of the relatively slender B/H ratios of these test fill, the EPS blocks were fixed around the perimeter base of the shake-table. In addition, the EPS blocks were bound together by metal connectors placed at a spacing of 2 connector per square meter. The maximum measured horizontal acceleration achieved in the embankment was 832, 916, 741 and 514 gals at the base, $1/3 \text{ H}$, $2/3 \text{ H}$ and top locations, respectively for a scaled Kobe earthquake input record which had a pga

Fig. 1 Free-standing EPS embankment for light-rail train system, Salt Lake City, Utah, USA



Fig. 2 8.5-m high free-standing EPS embankment test conducted by EDO and Hokkaido CERI in Japan Tsukamoto [3]



value of about 500 gals and a peak spectral acceleration of about 1700 gals from the period ranging from 0.4 to 1.0 s, which matched the spectrum for a design level 2 earthquake in Japan. Some vertical gaping between blocks occurred due to this rather severe motion which were typically 15–25 mm with one maximum gap of 40 mm. Based on these experimental results, Hotta et al. [2] conclude that “aseismic” (i.e., acceptable or anti-seismic) performance of EPS fills to tipping and “pulling out” can be assured for level 2 earthquake motions and that roads constructed on EPS fills should remain functional after major earthquakes. In addition, these authors noted that rocking was initiated during the tests and recommended that high stiffness EPS should be placed in the lowermost layer as a countermeasure (Fig. 2).

2 Design Guidance

In Japan, EDO has developed a “simplified” seismic design process for EPS embankments summarized by Tsukamoto [3] and Hotta [4]. This consists of the following steps: (1) determining the design horizontal seismic intensity coefficient, K_h , which is modified by factors accounting for variation in Japanese seismicity and the H/B ratio of the proposed embankment, (2) determining the fundamental period of the embankment using a simplified formula based on elastic beam theory (discussed later), (3) calculation of an amplification ratio which is used to modify K_h based on the size of the design earthquake and the fundamental period of the embankment. This modified K_h value is used to check the factor of safety against basal and interlayer sliding and overturning. In lieu of the simplified method, Japanese practice allows for a “detailed” method of evaluation to determine the seismic demand placed on the embankment system. Analysis methods under this category include a “response spectrum method,” which uses input spectral accelerations at the fundamental period of the embankment; and a “time history response analysis,” which uses direct input of seismic waves from earthquake records. In the latter method, the EPS embankment is treated as a linear elastic body with varying levels of damping employed based on the

level of input ground motion. The increased damping at higher levels of basal input motion was attributed to friction acting between the blocks which increases the damping occurring during excitation above that of routine material damping. Lastly, similar to the simplified method, the accelerations obtained from the detailed method(s) are used to check for sliding and overturning.

In the U.S., the National Cooperative Highway Research Program (NCHRP) has simplified design guidance regarding the seismic stability of EPS embankments including the potential for global stability and interlayer sliding found in NCHRP Report 529 [5, 6] and NCHRP Web Document 65 [5, 6]. More advanced techniques based on finite difference and discrete interface modeling have been proposed by Bartlett and Lawton [7], Bartlett et al. [8], Amini [9] and Bartlett and Neupane [10]. The following sections of this paper describe a simplified evaluation procedure based on the methods adopted in U.S. and Japanese practice.

3 Fundamental Period Evaluations

3.1 Analytical Methods

Simplified seismic evaluations of any geosystem requires the knowledge of its fundamental period or natural frequency of vibration. Embankment systems generate the maximum displacement response when excited at their fundamental period. In order to develop a rational design procedure, free-standing EPS embankment systems are evaluated numerically and compared with analytical solutions.

Geofoam blocks have a very low mass density, thus the vast majority of the mass in an EPS embankment is located at the top of the EPS flexible body. The potential for amplification of the base motion within the EPS embankment has led researchers to model the system as a classical single-degree-of-freedom (SDOF) system. In such an approach, the EPS geofoam embankment system is generally modeled as a fixed-end cantilevered beam with a concentrated mass on top. This simplifies the EPS geofoam embankment to a cantilevered Timoshenko beam, the length and width of which are equal to the height and width of the EPS geofoam embankment respectively [11, 12].

Stark et al. [5] have proposed Eq. 1 for calculating the fundamental period:

$$T_0 = 2\pi \left\{ \frac{\sigma'_{v_0} H}{E_{t_i} g} \left[4 \left(\frac{H}{B} \right)^2 + \left(\frac{12}{5} \right) (1 + v) \right] \right\}^{0.5} \quad (1)$$

where B and H are the width and height of the embankment respectively. σ'_{v_0} is vertical effective stress acting on top of the EPS, E_{t_i} and v are the initial tangent Young's modulus and Poisson's ratio of the EPS respectively, and g is the gravitational constant. The derivation of Eq. 1 considers flexural and shear stiffness of the beam. An alternative for calculating the fundamental period of the EPS geofoam embankment system, known as the Japanese Design Equation [4] is:

$$T_0 = 2\pi \left[\left(\frac{\sigma'_{v_0} H}{g E_{t_i}} \right) \left(4 \left(\frac{H}{B} \right)^2 + \left(\frac{12}{5} \right) (1 + v) + 1 \right) \right]^{0.5} \quad (2)$$

where all terms have been previously defined. This derivation includes the flexural, shear and axial stiffness of the beam.

3.2 Numerical Methods

The dynamic behavior of a vertical, free-standing, geofoam embankment has been simulated by Bartlett and Lawton [7] and Amini [9] using the finite difference method (FDM) as incorporated in the commercially-available 2D computer program named Fast Lagrangian Analysis of Continua 2D (FLAC 2D) [13]. The geometries modeled by Amini [9] included eight different heights, 5, 6, 7, 8, 9, 10, 12 and 15 m producing B/H aspect ratios of 0.6, 0.8, 1, 1.5, 2, 2.5 and 3, respectively. A 1-m thick, relatively stiff mass was modeled atop the EPS embankment body representing a concrete load distribution slab (LDS) and capping pavement section. The EPS geofoam was modeled as a coherent mass at this stage of the study rather than as individual blocks. Material properties indicated in Table 1 were used, and the properties of the lumped mass were adopted from work of Bartlett and Lawton [7].

A harmonic velocity wave comprised of only the horizontal component of motion was imposed at the base of the embankment. This input wave was set up in a way that at time zero, zero velocity would be applied to the model. No vertical wave was applied, and no material damping was assigned to the model; thus for these initial analyses, the system underwent forced, undamped vibration to evaluate the fundamental period, T_0 , of the EPS embankment. In addition, because the design ground motion is usually specified as a free-field motion at the ground surface, the input wave was applied at the base of the EPS embankment without including soil layers in the model. This approach assumes that there is minimal soil-structure interaction between the EPS embankment and the underlying soil. This is a reasonable assumption as verified by Amini [9] because of the relatively low mass of the EPS system, which minimizes inertial interaction; and the shallow embedment of the basal blocks, which minimizes kinematic interaction.

Table 1 EPS geofoam and material properties used for FLAC modeling [9]

Material	ρ (kg/m ³)	E (MPa)	v	G (MPa)	K (MPa)
EPS	19	7	0.1	3.2	2.9
Lumped mass	2321	30,000	0.2	12,712	15,625

ρ = mass density, E = Young's modulus, v = Poisson's ratio, G = shear modulus, K = Bulk modulus

A trial-and-error method was used to find the fundamental period of the EPS geofoam embankment. The procedure included manually changing the period of the input wave in the model and monitoring the displacement of the embankment at the uppermost nodes (i.e., top of the lumped mass). In the absence of damping, the system displayed an ever-increasing displacement at resonance. Once this behavior was observed for each model, the assigned input wave period was recorded as the fundamental period of the embankment system. The results of 56 analyses of embankments with various aspect ratios are presented in Fig. 3. In order to compare the results of the equations discussed above with those of the numerical modeling, the percent error of fundamental period values was calculated and normalized to the numerical results as follows:

$$\left[\frac{T_{Theoretical} - T_{FLAC}}{T_{FLAC}} \right] \times 100 \quad (3)$$

where $T_{theoretical}$ is the fundamental period calculated from either Eq. 1 [5, 6] or Eq. 2 (Japanese Design Equation). T_{FLAC} was calculated from the simulations.

Based on the results presented in this figure, Eq. 1 appears to underestimate the fundamental period value for all aspect ratios, whereas Eq. 2 generally overestimates the values of fundamental period for aspect ratios greater than 1. Based on this comparison, Eq. 1 is recommended for B/H aspect ratios of 1.5 or greater; whereas Eq. 2 is recommended for B/H aspect ratios less than 1.5. For other embankment configurations that are not rectangular prismatic in shape, these equations are not recommended; instead, T_0 should be evaluated used numerical methods in order to avoid considerable error [10].

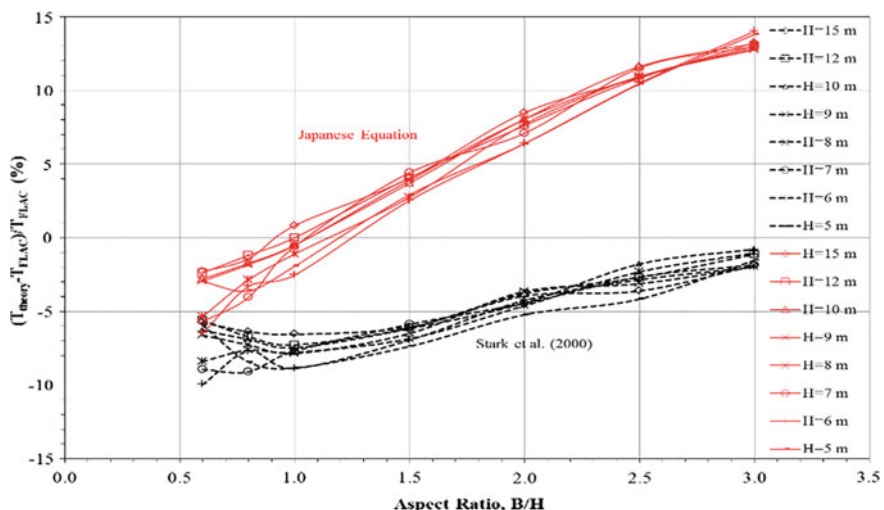


Fig. 3 8.5-m high free-standing EPS embankment test conducted by EDO and Hokkaido CERI in Japan Tsukamoto [3]

4 Design Acceleration

In the U.S. the acceleration response spectrum used for bridge design consists of spectral ordinates obtained from the United States Geological Survey [14]. For the site shown in Fig. 1, the design pga value is about 0.4 g and the S_{DS} (short period spectral acceleration) and S_{D1} (1 s period spectral acceleration) values are about 0.971 and 0.987 g, respectively, based on design guidance developed by the American Association of State Highway and Transportation Officials (AASHTO) and for a site class E profile (soft soil). The response spectrum for this is shown in Fig. 4 using information from AASHTO [15].

For countries that have not adopted probabilistic-based ground motions, it is possible to develop deterministic design spectra based on regional ground motion predictive equations.

5 Horizontal Inertial Force

The horizontal acceleration varies from the basal level to the crest of the embankment due to its flexible nature and potential for resonance. In order to calculate the maximum horizontal acceleration at different levels within the embankment, both NCHRP Web Document 65 and NCHRP 529 guidance recommend linear interpolation between the base acceleration (i.e., peak ground acceleration, pga) and the crest acceleration obtained from the design response spectrum at T_0 . This assumption was further investigated by Amini [9] using elastic FLAC analyses with 2% Rayleigh damping. A horizontal acceleration of 0.1 g was input at the base ($a_{b,max}$) and maximum acceleration at 1-m increments were

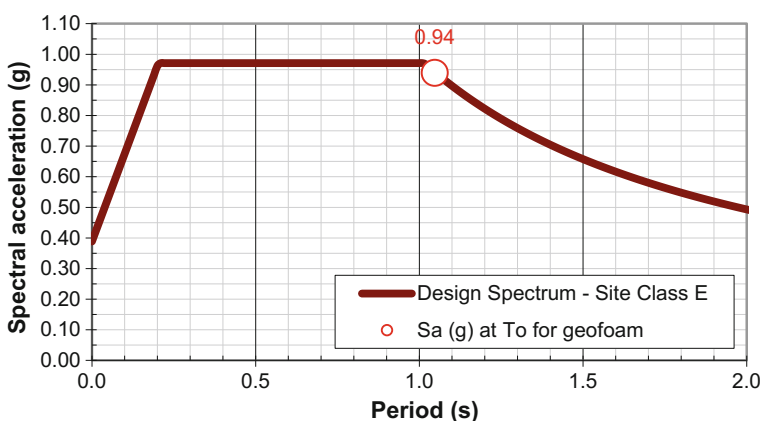
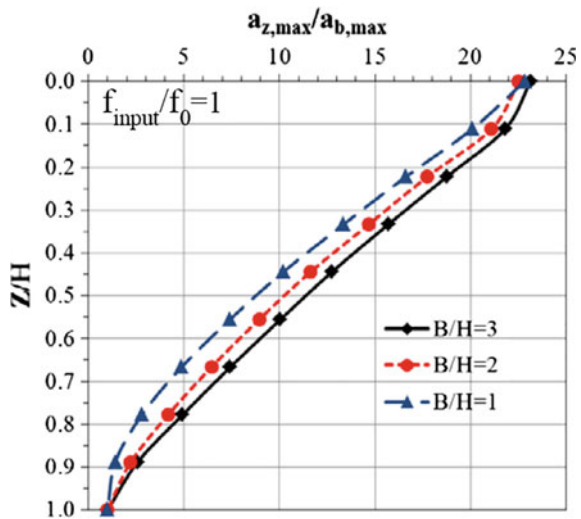


Fig. 4 Design acceleration response spectrum for 14-m high free-standing EPS embankment in Salt Lake City, Utah

Fig. 5 $a_{z,\max}/a_{b,\max}$ values as a function of Z/H for various B/H aspect ratio [9]



obtained ($a_{z,\max}$) within the model for various Z (depth below crest) to embankment height (Z/H) ratios for a 9 m high embankment. For 3 aspect ratios evaluated, the maximum normalized response ($a_{z,\max}/a_{b,\max}$) was about 23 times larger at the crest ($Z/H = 0$) than the input motion at the resonance frequency case (i.e., $f_{\text{input}}/f_0 = 1$). Notwithstanding this large amplification, the accelerations calculated at various levels suggest that the $a_{z,\max}/a_{b,\max}$ values vary in a linear approximation (Fig. 5), especially for B/H aspects ratios of 2–3, which are commonly found in bridge approach fills.

Higher modes of vibration were also investigated by Amini [9], but were found to be relatively unimportant when compared with the fundamental mode of vibration in determining the distribution of $a_{z,\max}/a_{b,\max}$ in the evaluated prototype embankments.

6 Sliding Resistance and Factor of Safety

For pseudostatic evaluations, the frictional sliding resistance at each interface is calculated using the normal stress (i.e., vertical stress) acting at the interface multiplied by coefficient of friction acting at the interface and by the percentage of area available to resist sliding. The weights and thicknesses of the pavement section and LDS are used to calculate the vertical stress obtained from 1D static calculations. Also, the weight of the EPS is typically neglected in these calculations due to its very low value. Interface coefficient of friction values should be determined from testing for the various materials. In our evaluations, the coefficient of friction for geofoam-to-geofoam and geofoam-to-soil interfaces were estimated to be 0.8 and 0.6, respectively, based on direct shear testing from the I-15 Reconstruction Project [16].

In addition, any potential bonding that develops between the EPS and the overlying concrete load distribution slab might be included if: (1) it can be reasonably obtained from experimental data, and (2) such a bond can be shown to persist throughout the design life of the embankment. Nonetheless, testing experience has shown that this is a relatively strong bond, and sliding at this interface is less likely due to the high friction and cohesion developed.

The factor of safety against sliding, FS, is calculated as:

$$FS = F_i/F_r \quad (4)$$

where F_i and F_r are the inertial and resisting forces, respectively acting at each interface. F_i equals the horizontal acceleration interpolated at each layer, as described in Sect. 5 and F_r equals the vertical stress per unit area times the interface coefficient of friction. A design FS value of 1.2 is recommended for all interfaces based on NCHRP guidance and Bartlett et al. [8].

7 Countermeasures

If the design FS values are too low, shear keys and/or adhesive bonding can be used in order to prevent interlayer sliding in EPS geofoam embankments [9]. Shear keys have been used in various EPS embankment construction projects to increase sliding resistance [8]. Commercially available adhesive may offer another efficient solution to prevent interlayer sliding. The use of adhesive prevents the EPS blocks from sliding atop each other thereby mobilizing the cohesive shear strength of the EPS geofoam in the glued blocks; hence forming a shear key. Lastly, for very large masses, such as light-weight bridges supported on EPS, a cabling restraint system has been proposed and evaluated by Bartlett and Neupane [10] in order to prevent interlayer sliding and excessive rocking of the EPS bridge support system.

8 Other Considerations

The methods thus far described herein have not accounted for potential damping effects within the embankment caused by the initiation of sliding. Once initiated, the acceleration response in the embankment is dramatically reduced. Results of non-linear interlayer sliding evaluations performed by Amini [9] show that relative movement between interfaces occurs relatively early in the FLAC dynamic model and is generally initiated at the lowest most interface and propagates upwards to the crest of the embankment. This relative movement appears to be a very efficient energy dissipation mechanism. Not only does it decrease the amount of dynamic sliding with time, but also once initiated, isolates the higher levels of the embankment from large horizontal accelerations. The initiation of sliding and its

attendant frictional damping is probably the reason why increased damping values were required in the numerical models summarized by Hotta [4] at higher levels of input motion (see Sect. 2 of this paper).

Figure 6 compares the maximum relative sliding between layers versus inputted basal sinusoidal horizontal acceleration for cases with and without the application of vertical motion. For the latter case, the applied vertical motion was input as 40% of the horizontal value and applied at a frequency equal to the vertical fundamental period of excitation.

These results suggests that significant interlayer sliding (i.e., sliding greater than 1 cm) begins at horizontal accelerations of 0.5–0.6 g. In addition, the presence of the vertical component of input motion leads to larger values of interlayer sliding; however its influence diminishes as the level of input motion increases; and it has no effect on sliding displacement at horizontal acceleration levels approaching 1 g. If sliding is prevented by construction countermeasures (e.g., shear keys, bonding, or cabling), the increase seismic energy due to less damping may introduce higher shear and compressional stresses at the base of the embankment as the embankment attempts to initiate rocking. For example, Fig. 7 shows that the basal corners of the EPS embankment may suffer from overstressing due to increased compressional and shear forces at the corners. For these zones, consideration should be given to using higher modulus EPS.

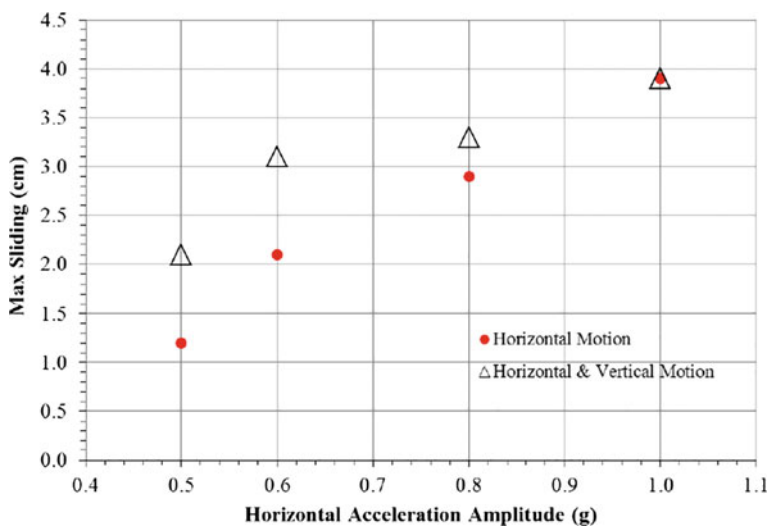


Fig. 6 Maximum block sliding versus input acceleration from FLAC interface modeling

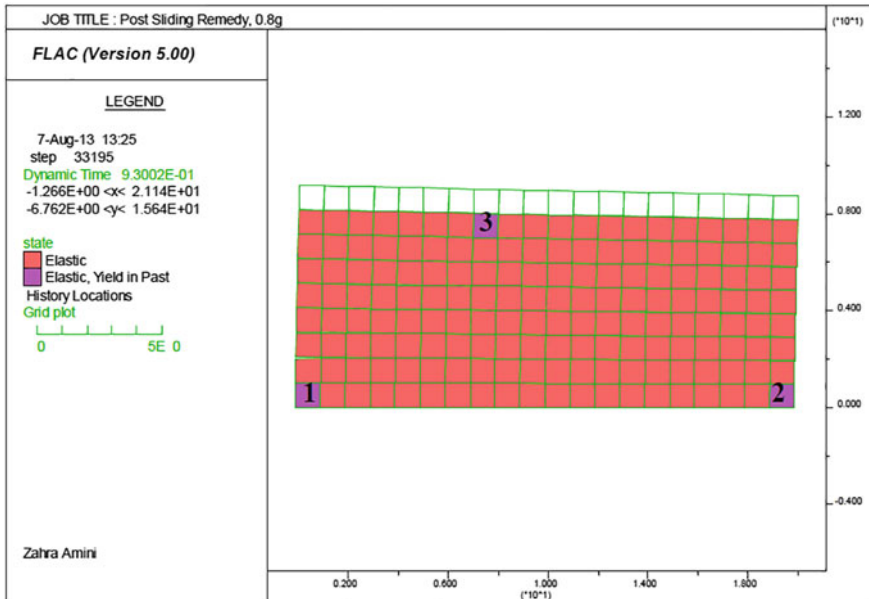


Fig. 7 Potential overstressing of corners of basal EPS blocks due to 0.8 g horizontal input acceleration

9 Conclusions

This paper has presented a straight-forward way of evaluating the dynamic stability of routine, free-standing vertical embankments based on a combination of pseudostatic and dynamic evaluations. Generally, horizontal accelerations of 0.5–0.6 g applied at the fundamental period of the embankment are necessary to initiate sliding. Such sliding can be easily prevented by using shear keys or adhesive in strategic areas of the embankment. However, in order to understand and evaluate the full dynamic behavior, it is important to consider the discrete block and layered nature of the embankment using evaluations based on more detailed dynamic models.

References

1. Kuroda S, Hotta H, Yamazaki F (1996) Simulation of shaking table test for EPS embankment model by distinct element method. In: International symposium on EPS construction method—EPS TOKYO '96, Japan, pp 83–92
2. Hotta H, Kuroda A, Nishi T (2001) Behavior of double-vertical-wall-EPS 2001 conference, Salt Lake City, Utah, USA type EPS fills during major earthquakes. Paper presented in *EPS 2001* conference, Salt Lake City, Utah, USA

3. Tsukamoto H (2011) History of R&D and design code for EDO-EPS method in Japan. Paper presented in EPS 2011 conference, Oslo, Norway
4. Hotta H (2001) Aseismic design of expanded poly-styrol fill in Japan. Paper presented in EPS 2001 conference, Salt Lake City, Utah, USA
5. Stark TD, Arellano D, Horvath, JS et al (2004a) Guideline applications in the design and construction of highway embankments. NCHRP Web Document Report 65, Transportation Research Board, Washington, D.C. <https://www.nap.edu/catalog/21944/geofoam-applications-in-the-design-and-construction-of-highway-embankments>. Accessed 9 Oct 2017
6. Stark T D, Arellano D, Horvath, JS et al (2004b) Guideline and recommended standard for geofoam applications in highway embankments. NCHRP Report 529, Transportation Research Board, Washington, D.C. <https://www.nap.edu/download/13759>. Accessed 9 Oct 2017
7. Bartlett SF, Lawton EC (2008) Evaluating the seismic stability and performance of freestanding geofoam embankment. In: 6th national seismic conference on bridges and highways, Charleston, SC, USA
8. Bartlett SF, Lawton EC, Trandafir AC, Lingwall BN (2011) Applications of EPS Geofoam in design and construction of earthquake resilient infrastructure. Paper presented in EPS 2011 Conference, Oslo, Norway
9. Amini ZA (2014) Dynamic characteristics and seismic stability of expanded polystyrene geofoam embankments. Dissertation, University of Utah
10. Bartlett SF, Neupane R (2017) Seismic evaluation of expanded polystyrene (EPS) geofoam bridge support system for overpass structure. Mountain Plains Consortium (MPC) Technical Report No. MPC-422, 133 p
11. Horvath JS (2004) A technical note regarding calculating the fundamental period of an EPS-Block-Geofoam embankment. Report No. CGT-2004-1, Manhattan College, School of Engineering, Bronx, NY, USA
12. Stark TD, Arellano D, Horvath JS, Leshchinsky D (2000) Guidelines for geofoam applications in embankment projects. Interim (Phase I) Report—National Cooperative Highway Research Program Project No. 24-11, submitted to the Transportation Research Board by the University of Illinois at Urbana-Champaign in cooperation with Horvath Engineering, P.C. and ADAMA Engineering, Inc
13. Itasca Consulting Group, Inc (2005) FLAC: Fast Lagrangian analysis of continua: structural elements, Version 5. Minneapolis, Minnesota
14. USGS (2017) <https://earthquake.usgs.gov/hazards/designmaps/usdesign.php>. Accessed 9 Oct 2017
15. AASHTO (2009) Guide specifications for LRFD seismic bridge design, 1st edn. <https://bookstore.transportation.org/>
16. Bartlett SF, Negussey D, Kimble M, Sheeley M (2000) Use of geofoam as super-lightweight fill for I-15 reconstruction. Transportation research board 79th annual meeting, Washington, DC

Expanded Polystyrene (EPS) Geofoam Columns in Expansive Soil: Preliminary Swelling Characteristics Evaluation



S. Selvakumar and B. Soundara

Abstract EPS geofoam is an excellent material for building road embankments on very soft soils, in slope stabilization, for reducing earth pressures acting on rigid structures, etc. Expansive soils give major challenges to geotechnical engineers because of high swelling and shrinkage characteristics that may severely damage the lightly loaded structures. Limited studies are available for the possible use of EPS geofoam for the reduction of vertical swelling of expansive soils. Columns techniques are preferable for deep stabilization of highly problematic soil. The use of compressible inclusion such as EPS geofoam column technique can be used to control the swelling potential of expansive soils. In this paper, an attempt has been made to study the effectiveness of EPS geofoam columns to control the vertical swelling of expansive soil with and without inclusions. For this study, EPS specimen with bulk density of 12 kg/m^3 (EPS12) was chosen and column diameters were varied to study the effect of area replacement ratio (A_r) on swelling characteristics. Laboratory swell tests have been carried out on statically compacted swelling clay with and without EPS geofoam columns (EPSC) with varying diameter. Tests results show that there is a reduction in the vertical swelling of soil with the inclusion of EPSC when compared to the soil without inclusion. Also with the increase in A_r of EPSC, there is significant reduction in the swell potential of the soil.

Keywords EPS geofoam column • Expansive soil • Swelling characteristics
Soil stabilization

1 Introduction

Expansive soils severely damaged the lightly loaded structures by uplift or volume changes as they swell when absorb the water and shrink upon evaporation of water [1]. Hence, it is necessary to place all the civil engineering structures on significant

S. Selvakumar (✉) · B. Soundara
Bannari Amman Institute of Technology, Sathyamangalam, India
e-mail: selva.geotech@gmail.com

depth and also on stabilized soils [2]. The worldwide estimated annual cost of damages of expansive soil is many billions [3]. In India, approximately one-third of land areas are covered with expansive soils (i.e., Black Cotton soils) predominantly spread over in the states of Madhya Pradesh, Maharashtra, Andhra Pradesh, Gujarat, Tamil Nadu, Karnataka and some other parts. These soil deposits in India are favourable to farmers but problematic to geotechnical engineers because of high swelling and shrinkage characteristics [4]. For any engineered construction activity on expansive soils, the primary step is to evaluate the problems by the determination of swelling or heave and swelling pressure in laboratory studies. Then the secondary step is to control the problems posed by expansive soils with some innovative techniques available for stabilization. Among all these techniques, the preferable solutions for deeper soil stabilization is column techniques [5–7]. Some of the traditional columns techniques such as Lime-slurry injection, Granular piles, Lime columns, Fly ash columns have been suggested for mitigating swelling or heave problems [1, 8, 9]. The functions and applications of soils with geosynthetics is now well defined and another innovative techniques to counteract swelling or heave [10, 11]. Very recently, some researchers reported the application of geosynthetics in expansive soils to reduce the swelling or heave and swelling pressure using geopiles reinforcement, EPS geofoam inclusions placed vertically and horizontally between expansive soil and rigid structures by laboratory studies [5, 12, 13]. The reliable results of the previous laboratory studies suggest placing of geopiles and geofoam inclusions in the field are possible but the material cost is quite high and also granular materials are scarce in many areas. So in this present study, a research attempt is aimed at using EPS geofoam as column inclusion in expansive soils for reducing the vertical and lateral swell. Also studied the effect of different diameter of EPS geofoam Column (EPSC) inclusion on the swelling potential of the soil.

2 Materials and Methods

2.1 Test Materials

2.1.1 Bentonite

The commercially obtainable sodium bentonite containing montmorillonite as a major constituent was used for this study. The reason for carried out laboratory tests on bentonite is due to its very high swelling properties. The physical index properties of the bentonite used in the experimental investigation are summarized in Table 1. The free swell tests were conducted on the bentonite sample as per IS 2720-40 and based on the differential free swell index value, it can be classified under clay with very high degree of expansiveness. According to USCS classification system, based on the soil plasticity it is classified as clay of high compressibility (CH).

Table 1 Index properties of bentonite

Property	Value
Specific gravity	2.80
Liquid limit (%)	278
Plastic limit (%)	32
Plasticity index (%)	246
Shrinkage limit (%)	8
Optimum moisture content (%)	37
Maximum dry unit weight (kN/m ³)	13.54
Unified soil classification	CH
Differential free swell index (%)	450
Principal clay mineral	Montmorillonite

2.1.2 EPS Geofoam Column

The rectangular blocks of EPS geofoam were obtained commercially from non-proprietary with the desired density. The significance of EPS geofoam in geotechnical application are briefly reported [14]. For performing the function of compressible inclusion applications, the lower density EPS geofoam up to 20 kg/m³ is advisable [15]. In this present study, EPS geofoam with an average (nominal) density of 12 kg/m³ referred as Type I as per ASTM C-578 standard is chosen to be the column material.

2.2 Tests Conducted

Laboratory swelling tests were performed for the reconstituted specimen at placement condition of Optimum Moisture Content (OMC) and Maximum dry density (MDD). The tests were conducted for soil specimen with and without EPSC inclusion. The details of the laboratory tests are given in the following sections.

2.2.1 Swell Test Apparatus

Swell tests on soil specimen with and without EPSC inclusion in California Bearing Ratio (CBR) mould was experimentally investigated. The perforated base CBR mould with an inner diameter of 150 mm and the height of 175 mm was used for this study. The apparatus consists of a perforated swell plate with an adjustable stem, lock nut and magnetic stand for placing the dial gauge. All accessories are corrosion resistant since they are fabricated with gunmetal.

2.2.2 Specimen Preparation

The commercial bentonite was used to study the swell characteristics of specimen with and without EPSC inclusion. The soil specimens were prepared at the respective OMC and MDD obtained from the standard proctor compaction curve. Before placing the sample in the mould, the inner surfaces of the mould were coated with silicone grease to reduce the internal friction. Then the specimen was statically compacted using prefabricated metal spacers placed above the sample to achieve the decided thickness of 100 mm. The remaining height (more than one-third height of mould i.e. 75 mm) is sufficient for the specimen to swell freely on imbibing water [2, 5]. A filter paper was placed on the top and bottom of the compacted specimen to prevent the clogging of soil grains into the pores of base plate and the swell pressure plate. Then the mould was fixed to the base plate by means of screws. A seating pressure of 1 kPa was applied over the soil specimen by providing 50 mm thick river sand. Then the test specimen was placed in the soaking tank for water inundation and the swell readings were monitored using dial gauges.

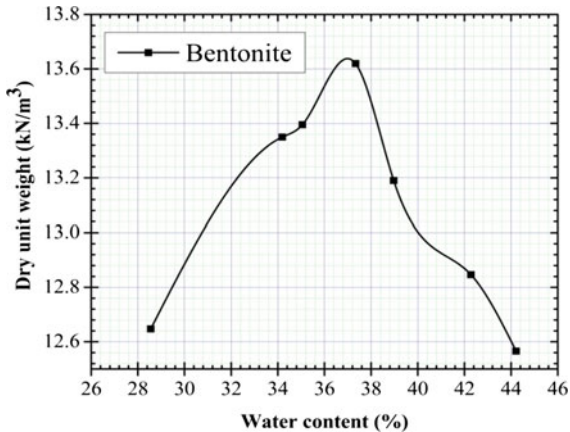
2.2.3 Column Preparation

For easy handling, the full-size blocks were cut into rectangular blocks at the factory itself where large foam cutting equipment is available; however, the cylinder/column shape cutting was done at the laboratory. Experience gathered from factory cutting indicates that adherence to make prefabricated compact size foam cutter with 240 V AC input and maximum 30 V output DC was fabricated and used to cut the rectangular EPS block into cylinder/column shape of 25 and 50 mm diameter and uniform length of 100 mm shown in Fig. 1a and used for the laboratory study.



Fig. 1 Column formation **a** EPSC, **b** vertical hole

Fig. 2 Compaction characteristics of bentonite



2.3 Laboratory Procedure

In order to analyze the variations of swelling behaviour of bentonite with and without EPSCs inclusion laboratory investigations were carried out to measure the swell/heave of the specimen. Initially, the index properties and compaction characteristics of bentonite were arrived by carrying out laboratory Atterberg limit and standard proctor compaction tests. The results of compaction studies (Fig. 2) such as OMC and MDD were used to prepare and compact the soil specimens for the swell pressure tests. The tests were performed on the statically compacted specimen in the CBR mould with surcharge load of 1 kPa mentioned in the ASTM D4546 [16].

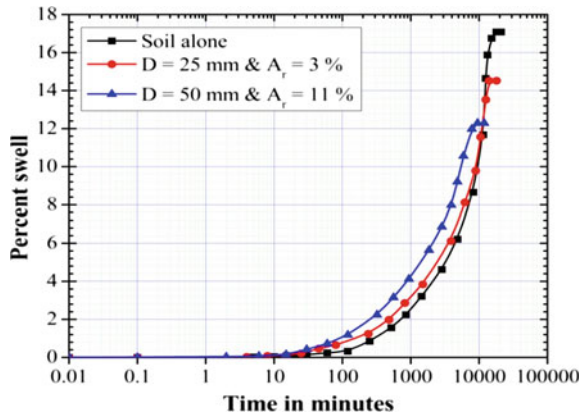
In the case EPSC tests, the vertical hole formation of 25 and 50 mm in the soil specimen by using steel tubes and appropriate top and bottom guide plates. The static compaction of the soil specimen was done by using a prefabricated metal spacer with maximum diameter hole at the center for forming varying diameter hole in the soil samples. Upon completion of static compaction, the desired thickness and diameter of the hole was formed shown in Fig. 1b. Utmost care was exercised not to disturb the surrounding soil while removing the guide plate and extruding the steel tube from the compacted specimen. The top and bottom guide plates were replaced with standard filter paper and the vertical hole was filled with an appropriate diameter of EPSC columns.

3 Results and Discussions

3.1 Effect of EPSCs in Swelling Behaviour

Figure 3 shows the time versus percent swell under seating pressure of 1 kPa and the plots are significant since they give the rate of swell occurring in the bentonite with and without EPSC inclusion. The results indicate that the maximum vertical

Fig. 3 Time versus percent swell for varying EPSC diameter



swell of the soil is decreased with the inclusion of EPSC. This is due to the fact that EPSC acts as a compressible inclusion in swelling clay and offered room to accommodate the lateral swell and hence reduce the vertical swell. Also, the rate of swelling was slightly faster with the inclusion of EPSC and this may be due to the water absorption capacity of EPS. The water absorption of EPS as per ASTM C272-12 standard test method shows the result of 4.65% for EPS12. Additionally, the authors feel it is appropriate to discuss the role of EPSC as a compressible inclusion in swelling clay since it has minimal influence on the rate of swelling because of its very low the water absorption capacity [17].

3.2 Effect of A_r on Max Percent Swell

The replacement of swelling clay is done by compressible EPSC inclusion with two different area replacement ratio (A_r) of 3 and 11% and the results in terms of maximum percent swell versus A_r is shown in Fig. 4. From Fig. 4, it is observed that with the increase in A_r , the maximum (Max) percent swell was decreased significantly when compared to the soil without inclusion, this is expected. The reason for this observation is due to the high compressible characteristics of EPSC, which can accommodate the lateral swell and hence there is reduction in the vertical swell.

The percentage reduction in the maximum swell for EPSC inclusion when compared with the soil alone are summarized in Table 2. From the table it can also be seen that with the increase in A_r , there is considerable amount of percentage reduction in the vertical swelling.

Fig. 4 Variation of max. percent swell versus area replacement ratio (A_r)

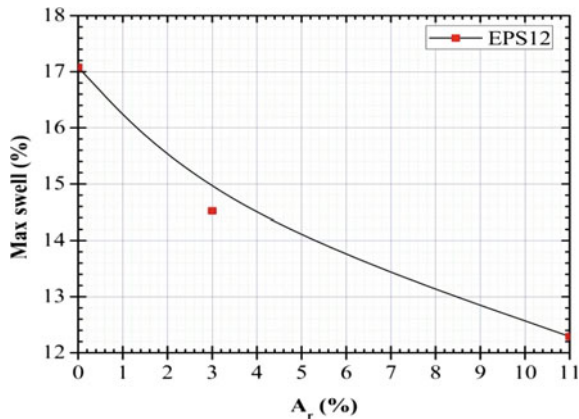


Table 2 Summary of the measured percent swell

$A_r (\%)$	Percent swell	Reduction in percent swell (%)
0	17.08	—
3	14.52	14.98
11	12.29	28.04

4 Summary and Conclusions

The preliminary swelling characteristics of high swelling sodium bentonite stabilized with two different diameter EPSCs are experimentally investigated. From the laboratory results, the following conclusions are drawn:

- The maximum vertical swell of the soil is decreased with the inclusion of EPSC. Expansive soils swell both vertical and lateral directions. Also, the rate of swelling was slightly faster with the inclusion of EPSC and this may be due to the water absorption capacity of EPS geofoam, which is marginal effect only.
- The diameter of EPSC controls the measured maximum percent swell which is specified in terms of area replacement ratio (A_r). With the increase in A_r there is a reduction in the maximum percent swell. However, further investigations are required to find out the optimal A_r for field applications.
- The present study only investigates the nominal density of EPS12 in swelling characteristics of bentonite with EPSC inclusion. More studies are needed to discover the optimal density of EPSC in swelling clay.
- EPSC inclusion can be installed in the expansive soil site to a greater depth by inserting the inclusion in a pre-bored hole extending up to the active depth and hence used to stabilize the deeper strata of expansive soils in cost-effective manner.

Acknowledgements This investigation was supported financially by Department of Science and Technology Science and Engineering Research Board (DST-SERB) India under Early Career Research scheme is gratefully acknowledged by the authors.

References

1. Chen FH (1988) Foundations on expansive soils. Elsevier Scientific Publishing Co., Amsterdam
2. Nagaraj HB, Munnas MM, Sridharan A (2009) Critical evaluation of determining swelling pressure by swell-load method and constant volume method. *Geotech Test J* 32:305–314. <https://doi.org/10.1520/GTJ102051>
3. Viswanadham BVS, Phanikumar BR, Mukherjee RV (2009) Swelling behaviour of a geofiber-reinforced expansive soil. *Geotext Geomembr* 27:73–76. <https://doi.org/10.1016/j.geotexmem.2008.06.002>
4. Katti RK (1979) Search for solutions to problems in black cotton soils. First IGS Annual Lecture, Indian Geotechnical Society at Indian Institute of Technology, Delhi, India
5. Sharma RS, Phanikumar BR (2005) Laboratory study of heave behavior of expansive clay reinforced with geopiles. *J Geotech Geoenvironmental Eng* 131:512–520. [https://doi.org/10.1016/\(ASCE\)1090-0241\(2005\)131:4\(512\)](https://doi.org/10.1016/(ASCE)1090-0241(2005)131:4(512))
6. Thyagaraj T, Suresh P (2012) In-situ stabilization of an expansive soil in desiccated state In-situ stabilization of an expansive soil in desiccated state. *Int J Geotech Eng* 6:287–296. <https://doi.org/10.3328/IJGE.2012.06.03.287-296>
7. Jamsawang P, Nuansrithong N, Voottipruex P, Songpiriyakij S, Jongpradist P (2017) Laboratory investigations on the swelling behavior of composite expansive clays stabilized with shallow and deep clay-cement mixing methods. *Appl Clay Sci* 148:83–94. <https://doi.org/10.1016/j.clay.2017.08.013>
8. Phani Kumar BR (1997) A study of swelling characteristics of Granular Pile Anchored Foundation system in expansive soils. Ph.D. Thesis, Jawaharlal Nehru Technological University, Hyderabad, India
9. Ingles OG (1970) Mechanism of clay stabilization with inorganic acids and alkalis. *Aust J Soil Res* 8:81–95
10. Koerner RM (2012) Designing with geosynthetics. Prentice-Hall, Upper Saddle River, NJ
11. Al-Omari RR, Hamodi FJ (1991) Swelling resistant geogrid-A new approach for the treatment of expansive soils. *Geotext Geomembr* 10:295–317. [https://doi.org/10.1016/0266-1144\(91\)90008-K](https://doi.org/10.1016/0266-1144(91)90008-K)
12. Ikizler SB, Aytekin M, Nas E (2008) Laboratory study of expanded polystyrene (EPS) geofoam used with expansive soils. *Geotext Geomembr*. <https://doi.org/10.1016/j.geotexmem.2007.05.005>
13. Ikizler SB, Aytekin M, Vekli M (2009) Reductions in swelling pressure of expansive soil stabilized using EPS geofoam and sand. *Geosynth Int*. <https://doi.org/10.1680/gein.2009.16.3.216>
14. Horvath JS (1994) Expanded polystyrene (EPS) geofoam: an introduction to material behaviour. *Geotext Geomembr* 4:263–280
15. Liu HL, Deng A, Chu J (2006) Effect of different mixing ratios of polystyrene pre-puff beads and cement on the mechanical behaviour of lightweight fill. *Geotext Geomembr* 24:331–338. <https://doi.org/10.1016/j.geotexmem.2006.05.002>
16. ASTM D4546-14 (2014) Standard test methods for one-dimensional swell or collapse of soils. ASTM International, West Conshohocken, PA
17. Beju YZ, Mandal JN (2017) Expanded polystyrene (EPS) geofoam: preliminary characteristic evaluation. *Procedia Eng*. <https://doi.org/10.1016/j.proeng.2017.05.038>

The Effect of EPS Geofoam Thickness on the Seismic Performance of Quay Walls



Ayşe Edinçliler and Yasin Sait Toksoy

Abstract Water front engineering structures have experienced earthquake induced damages from minor to catastrophic scales during the past few decades. Previous major earthquakes including the 1995 Kobe earthquake, the 1999 Kocaeli earthquake and the 2011 Tohoku earthquake showed that ports and all of its structural components are exposed to a great seismic risk. Thus, great attention should be paid by means of seismic performance in the design phase of such facilities. EPS geofoam inclusion as one of the several improvement methods can increase the seismic performance of the quay walls. It is a well-known method to reduce the magnitude of earthquake-induced dynamic forces against rigid earth retaining wall structures. The aim of this numerical study is to determine the effects of using different thicknesses of EPS geofoam cushion on the seismic performance of quay walls. Non-linear dynamic analyses were performed using the PLAXIS software. During the analyses, real earthquake records were used. Evaluation of the results reveal that inclusion of EPS geofoam as a seismic buffer decreases earthquake-induced dynamic forces against the rigid quay wall model successfully in comparison of the nominally identical structure with no compressible cushion layer. Increasing cushion thickness was found to have a positive effect on the selected performance indicators. More importantly transmitted peak accelerations within the quay wall model are reduced up to 84%. One limitation of using lightweight-compressible materials behind rigid walls may be the possibility of increased displacements and rotations which should be controlled carefully.

Keywords Quay walls · EPS geofoam · Earthquake · Seismic buffer
Seismic performance

A. Edinçliler (✉) · Y. S. Toksoy
Boğaziçi University, Istanbul, Turkey
e-mail: aedinc@boun.edu.tr

1 Introduction

Quay walls are earth-retaining structures at which ships can berth. Quay walls are used for the transhipment of materials and goods by cranes or heavy equipment that move alongside the ship. In the seismic design phases of quay walls; stability and safety in addition to the economy is considered and basic design criteria including sliding, overturning and allowable bearing stress are taken into consideration during the design stages. Quay walls can suffer significantly due to earthquake and economical and social impacts of this natural event can be devastating. It is very difficult to categorize all the earthquake damages observed on quay walls; however, it is possible to classify this earthquake damages considering these basic design criteria [1]. The factors governing seismic performance of a gravity quay wall include wall dimensions, thickness of soil deposit below the wall, liquefaction resistance of subsoil below and behind the wall, as well as levels of seismic shaking at the base layer [2].

Dynamic performance of water front structures such as gravity type quay walls, vertically composite structures, flexible retaining walls, anchored bulk heads etc. under earthquake loading is always a source of anxiety [3]. In the past 20 years, many port structures have failed due to earthquakes, including those in Los Angeles, USA in 1994; Kobe, Japan in 1995; Kocaeli, Turkey in 1999; Taiwan in 1999, South Asia in 2003; and Tohoku, Japan in 2011 [4].

Secondary effects of earthquakes may also cause serious problems to the stability of quay walls. Liquefaction is one of the major indirect effect of strong ground motion which is a great threat to the stability and integrity of marine structures. Liquefaction-induced damage on port structures has been observed in the recent major earthquakes in Turkey and Japan [5].

The 1995 Hyogo-ken Nanbu earthquake caused extensive damage to the Port of Kobe and illustrated how vulnerable port systems are to earthquakes. The 1999 Kocaeli Earthquake is another devastating example. Container cranes were overturned due to the settlement and the permanent displacement of the quay walls at Derince Port of Kocaeli, Turkey [6]. The 2010 Haiti Earthquake demonstrated that ports are also critical to the post disaster response of the region in which they are located. Despite their vulnerability to earthquakes and importance to the economy and post disaster response, such structures have received little attention from the earthquake community [7].

In the literature, there can be found a number of experimental and numerical studies related with the dynamic performance of quay walls under seismic loads. Performing shaking table and centrifuge tests, researchers aim to find out the reasons such as liquefaction that lead to the permanent displacement of quay walls [8–10]. The dynamic response of gravity quay walls is strongly affected by non-linear soil behaviour. Development of excess pore pressures and accumulation of shear and volumetric strains both at the retained and the foundation soil, produces shear strength degradation [11, 12].

The benefits of using vertical compressible layers against rigid soil retaining wall structures have been reported in the literature by many researches and the product of choice to perform this function is expanded polystyrene (EPS), which is called as geofoam [13].

Geofoam is a geosynthetic product composed of foam. This lightweight product takes increasing attention of researchers due to its unique static and dynamic properties. Both experimental and numerical studies have been performed to investigate the effectiveness of expanded polystyrene (EPS) geofoam buffers in reducing the earthquake induced seismic loads on geotechnical structures such as retaining walls. A smart extension of this application is to use vertical compressible inclusions of EPS geofoam to attenuate earthquake-induced dynamic earth pressures against rigid walls. It is known that EPS geofoam has superior cushion properties due to the individual air bubble body which is capable of reducing the impact and vibration effects [14]. The results from the parametric analyses have been compiled into design charts that quantify the efficiency of geofoam as a function of geofoam buffer thickness and density, wall height, dynamic stress-strain properties of the retained soil mass, and characteristics of the base input excitation [15–22].

Recent comparative numerical experiments reveal that inclusion of EPS geofoam as a seismic buffer successfully decreases earthquake-induced dynamic earth pressures and transmission of accelerations, which prove that it can be possible to mitigate earthquake hazards on quay walls by simply implementing geofoam cushions [23–25].

The aim of this study is to investigate the thickness effect on the use of EPS geofoam seismic buffer to improve the seismic performance of the quay walls. Two different EPS geofoam thicknesses of 2 and 3 m are selected for the proposed study. Dynamic performance analyses were performed using the real earthquake records of the 1999 Kocaeli Earthquake and the 1940 El Centro Earthquakes which are obtained from KOERI.

2 Numerical Study

In this study, quay wall models with EPS geofoam seismic buffers, which vary in thickness, are modelled by using PLAXIS software. Due to the super lightweight of the material and high energy absorption properties, quay wall models with EPS geofoam are expected to perform better both under static and dynamic load conditions. This numerical study presents the effects of the thickness of the geofoam buffer in addition to the earthquake characteristics on the seismic performance of the quay walls. The detailed information is given in the following parts.

2.1 FEM Modelling

FEM analyses were performed using the commercially available PLAXIS 2D software which is a multi-purpose finite element modelling program capable of modelling various types of real geotechnical applications. During the modelling phase, plain strain model is selected and 15-node triangle elements option is preferred. In the dynamic analysis, prescribed displacement along the x-axis is introduced to the model in order to apply the selected earthquake motions of this study. In order to prevent unexpected spurious wave reflections and stress concentrations at the boundaries, the model mesh is created as large as possible and absorbent boundaries are introduced to the model. Dynamic analyses were performed under undrained conditions to approximate the behavior of saturated soils under transient and cyclic loads during earthquakes.

Proposed caisson type quay wall model has the dimensions of H: 15 m and W: 10 m. The depth of the water is considered as 10 m and the quay wall itself retains 13 m high backfill soil. All dimensions except the thickness of geofoam buffer remain the same during the analyses. The finite element model is represented in Fig. 1.

2.2 EPS Block Geofoam

All soil types and geofoam buffer material are modelled by Mohr Coulomb soil model in FEM model. Quay wall is introduced as a plate element in the model. Flexural rigidity of the plate is EA: $7.5E^6$ with an element thickness of 1 m. The parameters of the geofoam buffers are obtained from the similar studies and ASTM 6817. Details of the material properties are given in Table 1.

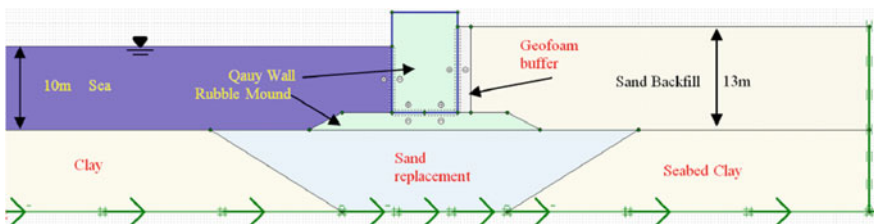


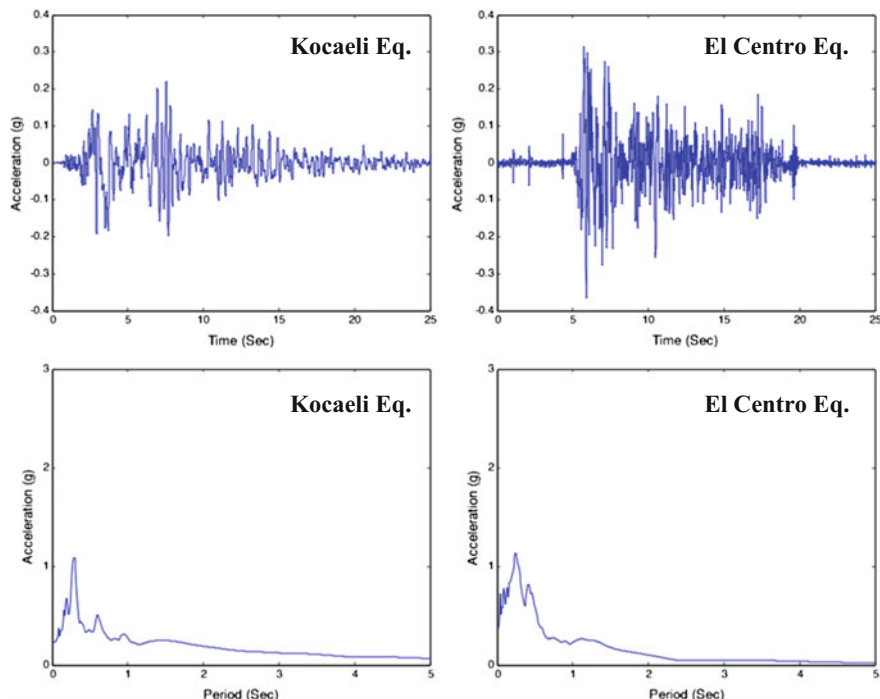
Fig. 1 FEM model for the proposed dynamic analyses

Table 1 Input parameters of materials for hardening soil model

	Sand	Clay	Foundation rubble	Fill	EPS
γ_{unsat}	16.5 kN/m ³	16 kN/m ³	17 kN/m ³	19 kN/m ³	0.20 kN/m ³
c'_{ref}	0 kN/m ²	14 kN/m ²	0 kN/m ²	5 kN/m ²	35 kN/m ²
\emptyset	33°	24°	35°	35°	30°
ψ	8°	0°	5°	10°	0°
E	13.560 kN/m ²	9000 kN/m ²	42.000 kN/m ²	200.000 kN/m ²	6000 kN/m ²

2.3 Dynamic Excitations

Dynamic response analyses were performed using the real earthquake records of the Kocaeli Earthquake (PGA = 0.23 g) and El Centro Earthquake (PGA = 0.36 g). Obtained from BU-KOERI-BDTIM database, these two earthquake records are carefully selected due to the difference of inherent characteristics in frequency domain which mostly governs the dynamic response of structures. Records are obtained from bedrock and used after baseline corrected and filtered from noise contamination. Predominant frequencies of the records are 3.5 and 4 Hz for Kocaeli and El Centro Earthquakes, respectively. Time-histories and Response spectra of ground motions are represented in Fig. 2.

**Fig. 2** Acceleration-time histories and response spectra of Kocaeli and El Centro earthquakes

3 Results

Numerical results obtained from quay wall models with and without EPS geofoam buffer included behind the model are represented by means of total displacements, rotations, axial and shear stresses and bending moments for all considered earthquake records and EPS thicknesses for each model. Model 1 corresponds to the quay wall model with no EPS geofoam buffer whereas Model 2 and Model 3 represents the models with EPS geofoam buffer thicknesses of 2 and 3 m, respectively. The results under different earthquake motions are given in the following parts. In addition, results are summarized in Table 1.

3.1 Results of the Kocaeli Earthquake

Under the Kocaeli Earthquake excitations, resultant total displacement contours for the models are represented in Fig. 3.

Results indicate that the inclusion of a cushion layer behind the quay wall model leads to a slight increase in total displacement values. Obtained 90 cm of displacement in Model 1 increased to 110 cm in Model 3 and 112 cm in Model 2. Similarly, earthquake induced rotations were occurred to be 1.34° in Model 1, 2.14° in Model 2 and 2.22° in Model 3.

Under current ground motion; axial and shear stresses and bending moments were significantly affected by the inclusion of the geofoam cushion. Axial stresses decreased from 470.8 to 457.1 kN/m in Model 2 and by means of shear stresses, results decreased from 433.9 to 423.0 kN/m in Model 3, where the 3 m-thick EPS cushion layer was used. Also, obtained bending moments follow the same trend as 1232 kN/m of moment force in Model 1 decreased to 1204 kN/m in Model 2. However, due to the superior cushion properties of EPS geofoam material, the obtained bending moment value was 1107 kN/m in Model 3.

Transmitted accelerations through the quay wall models are represented in Fig. 4 for the Kocaeli Earthquake motion.

As seen in Fig. 4, EPS geofoam buffer is capable of effectively and successfully reducing the peak transmitted accelerations from 2.35 to 0.59 g in Model 2 and to 0.38 g in Model 3.

3.2 Results of the El Centro Earthquake

Obtained total displacement contours for El Centro Earthquake excitations are represented for each model in Fig. 5. When subjected to El Centro Earthquake excitations, observed displacements are in the range of 89–97 cm and related rotations are obtained between 1.35° (Model 1) and 1.90° (Model 3) as revealed in Fig. 5.

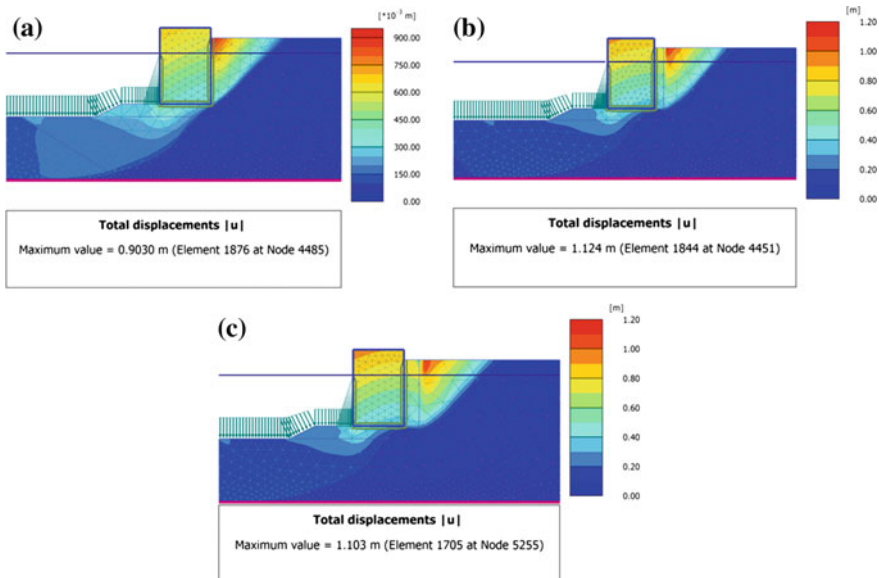


Fig. 3 Total displacement contours under the Kocaeli earthquake **a** Model 1, **b** Model 2, **c** Model 3

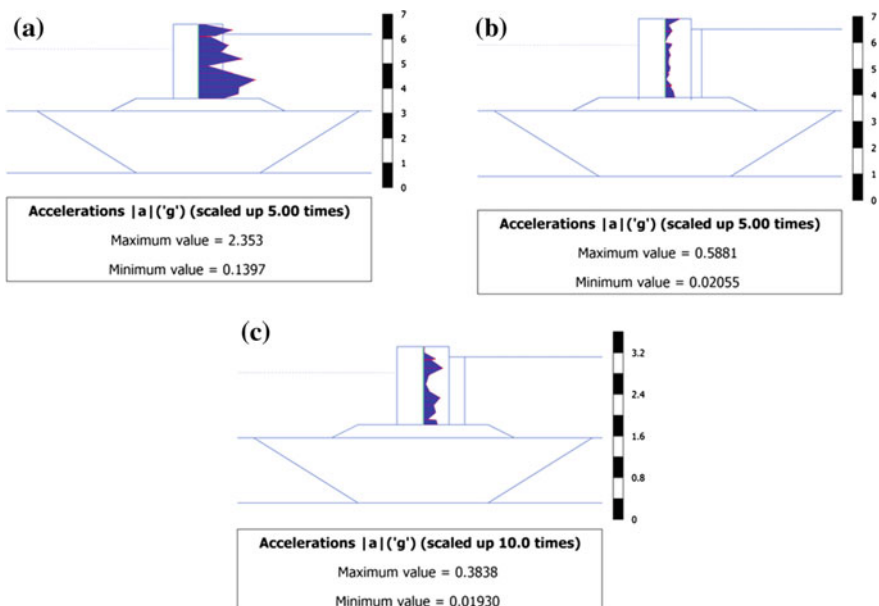


Fig. 4 Transmitted acceleration distribution under Kocaeli earthquake **a** Model 1, **b** Model 2, **c** Model 3

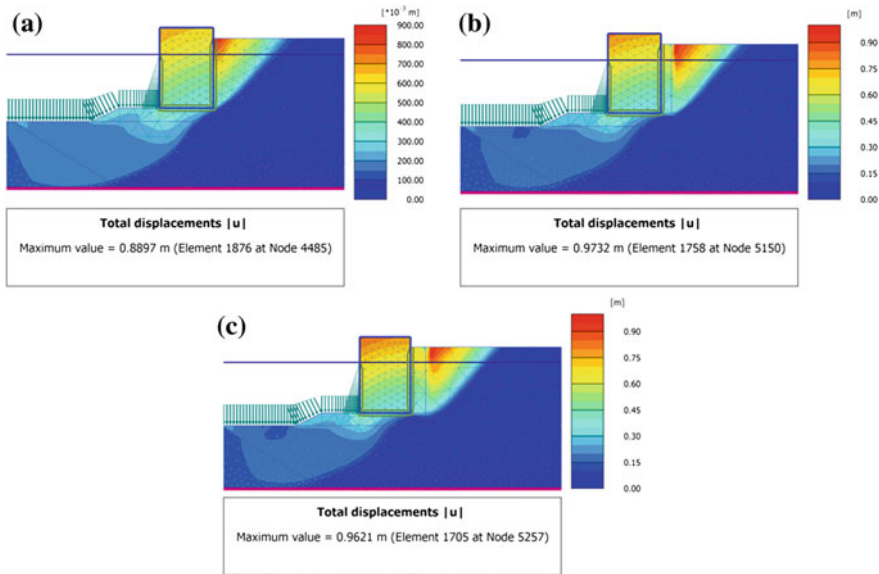


Fig. 5 Total displacement contours under Kobe earthquake **a** Model 1, **b** Model 2, **c** Model 3

Under current ground motions, obtained axial stresses are 493.5, 494.9, and 495.9 kN/m for Model 1, Model 2 and Model 3, respectively. On the other hand, the cushion effect of the proposed material is clearly seen in shear stress and bending moment parameters. Shear stresses were obtained to be 453.7 kN/m in Model 1 and it decreased to 440.8 kN/m in Model 3, where 3 m-thick EPS cushion is used. Earthquake induced bending moments found to be effectively diminished by the EPS geofoam inclusion as bending moment values are significantly reduced from 1172 to 1092 kN/m in Model 2 and to 1078 kN/m in Model 3. Transmitted acceleration distributions along the models are visualized in Fig. 6.

Transmitted acceleration values are found to be significantly influenced by the inclusion of cushion layer along the structure. Obtained 1.06 g of peak transmitted acceleration within the body of the structure decreased to 0.91 and 0.43 g in Model 2 and Model 3 respectively.

4 Discussion and Evaluation of Results

Numerical results obtained from proposed FEM software are summarized in Table 2 for the ease of evaluation.

Cushion thickness is found to have a negligible effect on the total displacement values in this study. Regardless of the seismic excitation, total displacements experience a slight increase with the application of EPS geofoam cushion.

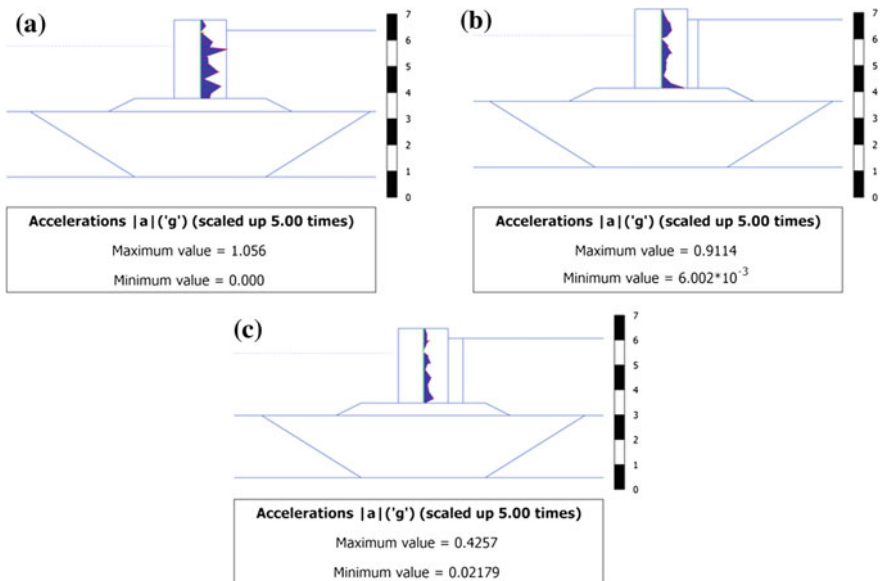


Fig. 6 Transmitted acceleration distribution under El Centro earthquake **a** Model 1, **b** Model 2, **c** Model 3

Table 2 Numerical results obtained from dynamic FEM analyses

	Kocaeli earthquake (0.23 g)			El Centro earthquake (0.36 g)		
	Model 1	Model 2	Model 3	Model 1	Model 2	Model 3
Total displacements (m)	0.90	1.12	1.10	0.89	0.97	0.96
Rotation (°)	1.34	2.14	2.22	1.35	1.76	1.90
Axial stress (kN/m)	470.8	457.1	462.8	493.5	494.9	495.9
Shear stress (kN/m)	433.9	423.3	423.0	453.7	443.4	440.8
Bending moment (kN/m)	1232	1204	1107	1171	1092	1078
Peak transmitted acceleration PGA (g)	2.35	0.82	0.38	1.06	0.91	0.43

However, results are slightly affected considerably by the changes in cushion thickness. The same statement also applies to the earthquake induced rotations of the models.

The inclusion of the proposed cushion material along the quay wall models has a direct effect on the earthquake induced axial and shear stress values and bending moments acting on the sea front structure. Axial stress values decrease around 5%

with the EPS geofoam. Increasing cushion thickness tend to increase the axial stress values. On the other hand, shear stress values tend to decrease with the increasing cushion thickness levels. It is investigated that the EPS geofoam cushion decreases the shear stresses up to 3%. Bending moment values seem to be affected more than axial and shear stress values by the inclusion of the EPS geofoam. As can be inferred from Table 2, increasing cushion thickness has a positive effect on results by means of bending moment and results are found to be up to 10% less when the quay wall model was cushioned with 3 m-thick EPS geofoam layer.

Assessment of the dynamic response analyses reveal that peak transmitted acceleration values within the quay wall model can be significantly decreased by simply introducing a cushion layer behind and along the models. As can be inferred from Table 2, peak transmitted accelerations decrease up to 84% for the models with EPS geofoam cushion when compared with the no-cushion model. Increasing cushion thickness has a favorable influence on peak transmitted accelerations by means of dynamic performance. Peak transmitted acceleration distributions under given ground excitations are also found noteworthy. Represented in Figs. 4 and 6; geofoam cushion inclusion diminishes transmitted accelerations and lead to a smoothened acceleration distribution along the quay wall models compared to the jagged distributions of Model 1.

5 Conclusions

In order to determine the effects of the EPS geofoam cushion thickness on the dynamic performance of quay walls, a comprehensive numerical study has been carried on by performing a series of numerical analyses using the finite element code PLAXIS. Three different finite element models are created and subjected to real earthquake records of Kocaeli Earthquake and El Centro Earthquake.

As can be inferred in Table 2, the inclusion of EPS geofoam cushion has a direct effect on obtained axial and shear stresses and bending moments. Inclusion of EPS geofoam layer across the quay wall model reduced the peak axial and shear stresses approximately 5% and bending moments up to 10% especially for the 3 m-thick EPS geofoam cushion case (Model 3).

The most striking outcomes of this study is related with peak transmitted acceleration values, transmitted acceleration distributions along the models. Peak transmitted accelerations are simply reduced by up to 84% with the inclusion of the EPS geofoam cushion. Increasing cushion thickness has a favorable influence on results by means of dynamic performance. Also, numerical analyses reveal that geofoam supported models are influenced by smoothened acceleration distributions along the structure compared to the jagged acceleration distributions of Model 1.

The obtained numerical results in this study are dependent on the model dimensions, material properties, and the earthquake characteristics. Different results may be achieved with different combinations of these parameters.

References

1. Li X, Wu Y, He S (2010) Seismic stability analysis of gravity retaining walls. *Soil Dyn Earthq Eng* 3:875–878
2. Ichii K, Iai S, Morita T (2000) Performance of the quay wall with high seismic resistance. *J Comput Civil Eng* 17(2):163–174
3. Madabhushi GSP, Cilingir U, Haigh SK, Hazarika H. (2008) Finite element modelling of the seismic behaviour of water front structures. In: The 12th international conference of international association for computer methods and advances in geomechanics (IACMAG), 1–6 Oct, Goa, India
4. Yuksel Y, Yuksel ZT, Cevik E, Orhan K, Berilgen M (2017) Evaluation of the seismic performance of a caisson and an L-type quay wall. *Soil Dyn Earthq Eng* 92:537–550
5. Sumer BM, Ansal A, Cetin KO, Damgaard J, Gunbak AR, Hansen NEO, Sawicki A, Synolakis CE, Yalciner AC, Yuksel Y, Zen K (2007) Earthquake-Induced liquefaction around marine structures. *J Waterw Port Coast Ocean Eng* 133(1):55–82
6. Boulanger RW, Iai S, Ansal A, Cetin KO, Idriss IM, Sunman B, Sunman K (2000) Performance of waterfront structures. *Earthq Spectra* 16:295–310
7. Jacobs LD, DesRoches R, Leon RT (2010) Large scale shake table test of a port container crane under strong motion excitation. *Structures Congress*, pp 2692–2701
8. Kohama E, Miura K, Yoshida N, Ohtsuka N, Kurita S (1998) Instability of gravity quay wall induced by liquefaction of backfill during earthquake. *Soils Found* 38(4):71–83
9. Kohama E, Miura K, Yoshida N, Ohtsuka N, Kurita S (2000) Behavior of gravity type quay wall during earthquake regarding dynamic interaction between caisson and backfill during liquefaction. In: 12th World conference on earthquake engineering, Auckland, NZ
10. Kim SR, Jang IS, Chung CK, Kim MM (2005) Evaluation of seismic displacements of quay walls. *Soil Dyn Earthq Eng* 25:451–459
11. Iai S, Ichii K, Morita T (1996) Analysis of damage to quay walls during 1995 great Hanshin Earthquake, Japan. In: 11th world conference on earthquake engineering, Acapulco, Mexico
12. Gerolymos N, Tasiopoulos P, Gazetas G (2015) Seismic performance of block-type gravity quay-wall: numerical modelling versus centrifuge experiment. *SECED 2015*, Cambridge, UK
13. Bathurst RJ, Zarnani S, Gaskin A (2007) Shaking table testing of geofoam seismic buffers. *Soil Dyn Earthq Eng* 27:324–332
14. Lin LK, Chen LH, Chen RHL (2010) Evaluation of geofoam as a geotechnical construction material. *J Mater Civ Eng* 22(2):160–170
15. Pelekis PC, Xenaki VC, Athanasopoulos GA (2000) Use of EPS geofoam for seismic isolation of earth retaining structures: results of an FEM study. In: Proceedings of the second European geosynthetics conference, Bologna, Italy, pp. 843–846
16. Hazarika H (2001) Mitigation of seismic hazard on retaining structures—a numerical experiment. In: Proceedings of the 11th international offshore and polar engineering conference, Stavanger, Norway, 17–22 June 2001, pp 459–464
17. Hazarika H, Okuzono S (2002) An analysis model for a hybrid interactive system involving compressible buffer material. In: Proceedings of the 12th international offshore and polar engineering conference, Kitakyushu, Japan, 26–31 May 2002, pp 622–629
18. Hazarika H, Okuzono S (2004) Modeling the behaviour of a hybrid interactive system involving soil, structure and EPS geofoam. *Soils Found* 44(5):149–162

19. Zarnani S, Bathurst RJ (2005) Numerical investigation of geofoam seismic buffers using FLAC. In: Proceedings of the North American geosynthetics society (NAGS)/GRI19 conference, Las Vegas, Nev, pp 14–16 Paper No. 5.10a
20. Zarnani S, Bathurst RJ (2006) Application of EPS geofoam as a seismic buffer: numerical study using FLAC. In: Proceedings of the 59th Canadian geotechnical conference, Vancouver, BC
21. Athanasopoulos GA, Niklopoulou CP, Xenaki VC, Stathopoulou VD (2007) Reducing the seismic earth pressure on retaining walls by eps geofoam buffers—numerical parametric study. In: Proceedings of the geosynthetics conference, Washington, DC
22. Zarnani S, Bathurst RJ (2009) Numerical parametric study of expanded polystyrene (EPS) geofoam seismic buffers. Can Geotech J 46:318–338
23. Edinçliler A, Toksoy YS (2016) Numerical study of improving seismic performance of quay walls. In: 12th international congress on advances in civil engineering, ACE (2016) Boğaziçi University, Istanbul, Turkey
24. Edinçliler A, Toksoy YS (2016) Effects of two different seismic cushions on seismic performance of quay walls: numerical study. In: 6th European geosynthetics congress, EuroGeo6, Ljubljana, Slovenia
25. Edinçliler A, Toksoy YS (2017) The influence of geofoam material parameters on the seismic performance of quay walls. In: G7 7th National geosynthetics conference, 11–12 May. Boğaziçi University, Istanbul, Turkey (in Turkish)

Opening Traffic for a Temporarily Remediated EPS Road After the 2016 Kumamoto Earthquake: A World First



Keiichi Taneichi, Takeharu Konami, Hideki Tsukamoto,
Tatsuro Kubota and Kazuya Yasuhara

Abstract In 2016, two successive gigantic earthquakes struck the Kumamoto area of Japan, damaging many private residences and some local roads. An EPS embankment in the Mashiki area near the earthquake epicenter also collapsed. In this EPS embankment, the EPS blocks were shifted sideways because of a landslide behind the EPS fill caused by the earthquake. Nevertheless, only part of the embankment collapsed. The road surface was temporarily remediated and was maintained as it was, for the opening of traffic. This case proves that EPS gives rise to great benefits: most importantly, the collapsed EPS road was put into practical use as a temporary road.

Keywords Geofoam block · Stability · Earthquake · Local road Reuse

K. Taneichi · T. Konami
Okasanlivic Co. Ltd., EDO, 1-8-27 Konan, Minato-ku, Tokyo 108-0075, Japan
e-mail: taneichi@okasanlivic.co.jp

T. Konami
e-mail: konami@okasanlivic.co.jp

H. Tsukamoto (✉)
CPC, Inc., EDO, 2-1-1 Awaza, Nishi-ku, Osaka 550-0011, Japan
e-mail: tsukamoto@cpcinc.co.jp

T. Kubota
CPC, Inc., EDO, 4-40-11 Takadanobaba, Shinjuku-ku, Tokyo 169-0075, Japan
e-mail: kubota@cpcinc.co.jp

K. Yasuhara
Institute for Global Change Adaptation Science (ICAS), Ibaraki University,
2-1-1 Bunkyo, Mito, Ibaraki 310-8512, Japan
e-mail: Kazuya.yasuhara.0927@vc.ibaraki.ac.jp

1 Kumamoto Earthquake

Devastation from the 2016 Kumamoto earthquake included 64 fatalities and 8336 complete failures of residences. The earthquake swarm included a Mj6.5 earthquake foreshock on April 14 and a Mj7.3 main shock earthquake that occurred soon after on April 16, striking Kumamoto and Oita prefectures.

From geotechnical engineering points of view, damage was characterized as explained below. (i) Landslides and liquefaction occurred respectively in volcanic mountainous and plain sites. (ii) Both gentle and steep embankments of residential areas founded on volcanic ash cohesive soil deposits flowed and collapsed during a period of maximum seismic intensity, measured as 7. Residences and local roads with retaining walls were the most severely damaged. (iii) Volcanic ash soil is an important keyword associated with geo-disasters. (iv) Rich groundwater in Kumamoto plain played an important role in exacerbating damage to earth structures and foundations. In addition, a road through the area collapsed. Traffic became impossible. Mountain slopes also collapsed. A large landslide occurred. This area, on the Median Tectonic Line lying in the Japanese archipelago, has many faults. These faults moved. Roads and rivers were shredded.

2 EPS Road in the Kumamoto–Mashiki Area

An Expanded Poly-Styrol (EPS) road was constructed in the Mashiki area in Kumamoto (Figs. 1, 2, 3, 4, 5, 6, 7, 8, 9 and 10). In the mountainous Mashiki area, many villages in the mountains are connected by a single road. Therefore, if these roads are closed, it will take hours to make a detour. It resembles a village in Norway's fjords.



Fig. 1 Deformation of EPS embankment seen from the temple side



Fig. 2 A 1-m-wide crack in the road surface after refilling

Fig. 3 Collapse of rear slope and temporary remediation





Fig. 4 Collapse of outer protective wall



Fig. 5 Displaced EPS blocks



Fig. 6 JMB remained in position



Fig. 7 Crack in intermediate concrete slab

The Mashiki road that was produced using EPS was planned for construction through slopes adjacent to a temple and tomb. Therefore, the local government adopted an EPS embankment, which is lightweight and which can therefore be terminated sideways with vertical walls.

However, the Kumamoto Earthquake caused ground movements in several places. The mountain behind the EPS embankment collapsed. The concrete retaining wall on the slope behind the EPS embankment was shattered. Moreover, the masonry retaining wall protecting the foundation of the EPS embankment collapsed. A nearby tombstone also nearly collapsed. Part of the shore on the opposite bank of a river collapsed, with a large-scale collapse occurring on a nearby mountain slope.



Fig. 8 EPS concrete foundation



Fig. 9 Collapse of hillside on the opposite shore of the river



Fig. 10 Remediated surface of collapsed EPS embankment with restricted road width

3 Collapsed EPS Embankment

Although the mountain behind the EPS embankment collapsed and the retaining wall that protected the foundation collapsed, the road was not completely destroyed. Because of ground motion caused by the earthquake, the protective wall on the vertical surface of the EPS road collapsed. The EPS blocks were shifted by landslides from the back and protruded out at the front. However, the EPS blocks were mutually supportive. They maintained the form of the embankment. Joint metal binders linking EPS blocks moved, but they kept the EPS blocks mutually connected. The concrete slab in the embankment was broken and a large crack with 1 m width occurred on the road surface. However, the road level remained even: it never collapsed completely. As a result, the EPS road was able to mitigate damage to neighboring temples and graveyards.

4 Opening Traffic on the Collapsed Road

The collapsed road is the only road that local mountain residents used every day. It would be a great inconvenience to the life of every resident in the area if the road had been closed for repair work.

It will take more than a year to recover from damage caused by the landslides behind the road and the deformed EPS embankment. For this reason, it was discussed whether the possibility exists of using the partly collapsed road as a temporary means of Kumamoto–Mashiki transportation. The council of the local government deliberated the question several times in the regional parliament. Eventually, it was decided to reopen the road conditionally. The difficult situations were, for example, that the road width was restricted to one lane (Fig. 10). There was a low speed limit. Furthermore, the road was supposed to be closed during periods of severe rainfall.

Currently, a design revision for this road is in progress. The design method is reconstruction of the new EPS embankment after stabilizing the rear slope reinforced with anchors.

5 Conclusion

The following conclusions were obtained from this case study of remediation of a temporarily collapsed EPS road in the Mashiki area. The road resisted a large-scale earthquake that occurred successively within a short period.

- (i) The EPS embankment was unable to resist the collapse of the rear slope and severe ground movement, but the EPS embankment did not collapse completely.

- (ii) Joint metal binders mutually connecting EPS blocks were effective even in strong earthquakes.
- (iii) The concrete slab cracked because of drastic deformation of the embankment, but it was effective for maintaining the road surface evenness after the collapse.
- (iv) The EPS embankment was deformed by landslides on the rear slope, but the blocks were mutually supporting. No complete collapse occurred.
- (v) The vertical embankment using EPS was able to minimize the influence on the surroundings, even in a large earthquake.
- (vi) The vertical EPS embankment was able to prevent road collapse by mutual block support even if partial deformation occurred.
- (vii) Results show that an EPS embankment undergoing substantial deformation and partial collapse was useful as a temporary road under additional reinforcement.

6 Future Research Necessary

The EPS Development Organisation in Japan (EDO) has planned to carry out advanced research on increasing earthquake resistance of EPS embankments:

1. *Improvement of joint metal binders*

Because the conventional joint metal binder is a rectangle with asymmetrical spikes, eccentric action from seismic forces might occur. Therefore, the shape should be square, but with an increased number of spikes. A shear test was conducted by attaching old and new joint metal binders to EPS blocks. Results confirmed that the new metal binder provides shear strength that is 1.5 times that of the old metal binders.

2. *Number and position of joint metal binders*

It is necessary to produce a 1/5 model EPS embankment, and to perform earthquake resistance experiments using a shaking table. The effect of several positions of joint metal binders will be confirmed by model tests on the shaking table. Currently, the experiment is being conducted using shaking table equipment at The University of Tokyo.

3. *Study the behavior of EPS embankments when strong earthquakes occur continuously, thereby strongly influencing EPS embankments*

Experiments in areas struck by large-scale earthquakes were conducted in 1997. Such attempts should be continued.

4. *In 2018, make real full scale EPS embankments and conduct earthquake resistance experiments*

The experimental EPS embankment will have 8-m height, 5-m length, and 3-m width. Experiments will be conducted at a large shaking table facility.

5. *Design specifications*

Based on these experimentally obtained results, a design system for large-scale earthquakes acting continuously on EPS embankments shall be established.

Acknowledgements The authors thank the road engineers and officials of Kumamoto Prefecture for their cooperation in providing necessary information to prepare this paper.

References

1. Tsukamoto H (2011) History of R&D and design code for EDO-EPS method in Japan, EPS 2011 NORWAY. In: Fourth international conference, Oslo, June 2011
2. EDO (EPS Development Organization: Japan) (2014) EDO-EPS method, designing/application code (in Japanese)

Development of Joint Metal Binder for Improving Earthquake Resistance of EPS Embankment



Keiichi Taneichi, Takeharu Konami, Hideki Tsukamoto,
Tatsuro Kubota and Kazuya Yasuhara

Abstract EPS embankments have been found to be able to ensure earthquake resistance by using joint metal binder between blocks. However, since the conventional joint metal binder is rectangular, it may act eccentric to a seismic force. There were also parts with no spikes around the metal edges, and it was pointed out that it provided a weak connection between blocks. This paper reports on the effectiveness of a new joint metal binder developed and improved on a shear testing machine.

Keywords Geofoam blocks · Lightweight · Stability · Seismic forces
Binders

1 Introduction

In an EPS embankment, the spikes of the Joint metal binder (hereinafter abbreviated as JMB) are inserted into blocks so that the blocks are connected to each other as an integral embankment. The seismic performance of an EPS embankment using the

K. Taneichi (✉) · T. Konami
Okasanlivic Co. Ltd, 1-8-27 Konan, Minato-ku, Tokyo 108-0075, Japan
e-mail: taneichi@okasanlivic.co.jp

T. Konami
e-mail: konami@okasanlivic.co.jp

H. Tsukamoto
CPC, Inc., EDO, 2-1-1 Awaza Nishi-Ku, Osaka 550-0011, Japan
e-mail: tsukamoto@cpcinc.co.jp

T. Kubota
CPC, Inc., EDO, 4-40-11 Takadanobaba, Shinjuku-ku, Tokyo 169-0075, Japan
e-mail: kubota@cpcinc.co.jp

K. Yasuhara
Institute for Global Change Adaptation Science (ICAS), Ibaraki University,
2-1-1 Bunkyo, Mito, Ibaraki 310-8512, Japan
e-mail: Kazuya.yasuhara.0927@vc.ibaraki.ac.jp

conventional JMB was confirmed by a model shaking table test and a full-scale shaking test carried out in 1997 [1, 2]. These tests indicated that when considering large scale seismic motion, JMBs should be densely distributed over the block surface in order to prevent misalignment and movement of the blocks. However, in the Kumamoto earthquake that occurred in 2016, a magnitude 6.5 scale sway was observed twice in succession. In the full scale shaking table test of 1997, the behavior in the case where a strong tremor acts multiple times has not been verified. Therefore, in order to make integration of the blocks more reliable, a new JMB was devised instead of the conventional one. In order to confirm the effect of the new JBM, shear tests of EPS blocks connected with old and new JMBs were conducted.

2 Effect of New JMB

Figure 1a shows the conventional JMB. The plate portion is a rectangle with a long side of 150 mm and a short side of 100 m, and six spikes are provided on each edge.

The new JMB is shown in Fig. 1b. The plate portion is a square with a side of 150 mm, and ten spikes are provided on each edge. The new JMB has an increased number of spikes by 1.67 times compared with the conventional one.

For this reason, the shear resistance of the spikes is increased, and even if strong ground motion or large ground deformation occur, the blocks can be more reliably kept in position. In addition, because the plate part of a JMB has conventionally been rectangular, it was considered to have a possible potential to cause rotational motion from seismic forces. Since the new JMB is square, it can control the rotational motion, and the mutual integration of the blocks can be made more reliable.

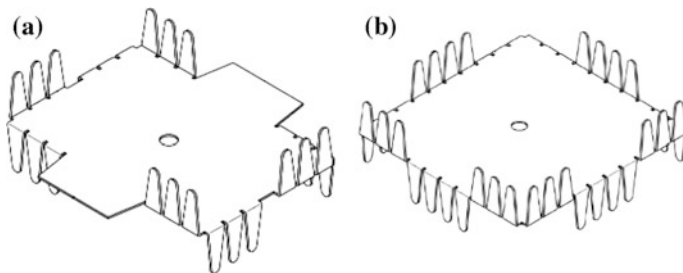


Fig. 1 **a** Conventional JMB. **b** New JMB

3 Test Block and JMB

EPS-20 and XPS-24 were used as test blocks. The dimensions of the blocks were 350 mm in length (upper block)/250 mm (lower block), 250 mm in width and 70 mm in thickness. The reason why the length is made large and small is that the mutual contact area should not change by horizontal movement of the upper block. The material used in the JMB is an alloy steel plate of aluminum and zinc.

4 Test Apparatus and Test Method

Figure 2 shows a schematic drawing of the test equipment. The apparatus is an improvement so that the block specimen could be tested with a soil shear test apparatus. First the lower block was fixed and a JMB was installed on the contact surface. Next, a vertical force was applied evenly from the lower surface of the lower block creating a vertical stress σ_v between the block surfaces. Then, the upper block was moved horizontally at a constant speed of 1 mm per minute, and the horizontal force and horizontal displacement were measured. Three cases of vertical stress σ_v were applied 2.5, 5.0, and 10.0 kN/m².

5 Test Results

Figures 3 and 4 show the relationship between shear stress τ and horizontal displacement δ when using the new JMB for the values of vertical stress σ_v selected.

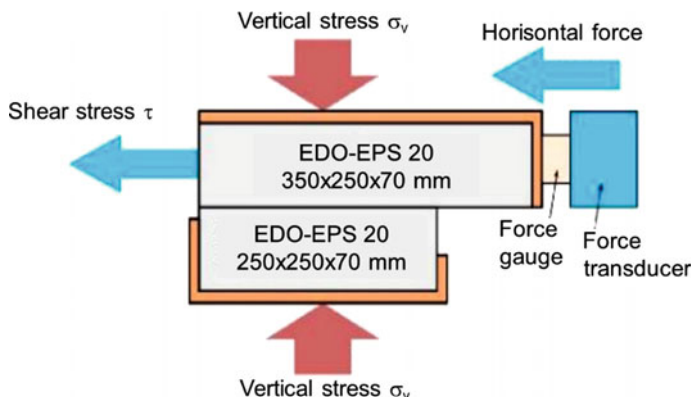


Fig. 2 Schematic drawing of test apparatus

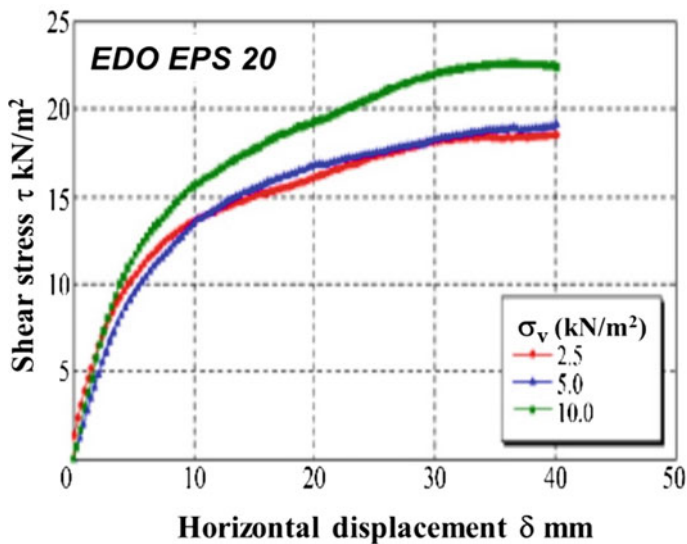


Fig. 3 Relationship between shear stress and horizontal displacement for EPS with new JMB

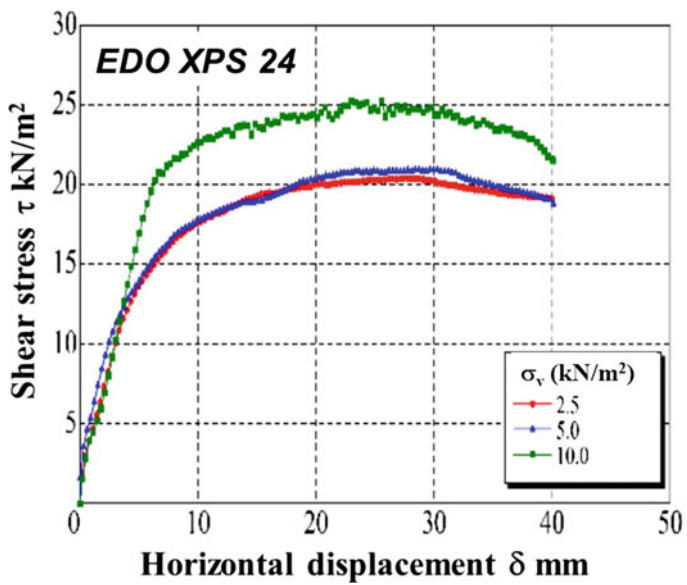


Fig. 4 Relationship between shear stress and horizontal displacement for XPS with new JMB

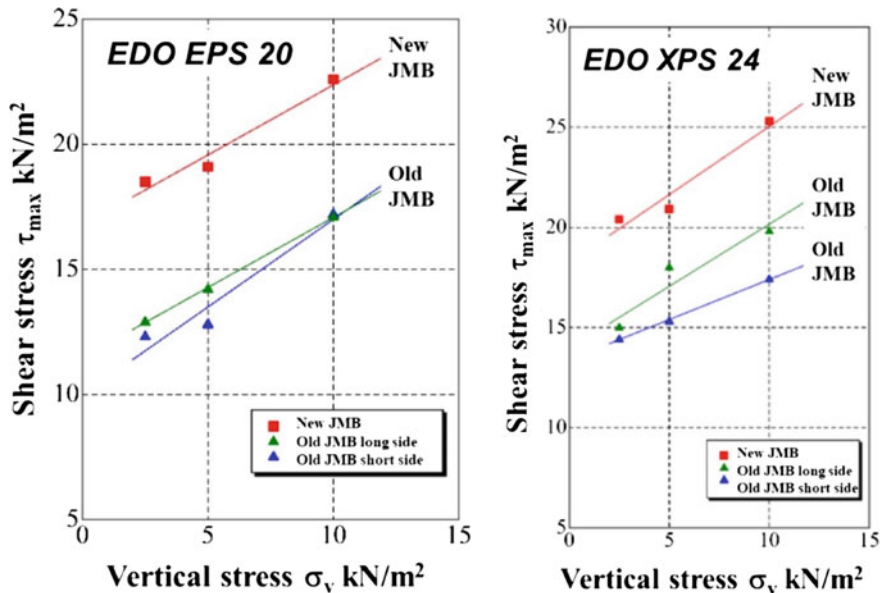


Fig. 5 Relationship between shear stress τ and vertical stress σ_v

The relationship between shear stress (maximum value) τ_{max} and vertical stress σ_v is shown in Fig. 5. In both cases shear stress τ versus vertical stress σ_v show a linear relationship. The shear stress of the new JMB is about 125–140% of the conventional metal binder within the range of the vertical stress values selected, and the effect of the new JMB is confirmed.

References

1. Hotta H, Kuroda S, Nishi T (2001) Behavior of double-vertical-wall-type EPS fills during major earthquakes, EPS geofoam 2001. In: 3rd international conference, Salt Lake City, Dec 2001
2. Tsukamoto H (2011) History of R&D and design code for EDO-EPS method in Japan, EPS 2011 Norway. In: 4th international conference, Oslo, June 2011
3. EDO (EPS Development Organization: JAPAN) (2014) EDO-EPS method designing/application code, Published in 2014 (in Japanese) (4)

Shaking Table Test of Scaled 1/5 EPS Embankment Model



Keiichi Taneichi, Tsuyoshi Nishi, Takeharu Konami, Tatsuro Kubota,
Junichi Koseki, Hiroyuki Kyokawa and Kazuya Yasuhara

Abstract A large earthquake in the Kumamoto district in the south of Japan in April 2016 occurred twice within 28 h with a magnitude class 6.5. Due to this earthquake many houses and roads collapsed. In order to investigate the behavior of EPS embankments when a large-scale earthquake acts consecutively, an EPS embankment model with a scale of 1/5 was built and a shaking table experiment was conducted using the shaking table (3 m × 2 m) at the University of Tokyo. The EPS embankment was found to cause rocking phenomenon due to seismic motion. As a countermeasure, in addition to the effect of an improved Joint Metal Binder (JMB), the effect of applying a larger number of JMBs was also investigated.

K. Taneichi · T. Konami
Okasanlivic Co. Ltd, 1-8-27 Konan, Minato-ku, Tokyo 108-0075, Japan
e-mail: taneichi@okasanlivic.co.jp

T. Konami
e-mail: konami@okasanlivic.co.jp

T. Nishi · T. Kubota (✉)
CPC, Inc, 4-40-11 Takadanobaba, Shinjuku-ku, Tokyo 169-0075, Japan
e-mail: kubota@cpcinc.co.jp

T. Nishi
e-mail: t_nishi@cpcinc.co.jp

J. Koseki · H. Kyokawa
Department of Civil Engineering, Faculty of Engineering, University of Tokyo,
7-3-1 Hongo, Bunkyo-ku, Tokyo 113-8656, Japan
e-mail: koseki@civil.t.u-tokyo.ac.jp

H. Kyokawa
e-mail: kyokawa@civil.t.u-tokyo.ac.jp

K. Yasuhara
Institute for Global Change Adaptation Scienceicas (ICAS), Ibaraki University,
2-1-1 Bunkyo, Mito, Ibaraki 310-8512, Japan
e-mail: Kazuya.yasuhara.0927@vc.ibaraki.ac.jp

Keywords Geofoam blocks • Lightweight • Stability • Seismic forces
Shaking table • Binders

1 Introduction

A shaking table test on an EPS embankment of 8 m in height carried out in 1997 [1, 2] showed high stability against large earthquakes. However, in Japan it is recently assumed that long earthquake motions such as the Tohoku earthquake that occurred in 2011 and continuous earthquakes of magnitude class 6.5 such as the Kumamoto earthquake in 2016, may reoccur. Therefore, the design of EPS embankments needs to consider such earthquakes. In order to evaluate the earthquake resistance of EPS embankments, it is planned to conduct a shaking table test with an embankment height of 8 m in 2018.

As a preliminary step, a shaking table experiment with an EPS embankment of scale 1/5 was carried out using a shaking table (3 m × 2 m) owned by the University of Tokyo.

2 Outline of Experiment

The experimental model was 1/5 of the actual model. The shape of the EPS embankment was rectangular at the base. The size of the EPS body was 1.0 m in length, 0.6 m in width and 1.6 m in height (16 layers of EPS blocks). Figure 1 shows the experimental model. The embankment shape assumes a high embankment with a height to width ratio of up to about 1.6, which is the same as the condition used in the 1997 shaking table test. The EPS embankment was modeled like an actual structure. In other words, slabs made of steel plates were installed for every 6 block layers, and the top was covered with a 30 mm thick steel plate simulating a pavement load.

Figure 2 shows Joint metal binders (JMB). The left side in the figure shows a new JMB developed for improving earthquake resistance. The right side shows the conventional JMB. The scale of JMBs used in the experiment was 1/5.

3 Experimental Conditions

Experiments were conducted by changing the arrangement and number of JMBs. Figure 3 shows an example of the arrangement of EPS blocks and JMBs with the old arrangement to the left and new to the right. The standard arrangement number is 15 (1 in 1 m² in actual arrangement). The arrangement pattern is a method of installing JMBs across adjacent EPS blocks (old method) and a method of installing

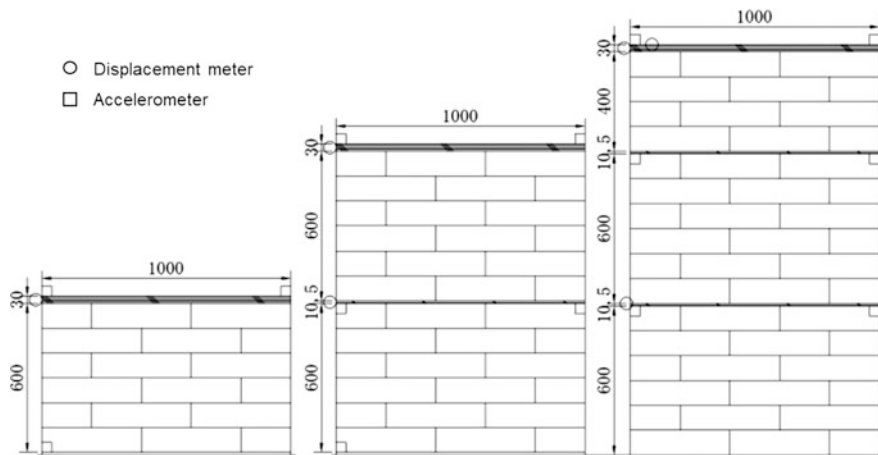


Fig. 1 Experimental model

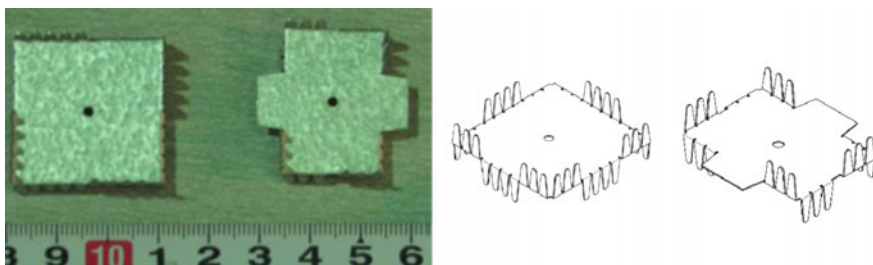


Fig. 2 Picture of JBMs 1/5 scale—left: new JBM—right: old JBM

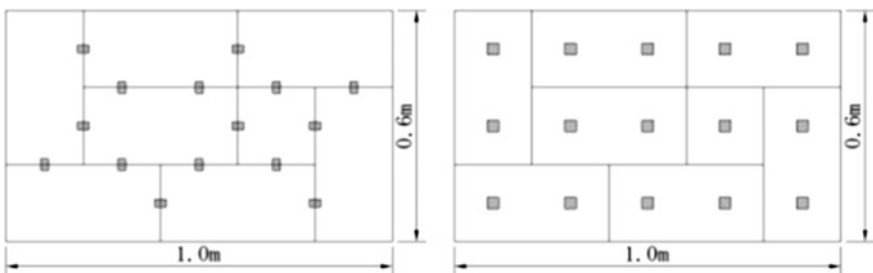


Fig. 3 Arrangement of EPS blocks and JBMs—left: old arrangement—right: new arrangement

JMBs in the center of the EPS block (new method). Tests were conducted with the case of 8 JBM (approximately half the standard value) and 30 JBM in a doubling arrangement.

The seismic motions used in the experiment were sine waves, inland type seismic waves and trench type earthquake waves.

The maximum acceleration used was three patterns of 100, 200 and 500 gal.

Inland seismic waves and trench type earthquake waves are assumed to be the largest earthquake motion observed in Japan so far, and the time axis is set to $\frac{1}{2}$ (Fig. 4).

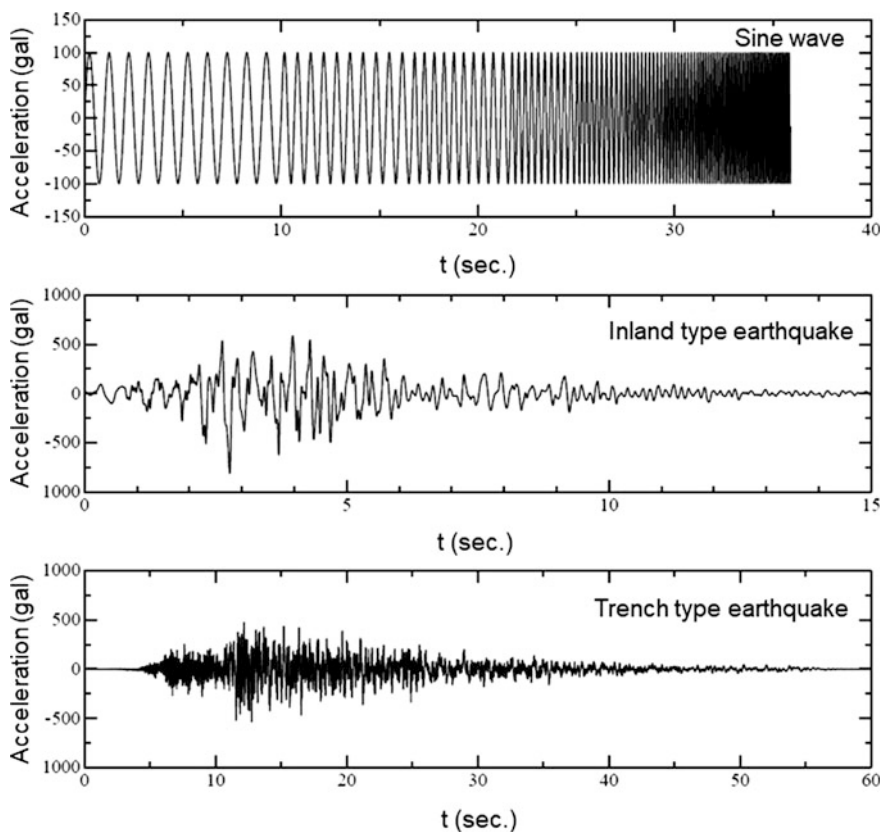


Fig. 4 Seismic wave used for experiment

4 Experimental Result

4.1 Effect of Joint Metal Binder (JMB)

In the experiment based on the presence or absence of JMBs, in the case without JMBs obviously, the movements were large, and the necessity for JMBs was confirmed. In the experiment, it was found that more than 15 JMBs (1 per 1 m² in actual arrangement) is necessary. Figure 5 shows experimental results.

In the experiments, it was found that the displacement between the shaking table and the EPS embankment placed there on, was large.

In each experiment, movement of the EPS embankment on the shaking table and movements between the EPS blocks and intermittent steel slabs were observed, but these are all caused by a rocking phenomenon. It was found that countermeasures against the rocking phenomena are necessary as measures against earthquake effects.

4.2 Rocking Phenomenon and Measures

When the embankment height was 1.6 m, the rocking phenomenon occurred near the third block layer measured from the base. A rotational moment is generated in the EPS embankment due to the horizontal inertia force caused by the excitation. Then, the deformation concentrates at the lower part where the moment is large.



Fig. 5 Picture of EPS embankment after test—left: no JMBs—right: new JMB arrangement



Fig. 6 JMB arrangements—left old system—right new system

This rotational moment causes vertical motion in the EPS embankment, and the EPS blocks were temporarily separated due to vertical movements between the blocks. That is, a phenomenon occurs in which the JMBs are disconnected. However, vertical motion caused by rotational moment does not mean that all EPS blocks are uniformly separated. Therefore, it was found that the JMBs provide smaller movements between blocks when arranged across blocks (Fig. 6).

The movements due to rocking confirmed by the experiment was more noticeable between the shaking table/intermittent steel slabs and the EPS blocks installed thereon than between the EPS blocks. Since there is nothing to constrain the EPS besides friction between EPS blocks and the shaking table/intermittent steel slabs, it was found that deformations are likely to occur.

As a method for suppressing these deformations, the following two alternative ideas were considered.

- ① A method of inserting spike-shaped protrusions on the shaking table/intermittent steel slabs extending into the EPS blocks.
- ② A method of installing L-shaped metal fittings at the side edges of the shaking table/intermittent steel slabs so that no horizontal movement may occur at the time of rocking.

Figure 7 shows displacement on intermittent steel slab (left) and the installation of L-shaped metal fittings according to idea ② (right). The left picture illustrates the situation after sine waves of 500 gal were applied with 2 waves. Displacement is seen in the lowest EPS block layer above the steel slab, but there is almost no change between the shaking table and the EPS blocks. By experiments, the effect of L-shaped metal fittings was found.



Fig. 7 Left—displacement on intermittent steel slab Right—effect of L-shaped metal fittings attached to intermittent slabs

5 Conclusion

Model experiments have revealed the effect of JMBs on EPS embankments during earthquakes, measures against rocking phenomena, and so on.

In 2018, it is planned to carry out a shaking table test using embankments of the same size as real objects of 8 m in height at large shaking table facilities owned by the country. Based on the results of this experiment, it is intended to develop and implement relevant new design specifications.

References

1. Hotta H, Kuroda S, Nishi T (2001) Behavior of double-vertical-wall-type EPS fills during major earthquakes, EPS Geofoam 2001. In: 3rd international conference, Salt Lake City, Dec 2001
2. Tsukamoto H (2011) History of R&D and design code for EDO-EPS method in Japan, EPS 2011 Norway. In: 4th international conference, Oslo, June 2011